GEOLOGICA ULTRAIECTINA

Mededelingen van de
Faculteit Aardwetenschappen
Universiteit Utrecht

No. 202

Fluxes, diagenesis and preservation of recent and Holocene sediments in the eastern Mediterranean

Arrian Rutten

Cover picture *Pigment concentrations in Mediterranean surface water measured by the Coastal Zone Colour Scanner, May 1980. Light colours indicate high pigment concentrations, darker colours low concentrations. Data are courtesy of NASA/GSFC.*

ISBN 90-5744-059-8

Fluxes, diagenesis and preservation of recent and Holocene sediments in the eastern Mediterranean

Fluxen, diagenese en preservatie van recente en Holocene sedimenten in de oostelijke Middellandse Zee.

(met een samenvatting in het Nederlands)

PROEFSCHRIFT

TER VERKRIJGING VAN DE GRAAD VAN DOCTOR
AAN DE UNIVERSITEIT UTRECHT
OP GEZAG VAN DE RECTOR MAGNIFICUS, PROF. DR. W.H. GISPEN,
INGEVOLGE HET BESLUIT VAN HET COLLEGE VOOR PROMOTIES
IN HET OPENBAAR TE VERDEDIGEN
OP WOENSDAG 18 APRIL 2001 DES MIDDAGS OM 14.30 UUR

DOOR

ARRIAN RUTTEN

geboren op 21 september 1972, te Dongen

Promotor: Prof. Dr. C.H. van der Weijden
Department of Geochemistry, Utrecht University,
Utrecht, The Netherlands

Co-promotor: Dr. G.J. de Lange
Department of Geochemistry, Utrecht University,
Utrecht, The Netherlands

The research described in this thesis was carried out at the Department of Geochemistry, Institute of Palaeo-environments and Palaeoclimate Utrecht (IPPU), Utrecht University, Budapestlaan 4, PO Box 80021, 3508 TA Utrecht, The Netherlands.
This study was supported by MARFLUX (MAST1-90022C), PALAEOFLUX (MAS2-CT93-0051) and SAP (MAS3-CT97-0137) European programmes.

“In the beginning the universe was created. This has made a lot of people very angry and been widely regarded as a bad move.”

Douglas Adams – The restaurant at the end of the universe

Contents

Chapter 1	Introduction and summary	*9*
Chapter 2	Recent terrestrial and carbonate fluxes in the pelagic eastern Mediterranean; a comparison between sediment trap and surface sediment	*15*
Chapter 3	Present-day coccolith fluxes recorded in central eastern Mediterranean sediment traps and surface sediments	*39*
Chapter 4	Deposition of sapropel S1 sediments in oxic pelagic and anoxic brine environments in the eastern Mediterranean; differences in diagenesis and preservation	*65*
Chapter 5	Sequential extraction of iron, manganese and related trace elements, tested on natural minerals and applied to eastern Mediterranean sediments	*85*
Chapter 6	A novel selective extraction for barite from marine sediments	*113*
Chapter 7	Sequential extraction of aragonite, calcite and dolomite from eastern Mediterranean sediments	*129*
	References	*147*
	Inleiding en samenvatting	*163*
	Acknowledgements	*171*
	Curriculum Vitae	*173*

Chapter 1

Introduction and summary

1.1 Setting

The Mediterranean Sea is a semi-enclosed basin, bordered in the south by the African continent and in the north by Eurasia. The only connection to the world ocean is via the shallow Strait of Gibraltar. The Mediterranean Sea itself is divided into two main parts, the western and the eastern Mediterranean (Fig. 1.1), which are separated by the sill in the Strait of Sicily. At present, evaporation exceeds precipitation, which results in an anti-estuarine circulation; nutrient-depleted Atlantic surface water flows into the Mediterranean, and nutrient-enriched Mediterranean Intermediate Water flows out. Due to this export of nutrients, the present-day Mediterranean Sea can be considered a nutrient desert. Overall organic matter production is very low compared to the world ocean, and 85% of the primary production in the eastern Mediterranean flows into the microbial foodweb (Turley, 1997). Phytoplankton populations are dominated by picoplankton, with the bacterial biomass constituting about 50% of total algal biomass (Robarts et al., 1996). Presently, eastern Mediterranean sediments consist mainly of terrestrial and carbonate fractions, whereas organic matter and opal contents are very low.

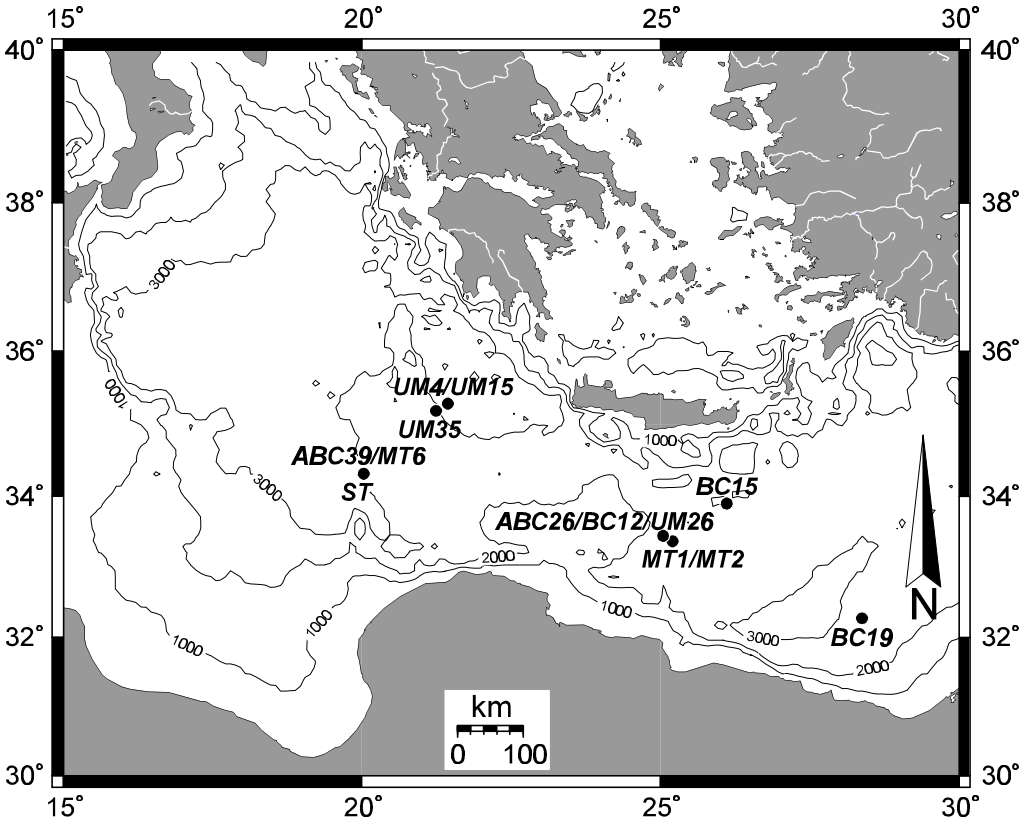

Figure 1.1 *Location of the sediment trap deployment (ST) and the boxcores of which results are discussed in this thesis.*

1.2 Sapropel formation

The 1948 Swedish Deep-Sea Expedition brought the first evidence for the existence of intervals with organic-rich sediments in the eastern Mediterranean (Kullenberg, 1952). In subsequent years, the cyclic occurrence of such organic-rich sediments within otherwise organic-poor intervals has been identified, in sediment cores (e.g. Cita et al., 1977; Kidd et al., 1978; Calvert, 1983; Pruysers et al., 1991; Van Santvoort et al., 1997; Nijenhuis et al., 1999) as well as in land sections (e.g. Sprovieri et al., 1986; De Visser et al., 1989; Van der Weijden et al., 1993; Van Os et al., 1994; Nijenhuis et al., 1996; Schenau et al., 1999). These organic-rich units, which can be dated back to the Miocene, have been named sapropels, for which Kidd et al. (1978) proposed the following definition: "discrete layers, greater than 1 cm in thickness, set in open marine sediment and containing greater than 2% organic carbon". However, this definition is rather restrictive, and for that reason Van Santvoort et al. (1996) proposed the following refinement: "discrete sediment layers with an organic carbon content that is significantly higher than that of the surrounding hemipelagic sediment and being deposited in an open marine environment". The cyclicity in eastern Mediterranean sediments has been related to variations in the eccentricity of the Earth's orbit and in the tilt (obliquity) and precession of the Earth's axis (e.g. Rossignol-Strick, 1983, 1985; Hilgen, 1991; Lourens, 1994; Hilgen et al., 1995). Sapropel formation is dominated by the precession cyclicity (~23 kyrs), with sapropel deposition occurring when Northern Hemisphere insolation is at its maximum caused by a minimum in the Earth's solar precession.

There is growing evidence that sapropels were formed during periods of wetter climatic conditions at times of the precession minimum (Rossignol-Strick et al., 1982; Rossignol-Strick, 1985; Kallel et al., 1997). These conditions caused enhanced river run-off and nutrient supply into the Mediterranean basin. It is, however, still a matter of debate what caused the high organic matter content of sapropels. The increased fresh water input may have resulted in the development of a low-salinity surface layer, which in turn reduced deep-water circulation. A stagnating water column may have led to anoxic bottom water conditions and a better preservation of organic matter (Olausson, 1961; Cita et al., 1977; Nolet and Corliss, 1990). Alternatively, it has been proposed that an increase in marine productivity rather than enhanced preservation of organic matter was the driving mechanism behind sapropel formation (Calvert, 1983; Calvert et al., 1992). Rohling and Gieskes (1989) combined both scenarios and argued that a distinct Deep Chlorophyll Maximum may have developed within the euphotic zone, thereby enhancing primary productivity.

1.3 Brine basins

In 1983, a deep basin filled with salt-saturated seawater was discovered in the eastern Mediterranean during the 1983 expedition of *R.V. Tyro* (De Lange and Ten Haven, 1983; Jongsma et al., 1983). A year later, another such basin was found by *R.V. Bannock* (Scientific staff of Cruise Bannock 1984-2, 1985). These brine basins, named after the ships that discovered them (Tyro Basin and Bannock Basin respectively), have persisting anoxic conditions due to the high density of the seawater in these basins, preventing ventilation. In

the Tyro Basin area, two formerly brine-filled basins, Kretheus and Poseidon Basins, were also discovered. In the mid-1990's, again three brine basins were found: Urania, Atalante and Discovery Basins (MEDRIFF Consortium, 1995).

These brine basins offer a unique opportunity to study contemporary oxic and anoxic sedimentation. The occurrence of perfectly preserved radiolarians and of sulphate reduction in anoxic brine sediments but not in contemporaneous oxic pelagic sediments in the eastern Mediterranean suggests that — assuming similar inputs to these two types of sediment — biogenic silica and reactive organic matter are preferentially preserved in these brine sediments (Björklund and De Ruiter, 1987; Troelstra, 1987; Aghib, 1996; Henneke et al., 1997).

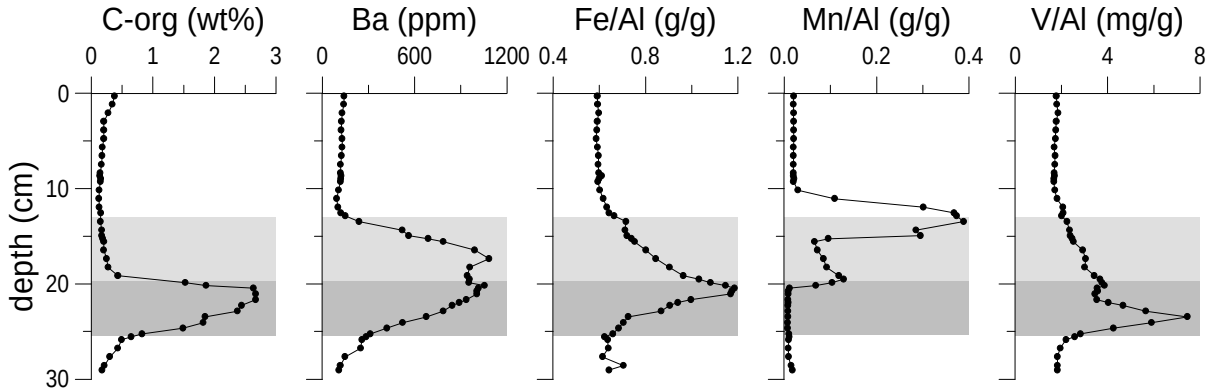

Figure 1.2 *Typical distributions of organic carbon, Ba, and the redox-sensitive elements Fe, Mn and V in Holocene eastern Mediterranean sediments. The metal contents are divided by Al to correct for carbonate dilution. The dark-grey area indicates the visible sapropel (its sediment is black-green in colour), the light-grey area the oxidised sapropel interval (its sediment is red-brown in colour). The shown results are from boxcore ABC26.*

1.4 Diagenesis of sapropel S1

After deposition sapropels undergo significant chemical alteration (diagenesis). It has been observed that organic matter profiles in Holocene sediments may vary significantly over the eastern Mediterranean basin, but that metal distributions are rather alike (e.g. Pruysers et al., 1991, 1993; Higgs et al., 1994; Thomson et al., 1995, 1999; Van Santvoort et al., 1996; see Fig. 1.2). These features resemble those found for organic-enriched turbidites in the Madeira Abyssal Plain (De Lange et al., 1989), which experienced diagenesis by a downward-moving oxidation front (e.g. Colley et al., 1984; Thomson et al., 1984, 1987; Wilson et al., 1985, 1986; Jarvis and Higgs, 1987). This has led to the hypothesis that sapropels, which are intercalated between organic-poor sediments, have been subject to a similar oxidation process, removing significant amounts of organic matter and other reduced species such as pyrite from the top of the sapropel and redistributing metal contents in the sediment column.

Most investigations have focussed on the most recent sapropel (S1), which was deposited in the Holocene. This sapropel contains the most fresh geochemical evidence of its

diagenesis and radiocarbon dating can be applied to it (e.g. Thomson et al., 1995, 1999). The "burn-down" of this sapropel has resulted in its partial or complete oxidation, leading to difficulties in the dating of the top of the sapropel. The time of deposition is now set between ~ 9000 and ~ 5000 years ago (Troelstra et al., 1991; Thomson et al., 1995; Mercone et al., 2000), where the top of the sapropel is set at the upper Mn enrichment (Fig. 1.2).

1.5 This thesis

In this thesis recent sediment fluxes to the pelagic eastern Mediterranean are studied, as well as the geochemistry of Holocene sediments, including sapropel S1, in normal and former brine settings in the eastern Mediterranean. Figure 1.1 shows the locations of the sediment trap deployment and the studied boxcores.

Chapters 2 and 3 deal with recent sediment fluxes to the pelagic eastern Mediterranean. These were measured in a sediment trap deployment from November 1991 to August 1994 at 3000 m water depth. Chapter 2 focusses on total mass fluxes and the fluxes of the most important terrigenous and carbonate-related elements (Al, Ca, Mg and Sr) and ^{230}Th, whereas Chapter 3 is concerned with biogenic fluxes, of which those of coccolithophores and calcareous dinoflagellates (thoracosphaerids) are the most important. A strong seasonality is observed for almost all fluxes, with the highest ones during early spring in 1992 and 1993, and during late-spring/early-summer in 1994. The only exception is the flux of whole coccospheres, which is at its maximum in winter. Comparison of historic annual satellite-derived chlorophyll records (Coastal Zone Colour Scanner) with the trap flux time series indicates a lag of 4 to 6 months between maximum primary production in the surface ocean and maximum flux recorded by the trap. Only the flux of coccospheres to the trap is at a maximum of about 1 month after maximum pigment concentrations in surface waters, a value commonly found in other areas. The trapping efficiency of the sediment trap, as calculated from the intercepted ^{230}Th flux, is only 23%. Compared to nearby uppermost sediments, the Al flux is similarly four times lower. Carbonate fluxes calculated from Ca are even lower relative to the Ca accumulation at the top of the sediment. The annual flux of coccolithophores is much lower than published data from most other oceanographic settings, even when corrected for the trap efficiency, emphasising the low primary productivity in the eastern Mediterranean. Carbonate dissolution is only a minor process at the trap depth and at the sea floor, as shown by the presence of fragile coccolithophore species. The relatively lower total carbonate flux compared to the lithogenic flux — the latter indicated by the Al flux — is partly due to the very low abundance of large (>32 μm) foraminifera and pteropods in the trap material compared to the surface sediment. Quantification of the lithogenic flux to the trap indicates that Saharan dust is likely to be the major contributor to the trap mass flux. Coccolithophores are the main constituents of the biogenic carbonate flux in the eastern Mediterranean, followed by thoracosphaerids. *Emiliania huxleyi* and *Florisphaera profunda* are dominant coccolithophore species in both sediment trap samples and surface sediments.

Chapters 4 to 7 focus on solid metal contents and speciation in normal and in former brine sediments of the eastern Mediterranean, with the emphasis on the diagenesis of sapropel

S1 sediments, or lack thereof, and the resulting relationships between metals and organic matter.

Chapter 4 deals with the recent history of sediments from the previously anoxic brine-filled Poseidon Basin. The geochemistry of these sediments is compared to those deposited in a normal eastern Mediterranean environment. On the basis of AMS-radiocarbon ages and of foraminiferal and geochemical zonations, three main sedimentary intervals can be distinguished in the boxcore. From the base of the core upwards these are: (1) Organic-rich sediment redeposited from within the brine and contemporaneous with sapropel S1 in normal sediments; (2) Sediment containing a cold foraminifera fauna redeposited from above the brine into the basin while the brine was still present; (3) Oxic pelagic sediment accumulated since the reoxygenation of Poseidon Basin which occurred about 1800 yrs BP. Near the base of the latter unit, a Mn oxide peak has formed, marking the present boundary between oxic and suboxic environments. A progressive downward oxidation front, which is usually found in normal sapropel S1 sediments, has never formed in Poseidon Basin sediments. This has resulted in the preservation of the relationship between organic carbon and organic-related trace elements e.g. selenium in the organic-rich sediments of Poseidon Basin, whereas such a relationship has been obliterated in normal sapropel S1 sediments. The high opal content of Poseidon Basin organic-rich sediments shows that biogenic opal is much better preserved than in normal sapropel S1 sediments. The carbonate content of the brine sediments is also slightly higher than that of contemporaneous nearby normal sediments, suggesting a somewhat better preservation of carbonates in the brine basin.

In Chapter 5, the findings in Chapter 4 are explored in more detail using a detailed sequential extraction scheme (MESEX) applied to Poseidon Basin as well as normal eastern Mediterranean Holocene sediments (see Fig. 1.2 for typical metal distributions in these normal sediments). The Mn(II)/Mn(III,IV) redox boundary in both types of sediment is clearly distinguished, with carbonate-related Mn being enriched below the boundary, and Mn oxides only being present above it. A clear Fe(II)/Fe(III) redox boundary is present in the normal eastern Mediterranean sediments and is located just below the Mn(II)/Mn(III,IV) redox boundary. The Fe(II)/Fe(III) boundary closely coincides with the visible boundary between the lower unoxidised and the upper oxidised part of the initial sapropel S1 interval. Pyrite is only present in the unoxidised interval, whereas oxides are abundant above it. The spacing between the Mn(II)/Mn(III,IV) and Fe(II)/Fe(III) redox boundaries in the sediments of the former brine basin confirms that no active oxidation has taken place into the organic-rich unit in these sediments, resulting in the preservation of trace metal to organic carbon relationships. This is further substantiated by the profiles of vanadium, another redox-sensitive metal. In normal eastern Mediterranean sediments, where a strong diagenetic V peak has been formed below the oxidation front, MESEX results suggest that this mobilised V is probably sorbed as vanadyl to organic matter, but the correlation of this excess V with organic matter has been obliterated. In the former brine sediments, V has not been mobilised as shown by the close correlation of excess V and organic matter. MESEX also indicates, by comparing the results of two sediment cores very close to each other, that the fraction of Mn and Co residing with reduced mineral phases is mainly associated with pyrite, whereas Ni, Cu and Zn

in this fraction are more related to organic matter. In the remaining, visible sapropel of normal eastern Mediterranean sediments, these latter elements still have the original relationships towards organic carbon, as shown by the comparison with the former brine sediments. On the basis of MESEX, slight variations have also been detected in the terrigenous fraction, i.e. aluminosilicates. $(Fe/Al)_{clay}$ and $(Mg/Al)_{clay}$ ratios are somewhat higher in sapropelic than in non-sapropelic sediments, which suggests an increased chlorite content in the former. Several trace element to Al ratios behave similarly. These results suggest that sources of terrigenous material have been different during sapropel times compared to the period immediately after it. On the other hand, the K/Al_{clay} ratio remains fairly constant with depth in the sediment, suggesting that no major changes may have occurred in the relative contribution of illite to the clay mineral fraction.

Chapter 6 introduces a novel sequential extraction scheme (BASEX) that separates barite successfully from other Ba containing mineral phases. Application of BASEX to Poseidon Basin as well as normal eastern Mediterranean Holocene sediments reveals that most of the high Ba concentrations in sapropel S1 (Fig. 1.2) consists of barite. The relationship of barite-Ba (= biogenic Ba) with organic carbon in unoxidised sapropelic sediments appears to be independent of water depth, organic matter fluxes and sedimentation rates for cores ranging from 2150 – 3300 m water depth. This indicates that organic carbon remineralisation has been virtually absent in the water column deeper than 2150 m. This might be caused by the suboxic to anoxic conditions present in the deep eastern Mediterranean basin during the formation of sapropel S1. Although our C_{org}/Ba_{bio} ratios fall in the same range as other published values, we think that, because we have directly measured biogenic Ba, our data set is more consistent than other ones which are based on estimated biogenic Ba contents. Because of the similar relationship between barite and organic carbon throughout the eastern Mediterranean, the high barite content of the oxidised sapropel zone can be used to quantify the original organic carbon content of the sediment.

In Chapter 7 a sequential extraction method (CASEX) is presented that can separate different carbonate phases, such as aragonite, calcite and especially dolomite. In addition, Mg/Ca and Sr/Ca ratios for bulk $CaCO_3$ can be determined without the influence of dolomite. CASEX was applied to Poseidon Basin as well as normal eastern Mediterranean Holocene sediments. The sedimentary dolomite content and the Mg/Ca ratio of $CaCO_3$ are lower during the deposition of sapropel S1 than they are during the period immediately thereafter. These observations correspond to the formation of the sapropel during a relatively humid period with relatively low dust deposition rates and a relatively high river run-off. In this respect the dolomite content indicates the relative contribution of dust to the terrigenous fraction. The lower Mg/Ca ratios in sapropelic sediments are mainly due to lower surface water salinities. Differences in the species composition of flora and fauna may also contribute to a lower ratio. In contrast, most of the change in the Sr/Ca ratio must be caused by a change in ecology.

Chapter 2

Recent terrestrial and carbonate fluxes in the pelagic eastern Mediterranean; a comparison between sediment trap and surface sediment*

Abstract – A sediment trap mooring has been deployed in the central eastern Mediterranean from November 1991 to August 1994. At 3000 m water depth, total mass, Al, Ca, Mg, Sr and ^{230}Th fluxes recovered by the sediment trap are highly seasonal, with highest fluxes during early spring in 1992 and 1993, and during late-spring/early-summer in 1994. Comparison of historic annual satellite-derived chlorophyll records with the trap flux time series indicates a lag of 4 to 6 months between maximum primary production in the surface ocean and maximum flux recorded by the trap. Only the flux of coccospheres to the trap is at a maximum ~ 1 month after maximum pigment concentrations in surface waters, a value commonly found in other areas. Quantification of the inorganic (lithogenic) flux to the trap indicates that Saharan dust is likely to be the major contributor to the trap mass flux. The trapping efficiency of the sediment trap, as calculated from the intercepted ^{230}Th flux, is only 23 %, and the trap Al-flux is similarly four times lower than Al fluxes measured in nearby uppermost sediments. Compared with surface sediments, the trap-intercepted carbonate fluxes are even nine times lower than the corresponding lithogenic fluxes. This is partly due to the very low abundance of large (>32 μm) foraminifera and pteropods found in the trap material compared to the surface sediment. We speculate that the period of our sediment trap deployment has been insufficiently long to recover episodical large fluxes, such as may be triggered by variations in the North Atlantic Oscillation.

2.1 Introduction

The eastern Mediterranean Sea is an area that is particularly sensitive to climate change. One expression of this is the recurrent presence of numerous organic carbon rich layers (sapropels; Kidd et al., 1978) in marine cores as well as in marine sections on land, dating back as far as the Miocene (e.g. Cita et al., 1977; Thunell et al., 1977; Kidd et al., 1978; Sigl et al., 1978; Calvert, 1983; Pruysers et al., 1991; Rohling, 1994; Nijenhuis et al., 1996). The regular occurrence of sapropels has been shown to be related to Milankovitch cycles (e.g. Rossignol-Strick, 1985; Hilgen, 1991; Lourens, 1994). Sapropels are thought to represent periods of high primary productivity and of wet climate (see review by Rohling, 1994) related to maximum Northern Hemisphere insolation caused by a minimum in the Earth's solar precession. At present, during a period of dry climate and close to a precession maximum, the eastern Mediterranean basin is an oligotrophic water body with low primary production. Furthermore, the Saharan desert is an important contributor to the sedimentation

* This chapter has been published as: A. Rutten, G.J. de Lange, P. Ziveri, J. Thomson, P.J.M. van Santvoort, S. Colley and C. Corselli, 2000, *Palaeogeography, Palaeoclimatology, Palaeoecology*, 158, 197–213.

during present time (e.g. Guerzoni et al., 1997, and references therein) due to the prevailing dry climate. However, its contribution is known to strongly decrease during a wet climatic period (e.g. Dominik and Stoffers, 1978). Such alternation leads to variations in the amount and origin of terrestrial matter input into the eastern Mediterranean, which is related to precession cycles.

The overall sedimentation rate in the deep eastern Mediterranean is in the order of 2 – 4 cm kyr^{-1} (e.g. Thomson et al., 1995; Van Santvoort et al., 1996). Bioturbation causes a mixed depth of 1–2 cm (Thomson et al., 1995), thereby obscuring changes in the sediment flux on yearly and decadal time scales in the geological record. This means that the relation between primary production, climate and seasonal fluxes to the sediment cannot be assessed directly from the sediment record. This relation needs to be better understood so as to obtain insight in the diversity of processes that govern the eastern Mediterranean ecosystem. In addition, this relation is needed for the development of better models for the prediction of the response of the Mediterranean ecosystem to changing climate. One approach to assess seasonal mass fluxes is by using time-series sediment traps.

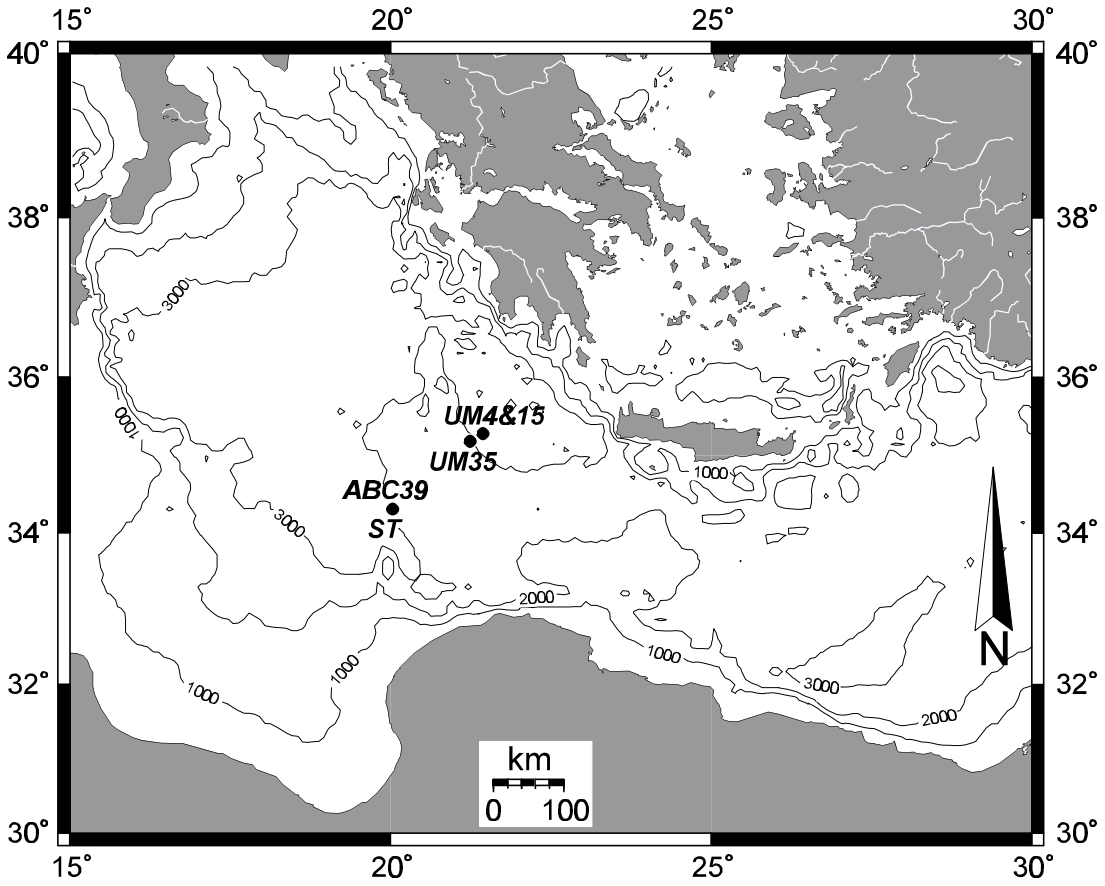

Figure 2.1 *Location of the sediment trap (ST) and the boxcores (UM4, UM15, UM35 and ABC39) in the eastern Mediterranean.*

A sediment trap deployment was undertaken from November 1991 to August 1994 in the central eastern Mediterranean. In this chapter, we report chemical data on terrestrial and carbonate fluxes, and discuss its relevance in view of seasonal changes. Furthermore, these results will be compared to those estimated from the uppermost sediment of boxcores from nearby sites.

2.2 Materials and methods

2.2.1 Material

2.2.1.1 Sediment trap

Two 1 m^2 sediment traps (Technicap PPS5/2) were deployed in a time series in the southwestern Bannock Basin (34˚ 18' N, 20˚ 01' E; Fig. 2.1). This basin is filled with a brine below 3150 m water depth (Fig. 2.2). The upper trap was located at 3000 meters water depth, well above the sea-water / brine interface in oxygenated conditions, whereas the lower trap at 3500 meters water depth was situated in anoxic brine conditions ~ 20 m above the basin floor (Fig. 2.2). Four time series deployments of 24 samples each were collected in both traps over a nearly continuous period of 34 months (Table 2.1). No preservatives were used in the sample bottles. However, this will not have altered our results significantly (Peterson et al., 1993; Khripounoff and Crassous, 1994). In this study we focus on the upper, oxic trap.

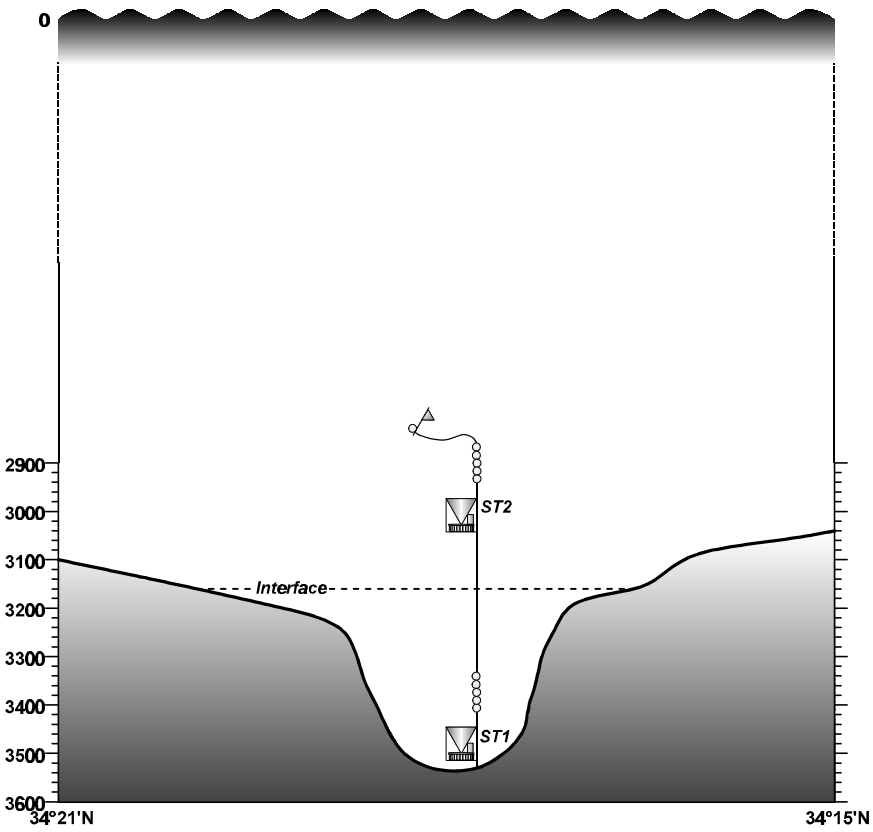

Figure 2.2 *Sediment trap mooring in Bannock Basin.*

2.2.1.2 Boxcores

The upper few centimetres of three eastern Mediterranean boxcores, from different water depths and located near the sediment trap, were analysed (Fig. 2.1; Table 2.2). The tops of UM4, UM15 and UM35 contained an oxic, light-brown ooze, which overlay a red-brown, oxidised zone. A double manganese peak, indicative of a burn-down front (Thomson et al., 1995; Van Santvoort et al., 1996; Chapters 1, 4, 5), was found in all three cores. Below the oxidised zone, black-green sapropel S1 sediments were found. All boxcores are rich in pteropods and foraminifera throughout. Cores UM15 and UM35 are described in more detail in Van Santvoort et al. (1996). For the analysis of individual pteropods, the top of boxcore ABC39, containing oxic sediment and located close to the sediment trap site, was available.

Table 2.1 *The periods of deployment of the sediment traps (3000 and 3500 m depth) in Bannock Basin (water depth 3520 m). Both sediment traps have the same sampling intervals.*

Mooring	Start date	End date	Deployment (days)	Sample interval (days)
ST2	10 Nov 1991	10 May 1992	182.5	5–10
MT4O	1 Jun 1992	19 Feb 1993	263	9–14
MU-B	1 Apr 1993	16 Sep 1993	168	7
UM1STO	20 Oct 1993	29 Aug 1994	313	10–20

2.2.2 Methods

2.2.2.1 Sediment traps

Upon retrieval of the sediment trap, the samples were divided on board into eight aliquots using a pneumatic splitter (Tennant and Baker, 1992). Seven aliquots were filtered using a gas pressure system; four of which were filtered on 0.2 μm cellulose acetate filters, three on 0.8 μm glass fiber filters. The remaining aliquot was either filtered on a cellulose acetate filter or maintained in solution (the last series (UM1STO; Table 2.1) only). All samples were stored at 4°C in air-tight containers until analysis.

For total elemental analysis one cellulose acetate filter was dried at 40˚C and weighed. Subsequently, the filter was sealed in a Teflon bomb with 2.5 ml HF and 2.5 ml $HClO_4/HNO_3$ and dissolved by oven heating at 90˚C for 5 hours. The solution was evaporated to dryness and redissolved in 7.5 ml 1 M HCl, and analysed with an inductively coupled plasma atomic emission spectrometer (ICP-AES; Perkin Elmer Optima 3000) for Al, Ca, Mg and Sr. Filter blanks as well as a calibration series of an in-house standard were simultaneously processed and used to calculate separate calibration lines for each element. In Appendix 2-A, the procedure is given in detail.

Table 2.2 *Location of the boxcores. ABC39 was recovered during the 1987 cruise of R.V. Tyro, the other three during the 1994 cruise of R.V. Urania.*

Boxcore code	Water depth (m)	Latitude	Longitude	Environment
ABC39	2800	34˚19.3' N	20˚01.6' E	oxic, pelagic
UM4	3309	35˚17.30' N	21˚24.85' E	oxic, pelagic
UM15	3308	35˚17.39' N	21˚24.82' E	oxic, pelagic
UM35	2672	35˚11.04' N	21˚12.54' E	oxic, pelagic

Total mass was determined in two ways, namely from: 1) The difference between the total weight of the filter after drying and the average weight of the filter alone; 2) The total of all elements measured with ICP transferred into oxides (except $CaCO_3$ and $SrCO_3$). Both methods give similar results.

Supernatant water was collected immediately after opening the sampling bottles of the sediment trap and stored at 4°C in polyethylene flasks for further analysis. The water samples were diluted eight times for Ca analysis by ICP-AES (Perkin Elmer Optima 3000). The quality of the analyses was monitored by the inclusion of sea water standards.

Current meter (NBA) data were only available for the third (MU-B; Table 2.1) series.

2.2.2.2 Thorium-230 and trap efficiency

Radionuclides were measured on a separate cellulose acetate filter. Due to the small mass of many samples and the low overall levels of radioactivity, a combination of samples was made, such that 39 samples each covering a similar time period were analysed for the natural alpha-emitting uranium and thorium isotopes and ^{210}Pb (Colley et al., 1995). Even with the combination of samples, these were demanding low-level radiochemical measurements, and counting times were typically 7 days and frequently longer.

Recent applications of ^{230}Th data generally involve the assumption that this natural radionuclide provides the best approximation to a constant flux tracer from the ocean to the sediments (Bacon, 1984). ^{230}Th is continuously produced from the ^{234}U present in the sea water, and its short residence time in the water column gives rise to a predictable $(^{230}Th_{excess})_0$ flux to the underlying sediments which is a linear function of water depth:

$$\text{Flux } (^{230}Th_{excess})_0 = \beta \times z = 0.00263 \times z \ \ (\text{dpm cm}^{-2}\ \text{kyr}^{-1}) \qquad (1)$$

where β is the production rate of ^{230}Th from the constant ^{234}U concentration in sea water (Chen et al., 1986) and z is the water column depth in m. For sediment traps, the formula is best used over a long time period (at least a year; Bacon et al., 1985) because of the usual good correlation between the total mass flux and the fluxes of radionuclides in sediment traps (e.g. Fisher et al., 1988; Moore and Dymond, 1988).

2.2.2.3 Boxcores

Dried boxcore subsamples (250 mg) were sealed in Teflon bombs with a mixture of HF, HNO_3, and $HClO_4$, and oven digested at 90°C. The solution was subsequently evaporated to dryness. Final solutions were made in 1 M HCl and analysed with ICP-AES (Perkin Elmer Optima 3000) for Al, Ca, Mg, and Sr. The quality of the analyses was monitored by the inclusion of in-house and international standards and precisions were always better than 2 %.

The average sedimentation rates for the upper, oxic, interval of boxcores UM4, UM15 and UM35 were calculated by extrapolation from a known time-marker, i.e. the upper Mn peak (average age of 5 kyr; Thomson et al., 1995). Mean porosity was taken into account in each boxcore for the calculation of mass accumulation rates from the sedimentation rate. The following equation was, therefore, used:

$$MAR = DBD \times SR \quad (2)$$

where MAR is the mass accumulation rate (mg cm^{-2} yr^{-1}), DBD the dry bulk density (g cm^{-3}) and SR the sedimentation rate (cm kyr^{-1}). The dry bulk density was calculated as follows:

$$DBD = (1 - por) \times \rho \quad (3)$$

where por is the mean porosity of the upper, oxic interval and ρ is 2.5 g cm^{-3}.

For the average composition of each boxcore top, the samples from the upper 1 to 2 cm, i.e. the surface mixed layer (Thomson et al., 1995), were averaged. Part of the top two samples of UM4 were wet-sieved to discriminate fractions smaller and larger than 32 μm. The separate size fractions were analysed the same way as the sediment samples above.

Clean pteropods from the top of boxcore ABC39 were handpicked and divided in 10 – 15 mg samples (4 samples, 3 – 4 pteropods per sample). Each sample was dissolved in 1 M HNO_3. The solutions were analysed with ICP-AES (Perkin Elmer Optima 3000) for Ca and Sr. A blank was included, and ICP analysis was monitored by the inclusion of standards.

2.3 Results

2.3.1 Sediment trap fluxes

The observed particle fluxes for the sediment trap deployments are highly seasonal, varying between 0.28 – 446 mg m^{-2} day^{-1} (Fig. 2.3). Marked peaks occur in April 1992, June – July 1992, April – June 1993, and June – August 1994, and have a magnitude between 42 – 80 mg m^{-2} day^{-1}. Small maxima are present in the period between November 1993 and April 1994. The three samples collected between April 20 and May 5 1992 are unusual in that the sampling bottles were all empty, whereas the next sample collected from 5 – 10 May 1992 recorded a large flux of 446 mg m^{-2} day^{-1}. These four samples are unlikely to be affected by a technical failure, as the sediment trap's performance registration did not indicate a deviation. In addition, a similar anomalously high flux was recorded in the anoxic trap at the same time, but here the three previous samples do contain sediment. Consequently, this high flux appears to be genuine, and has been included in all calculations.

Individual fluxes of Al, Ca, Mg and Sr show the same trend as the total mass flux

(Fig. 2.3). However, there are subtle differences between biogenic elements such as Ca and Sr on the one hand and terrestrial elements like Al and Mg on the other. In particular, the 1993 flux maximum of Ca and Sr is relatively high compared to those in 1992 and 1994, whereas it is relatively low for Al and Mg.

2.3.2 Thorium-230

The flux of ^{230}Th to the sediment trap is highly seasonal (Fig. 2.3) and correlates linearly with the total mass flux (Fig. 2.4; $r^2 = 0.94$). The slope of the regression line indicates an observed average ^{230}Th concentration of 3.13 dpm/g in the sediment trap samples. The average measured mass flux over the complete deployment of 34 months is 15.9 mg m^{-2} day^{-1} (0.58 g cm^{-2} kyr^{-1}), giving a mean measured ^{230}Th flux of 1.82 dpm cm^{-2} kyr^{-1}. The ^{230}Th flux calculated for a trap at 3000 m is 7.89 dpm cm^{-2} kyr^{-1} (using equation (1)). The average sediment trap efficiency is, therefore, 23 %.

2.3.3 Composition of sediment trap samples

The average carbonate content in the sediment trap samples, calculated from total Ca, is 31.5 wt%. Biogenic carbonate is the main carbonate contributor and mostly consists of coccolithophorids, calcareous dinoflagellates and juvenile foraminifers (Ziveri et al., 1995; Chapter 3). Pteropods and large foraminifers, i.e. the coarse fraction, have a notably low abundance. The major component of the mass flux in the sediment trap is lithogenic material (60.4 wt%). This amount was estimated in two ways, namely from: 1) The constant ratio of lithogenic material to Al (Terr/Al = 0.0885, calculated from the anoxic trap samples); 2) The difference between 'total mass' and the biogenic components ($CaCO_3$ and organic matter). Both estimates give similar results.

2.3.4 Boxcores

Average total mass fluxes calculated for oxic boxcore tops (UM4, UM15 and UM35) correspond to 85 – 115 mg m^{-2} day^{-1} (Table 2.3). Fluxes of Al and Ca vary between 3.56 – 5.40 and 17.7 – 23.4 mg m^{-2} day^{-1} respectively. The Ca content, mainly from $CaCO_3$, is around 20 wt%, resulting in a carbonate content of ~ 50 wt%. Aluminium concentrations are 4.2 – 4.7 wt% and are indicative of the lithogenic component.

The size fraction analysis of the topmost sample in oxic boxcore UM4 (0 – 0.5 cm) reveals distinctively different compositions for the two size classes (Table 2.4). The >32 μm fraction contains a high amount of Ca (~ 31 wt%), low Al (~ 2 wt%) and a low Sr/Ca ratio (~ 3.2 mg/g), whereas the <32 μm fraction is characterised by a Ca content of ~ 15 wt%, high Al (~ 5.4 wt%) and high Sr/Ca ratios (~ 5.5 mg/g). The sample immediately below the topmost sample (0.5 – 1 cm) yielded similar results. The individual analysis of the Sr/Ca ratio of eastern Mediterranean pteropods yields a ratio of 3.60 ± 0.03 mg/g.

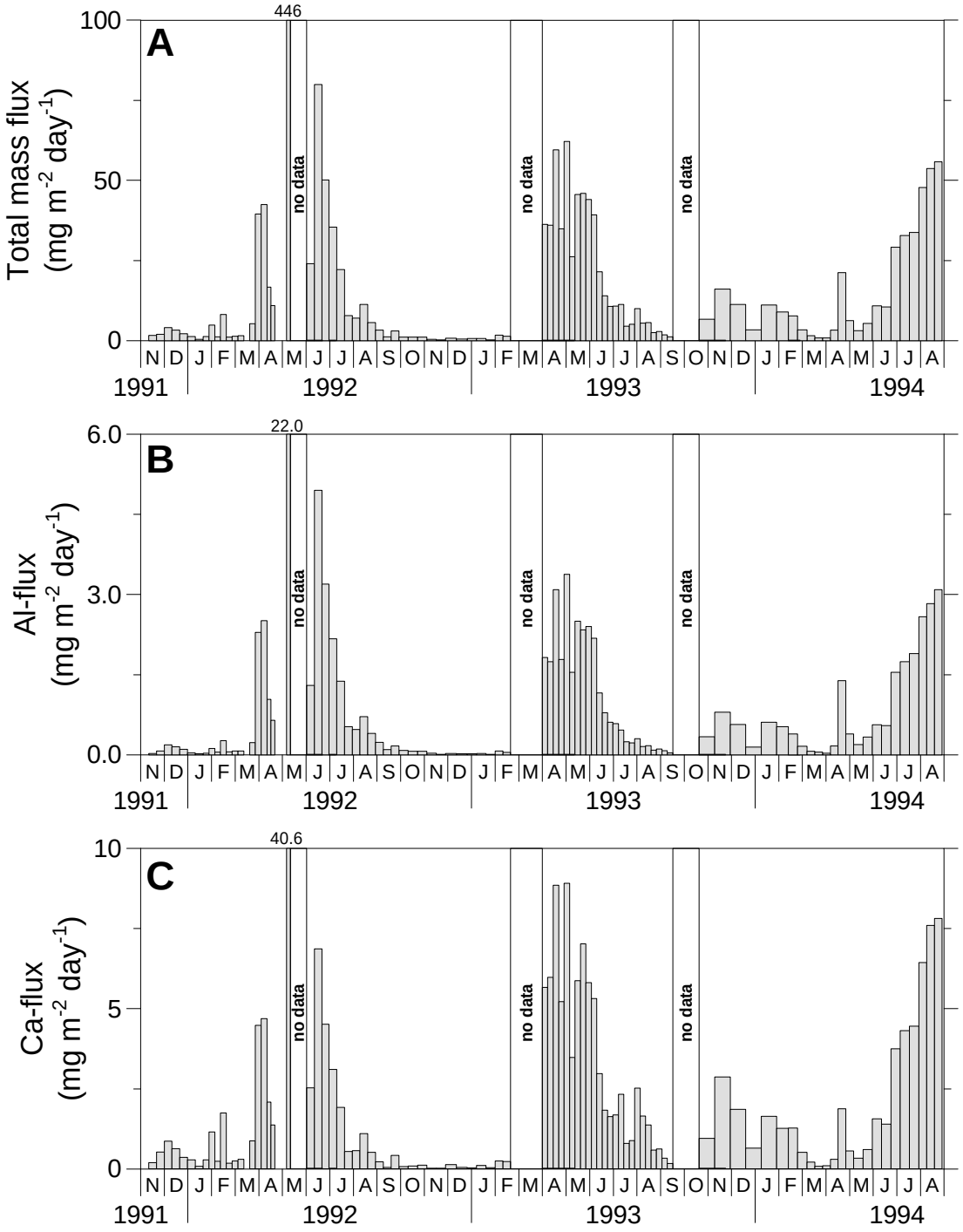

Figure 2.3 *Fluxes intercepted during the deployment of the sediment trap in Bannock Basin: A) Total mass flux; B) Al-flux; C) Ca-flux; D) Mg-flux; E) Sr-flux; F) ^{230}Th-flux (including 2σ error bars).*

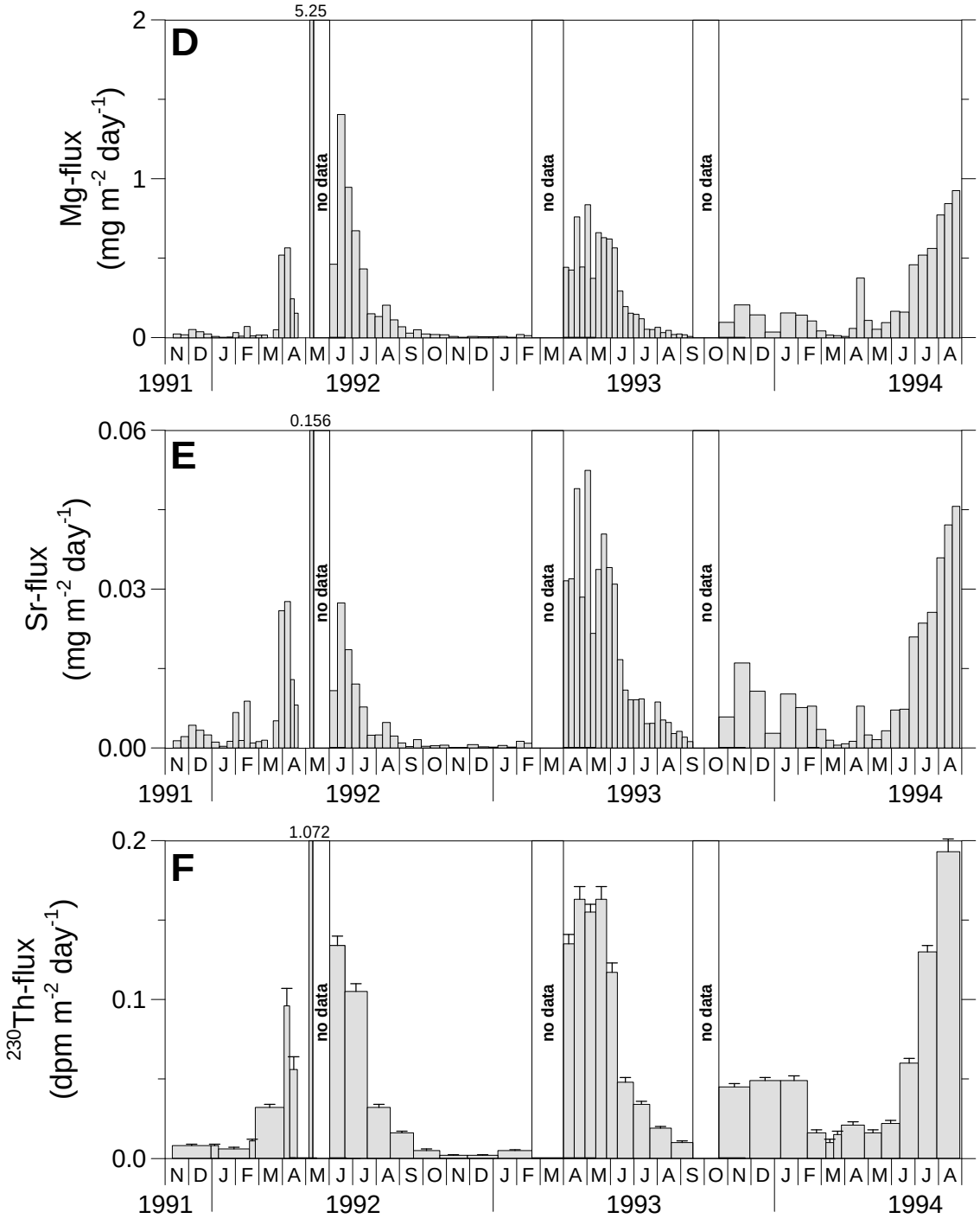

Figure 2.3 (continued)

2.4. Discussion

2.4.1 Seasonal variations recovered in the sediment trap samples

A profound seasonality is recorded in the sediment trap samples recovered between November 1991 and August 1994 (Fig. 2.3). Maximum fluxes occur between April and July in 1992 and 1993, and between June and August (end of the recording period) in 1994. The timing of the flux peaks, therefore, differs per year, as do the flux maxima. The major contributors to the mass flux out of the photic zone appear to be lithogenic material and carbonates (Table 2.5), the latter indicative of primary production, although some carbonate may have a terrestrial origin through the transport of Saharan dust (e.g. Chester et al., 1977; Correggiari et al., 1989). Organic matter and biogenic opal comprise relatively minor fractions. We will now compare the fluxes found in the sediment trap samples with parameters obtained by remote sensing satellite, such as chlorophyll concentrations and desert dust mass.

Table 2.3 *Average fluxes and composition of the sediment trap and top sediment samples. The fluxes in the trap have not been corrected for trap efficiency.*

	Average flux					**Average composition**				
	Al	Ca	Mg	Sr	Tot.[a]	Al	Ca	Mg	Sr	Sr/Ca
	(mg m^{-2} day^{-1})					(wt%)	(wt%)	(wt%)	(ppm)	(mg/g)
Trap	0.85	2.0	0.23	0.010	15.9	5.37	12.6	1.45	651	5.17
UM4	5.12	21.4	1.73	0.101	109.7	4.67	19.5	1.58	919	4.71
UM15	5.40	23.4	1.98	0.107	114.7	4.71	20.4	1.72	932	4.57
UM35	3.56	17.7	1.41	0.077	85.5	4.17	20.7	1.65	905	4.37

[a] *Tot. = total mass flux.*

Historic satellite-derived chlorophyll data from the Coastal Zone Colour Scanner are only available for the period 1979 – 1985. Data for each month have been averaged for that time period to give the average annual trend (Fig. 2.5). The original chlorophyll data (not shown) indicate that maximum primary productivity occurs, without exception, from December to March, with maximum concentrations in January – February. Although a strong inter-annual variability occurs in the size of the pigment concentrations (indicated by the gray area in Fig. 2.5), the position of the maxima, i.e. mostly January – February, remains the same. Because of this relatively constant behaviour in seasonality of the chlorophyll concentrations, it is justified to compare the seasonality recorded in our sediment trap with the only available, but non-contemporary chlorophyll data. When the timing of the flux

maxima in the sediment trap is compared to that of the pigment data, an average time-lag of 4 to 6 months is apparent. Such a lag is at variance with the sinking rate of particles through the water column usually observed, namely about 100 m day^{-1} (e.g. Neuer et al., 1997, and references therein), which would result in an expected lag of about 30 days. A possible indicator for relatively high primary production is the occurrence of high coccosphere fluxes. A coccosphere represents the complete calcite test of coccolithophores, pelagic unicellular algae that secrete calcite plates (coccoliths). Coccolithophores are the most important primary producers that also manufacture a skeleton in the present-day eastern Mediterranean (Knappertsbusch, 1993; Ziveri et al., 1995; Chapter 3). Maximum fluxes of coccospheres were recorded mostly from January to April (Chapter 3), indicating a time-lag of about 1 month between maximum primary production in the photic zone and its interception at 3000 m water depth. Consequently, the flux of coccospheres appears to be directly linked to the associated surface production. However, the major flux of Ca and individual coccoliths, the latter being three or more orders of magnitude higher than that of coccospheres, occurs at the same time as the main flux of the lithogenic component, i.e. 4 to 6 months after the peak in surface water productivity. The major flux of biogenic particles from the photic zone to the deep water is, therefore, not directly related to primary production.

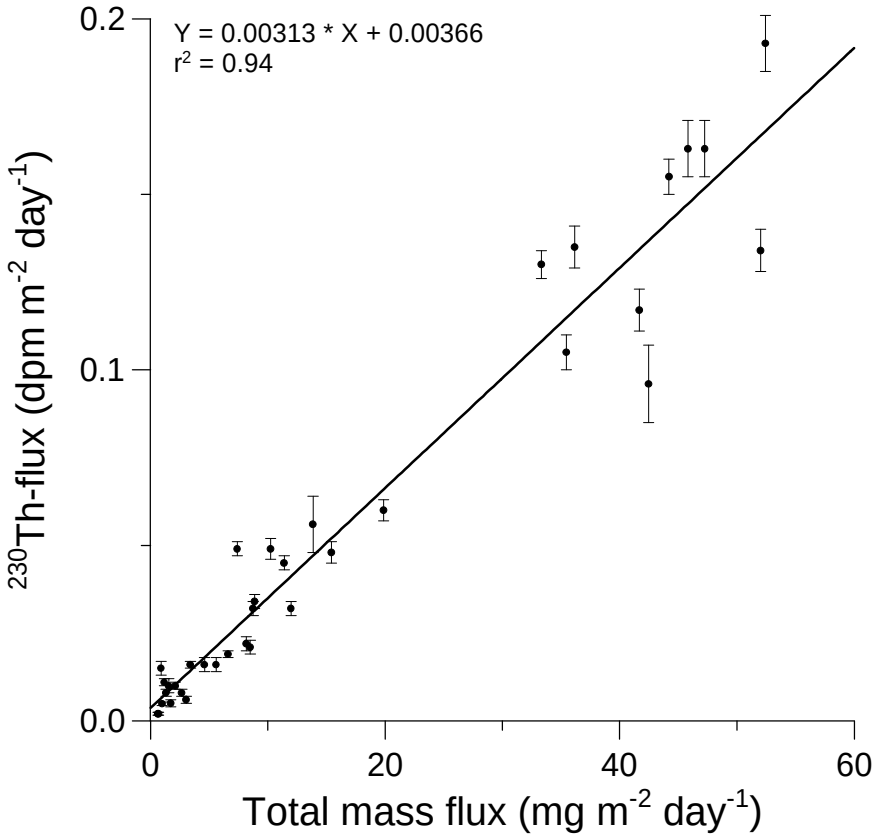

Figure 2.4 *Total mass flux vs. ^{230}Th flux during the sediment trap deployment in Bannock Basin. The vertical error bars designate the error due to counting statistics. The sample collected between 5–10 May 1992 is not shown.*

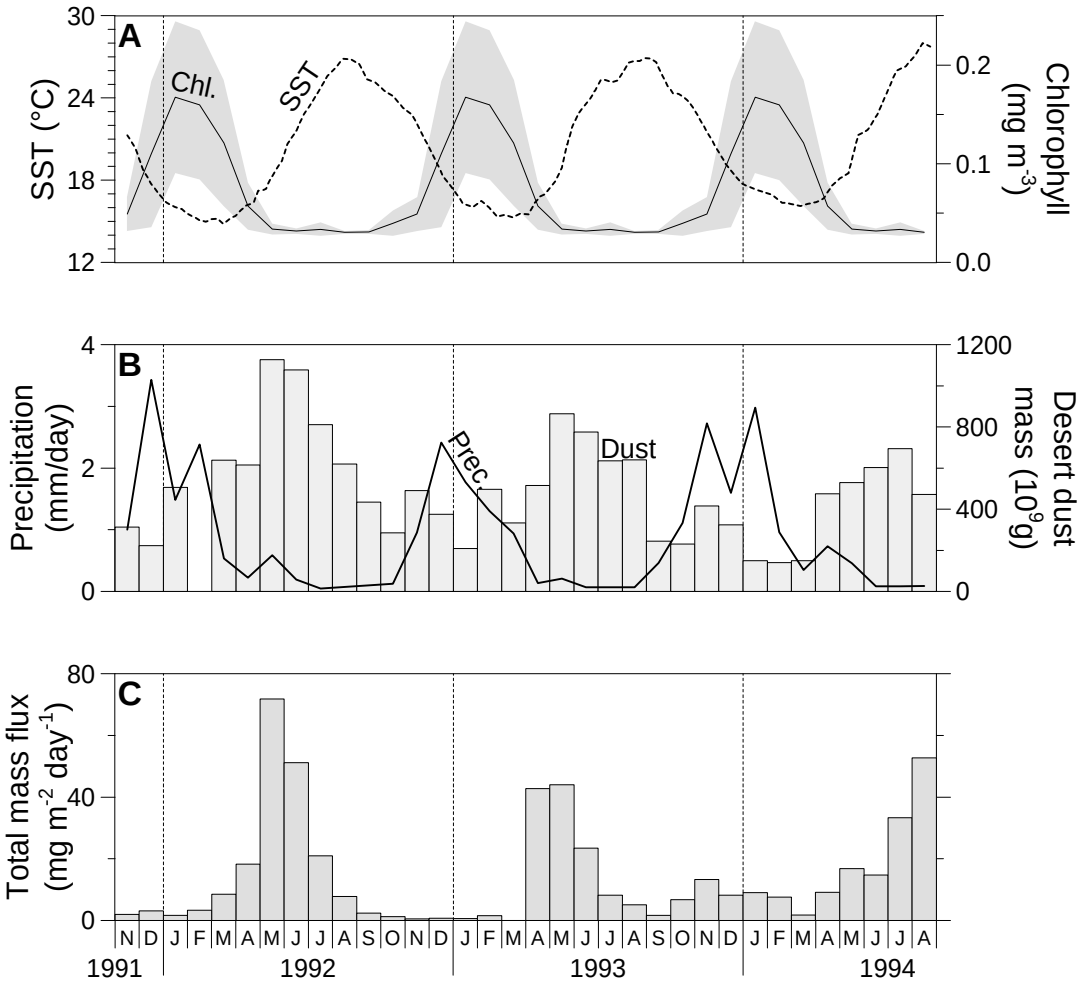

Figure 2.5 *Satellite data for the sediment trap location and the monthly averaged total mass flux intercepted by the sediment trap: A) Chlorophyll concentrations (solid line) and sea surface temperature (dashed line). Chlorophyll data were averaged from 1979–1985 monthly CZCS data, with the gray area indicating the 1σ standard deviation for each month. SST data are actual satellite observations made during the deployment period; B) Precipitation and desert dust mass. These are also actual satellite observations made during the deployment period. The dust data were redrawn after Dulac et al. (1996); C) Monthly averaged total mass flux intercepted by the sediment trap. No data were available for March 1993 (see Table 2.1).*

Dulac et al. (1996) have derived the monthly desert dust mass above the Mediterranean Sea. Their data indicate that dust concentrations in the atmosphere are high all year long, and at a maximum between May and August (Fig. 2.5). Actual dust deposition is, however, affected by precipitation (Molinaroli et al., 1993), which is high from November to March (Fig. 2.5). Unfortunately, no data are available on actual dust deposition rates in the sediment trap area. Molinaroli et al. (1993) have calculated the dust input into the central Mediterranean (near Sardinia) to be between 0.75 – 1.0 mg cm^{-2} yr^{-1}, which has been

corroborated by Guerzoni et al. (1997), who have reported the dust input into the western and eastern Mediterranean Sea to be 1 mg cm^{-2} yr^{-1} and 2 mg cm^{-2} yr^{-1} respectively. When we take the average lithogenic composition of the sediment trap samples (60.4 wt%), the mean total flux of 15.9 mg m^{-2} day^{-1} (Table 2.3) and account for the average trap efficiency of 23 %, then the total detrital flux derived from the sediment trap data is calculated as 1.52 mg cm^{-2} yr^{-1}. This flux falls in the range reported by Guerzoni et al. (1997), suggesting that Saharan dust is the most important contributor to the lithogenic material in the sediment trap. We have neglected a possible contribution of rivers to the lithogenic material. A way to estimate the relative contributions of riverine and dust lithogenic material is by making use of the Ti/Al ratio. For rivers, this ratio is reported to be between 48.2 and 59.6 mg/g (Gordeyev and Lisitsyn, 1978; Martin and Meybeck, 1979), whereas dust has a ratio between 57.8 and 69.6 mg/g (Bonelli et al., 1996; Güllü et al., 1996). The average Ti/Al ratio of the sediment trap samples is 68.0 mg/g, also pointing to dust as the major contributor to the lithogenic fraction.

The high fluxes of biogenic and terrigenous material to the sediment trap at 3000 m are coincidental, with a time-lag of 4–6 months after maximum primary production. In most sediment trap studies, the interception of these two types of material is found to occur at the same time (e.g. Honjo et al., 1982; Ramaswamy et al., 1991; Neuer et al., 1997). This relation is established by the incorporation of biogenic as well as lithogenic material in faecal pellets. These sink very fast compared to small particles like coccoliths and clay minerals, which can remain in suspension for long time periods (Lal, 1977; Buat-Ménard et al., 1989). We have found no data on faecal pellet fluxes in the eastern Mediterranean, but in the western Mediterranean, zooplankton grazing activity, resulting in faecal pellet production, was inferred to be mostly responsible for the sedimentation of terrigenous iron (Quétel et al., 1993). This grazing activity was particularly intense from April to June, the same period in which we find the highest mass fluxes in the sediment trap in 1992 and 1993. This might, therefore, explain the co-sedimentation of biogenic and terrigenous particles in this particular period.

The satellite data (Fig. 2.5) indicate that pigment concentrations are highest when sea surface temperature (SST) is lowest. The latter indicates a wind-induced oceanographic change from a summer stratified upper water mass to a deep winter mixing (Krom et al., 1992). This results in the fertilisation of the photic zone, important because the eastern Mediterranean is nutrient-depleted and phosphorus-limited (Zohary and Robarts, 1998). However, dust deposition, mainly occurring in the same period, might also contribute to higher P concentrations in the upper water column. Bergametti et al. (1992) found that the atmospheric input of phosphorus could be significant to northwestern Mediterranean surface waters, especially in summer.

2.4.2 Comparison between trap and sediment

2.4.2.1 Efficiency of the sediment trap

To compare fluxes recorded in a sediment trap with those of surface sediments, it has to be established first whether the flux is efficiently trapped. A widely used method is that by applying ^{230}Th (see section 2.2.2.2). The calculated value of 23 % is extremely low when compared to other sediment trap studies (Anderson et al., 1983a; Bacon et al., 1985; Fisher et al., 1988; Colley et al., 1995). The low efficiency may be the result of three phenomena, namely 1. Boundary scavenging; 2. A water column with unusually low U concentrations; and 3. High current velocities.

Boundary scavenging, i.e. lateral export of ^{230}Th away from the water column above the sediment trap, has not been accounted for in the model calculation. Comparison of ^{230}Th and ^{231}Pa inventories in pelagic as well as near-coastal traps and sediments has shown that a net export of these radionuclides out of the pelagic realm to the ocean boundaries must occur (e.g. Kadko, 1980; Anderson et al., 1983a,b). Because of the pelagic location of our sediment trap, this might also happen at the Bannock site. However, to the best of our knowledge, no ^{231}Pa data for eastern Mediterranean sediments have yet been published. Therefore, no quantification of this boundary scavenging effect can be made. Kadko (1980) found an average of 30 % deficit of $^{230}Th_{excess}$ in deep open ocean sediments. This value can, therefore, not fully explain the observed deficit of 77 % in our sediment trap samples (see also next section).

A much lower concentration of ^{234}U in the Mediterranean water column relative to the open ocean might also result in lower ^{230}Th fluxes to the sediment trap. This, however, is ruled out by the long residence time and stability of dissolved U in sea water. Furthermore, the actual U concentration is even slightly higher than average sea water just above the Bannock brine interface (Van der Weijden et al., 1990).

The occurrence of high current velocities would seriously hamper the collection of particles. However, the current meter data from the third (MU-B; Table 2.1) series indicate low velocities, mostly below the detection limit of 1 cm s^{-1}. Speeds were never higher than 7 cm s^{-1}. In addition, the tilt meter mounted on the sediment trap indicates no deviations from the vertical during the sampling period. Consequently, hydrodynamic biases were negligible for the particle flux data (Baker et al., 1988; Gust et al., 1992).

Overviewing these three influencing factors, we believe that only boundary scavenging, if similar to the open ocean, may explain part of the low trapping efficiency as calculated by the ^{230}Th method. Because we cannot quantify this process on the basis of ^{230}Th trap data alone, we will compare fluxes between the sediment trap and top sediment in the following section.

2.4.2.2 Comparison of fluxes and composition

Obviously, average mass fluxes are much lower in the sediment trap samples than in surface sediments (Table 2.3). We will compare the fluxes in the sediment trap with those found in boxcores UM4, UM15 and UM35. These boxcores are not in the immediate vicinity of the sediment trap location. However, a gravity core taken in Bannock Basin, containing

Table 2.4 *Composition of the two top samples of boxcore UM4. A part of the sample was sieved to gain two size fractions, which were analysed together with an unsieved sample.*

	UM4: upper 0.5 cm			
Component	<32μm	>32μm	total[a]	*calc/tot*[b]
Al (wt%)	5.41	1.99	4.50	*1.00*
Ca (wt%)	15.8	31.1	19.6	*1.01*
Mg (wt%)	1.95	0.72	1.54	*1.05*
Sr (ppm)	875	1000	923	*0.98*
Sr/Ca (mg/g)	5.55	3.21	4.72	*0.97*

[a] *analysis of the total sample.*

[b] *calculated total (from the two fractions by using the weight fraction) divided by the measured total; weight fraction used: >32 μm = 0.265.*

oxic top sediments and sapropel S1 (GC17; Van Os et al., 1991), has a sediment composition and an accumulation rate comparable to that in UM35. Therefore, a comparison between the oxic boxcores and the sediment trap is justified. We will mainly concentrate on the fluxes in UM35 because of the similar accumulation rate compared to sediments near the trap location.

The Al flux in the sediment trap is about four times lower than it is in UM35 (0.85 *vs.* 3.56 mg m^{-2} day^{-1}), which is close to the estimated trap efficiency of 23 %. This similarity indicates that boundary scavenging of ^{230}Th is not significant and that the estimated trap efficiency is reliable. Because current velocities are low and tilt meter data show no offset from the vertical, we think that the low sediment trap efficiency cannot be caused by either hydrodynamic bias or boundary scavenging of ^{230}Th. A possible alternate explanation which may be significant for these low mass fluxes, is the sticking of settling particles to the inner cone of the trap.

The fluxes of Ca, Mg and Sr in the sediment trap are relatively even lower when compared to the surface sediment samples. For Ca, this factor is ~ 9, for Mg ~ 6, and for Sr ~ 8. In the eastern Mediterranean, Ca and Sr reside almost exclusively in the carbonate fraction, whereas Mg is found in both clay minerals (i.e. the lithogenic fraction) and carbonates (Chapters 5 and 7). Aluminium is indicative for clay minerals. The magnitude of the flux and the correlation of Al with other terrigenous elements (K, Ti) must dominate any biogenic scavenging of Al as found by Murray and Leinen (1996) in the central equatorial Pacific Ocean. Consequently, variations in Al content cannot be related to variations in biogenic scavenging but rather to changes in terrigenous input alone. It appears, therefore, that the carbonate component of the total flux is relatively more undertrapped than the terrigenous one. From the faunal and floral analysis of the sediment trap samples, it is clear that the large biogenic carbonate particles, i.e. pteropods and large foraminifers, are rare (Chapter 3), whereas they are common in surface sediments of the eastern Mediterranean. To

investigate this geochemically, two size fractions of surface sediment from UM4, namely one (<32 μm) containing the small biogenic fraction (e.g. coccoliths, calcareous dinocysts, juvenile foraminifers) and the other (>32 μm) including large biogenic particles (foraminifers and pteropods), were analysed. The results indicate that the fine fraction contains only half as much Ca (16 wt%) as the large fraction (30 wt%; Table 2.4). The Sr/Ca values in the fine fraction are distinctly higher than they are in the coarse fraction. Although higher Sr/Ca values are often interpreted to be due to enhanced pteropod contents (Winland, 1969; Sutherland et al., 1984), Krinsley and Bieri (1959) observed a relatively low average Sr/Ca of 2.5 mg/g for eastern Mediterranean pteropods from plankton tows as well as surface sediment. We have also analysed pteropods from the top of a nearby boxcore, and have found a Sr/Ca ratio of 3.60 ± 0.03 mg/g. The latter Sr/Ca ratio is comparable to the one found in our coarse sediment fraction. In contrast, the sediment trap samples have a much higher Sr/Ca ratio, namely 5.2 mg/g, close to that of the fine surface sediment fraction (5.5 mg/g) (compare Tables 3 and 4). All evidence given above, therefore, is consistent with the scarcity of the coarse carbonate fraction in the sediment trap samples. At this moment, however, it is not clear why this fraction is absent in the trap. Hydrodynamic bias in trapping, if at all present, would be expected to lead to a greater loss of smaller particles rather than larger ones. Dissolution can also be ruled out; coccoliths, even delicate forms, are well preserved (Chapter 3), and the Ca concentration of the supernatant water in sediment trap sampling bottles is similar to the sea water value. The observed deviation might arise from the distribution of the coarse size fraction of biogenic carbonate through time. As juvenile foraminifers are always present in the trap samples, the distribution of the large foraminifers and pteropods could be highly variable in time and in place. The resulting magnitude of fluxes at one site may, therefore, have varied over the course of time. A bloom associated with a major hydrodynamic or atmospheric event, and occurring, for example, once every ten years has a large probability of not being trapped during a three-year deployment. An example of such a phenomenon was reported at the Cap Blanc sediment trap site, off the coast of Northwest Africa (Wefer and Fischer, 1993). In a single sampling interval of 17 days, out of three years, an extremely high flux was recorded in the >1 mm size fraction. This fraction contained a monospecific assemblage of pteropods (Kalberer et al., 1993). Another example is a sediment trap study conducted during more than 19 years in the deep Sargasso Sea, which exhibited an episodic occurrence of large, short-lived flux maxima that are not associated with the annual spring bloom in that area and do not necessarily occur every year (Conte et al., 1998). A phenomenon, similar to the ones at Cap Blanc or in the Sargasso Sea, and possibly related to North Atlantic Oscillation (NAO), might occur in the usually low-productive eastern Mediterranean. Moulin et al. (1997) have shown that atmospheric export of Saharan dust to the Mediterranean and North Atlantic Ocean is controlled by NAO. Clearly, long time series sediment trap sampling is needed so as to fully understand the dynamics of seasonal and annual variations in the eastern Mediterranean biogeochemical fluxes.

We will now evaluate if an additional (coarse) fraction in the sediment trap samples might explain the difference between sediment trap and surface sediments. When such a coarse fraction, containing 31.1 wt% Ca (i.e. 77.7 wt% $CaCO_3$) and having a weight fraction

of 0.265 (as found in the uppermost sample of UM4 (Table 2.4)), is added to the average sediment in the trap, the $CaCO_3$ content would rise to 43.7 wt%, much closer to the concentrations found in the oxic boxcores (Table 2.5). The $CaCO_3$ flux would, when including the trap efficiency correction, increase to 41.0 mg m^{-2} day^{-1}. This flux is still lower than that found in the oxic boxcore tops, although close to the Ca-flux in UM35 (Table 2.5), possibly reflecting subtle differences in the primary production in the photic zone, hence export production, at the different locations (e.g. sediment trap site vs. UM35 or UM4/UM15 site).

We have related the lithogenic flux in the trap to the input of Saharan dust. For UM35, the lithogenic flux is 1.48 mg cm^{-2} yr^{-1}, and for UM4 and UM15 2.01 mg cm^{-2} yr^{-1}. These values are in the same range as those reported by Guerzoni et al. (1997), discussed earlier. Therefore, the sediment trap and boxcore samples are both consistent with the notion that Saharan dust input is the major source for lithogenic matter in this region at present.

Table 2.5 *Observed and recalculated total, carbonate and lithogenic fluxes, and composition, for the sediment trap. Organic matter and biogenic opal, the other two contributors to the total mass flux, are not shown. Observed fluxes and composition for the three normal 'oxic' boxcores (UM4, UM15 and UM35) are also listed.*

	Flux (mg m^{-2} day^{-1})					
	Trap	**Trap***	**Trap****	**UM4**	**UM15**	**UM35**
Total	15.9	68.9	93.8	109.7	114.7	85.5
Carbonate	5.0	21.7	41.0	53.4	58.4	44.2
Lithogenic	9.6	41.6	47.5	55.2	55.1	40.6

	Composition (wt%)					
	Trap	**Trap***	**Trap****	**UM4**	**UM15**	**UM35**
Carbonate	31.5	31.5	43.7	48.7	50.9	52.7
Lithogenic	60.4	60.4	50.6	50.3	48.1	47.4

* *Numbers corrected for a sediment trap efficiency of 23 %. Possible lateral export of ^{230}Th is neglected.*
** *Numbers also corrected by adding a coarse fraction (26.5 wt%) having a composition comparable to that found for the uppermost sample (>32 μm) of UM4.*

2.5 Conclusions

The total flux of suspended material out of the photic zone to the deep water is low and highly seasonal in the pelagic eastern Mediterranean. The coccosphere-indicated primary productivity maximum reaches the trap about one month after the satellite-inferred chlorophyll maximum. However, the major sediment flux, containing a lithogenic as well as a biogenic fraction (the latter comprised mainly of coccoliths), does not coincide with the coccosphere flux, but rather is recorded 4 to 6 months later, probably due to intense zooplankton grazing, resulting in high faecal pellet production, from April to June. Because coccoliths and clay minerals, comprising most of the biogenic and lithogenic material respectively, can remain in suspension for a long time, they are scavenged and quickly transported by faecal pellets. Quantification of the lithogenic flux indicates that desert dust is likely to be the major component of the detrital matter. The Th-230 based trap efficiency is low (23 %), but is substantiated by the four times lower Al flux of samples in the sediment trap compared to those in boxcore top sediments. Boundary scavenging of ^{230}Th, the most common factor determining the trapping efficiency of ^{230}Th is, therefore, unlikely to be the major cause for the low trap efficiency. Due to the absence of hydrodynamic bias, sticking of settling particles to the inner cone of the sediment trap might have significant influence on the low mass flux. The relative recovery of carbonate in samples from the trap compared to those in the sediment is even lower (1/9). The near absence of the coarse carbonate fraction consisting of large foraminifers and pteropods in the trap samples, compared to their abundant occurrence in top sediment samples, may account for most of this deficiency. Episodically occurring major blooms may have resulted in brief intervals of major coarse carbonate (large foraminifers and pteropods) fluxes that have not been recorded during the time period of our sediment sampling (i.e. from November 1991 to August 1994) and are possibly related to NAO. Clearly, long time series sediment trap observations are needed for this area that is sensitive for recording subtle global climatic variations, so as to fully understand the dynamics of seasonal and annual variations.

Acknowledgements – G. Nobbe and H. de Waard are thanked for their analytical assistence. The pigment data are courtesy of the Joint Research Centre (European Commission / European Space Agency). The SST data were extracted from the Weekly NCEP SST Database at the NOAA/WRC Server Ferret and the precipitation data from the GPCP Global Combined Precipitation Dataset (part of the Climatology Interdisciplinary Data Collection). This chapter greatly benefited from the comments of two anonymous reviewers.

This study was supported by MARFLUX (MAST1-90022C), PALAEOFLUX (MAS2-CT93-0051) and SAP (MAS3-CT97-0137) European programmes.

This is Netherlands Sedimentary Research School (NSG) contribution 990402.

Appendix 2-A: Determination of the inorganic composition, including silica, using total digestion on sediment trap samples

Sediment trap samples, especially those from the oxic trap in the oligotrophic open eastern Mediterranean, are too small to perform separate analyses for total silica and for other major and minor elements by traditional ICP-AES techniques. In the latter preparation, a HF/acid mix total digestion is followed by evaporation of the acids, and the subsequent dissolution in 1 M HCl. During the evaporation step, however, silica is removed as volatile Si fluorides. In addition, routinely such total digestions prior to ICP-AES analyses are done one 250 mg of sample, whereas the one eighth (aimed for inorganic geochemical analysis) sediment trap samples mentioned above frequently were only a few mg in size.

In this appendix, a method is described to obtain the conventional ICP-AES determined element concentrations as well as the total Si concentration using a single total digestion.

In brief

The sediment trap samples had originally been filtered on board ship, using cellulose acetate filters. In the home laboratory these samples were dried at 40°C in an oven or were freeze-dried. The samples including the filter were then added to a Teflon vessel. A calibration series of MM91, an in-house standard, was also weighed into separate vessels (2, 4, 8, 16, 32, 64, 128 mg). A fresh cellulose acetate filter was added to make the matrix uniform to that of the sediment trap samples. Also, three 'blanks', containing only a cellulose acetate filter, were run. To all these vessels 2.5 ml HF and 2.5 ml mixed acid (60 vol% $HClO_4$, 30 vol% HNO_3 and 10 vol% distilled water) were added and the closed vessels were put in an oven at 95°C for 5 hours. After cooling down, 200 µl of the HF/mixed acid solution was transferred to a pre-cleaned polyethylene vial already containing 10 ml Milli-Q water. This subsample is subsequently used for the spectrophotometric determination of total Si. The (open) vessels with the remaining 4.8 ml of fluid were then put upon a sand bath at 240°C and the solution was vaporised to near-dryness. The remaining material was redissolved in 7.5 ml 1 M HCl and analysed by Inductively Coupled Plasma Atomic Emission Spectrometry (ICP-AES). The MM91 calibration series was used to calculate separate calibration lines for each element.

In detail

1. Freeze-dry the filter containing the sediment trap sample.
2. Weigh Teflon vessel (small format; 25 ml) including the lid.
3. Weigh filter containing the sediment trap sample.
4. Add the filter containing the sediment trap sample to the Teflon vessel.
5. Weigh Teflon vessel + lid → extra check on the filter+sample weight.
6. Add 2.5 ml HF and 2.5 ml HNO_3/$HClO_4$ to the Teflon vessel.
7. Put the lid firmly on the Teflon vessel and weigh it → weight of HF+HNO_3/$HClO_4$ is now known.

8. Put the Teflon vessel for 5 hours in an oven at 95°C.
9. Weigh polyethylene vial including closing cap.
10. Fill vial with 10 ml Milli-Q water and put cap on vial.
11. Weigh filled vial → weight of 10 ml Milli-Q water is now known.
12. Take the Teflon vessel after the 5 hours heating out of the oven, let it cool down, and weigh (to check for possible loss).
13. Unscrew cap and put 200 µl of the solution into the vial containing Milli-Q water.
14. Evaporate the remaining solution in the Teflon vessel to near-dryness.
15. Weigh the closed vial → the weight of 200 µl HF+HNO_3/$HClO_4$ is now known.
16. Add 7.5 ml 1 M HCl to the Teflon vessel, close the vessel and put it for 2 hours in an oven at 95°C.
17. After 5 hours heating, the Teflon vessel is removed from the oven and cooled down.
18. Weigh the Teflon vessel → the weight of the 7.5 ml 1 M HCl solution (thus including the dissolved elements) is now known.
19. Put the solution into a polyethylene vial for measurement with ICP-AES.

The polyethylene vial containing 10 ml Milli-Q water + 200 µl HF+HNO_3/$HClO_4$ is used for the spectrophotometric determination of Si.

Notes:

1) Steps 9 to 11 and step 13 are meant for the determination of Si.
2) The repeated weighing is essential for the calculation of dilution factors.

The spectrophotomethic measurement of silica

Total silica content can be reliably determined by the following method using a small subsample of the hydrofluoric/mixed acid mixture. The basic solution is a 50 times diluted acid/sample mixture (200 µl in 10 ml Milli-Q water). Prior to evaporation, no silica will have been removed from solution by the HF reagent. However, the presence of HF in the solution does imply that certain precautions have to be taken (such as for safety, always work in a well-ventilated fume-hood and always wear plastic gloves; do not use glassware anywhere in the procedure, and certainly not glass cuvettes!!).

Reagents

- *MOLYBDATE REAGENT **(AMMO)**:* Dissolve 4 g of ammonium paramolybdate, $(NH_4)_6MO_7O_{24}.4H_2O$ (preferably fine crystalline), in ~ 300 ml Milli-Q water using a 500 ml plastic volumetric flask. Add 12 ml concentrated hydrochloric acid (12 N), mix, and make up the volume to 500 ml with Milli-Q water. This reagent is colourless and is stable for many months if stored in a dark bottle. The reagent should be discarded immediately when any white precipitate forms. If unable to store properly, or if time permits, make fresh for each run.

- *METOL SULPHITE SOLUTION (**METOL**):* Dissolve 6.0 g anhydrous sodium sulphite, Na_2SO_3, in a 500 ml plastic volumetric flask. Add 10 g Metol (p-methylaminophenol sulphate) and then Milli-Q water to make the volume to 500 ml. When the metol has dissolved, filter the solution through a Whatman no. 1 filter paper and store in a clean, dark, polyethylene bottle, which is tightly stoppered in the refrigerator. This solution may deteriorate quite rapidly and erratically so it should be prepared fresh every month.

- *OXALIC ACID SOLUTION (**OXAL**):* Prepare a saturated oxalic acid solution by shaking 50 g of analytical-grade oxalic acid dihydrate, $(COOH)_2.2H_2O$, with 500 ml of Milli-Q water. Let stand overnight. Decant solution from crystals before use. This solution is stable and can be stored in a polyethylene bottle.

- *SULPHURIC ACID SOLUTION (**SULF**): 50% V/V.* Using a 500 ml plastic volumetric flask, pour 250 ml concentrated analytical-grade sulphuric acid into ~ 200 ml Milli-Q water. Cool to room temperature and bring volume to 500 ml with a little extra Milli-Q water. Store in a polyethylene bottle.

Standards

A standard series with the following Si concentrations was used for calibration:

0; 6.25; 12.5; 25; 50; 100; 200; 300; 400; 600; 800; 1600; 2600 µM.

To 50 ml of each standard solution, 1 ml of HF/mixed acid was added to assure a matrix similar to that of the samples. All standards were measured in duplicate.

Preparation of reducing solution (RED)

Mix 50 ml METOL with 30 ml OXAL. Add slowly, with mixing, 30 ml SULF and bring volume to 150 ml with Milli-Q water. This solution should be made daily, just before using it.

Method for the silica measurements

1. First, make sure that all reagents are prepared ahead of time. The method has a time factor built in, and therefore it is of great importance to have all necessary reagents ready to go.
2. Label and set up 4.5 ml polystyrene cuvettes (4 clear sides).
3. Put 1.400 ml Milli-Q water into the cuvettes.
4. Add 0.100 ml of sample, standard, or blank, and mix.
5. Record time.
6. Add 1.000 ml of AMMO, and mix. A yellow colour will develop, and this is allowed to mature for exactly 15 minutes (± 15 seconds). Then add 1.50 ml of RED, and mix again. Cover the cuvettes with Parafilm and wait for at least 4 hours.
7. Read absorbances on the Perkin Elmer Lambda 1 UV/VIS Spectrophotometer at 812 nm.

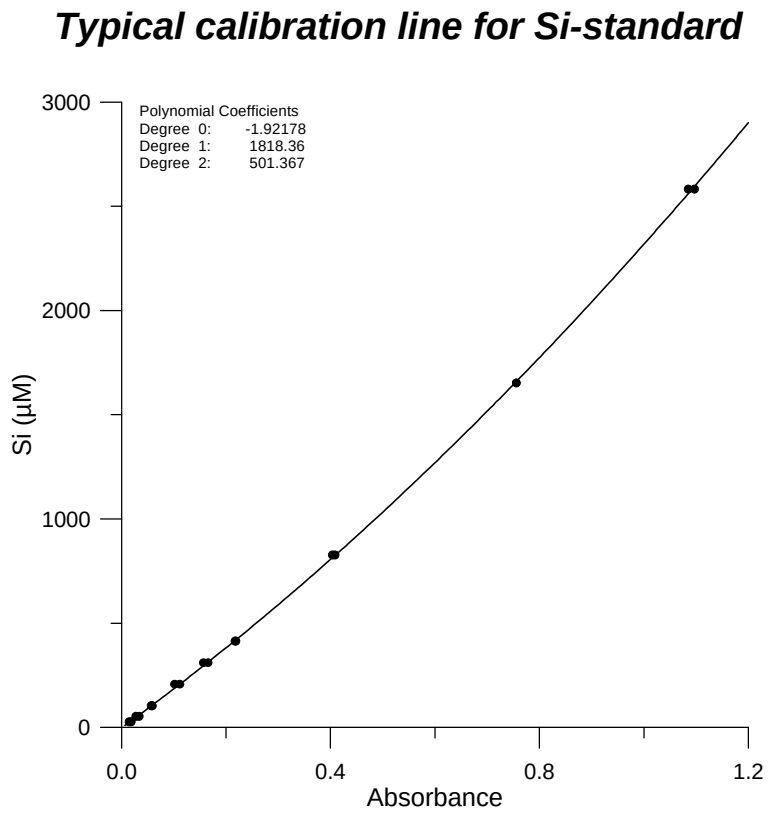

Figure 2-A.1 *A typical calibration line for the Si-standard. The absorbance of the Si-standard samples is plotted against the known Si concentration. This calibration line is then used to calculate concentrations from the absorbances of the sediment trap samples and the MM91 calibration series.*

Calculation of the Si content of the sediment trap samples

The first step consists of plotting the absorbance of the Si-standard calibration series against the Si concentration of the original solution (Fig. 2-A.1 shows the calibration line from the UM-series of the oxic trap). From this plot a calibration line can be calculated, so as to transform the measured absorbances of the sample solutions into the concentration of the 10 ml Milli-Q water + 200 µl HF/mixed acid. Using the previously measured weights, the amount (in mg) of Si in total HF/mixed acid can be calculated. Then, the measured Si amounts of the MM91 standards are plotted against the expected Si amounts, which are calculated by using the weight of the samples and the known Si content (13.13 wt%) (Fig. 2-A.2 shows the MM91 calibration for the UM series of the oxic trap). The measured Si amount of the sediment trap samples is then transformed into standard-calibrated values so as to avoid procedural artifacts. These Si amounts can be recalculated as Si fluxes. Note: the absorbances of the MM91 calibration series and the sediment trap samples are in the full range of the Si calibration line.

Procedural notes

- Do not handle more than about 60 samples at a time in order to ensure that the 15-minute time limit can be adhered to. Make sure that there are no wild fluctuations in room temperature.

- Although it is suggested that strict adherence to the 15-minute time limit is advisable, tests have shown that there is some leeway, i.e. the yellow molybdate complex is stable from 10 to 20 minutes. However, consistency in the time limit will eliminate any potential error.

- It is important to wait at least 3 hours for the blue colour to develop; the higher the concentration, the longer the time. The colour remains stable for many more hours, and reading after 4 or 5 hours may, in fact, be a good idea. Again, consistency in time limits is advisable.

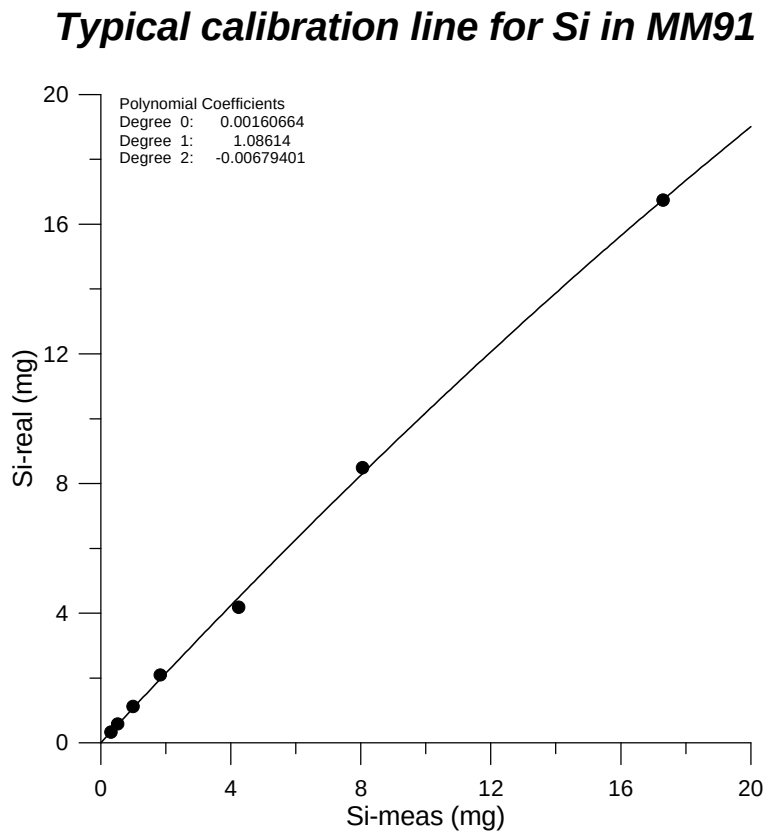

Figure 2-A.2 *A typical calibration line for the MM91 series. The known amount of Si is plotted against the measured Si content. From this calibration line, the final amounts of Si in the sediment trap samples are calculated from the measured amount of Si so as to avoid procedural artifacts.*

Calculation of the mass accumulation rates

The calculation of the total mass on a filter was done in two ways: 1) by assuming a constant weight for each filter and substracting this from the weights of the dried filter including the sample, and 2) by normalizing all elements to oxides (except Ca and Sr, which are normalized to carbonates). Both values appeared to agree well. The mass accumulation rates were then derived by multiplying with the split factor (4 for the first series, 8 for the remaining three) and by dividing with the number of collection days for each sample and the sediment trap aperture (1 m^2).

Because the oxic sediment trap samples were too small to allow a separate analysis of biogenic Si (opal), clay-Si had to be calculated by assuming a constant Si/Al for clays of 2.6 (this value, corrected for the known quartz and opal content, is found in MM91, which consists of mixed eastern Mediterranean sediments). By multiplying the total accumulated Al by Si/Al_{clay}, clay-Si is then derived. This value is substracted from total Si to give Si_{rest}, which consists of quartz and biogenic Si. Because these two cannot be separated, all Si_{rest} is assumed to be biogenic Si, which is an upper limit for the real value.

Chapter 3

Present-day coccolith fluxes recorded in central eastern Mediterranean sediment traps and surface sediments*

Abstract – Two sediment traps were deployed in time series collection from November 1991 to August 1994 at 3000 m and 3500 m, respectively, above and below the oxygenated sea water/anoxic brine interface in Bannock Basin, central eastern Mediterranean. Here the coccolithophore flux and its contribution to the carbonate particulate flux is presented for the 3000 m trap, and compared with the record in eastern Mediterranean surface sediments. A marked seasonal variation is observed in the fluxes of total mass, total coccoliths and whole coccospheres, with flux maxima in late winter and spring. The annual coccolith flux of 1.0×10^{10} coccoliths m^{-2} yr^{-1} measured in the deep waters of Bannock Basin is much lower than published data from most other oceanographic settings, even when corrected for the trap efficiency of about 23% calculated from the ^{230}Th flux. The biogenic and lithogenic fluxes are primarily controlled by coccolithophore production and Saharan dust input, respectively. The calculated coccolith and coccosphere settling rates estimated from the comparison of maximum pigment concentration in the surface ocean and arrival of maximum flux at 3000 m water depth ranged from 17 – 25 m day^{-1} for coccoliths and 100 m day^{-1} for coccospheres. At the study site, carbonate dissolution is a minor process at both the trap depth and at the sea floor in both oxic and anoxic conditions, and there is a high preservation of coccolith $CaCO_3$. Coccolithophores are the main contributor to the biogenic carbonate flux, followed by thoracosphaerids. *Emiliania huxleyi* and *Florisphaera profunda* followed by *Syracosphaera*, *Helicosphaera carteri* and *Calcidiscus leptoporus* are the dominant species in the sediment trap and surface sediments.

3.1 Introduction

The eastern Mediterranean is an area with extremely oligotrophic or ultra-oligotrophic conditions (Berland et al., 1988; Dugdale and Wilkerson, 1988; Yacobi et al., 1995). Heterotrophic bacterial production is tightly coupled with primary production. In particular, 85% of the primary production in the eastern Mediterranean flows to the microbial food web (Turley, 1997). Phytoplankton populations are dominated by picoplankton (Li et al., 1993) with the bacterial biomass constituting about 50% of total algal biomass (Robarts et al., 1996). The central eastern Mediterranean is net phototrophic, resulting in a sink for atmospheric CO_2. Although eastern Mediterranean primary production estimates are generally low (Dugdale and Wilkerson, 1988), however, so far no one has studied how the productivity changes over the annual cycle in detail.

Coccolithophores are pelagic unicellular algae that secrete calcite plates. They are a

* This chapter has been published as: P. Ziveri, A. Rutten, G.J. de Lange, J. Thomson and C. Corselli, 2000, *Palaeogeography, Palaeoclimatology, Palaeoecology*, 158, 175-195.

major constituent of marine phytoplankton and make the major contribution to the biogenic carbonate content in deep-sea sediments (Bernard & Lecal, 1953; Milliman and Muller, 1973; Milliman, 1993)., With their fast turnover, coccolithophores may have an important effect on the CO_2 cycle in the global ocean. They influence the global climate system through the organic carbon and carbonate pumps and by the emission of dimethyl sulfide which may affect cloud albedo (Andreae, 1986; Matrai and Keller, 1993; Charlson et al., 1987; Westbroek et al., 1993). Satellite imagery by the Coastal Zone Color Scanner (CZCS) revealed the formation of extensive blooms of the coccolithophore *Emiliania huxleyi* at higher latitudes in cooler, nutrient-rich waters (Holligan et al., 1983, Balch, 1997; Brown and Yoder, 1994). A better understanding of coccolithophore ecology is further required to use them as a biotic proxy of past climate change and to assess the quality and accuracy of the information preserved in the sediment record.

In the central eastern Mediterranean, coccolithophores are the dominant phytoplankton group that produces carbonate (Ziveri et al., 1995). In this study, we concentrate on the coccolithophore flux (number m^{-2} day^{-1}) and its seasonality. In addition, annual fluxes will be compared with those estimated for nearby surface sediments. Present-day coccolithophore fluxes in the eastern Mediterranean have been measured by two automated sediment traps capable of collecting particles for specified time intervals over a long period.

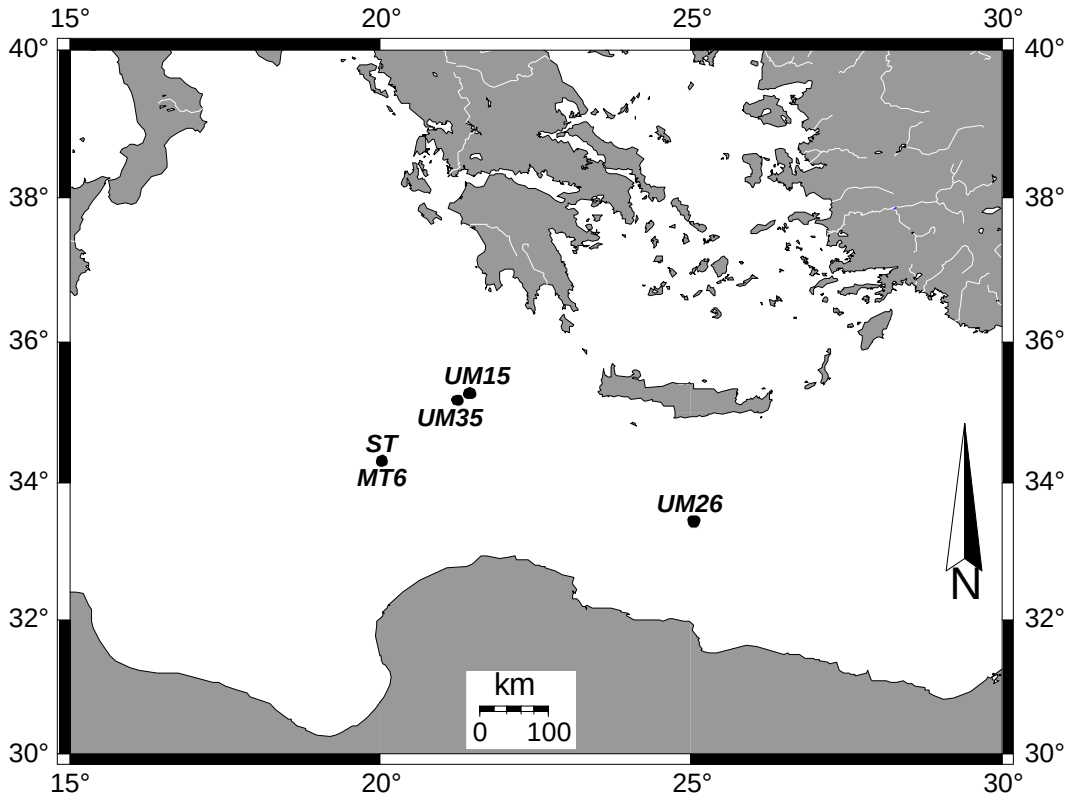

Figure 3.1 *Map of the central eastern Mediterranean showing the locations of the sediment trap mooring (ST) and boxcores (MT6, UM15, UM35 and UM26) used in this study.*

3.2 Material and methods

Two time-series sediment traps (Technicap PPS5/2) were deployed in the southwestern Bannock Basin (Libeccio subbasin; 34º18'N; 20º01'E), a central eastern Mediterranean anoxic basin (Scientific staff of Cruise Bannock 1984-12, 1985) (Fig. 3.1). Collection was from November 1991 until August 1994. During the 927-day deployment, each sediment trap opened and closed 96 times, providing a near-continuous time-series (Table 3.1). The upper trap was located at 3000 m, above the sea-water / brine interface in oxygenated conditions, whereas the lower trap, at 3500 m, was located in anoxic brine close to the bottom of Libeccio Basin (Fig. 2.2 in Chapter 2). Samples 21, 22, 23 (from 20-04-1992 to 05-05-1992) collected by the trap at 3000 m were empty, whereas sample 24 was unusually large, but no technical failure was apparent. In addition, a high mass flux was recorded in the anoxic trap at the same time in the synchronous sample 24. For this reason, we include all samples in all calculations.

A detailed description of the deployment and recovery of the sediment traps, sample additives, integrity and analytical methods are reported in Chapter 2 and by Ziveri et al. (1995). Sediment trap efficiency was evaluated using the flux of the long-lived radionuclide ^{230}Th (Chapter 2).

The surface sediment of four eastern Mediterranean boxcores, from 2160 – 3520 m water depth, were analysed for comparison with the accumulation rates and taxonomic composition of the coccolithophores estimated from the traps (Fig. 3.1, Table 3.2).

3.2.1 Coccolithophore sediment trap sample preparation

All samples were split on recovery on board ship into equal fractions using a pneumatic splitter (Tennant and Baker, 1992). For coccolith analysis, the first three series of samples (1 – 72) were collected on board upon 0.45 μm cellulose acetate (samples 1 – 48: 47 mm diameter; samples 49 – 72: 25 mm diameter) using a gas pressure system. The final set of samples (73 – 96) were maintained in solution and then split and filtered in the laboratory of the Department of Biology, University of Milan. After stirring the solution, a small portion of the sample was collected using a precision pipette and filtered on to a 0.45 μm cellulose acetate filter (47 mm diameter).

Table 3.1 *Sediment trap mooring phases, sampling period per phase, sample interval and deployment days per sampling phase. Sediment trap position: 34°17.84'N 20°00.89'E. Sediment trap depth: 3000 m. Water depth: 3530 m.*

Mooring Phase	Phase Start date	Phase End date	Deployment (days)	Sample interval (days)
ST2	10 Nov 1991	10 May 1992	182.5	5–10
MT4O	1 Jun 1992	19 Feb 1993	263	9–14
MU-B	1 Apr 1993	16 Sep 1993	168	7
UM1STO	20 Oct 1993	29 Aug 1994	313	10–20

Table 3.2 *Boxcore position, sampling interval, water depth, type of sediment and data used for the calculation of the coccolith accumulation rates (excluding coccolith concentration). These data include the sedimentation rates (cm kyr^{-1}), dry bulk densities (g cm^{-3}), percent mass accumulation rates (mg cm^{-2} kyr^{-1}) and $CaCO_3$ content (%) of the surface sediments analysed in the present study. The sedimentation rates and the dry bulk densities are from Van Santvoort et al. (1996), excluding the data for MT6 (see Appendix 3-A).*

Boxcore	Position (latitude, longitude)	Sampling Interval (cm)	Water Depth (m)	Sediment Type	Sed. Rate (cm kyr^{-1})	Dry Bulk Density (g cm^{-3})	Mass. Accum. Rate (g cm^{-2} kyr^{-1})	Total $CaCO_3$ Weight (%)
UM15	35°17.39'N 21°24.82'E	0.0 – 1.0	3307	Oxic, homogenised	4.7	0.8	4.2	51.3
UM26	33°23.58'N 25°00.93'E	0.0 – 0.5	2160	Oxic, homogenised	2.7	0.8	2.6	53.7
UM35	35°11.04'N 21°12.54'E	0.0 – 1.0	2670	Oxic, homogenised	3.3	0.9	3.1	54.5
MT6	34°17.09'N 20°01.16'E	0.0 – 0.5	3520	Anoxic, laminated	14.1	0.2	6.1	37.7

For the coccolith analysis of samples 1 to 72, the material on the filter had to be resuspended off the filter. Each filter was put into a glass culture tube containing a known volume of filtered (0.2 μm) distilled water buffered with sodium borate. The solution was stirred for a few minutes to allow detachment of the material from the fiber filter. A portion (1/8 – 1/1000 of the original sample) of the solution was collected by precision pipette and refiltered on to a 0.45 μm cellulose acetate filter (47 mm diameter). A 1 to 2 mm^2 area of each filtered membrane was subsequently analysed using a polarised light optical microscope (LM) at 1250× magnification to determine the total coccolith, coccosphere and calcareous dinocyst fluxes and the fluxes of the individual coccolithophore species (Ziveri and Thunell, 2000). A larger area (about 30 mm^2) was then used to quantify fluxes of coccospheres and calcispheres of thoracosphaerids (calcareous dinocysts). A scanning electron microscope (SEM) was used to evaluate the sample preparation, the coccolithophore taxonomical composition and coccolith preservation. The flux results on the other major biogenic contributors will be given in Ziveri et al. (in prep.).

The evenness of the distribution of coccoliths across the filter surface was confirmed by quantifying their distribution on different areas across the filter on samples from different production episodes. An average of 709 (405 – 1302) coccoliths were counted per sample; the number of coccospheres counted per sample ranged from 0 – 340.

3.2.2 Coccolithophore surface sediment sample preparation

Total coccoliths per gram of dry sediment (coccoliths g^{-1}) and the coccolith taxonomic composition were determined in the <32 μm fraction from the top sediment of four boxcores (upper 0.5 to 1 cm) located close to the trap mooring (UM15, UM35, MT6) and at a more eastern site (UM26).

The <32 μm and 32 – 1000 μm fractions for each sample were obtained by wet sieving 0.25 – 0.5 g of freeze-dried sediment following the filtration method described in Lototskaja et al. (1998). Each size fraction was collected on to 0.45 μm Millipore filters (47 mm diameter) using prefiltered distilled water with a sodium borate buffer. A low-pressure vacuum pump was used for filtration in order to improve the even distribution of the particles on the filter. Each membrane was oven-dried at 40˚C and stored in an air-tight container. Coccolithophore quantification was carried out on the <32 μm fraction; the >32 μm fraction was qualitatively analysed to evaluate the sieving efficiency. The weight percentage of the >32μm and <32μm size fractions for samples of UM15, UM26 and UM35 was obtained by wet-sieving 0.5 g sediment and subsequent oven drying.

The sedimentation rates (cm kyr^{-1}), dry bulk densities (g cm^{-3}), mass accumulation rates (mg cm^{-2} kyr^{-1}) and $CaCO_3$ content (wt%) of the surface sediments analysed in this study are presented in Table 3.2. The sedimentation rates and the dry bulk densities are from Van Santvoort et al. (1996), excluding the data for MT6 (see Appendix 3-A). The carbonate content of the fine fraction was determined by gasometric techniques, with a precision of ±2%

Coccolith accumulation rates were calculated using the following formula (Lototskaya et al, 1998; Ziveri and Thunell, 2000):

$$ARc = Dc \times DBD \times SR \quad (1)$$

where ARc is the coccolith accumulation rate (number of coccoliths cm^{-2} yr^{-1}), Dc the coccolith density (number of coccoliths g^{-1}), DBD the dry bulk density (g cm^{-3}), and SR the sedimentation rate (cm yr^{-1}).

The coccolith taxonomic composition of the top sediments was determined by LM in the same way as the trap samples and 500 specimens were counted for each; SEM was used to evaluate the preparation of the samples, the coccolith carbonate preservation and species diversity.

Taxonomic identification for the determination of the species diversity follows Ziveri et al. (1995). For quantification, all holococcoliths were classed as holococcolith spp., and the *Syracosphaera* group includes all *Syracosphaera* species excluding *S. pulchra* and *S. histrica*.

3.3 Results

3.3.1 Sediment trap

The seasonal pattern of coccolithophore deposition recorded in the 3000 m Bannock Basin sediment trap exhibits highest coccosphere fluxes during January – May 1992, April – May 1993 and January 1994, and highest individual coccolith fluxes during late March – mid July 1992, April – June 1993 and late October – January 1994 (Fig. 3.2). Maximum coccolith and coccosphere fluxes occur in April 1993, reaching values of 3.0×10^8 coccoliths m^{-2} day^{-1} and 6.2×10^4 coccospheres m^{-2} day^{-1}, respectively. The contribution of intact coccospheres to the total coccolith flux is relatively small in comparison to the settling of individual coccoliths.

The coccolithophore flux peaks are caused mainly by an increased flux of *E. huxleyi* (Fig. 3.3). The taxonomic composition of the coccolithophore assemblages in the trap samples is dominated by *E. huxleyi* (on average 82.2% of the total coccolith assemblage; range between 6.3 and 95%) and secondarily by *F. profunda* (average 5.3%; range 0 – 50.4%), *Syracosphaera* (average 3.9%; range 0 – 31.9%) and *H. carteri* (average 3.1%; range 0 – 31.2%) (Fig. 3.3).

The fifty coccolithophore species identified in the sediment trap samples are listed in Table 3.3. The 500 specimens counted for each sample lead to a 95% probability level of detecting a species present in the population at 1%.

Maximum fluxes of thoracosphaerids are recorded during April till June 1992 and 1993, and from November 1993 to January 1994 and July to August 1994 (Fig. 3.2). The mean flux is 6.5×10^4 calcispheres m^{-2} day^{-1}.

Coccolithophores are the major contributor to the biogenic carbonate flux in Bannock Basin, and are also the dominant phytoplankton group detected in the trap samples (Ziveri et al., 1995). Calcareous dinoflagellates, mainly *Thoracosphaera hemii*, are the only additional calcareous component that contribute considerably to the biogenic carbonate fluxes (average of 17%). Foraminifers are present mainly as juvenile forms and have low fluxes. An increase in juvenile foraminifer flux has been recorded in July–August 1994 (Ziveri et al., in prep.).

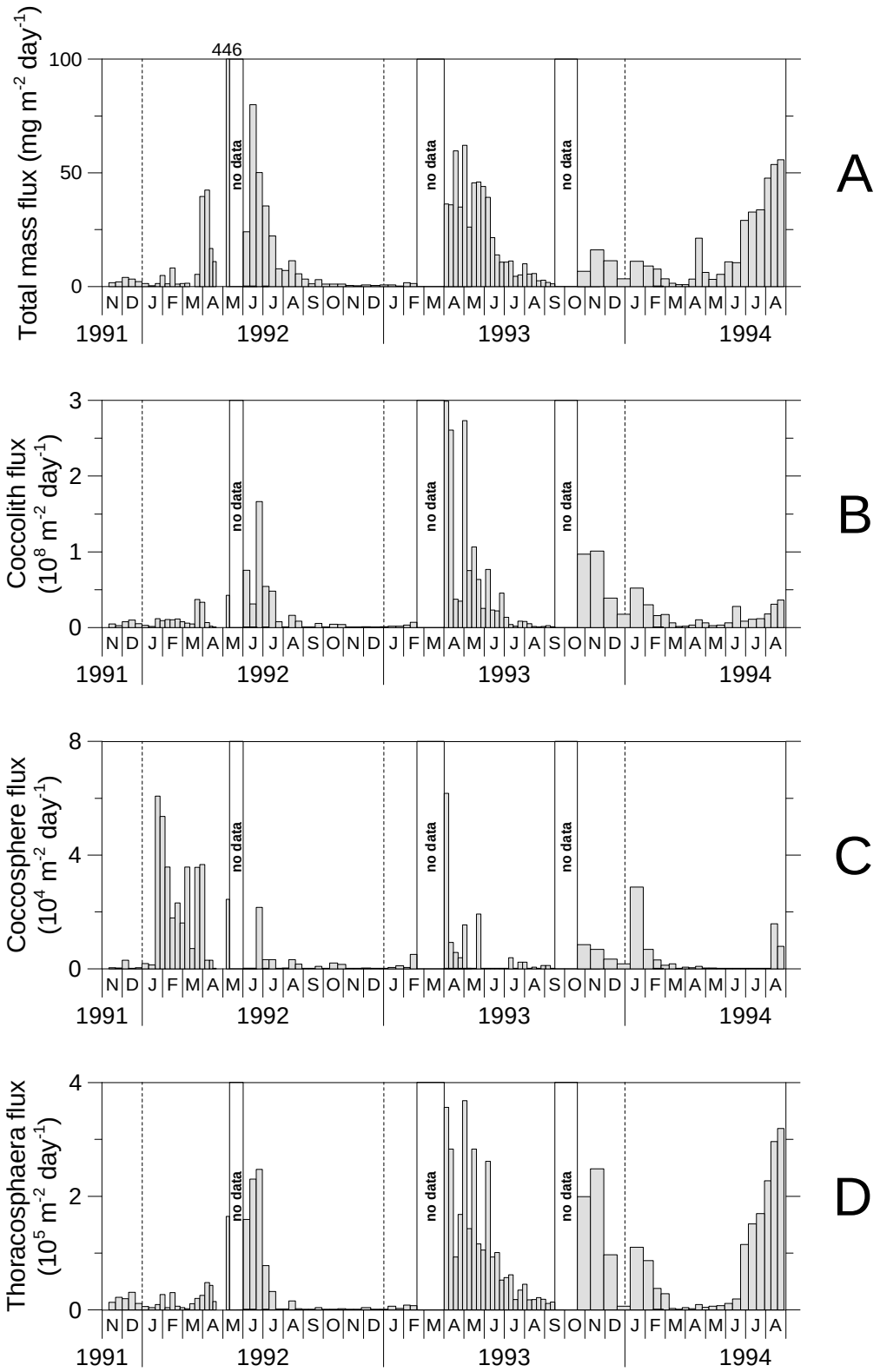

Figure 3.2 *Flux records for: A) Total mass (mg m^{-2} day^{-1}); B) Total coccoliths (number m^{-2} day^{-1}); C) Coccospheres (number m^{-2} day^{-1}); D) Thoracosphaerids (number m^{-2} day^{-1}), at Bannock Basin at 3000 m water depth.*

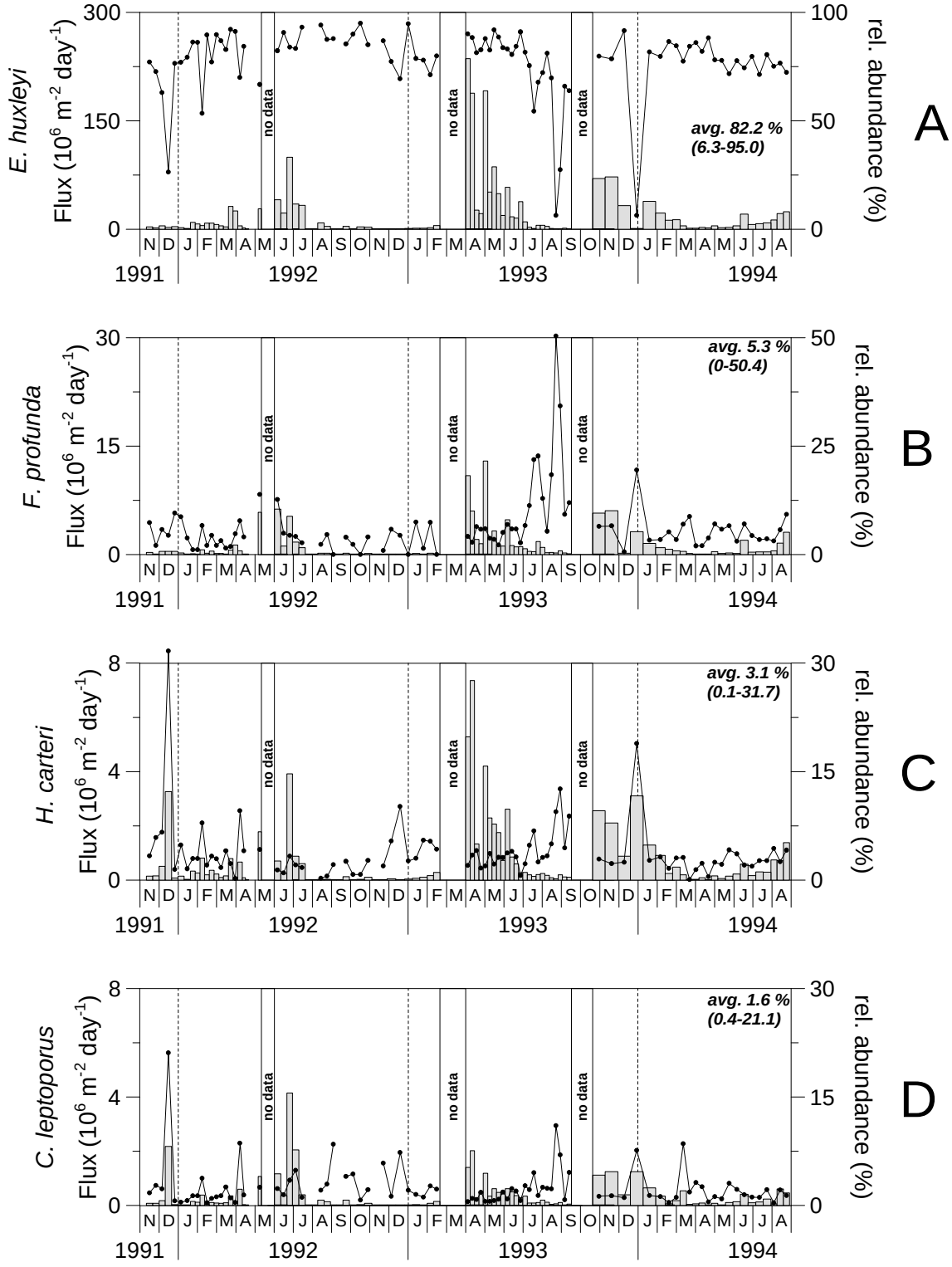

Figure 3.3 *Coccolith flux (number m^{-2} day^{-1}) (bars) and relative abundance (% of total coccolith flux) (lines) records of the major individual species of coccolithophores. The relative abundance is defined as flux of a certain species (number m^{-2} day^{-1}) divided by total coccolith flux (number m^{-2} day^{-1}) and multiplied by 100%.*

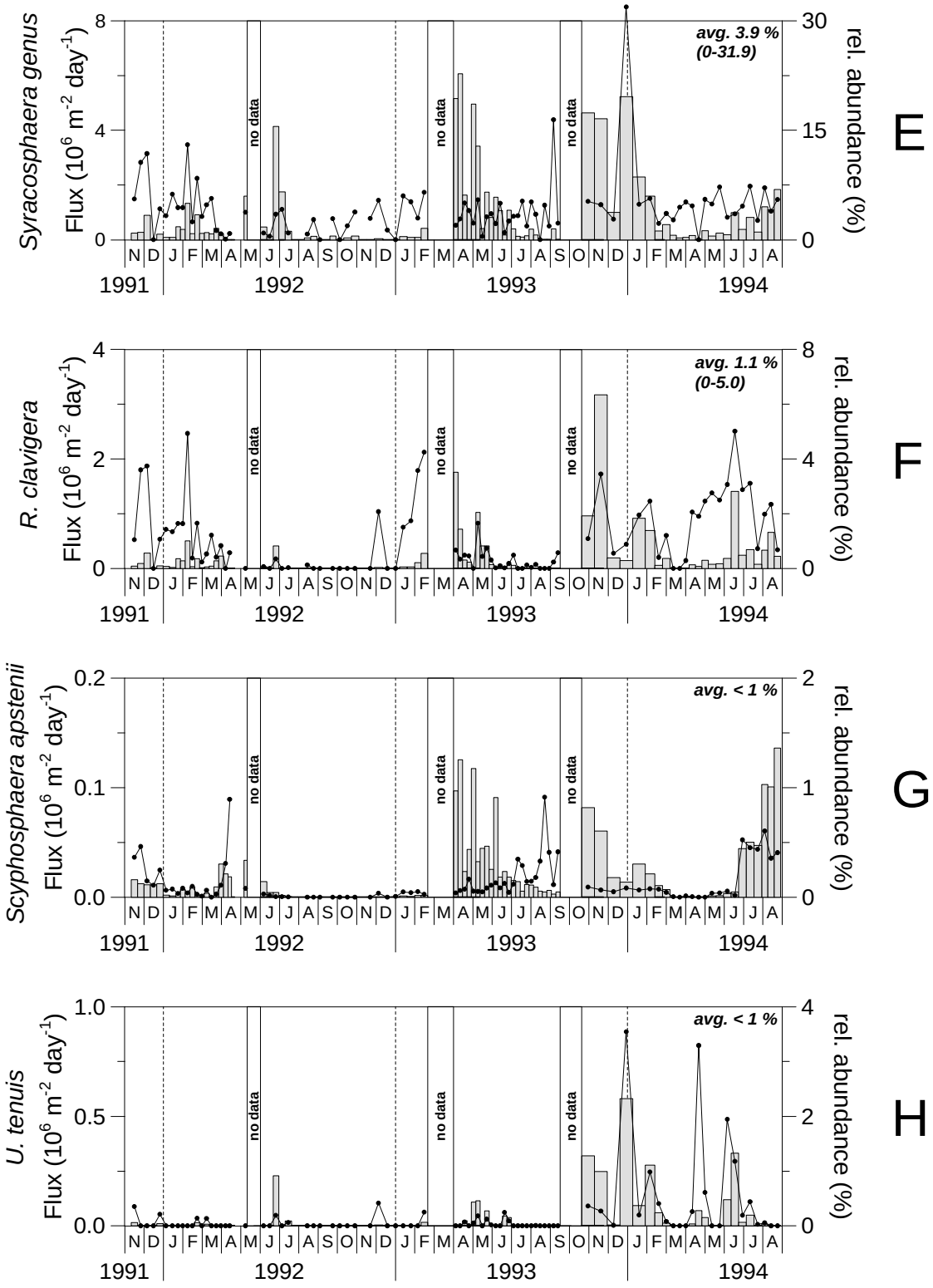

Figure 3.3 (continued)

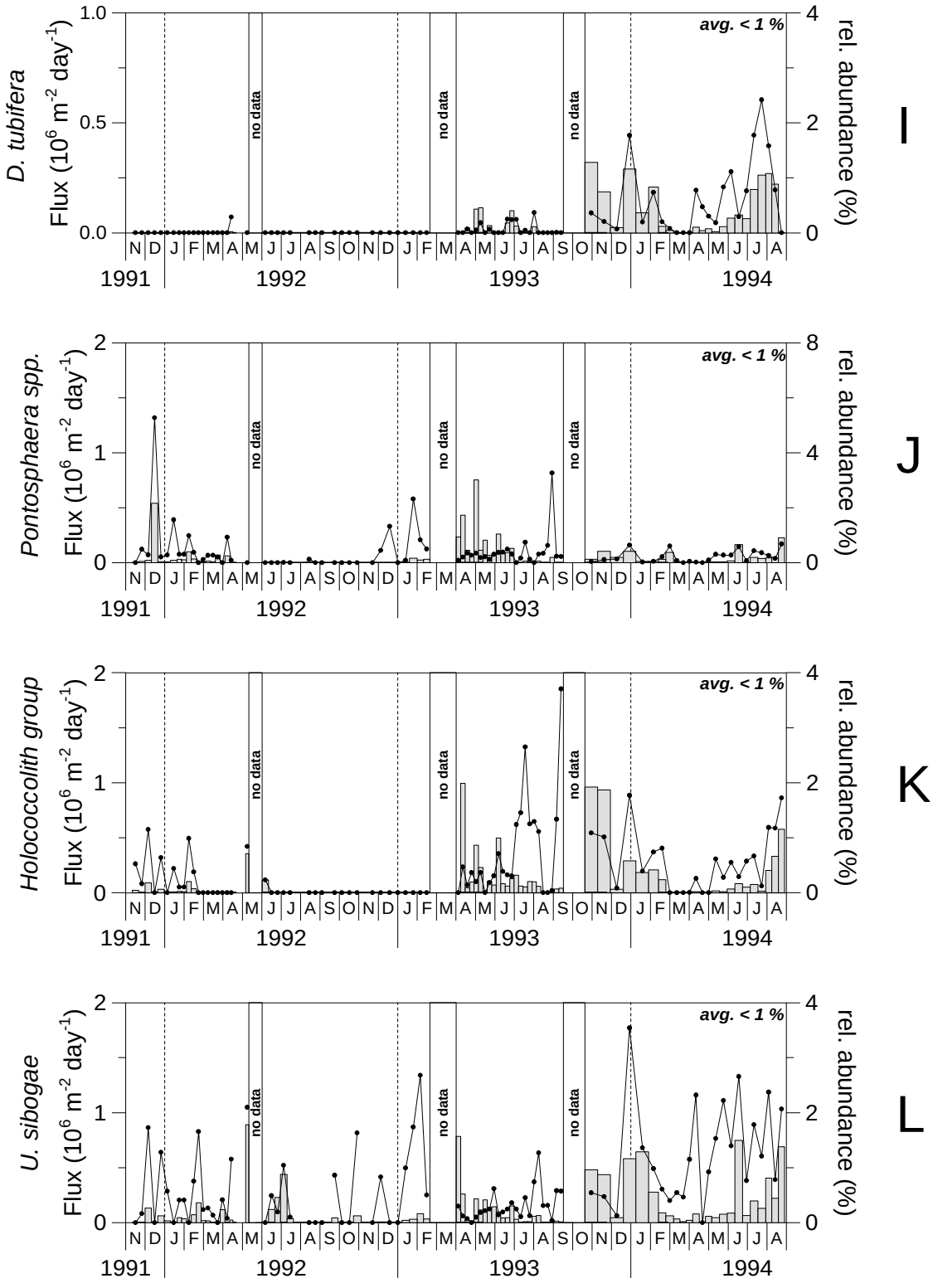

Figure 3.3 (continued)

3.3.2 Surface sediments

The Ca content of the surface sediments of boxcores UM15, UM26 and UM35 varies from 18 to 24 wt% and is 15 wt% for boxcore MT6, located in the anoxic brine basin. Higher annual coccolith accumulation rates were found in the anoxic surface sediments (core MT6) from Bannock Basin (Fig. 3.4; Table 3.4). The coccolith accumulation rates range from 2×10^{12} to 3.9×10^{13} coccoliths m^{-2} kyr^{-1}. *Emiliania huxleyi* dominates the sediment assemblage, followed by *F. profunda*, *H. carteri* and *C. leptoporus* (Fig. 3.4; Table 3.4).

3.4 Discussion

3.4.1 Seasonal trend of coccolithophore and thoracosphaerid fluxes

During the 3-year time series the mass flux pattern was characterised by low mass particle fluxes with an average of about 16 mg m^{-2} day^{-1}. This value is several times lower than the average mass flux measured at 1000 m depth in the North Balearic Northwestern Mediterranean (185–588 mg m^{-2} day^{-1}), Adriatic sea (341 mg m^{-2} day^{-1}) and west of Crete (46 – 210 mg m^{-2} day^{-1}) (Heussner and Monaco, 1996), and in the Alboran Sea (197 mg m^{-2} day^{-1}; Dachs et al., 1986). It is, however, similar to the flux recorded in the western Mediterranean northwest of Corsica (22 mg m^{-2} day^{-1}; Miquel et al., 1994).

The total mass and coccolith fluxes recorded in Bannock Basin present a strong seasonal pattern with a general increase in late winter to early spring. The major component of the mass flux in the sediment trap appears to be of terrigenous origin (60 wt%) (Chapter 2). The average total carbonate content is relatively low (31.5 wt%) compared to those in the top sediments of the eastern Mediterranean. In contrast, the biogenic particle fluxes in the sediment trap at the Bannock Basin site are largely dominated by carbonate (~70%). Dilution of the biogenic components is, therefore, an important process. The dilution effect by terrigenous input is demonstrated by the general inverse trends of the Al flux (an indicator of terrigenous input) and the coccolith concentrations obtained by dividing coccolith flux by mass flux (Fig. 3.5).

Little work has been performed in the eastern Mediterranean on living coccolithophores and almost nothing is known about their spatial and temporal distribution or their export production to the sea floor. One previous investigation (Knappertsbusch, 1993) in the eastern Mediterranean in 1986 to 1988 registered a very high seasonal variability in coccolithophore production. The highest production was found in February to March, largely dominated by *E. huxleyi*. Preliminary results from the oligotrophic waters of the south Aegean Sea and the Straits of Cretan Arc show that coccolithophores were the dominant phytoplankton group in March and September (Balopoulos et al., 1996).

The annual coccolith flux of 1.0×10^{10} coccoliths m^{-2} yr^{-1} measured in the deep waters of Bannock Basin is much lower than most published data recorded in other oceanographic settings (10^{11} – 10^{12} coccoliths m^{-2} yr^{-1}; Steinmetz, 1991; Broerse et al., 2000; Haidar et al., 2000; Sprengel et al., 2000; Ziveri and Thunell, 2000). This result remains low even after we correct the value for the trap efficiency of 23% calculated from the ^{230}Th (Chapter 2).

Thoracosphaera fluxes parallel the mass flux (r= 0.72). Data on thoracosphaerid fluxes

in the ocean still remain scarce. Their annual fluxes (2.4×10^7 calcispheres m^{-2} yr^{-1}) in Bannock Basin are higher than those recorded in open ocean Northeast Atlantic stations at 48ºN21ºW however, and are comparable to the data collected at 38ºN 21ºW (Broerse et al., 2000). Enhanced calcareous cyst production can be observed in regions and time intervals with stratified, oligotrophic conditions in the upper water masses (Höll et al., 1999; Zonneveld et al., 1999).

Table 3.3 *List of the coccolithophore species recorded in the sedimen trap (extrapolated by 926-day deployment) in Bannock Basin and sediment samples from Bannock Basin and the eastern Mediterranean. The relative abundances (%) of the main coccolithophore species in the sediment trap and surface sediments are shown in Table 3.4.*

Species	Sediment Trap	Surface Sediments			
	Bannock Basin (3000 m)	UM15 (3307 m)	UM26 (2160 m)	UM35 (2670 m)	MT6 (3520 m)
Heterococcolithophores					
1. *Algirosphaera oryza* Schlauder 1945	Yes	Yes	Yes	Yes	No
2. *Anopsolenia brasilianensis* (Lohmann 1919) Deflandre 1952	Yes	Yes	No	No	No
3. *Braarudosphaera bigelowi* (Gran and Braarud 1935) Deflandre 1947	Yes	No	No	No	No
4. *Calcidiscus leptoporus* (Murray and Blackmann 1898) Loeblich and Tappan 1978	Yes	Yes	Yes	Yes	Yes
5. *Ceratolithus cristatus* Kamptner 1950 var. cristatus	Yes	No	Yes	No	No
C. cristatus var. *telesmus* (Norris 1965) Jordan and Young 1990	Yes	No	No	Yes	No
6. *Coccolithus pelagicus* (Wallich 1877) Aciller 1930 f. *pelagicus*	Yes	No	No	No	Yes
7. *Coronosphaera mediterranea* (Lohmann 1902) Gaarder and Heimdal 1977	Yes	Yes	Yes	Yes	Yes
8. *C. binodata* (Kamptner 1927) Gaarder and Heimdal 1977	Yes	No	No	No	No
9. *Discosphaera tubifera* (Murray and Blackman 1989) Ostenfeld 1900	Yes	Yes	No	No	No
10. *Emiliania huxleyi* (Lohmann 1902) Hay and Mohler, in Hay et al. 1967	Yes	Yes	Yes	Yes	Yes
11. *Florisphaera profunda* Okada and Honjo 1973	Yes	Yes	Yes	Yes	Yes
12. *Gephyrocapsa caribbeanica* Boudreaux and Hay, in Hay et al. 1967	Yes	Yes	Yes	Yes	Yes
13. *G. ericsonii* McIntyre and Bé 1967	Yes	Yes	Yes	Yes	Yes
14. *G. ornata* Heimdal, 1973	Yes	No	No	No	No
15. *G. muellerae* Breheret 1978 type A	Yes	Yes	Yes	Yes	Yes
16. *G. oceanica* Kamptner 1943	Yes	Yes	Yes	Yes	Yes
17. *Gladiolithus flabellatus* (Halldal and Markali 1955) Jordan and Chamberlain 1993	Yes	Yes	Yes	Yes	Yes
18. *Helicosphaera carteri*(Wallich 1978) Kamptner 1954	Yes	Yes	Yes	Yes	Yes
19. *H. pavimentum* Okada and McIntyre 1977	Yes	No	Yes	No	No
20. *Neosphaera coccolithomorpha* Lecal-Schlauder 1950	Yes	No	No	No	Yes

Species	Sediment Trap Bannock Basin (3000 m)	Surface Sediments			
		UM15 (3307 m)	UM26 (2160 m)	UM35 (2670 m)	MT6 (3520 m)
21. *Oolithotus fragilis* (Lohman 1912) Okada and McIntyre 1977	Yes	Yes	Yes	Yes	No
22. *Ponthosphaera japonica* (Takayama 1967) Nishida 1971	Yes	No	Yes	No	No
23. *P. discopora* Schiller 1925	Yes	Yes	Yes	Yes	Yes
24. *P. syracusana* Lohmann 1902	Yes	Yes	No	No	No
25. *Reticulofenestra parvula* (Okada and McIntyre 1977) Biekart 1989	Yes	Yes	Yes	Yes	Yes
26. *Reticulofenestra* "overcalcified" sp.	Yes	Yes	Yes	Yes	Yes
27. *Rhabdosphaera clavigera* Murray and Blackman 1989	Yes	Yes	Yes	Yes	Yes
28. *R. xiphos* (Deflandre and Fert 1954) Norris 1984	Yes	No	No	No	No
29. *Scyphosphaera apstenii* Lohman 1902	Yes	No	No	No	Yes
30. *Syracosphaera anthos* (Lohman 1912) Jordan and Young 1990	Yes	Yes	No	No	No
31. *S. corrugis* Okada and McIntyre 1977	Yes	No	No	No	No
32. *S. halldalii* (Weber-van Bosse, 1901) Gaarder 1970	Yes	Yes	No	Yes	Yes
33. *S. histrica* Kamptner 1941	Yes	No	No	No	No
34. *S. pulchra* Lohmann 1902	Yes	Yes	Yes	Yes	Yes
35. *Umbellosphaera irregularis* Paashe, in Markali and Paashe 1955	Yes	No	No	No	No
36. *U. tenuis* (Kamptner 1937) Paashe, in Markali and Paashe 1955	Yes	Yes	Yes	Yes	Yes
37. *Umbilicosphaera hulburtiana* Gaarder 1970	Yes	No	No	No	No
38. *U. sibogae* (Weber-van Bosse 1901) Gaarder 1970	Yes	Yes	No	No	No
Holococcolithophores					
39. *Antosphaera fragaria* (Kamptner 1953) Kleijne 1991	Yes	No	No	No	No
40. *Calyptrolithina multipora* (Gaarder, in Heimdal and Gaarder 1980) Norris 1985	Yes	No	No	No	Yes
41. *C. wettsteinii* (Kamptner 1937) Kleijne 1991	Yes	Yes	Yes	No	No
42. *Calyptrolithophora papillifera* (Halldal 1953) Heimdal, in Heimdal and Gaarder 1980	Yes	No	No	No	Yes
43. *Calyptrosphaera oblonga* Lohmann 1902	Yes	Yes	No	Yes	Yes
44. *Calyptrosphaera pirus* Kamptner 1937	Yes	No	Yes	No	No
45. *Gliscolithus amitakarenae* Norris 1985	No	Yes	No	No	No
46. *Homozysosphaera vercellii* Borsetti and Cati, 1979	Yes	No	No	No	No
47. *S. dalmaticus* (Kamptner 1927) Loeblich and Tappan 1963	Yes	No	No	Yes	No
48. *S. quadriperforatus* (Kamptner 1937) Gaarder 1962	Yes	Yes	No	Yes	No
49. *Syracolithus confusus* Kleijne 1991	Yes	No	No	No	No
50. *Zygosphaera hellenica* Kamptner 1937	Yes	No	No	Yes	No

Table 3.4 *Estimated annual coccolith flux (coccoliths m^{-2} yr^{-1}) in the sediment trap (extrapolated by 926-day deployment) and surface sediments, and relative abundances (%) of the main coccolithophore species in the sediment trap and surface sediments*[a].

	Coccolith species abundance (%)				
	Sediment trap[b]	Boxcore UM15[c]	Boxcore UM26[d]	Boxcore UM35[e]	Boxcore MT6[f*]
C. leptoporus	1.61	<1	<1	<1	1.34
D. tubifera	<1	1.72	2.90	1.06	<1
Reticulofenestra "overcalcified" sp.	<1	4.58	31.10	19.84	3.32
E. huxleyi	82.22	68.19	28.10	57.14	55.52
F. profunda	5.28	9.16	12.98	5.17	9.03
G. flabellatus	<1	1.15	2.48	<1	<1
G. oceanica	<1	<1	<1	<1	1.34
H. carteri	3.06	<1	<1	<1	1.67
N. coccolithomorpha	<1	3.72	4.99	5.03	0.00
Oolithothus spp.	<1	<1	1.14	<1	<1
R. clavigera	1.07	<1	<1	2.38	0
R. xiphos	<1	2.01	2.17	1.85	0
S.pulchra	<1	<1	2.57	1.59	<1
Syracosphaera .spp.	3.92	1.15	1.29	<1	1.67
S. fossilis	<1	2.01	1.63	<1	0
U. tenuis	<1	1.15	1.61	<1	1
U. sibogae	<1	<1	2.03	<1	1
Holococcoliths	<1	<1	2.41	1.32	<1

[a] *MT6 = boxcore located in anoxic environment.*
[b] *Annual coccolith flux (number per m^{-2} y^{-1})=1.0×10^{10}.*
[c] *Annual coccolith flux (number per m^{-2} y^{-1})=1.0×10^{10}.*
[d] *Annual coccolith flux (number per m^{-2} y^{-1})=2.31×10^{9}.*
[e] *Annual coccolith flux (number per m^{-2} y^{-1})=5.87×10^{9}.*
[f] *Annual coccolith flux (number per m^{-2} y^{-1})=3.9×10^{10}.*

3.4.2 Factors controlling the temporal and spatial variability of coccolithophores, and the transfer processes to the deep Mediterranean waters

The particle flux in the ocean is mainly controlled by biological processes, occurring in the upper ocean, and by eolian and riverine input. Our work suggests that, in the central eastern Mediterranean, these two main particle flux sources of biogenic and lithogenic origin are primarily controlled by coccolithophore production and Saharan dust input, respectively.

Satellite derived, 7-year average (1979 – 1985), monthly surface pigment concentrations were estimated using data collected by the Coastal Zone Color Scanner (CZCS) (courtesy of the Joint Research Centre, European Commission/European Space Agency) and show an annual variation in primary production (Fig. 3.6). The pigment concentration record is used as a proxy for surface primary productivity and is very similar from year to year. In the eastern Mediterranean, the overall pigment concentrations are low when compared to other oceanic basins, even during the high-productivity season, and most of the production occurs in the period from December to March.

Sea surface temperatures (SST) were derived from Advanced Very High Resolution Radiometer (AVHRR) data for the study period (November 1991 to August 1994) and have

been generated using weekly composite AVHRR data for the Bannock Basin trap location (Fig. 3.6). The sea surface temperature varies between 15 and 28˚C at Bannock Basin, with highest temperatures in summer and fall (Fig. 3.6). The average SST in the summer and winter of 1994 appears to be 1˚C higher than those in 1992 and 1993.

Massive airborne plumes of desert dust from Sahara are exported to the Mediterranean all year long (Bergametti et al., 1989; Moulin et al., 1997). Although dust concentrations in the Mediterranean atmosphere and chlorophyll concentrations correlate negatively, there are differences between the dry and wet dust deposition. In the Mediterranean, wet dust deposition contributes 65 – 80% to the total dust deposition (Molinaroli et al., 1993). Because precipitation only occurs in winter, most of the yearly dust deposition to the sea water occurs in this period. A relationship between dust input and primary production was shown by the results of the Ironex II program, which established physiological limitation of phytoplankton

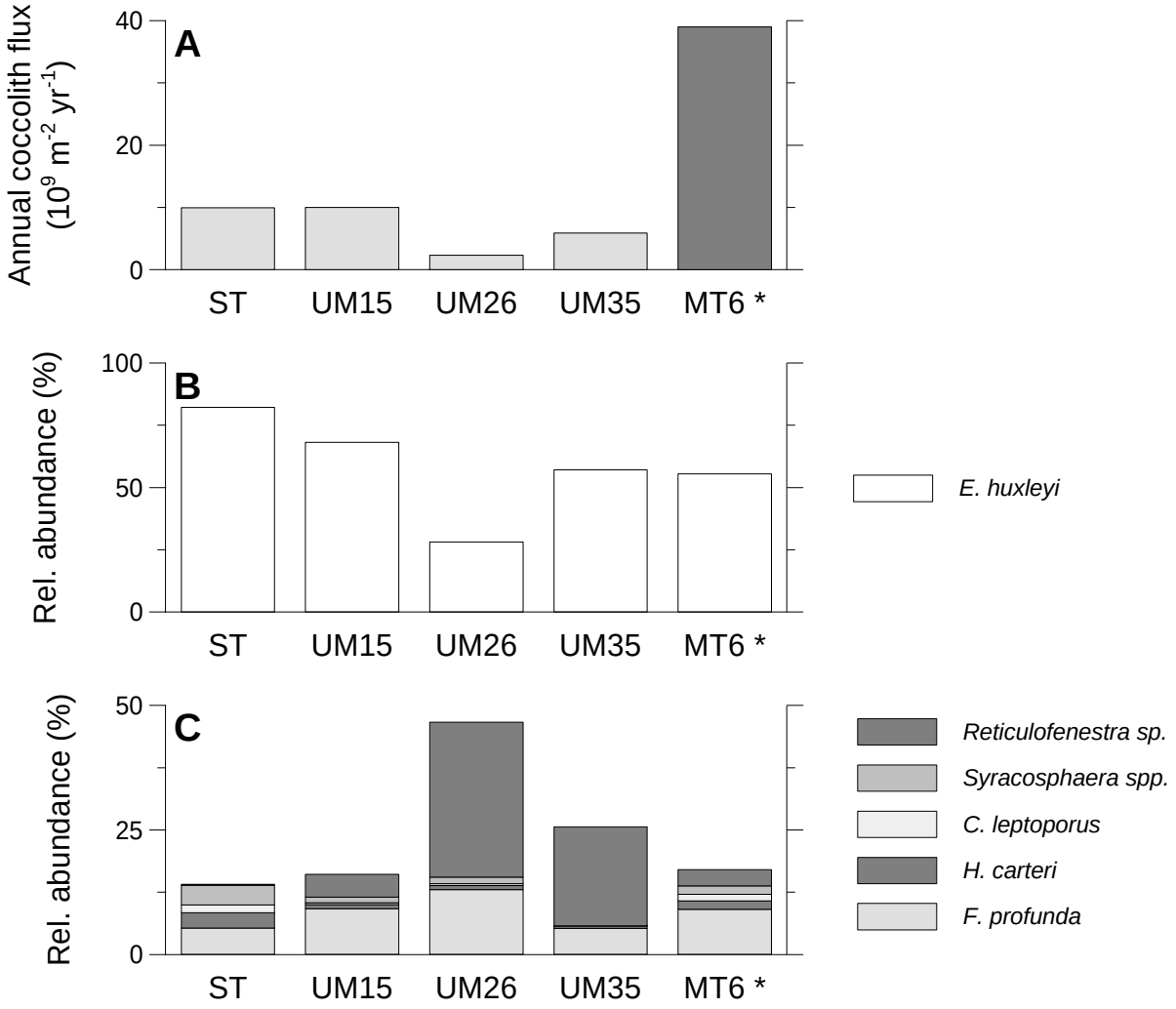

Figure 3.4 *Comparison of sediment trap (ST) and surface sediment (boxcores MT6, UM15, UM35 and UM26) results: A) Annual coccolith flux (number m^{-2} yr^{-1}); B) Relative abundance (%) of E. huxleyi; C) Relative abundance (%) of the major coccolith species excluding E. huxleyi.*

by iron as the cause of the high nutrient, low chlorophyll phenomenon at eastern equatorial Pacific Ocean (Martin et al., 1994; Behrenfeld et al., 1996). We are aware of the fact that phosphorus, not iron, is the limiting nutrient in the eastern Mediterranean (Krom et al., 1991; Zohary and Robarts, 1998), but the atmospheric source can also contribute phosphorus to the photic zone, as was shown for the western Mediterranean (Bergametti et al., 1992). Because *E. huxleyi* is an excellent competitor for phosphorus (Riegman et al., 1998), increases in production of this most abundant coccolithophore species are expected in P-controlled systems such as the eastern Mediterranean.

Our work on particle fluxes in Bannock Basin suggests that the productivity pattern could be the result of fertilisation in the upper euphotic zone. The increase in pigment concentration is observed when both wind-induced oceanographic changes from a summer stratified upper water mass to a deep winter mixing (Krom et al., 1992) and wet deposition of Saharan dust occur (compare also Figs. 3.2 and 3.6).

The vertical stability of the water column may play a vital role in determining the productivity of Bannock surface waters. The breakdown of this stability is most important in initiating the late fall increase in plankton production. Coincident with the changes in winds that occur in late fall, surface waters begin to cool and evaporation is highest at this time. Nutrients are scarce in the Mediterranean compared with the rest of the world ocean, because the main input comes from the surface waters of the Atlantic through the Strait of Gibraltar. As a consequence, the central eastern Mediterranean is characterised by an extremely oligotrophic regime (Berland et al., 1988; Dugdale and Wilkerson, 1988).

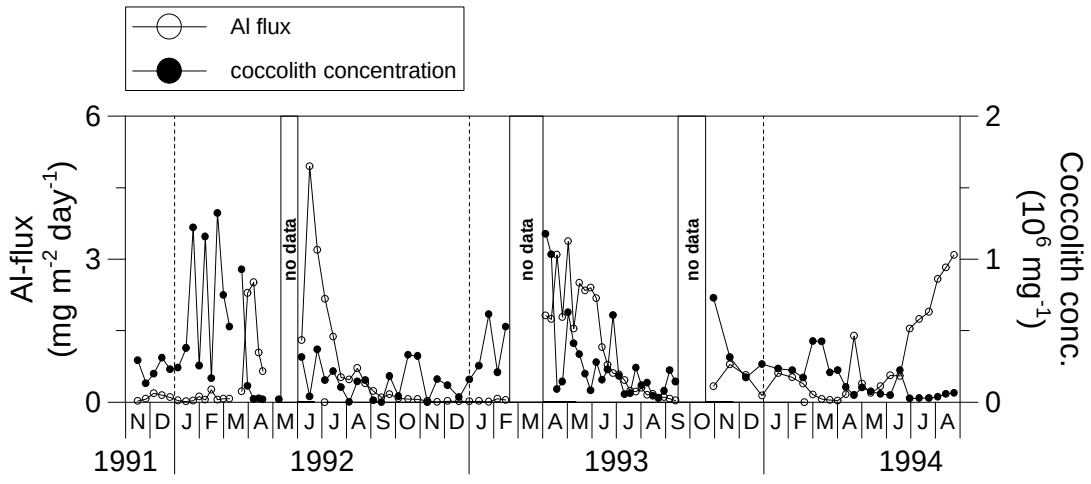

Figure 3.5 *Flux record for Al (mg m^{-2} day^{-1}) and coccolith concentration (number mg^{-1}).*

The trap station in Bannock basin is located in the Ionian Sea province of Antoine et al. (1995) in which the winter bloom, as revealed by CZCS, coincides with the breakdown of stratification, and it is of moderate intensity because the nutrient levels are never high. Zohary and Robarts (1998) concluded that phosphorus was the primary limiting nutrient when other factors (such as light and grazing) did not control microbial biomass or activity.

The coccolith and coccosphere sinking rates were calculated from the time lag between

associated pigment maxima at the sea surface (Fig. 3.6) and the coccolith/coccosphere flux maxima in the trap samples and the vertical distance (3000 m). The coccolith sinking rates are very low, ranging from 17 – 25 m day^{-1} (average time-lag of 4 to 6 months). In contrast, maximum fluxes of coccospheres were recorded mostly from January to April indicating that the time-lag between maximum primary production and maximum export flux at 3000 m water depth was about 1 month. Consequently, it appears that in the eastern Mediterranean, coccospheres sink individually with a rate of approximately 100 m day^{-1}. This settling speed concords with the previous estimations of the sinking speed of particles through the water column (Honjo, 1982; Neuer et al., 1997). Therefore, a possible indicator for primary production in the sediment trap located in the oligotrophic waters of the eastern Mediterranean might be the occurrence of high coccosphere fluxes. However, the contribution of intact coccospheres to the total coccolith flux is relatively small in comparison to the settling flux of individual coccoliths probably associated with small-sized macroaggregates and fecal pellets (considering also that grazing activity and organic matter production is very low in the central eastern Mediterranean). The coccosphere-coccolith flux ratio ranges from 0 to 5.8×10^{-3} (average 5.1×10^{-4}). Individual coccoliths may have been resuspended and redeposited from the shelf into the deep sea, through currents and winds. In contrast, intact coccospheres disintegrate relatively rapidly after the cell dies and are rarely found in sediments. Consequently, the occurrence of coccospheres directly refers to overlying surface water productivity whereas coccoliths may also have a different origin (e.g. compare Figs. 3.2B and 3.2C for January to March 1992).

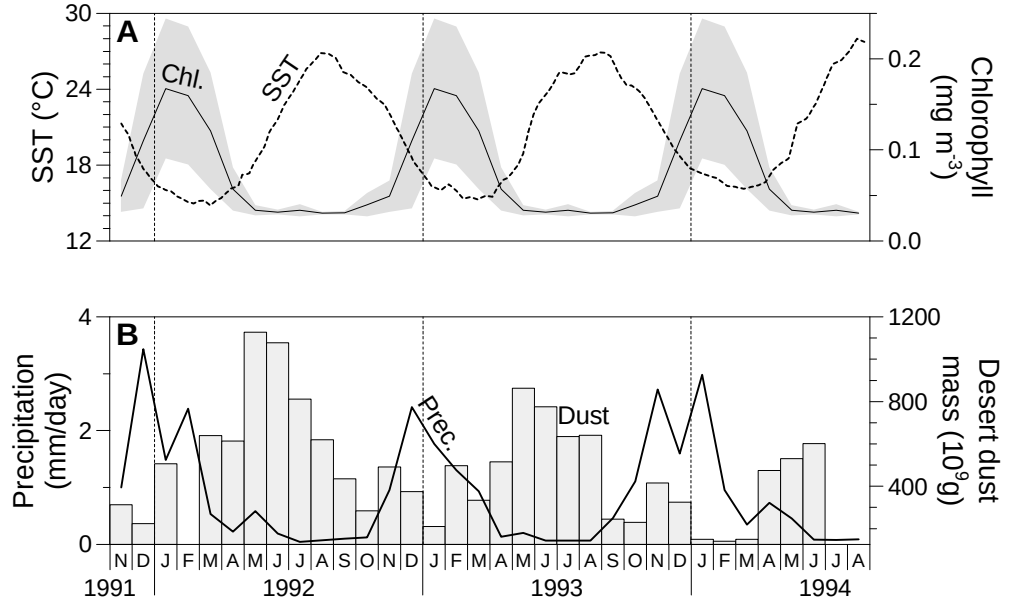

Figure 3.6 *Satellite observations: A) Monthly averaged pigment concentrations observed for the period 1979 to 1985 derived from CZCS data (solid line) at the trap location, with the gray area indicating the 1σ standard deviation for each month, and the weekly composite AVHRR sea surface temperature record at the trap location during the deployment period (dashed line). B) Precipitation at the trap location (line) and desert dust mass over the Mediterranean (bars) during the deployment period. The dust data were redrawn after Dulac et al. (1996).*

3.4.3 Flux patterns of Coccolithophore species

The most abundant and cosmopolitan coccolithophorid species, *Emiliania huxleyi*, largely dominates the observed assemblage of the fifty coccolithophore species recorded in the trap samples (38 heterococcolith and 12 holococcolith species; Fig. 3.3; Tables 3.3, 3.4). The seasonal trend recorded in coccolith species fluxes is mainly driven by changes in the flux of this species, a dominance of this species already observed in the Mediterranean surface waters by Knappertsbusch (1993) and Kleijne (1993).

The high correlation (r = 0.90) between *E. huxleyi* and the deep-dwelling species *Florisphaera profunda* suggests coccolithophore production throughout the water column. *F. profunda* is restricted to the lower euphotic zone in low-middle latitude regions (Okada and Honjo, 1973), and changes in the *F. profunda* abundance through time have been used as a proxy to model palaeonutricline dynamics (Molfino and McIntyre, 1990). The inverse relationship between the *F. profunda* flux and the diatom export production shows that *F. profunda* is inversely related to the intensity of upwelling (Jordan et al., 1996; Ziveri and Thunell, 2000). The relative abundance of *F. profunda* in the coccolith assemblages of eastern Mediterranean sapropelitic sediments has been used to infer palaeonutricline dynamics (Castradori, 1994).

Coccolith fluxes of *Helicosphaera carteri* and *Calcidiscus leptoporus* show a similar seasonal trend (r = 0.79) and abundance (Fig. 3.3). This similarity was previously observed in the Quaternary sediments from the North Atlantic and in sediment trap samples from the Southern California Bight and Gulf of California (Gard, 1989; Ziveri et al., 1995, Ziveri and Thunell, 2000). In the Southern California Bight, the highest fluxes of the two species were associated with low to intermediate nutrient concentrations prior to upwelling when total coccolithophore productivity was high. In the Gulf of California both species tend to decrease when the zooplankton grazing pressure increases.

The *Syracosphaera* spp. fluxes represent all of the *Syracosphaera* species recorded in Bannock Basin except *S. pulchra* and *S. histrica*, which have a very low abundance in our samples. The fluxes of *Syracosphaera* spp. show a seasonal signal comparable to *C. leptoporus* and *H. carteri* (Fig. 3.3). The remaining coccolithophore species account for approximately 3.7% of the total assemblage. *Umbellosphaera tenuis* and *U. irregularis* have seasonal trends similar to that of *H. carteri* (Fig. 3.3). Both species are typical of warm, tropical-subtropical waters (McIntyre et al., 1970). The Rhabdospheraceae represents only a small part of the species recorded in the present study and are present as *D. tubifera* and *R. clavigera* ad *R. xiphos*. Okada and McIntyre (1979) have described *D. tubifera* and *R. clavigera* as warm water species of the upper water layers. These two species have a subtropical temperature preference, of which *R. clavigera* (3 – 29ºC) has a wider temperature range than *D. tubifera* (optimum 21 – 29ºC; total range 14 – 30ºC). *D. tubifera* is more abundant in oligotrophic water conditions, occurring outside the upwelling areas and has also been described in the warmer areas of the eastern Mediterranean (Kleijne, 1993). In our study, *D. tubifera* is always less than 3% of the coccolith assemblage, but is remarkable in that the increase in both fluxes and relative abundance during the last sampling year (1994) is associated with a low coccolith flux and SST being a few degrees higher than the previous

sampling years. *Scyphosphaera apstenii*, *Umbellosphaera tenuis* and holococcoliths show the same increase during 1994.

3.4.4 Comparison of sediment trap and surface sediment results (Pl. 3.1 and 3.2)

The importance of coccolith calcite in the eastern Mediterranean deep-sea sediments has been established previously (Bernard & Lecal, 1953; Milliman and Muller, 1973). Coccolithophores are the most abundant primary producers that are being preserved in surface sediments in the eastern Mediterranean. This is confirmed by our results on particle fluxes in Bannock Basin, where coccoliths constitute the major part of the biogenic component.

The coarse-size fraction of the biogenic particle flux, including foraminifers, pteropods, and radiolarians, has not been quantified in the trap samples. However, during the analyses of the complete fraction aliquot under both binocular microscope (400×) and LM, it was noted that this fraction was consistently very low. In Bannock Basin, coccolithophores are the dominant phytoplankton group that manufactures a skeleton, and together with calcareous dinoflagellates (mainly *Thoracosphaera heimii*) are also the major contributors to the biogenic carbonate flux. In contrast, in the surface sediment, the >32 μm fraction constitutes approximately 25% of the bulk sediment and contains about 75% biogenic carbonate (mainly foraminifers and pteropods; Plate 3.2) (Chapter 2).

There is no evidence of carbonate dissolution in the trap samples collected at 3000 m water depth in Bannock Basin. The preservation of delicate coccoliths such as *Oolithothus fragilis, Discosphaera tubifera* and *Umbilicosphaera* spp. (Roth and Berger, 1975; Schneidermann, 1977) is very good. Perfectly preserved spines of foraminifers were also detected suggesting a good carbonate preservation.

The rest of the flora consists of diatoms and silicoflagellates. They show a flux pattern similar to coccoliths (Ziveri et al., in prep.). The fauna is poorly represented by radiolarians and planktic foraminifers, the latter mainly as juvenile forms. The occurrence of mainly juvenile foraminifers is probably due to the combination of two factors. Firstly, extremely oligotrophic conditions seriously hampers heterotrophic production in the eastern Mediterranean (Turley, 1997). Secondly, the small size of juvenile foraminifers (approximately 20 – 60 μm) allows for easy lateral transport from higher production areas to the Bannock Basin site.

The carbonate content of sediment trap samples and surface sediment samples shows large regional variations. The carbonate content in the trap resembles that found in boxcore MT-6, but is much lower that in the other boxcores. Aluminium correlates inversely with coccolith concentrations (coccoliths mg^{-1}), suggesting the dilution of coccolith carbonate by terrigenous input (Fig. 3.5).

The annual coccolith flux obtained by the sediment trap at 3000 m is comparable to the coccolith accumulation rates of the aerobic surface sediment of boxcore UM15 and is about one third of the coccolith accumulation rate calculated in the anaerobic surface sediment of Bannock Basin (MT6) (Fig. 3.4). Differences with a similar order of magnitude have been obtained by the comparison of the coccolith fluxes in the two traps in the aerobic (this chapter) and anaerobic water conditions (Ziveri et al., 1996). The main difference

between the coccolith assemblages of sediment trap and surface sediment samples is the presence of *Reticulofenestra* "overcalcified" sp. in the surface sediment. Because this species has a very low abundance in the sediment trap, we conclude that, in combination with the same trend for the large-size fraction (high in surface sediments, low in the sediment trap), the long-term variability in faunal and floral assemblages is not captured by the sediment trap, possibly due to irregular blooms (see also Chapter 2).

3.5 Summary and conclusions

This work, concentrating on coccolithophores and thoracosphaerid fluxes as the major contributors to the biogenic carbonate flux recorded at 3000 m in the oligotrophic waters of the central eastern Mediterranean Sea, has shown that:

1. A strong seasonal variation in the total mass flux is recorded by the total coccolith and coccosphere flux, with maximum fluxes occurring in late winter and spring.
2. The annual coccolith flux of 1.0×10^{10} coccoliths m^{-2} yr^{-1} measured in the deep waters at 3000 m water depth is much lower than most published data recorded in other oceanographic settings, even when corrected for the trap efficiency (23%).
3. The biogenic and lithogenic fluxes are primarily controlled by coccoliths and Saharan dust input, respectively.
4. The calculated coccolith and coccosphere settling speeds estimated from the comparison of maximum pigment concentration at the sea surface and maximum flux at 3000 m water depth were 17 to 25 m day^{-1} for coccoliths and 100 m day^{-1} for coccospheres.
5. *Emiliania huxleyi* and *Florisphaera profunda*, followed by *H. carteri* and *C. leptoporus*, are the dominant coccolith species in sediment trap samples as well as surface sediments. *Reticulofenestra* "overcalcified" sp. is a major species in the surface sediments only. This anomaly is comparable to that observed for the large-size (>32 μm) fraction, which is nearly absent in the sediment trap, but abundant in surface sediments. Both might be related to long-term differences in faunal and floral assemblages, possibly due to irregular blooms.

Acknowledgements – P.J.M. van Santvoort, G. Nobbe and H. de Waard are thanked for their analytical assistance. We are greatful to Agostino Rizzi, (University of Milan) and Saskia Kars (Vrije Universiteit Amsterdam) for operating the SEM. The chapter benefited greatly from comments by E. Erba and R. Thunell. The pigment data are courtesy of the Joint Research Centre (European Commission / European Space Agency). The SST data were extracted from the Weekly NCEP SST Database at the NOAA/WRC Server *Ferret* and the precipitation data from the GPCP Global Combined Precipitation Dataset (part of the Climatology Interdisciplinary Data Collection). This study was supported by MARFLUX (MAST1-90022C), PALAEOFLUX (MAS2-CT93-0051) and SAP (MAS3-CT97-0137) European programmes.

This is Netherlands Sedimentary Research School (NSG) contribution 990309.

Plate 3.1 *Sediment trap samples*

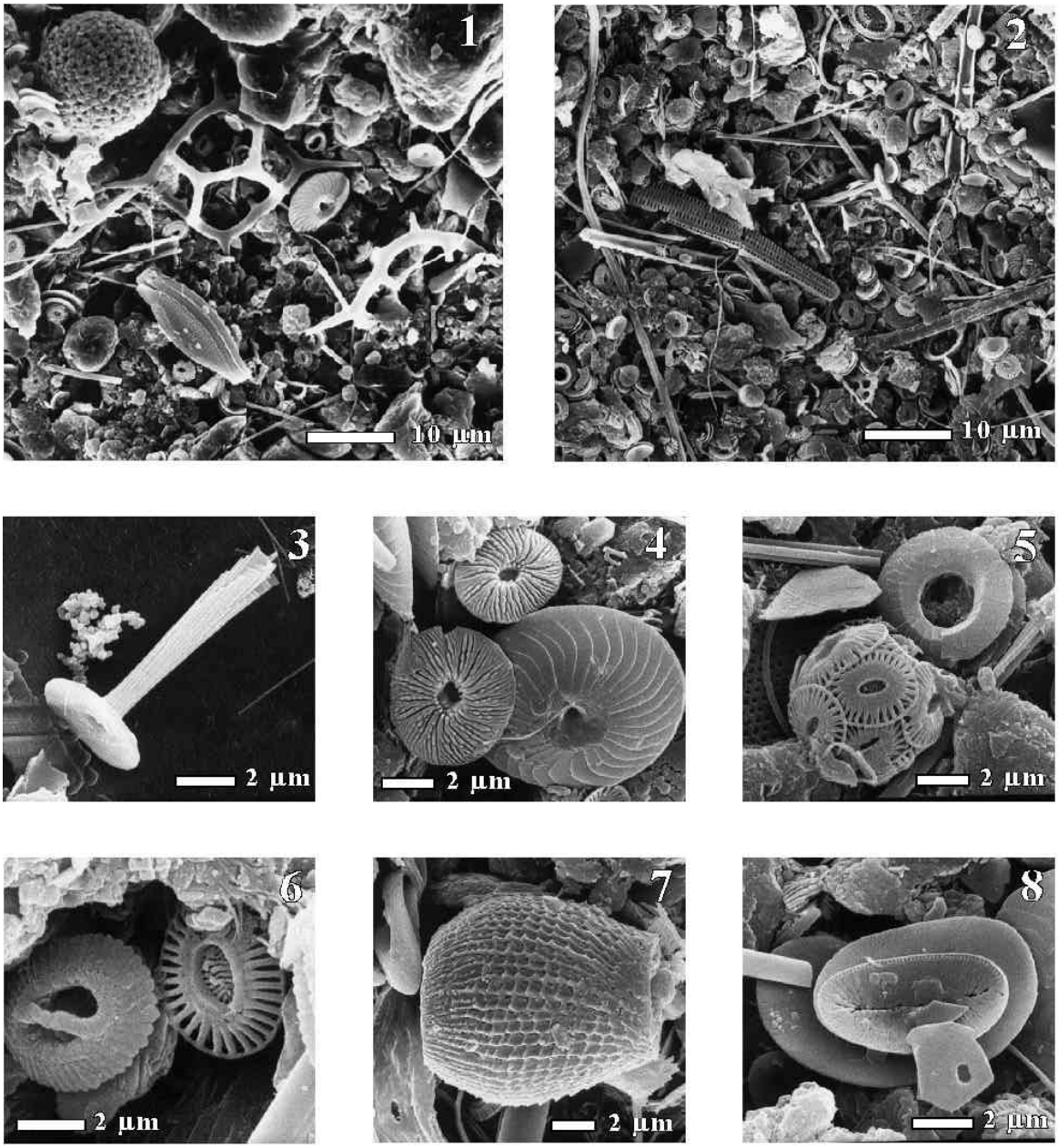

1. Assemblages of sample MT4O-1
2. Assemblages of sample MUB-1
3. *Rhabdosphaera clavigera* var. *clavigera*, rhabdolith, (sample MT4O-18)
4. *Umbilicosphaera tenuis*, umbelloliths, and *Calcidiscus leptoporus*, distal view of the distal shield, (sample MT4O-16)
5. *Emiliania huxleyi*, coccosphere, and *Umbilicosphaera sibogae*, distal view of the distal shield, (sample ST2-20)
6. *Emiliania huxleyi* and gephyrocapsid, distal view of the distal shields (sample MT4O-1)
7. *Syracosphaera apstenii*, lopadolith, (sample MUB-10)
8. *Helicosphaera carteri*, proximal view of coccolith, and *F. profunda*, coccolith, (sample MUB-1)

Plate 3.2 *Surface sediment samples*

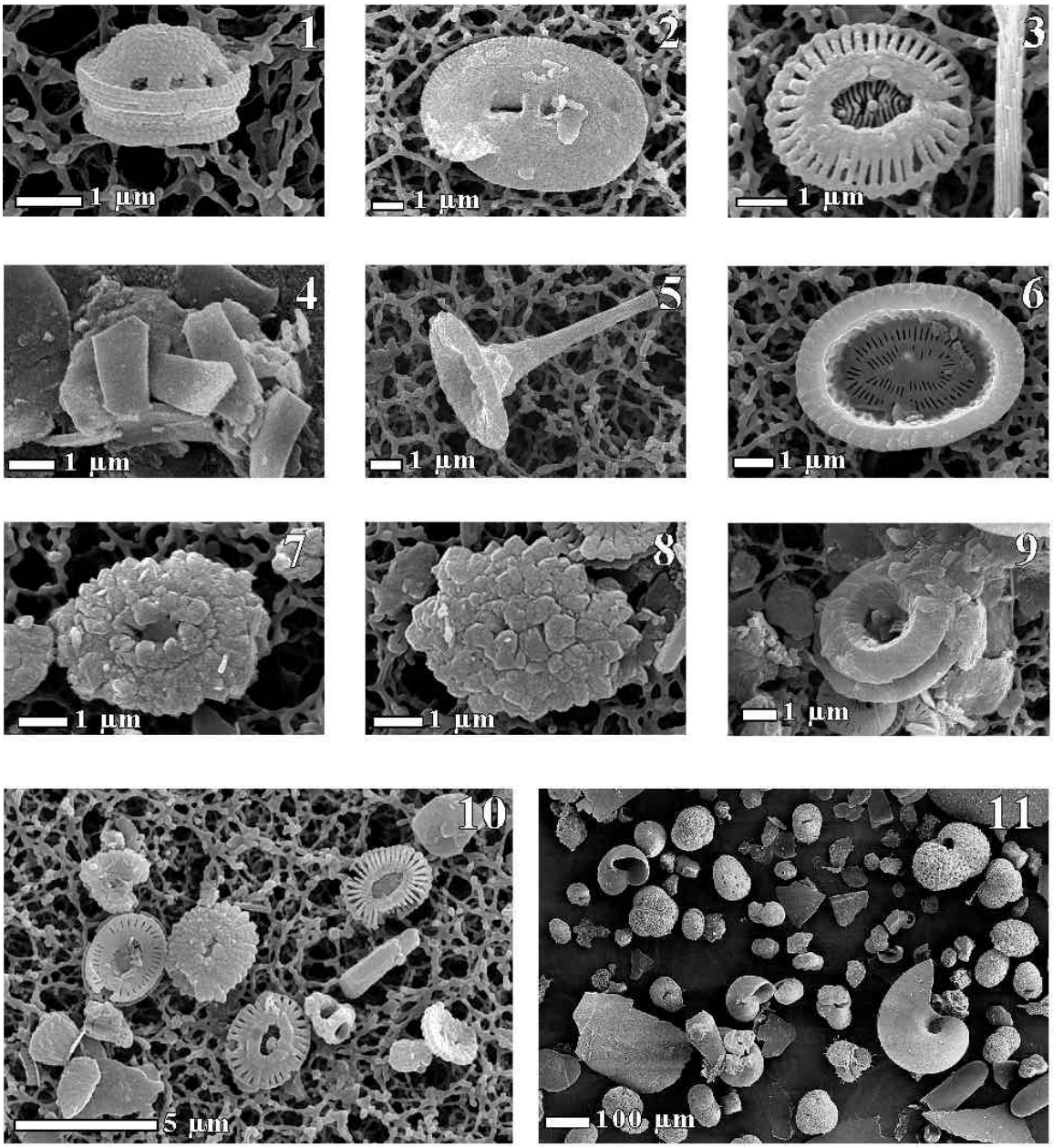

1. *Calyptrosphaera pirus*, areolith, (sample UM15 <32 µm)
2. *Helicosphaera carteri*, distal view, (sample UM35 <32 µm)
3. *Emiliania huxleyi*,. distal view, (sample UM26 <32 µm)
4. *Florisphaera profunda* coccoliths, (sample MT6)
5. *Discosphaera tubifera*, rhabdolith, (sample UM35)
6. *Syracosphaera pulchra*, caneolith, distal view, (sample UM35)
7. *Reticulofenestra* "overcalcified" sp., distal view, (sample UM26 <32 µm)
8. *Reticulofenestra* "overcalcified" sp., distal view, (sample UM26 <32 µm)
9. *Umbilicosphaera sibogae*, distal view, (sample UM15 <32 µm)
10. Assemblages of sample UM15 <32 µm
11. Assemblages of sample UM15 >32 µm

Appendix 3-A

The anoxic boxcore MT6 has an almost ideal ^{210}Pb profile (Fig. 3-A.1) from which the mass accumulation rate can be determined. Mean porosity is taken into account in the boxcore for the calculation of the average linear sedimentation rate from the mass accumulation rate. The determined mass accumulation rate is 166.0 mg m^{-2} day^{-1}. The average dry bulk density is 0.429 g cm^{-3}. Dividing the mass accumulation rate by the dry bulk density gives an average linear sedimentation rate of 14.1 cm kyr^{-1}.

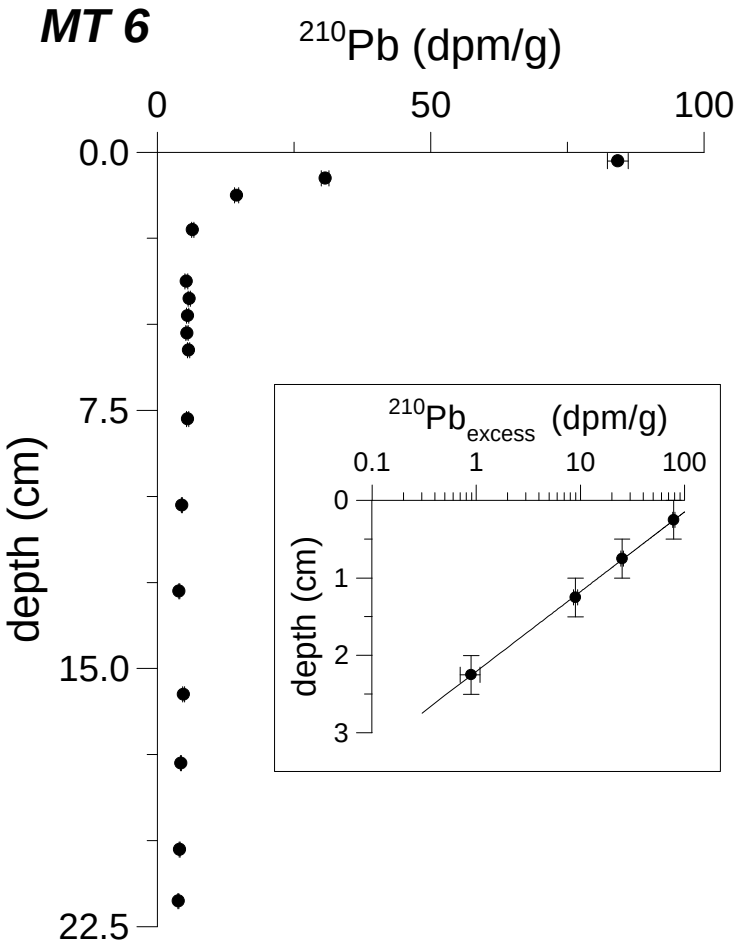

Figure 3-A.1 *Pb-210 (dpm/g) vs. depth in boxcore MT6.*

Chapter 4

Deposition of sapropel S1 sediments in oxic pelagic and anoxic brine environments in the eastern Mediterranean; differences in diagenesis and preservation*

Abstract – Sediments from a boxcore in the previously anoxic brine-filled Poseidon Basin, eastern Mediterranean, have been studied and compared to sediments deposited in a normal eastern Mediterranean environment. The boxcore can be divided into three main sedimentary intervals based on AMS-radiocarbon ages, foraminiferal and geochemical zonations. From the base of the core upwards these are 1) 12.3 – 31.2 cm: Organic-rich sediment redeposited from within the brine; 2) 6.6 – 12.3 cm: Sediment containing a cold foraminifera fauna redeposited from above the brine into the basin while the brine was still present; 3) 0 – 6.6 cm: Oxic pelagic sediment accumulated since the reoxygenation of Poseidon Basin which occurred about 1800 yrs BP. Near the base of the latter unit, a Mn oxide peak has formed and marks the present boundary between oxic and suboxic environments. A progressive downward oxidation front, which is usually found in normal sapropel S1 sediments, has never formed in Poseidon Basin sediments. This has resulted in the preservation of the relationship between organic carbon and organic-related trace elements e.g. Se in the organic-rich sediments of Poseidon Basin, whereas such a relationship has been obliterated in normal sapropel S1 sediments. On the basis of the carbonate content as well as the Sr/Ca ratio** , preservation of carbonates appears to be better in the brine sapropel sediments of BC15 than it is in normal sapropel S1 sediments. The high opal content of BC15 shows that biogenic opal is also much better preserved. The overall lower C_{org} / Ba ratio in BC15 suggests a better preservation of barite relative to that of organic carbon in shallow brine sediments*** , but is as yet inconclusive for the organic carbon preservation potential of brine relative to normal unoxidised sediments.

---

* This chapter has been published as: A. Rutten, G.J. de Lange, A. Hayes, E.J. Rohling, A.F.M. de Jong and K. van der Borg, 1999, *Marine Geology*, 153, 319-335.

** Continuing research (Chapter 7) shows that the Sr/Ca ratio is not conclusive regarding differences in the carbonate preservation between normal and brine sediments.

*** Further research (Chapter 6) reveals that the relationship between biogenic Ba and organic carbon is the same in normal and brine sediments. The apparent difference in preservation of barite is caused by total-Ba rather than barite-Ba being plotted against organic carbon. A relatively lower contribution of clay-bound Ba in the brine sediments causes total Ba to be relatively lower for a certain C_{org} value compared to normal sediments.

4.1 Introduction

A common feature in eastern Mediterranean sediments is the occurrence of marked intervals enriched in organic matter (sapropels). Sapropels were originally defined by Kidd et al. (1978) as "discrete layers, greater than 1 cm in thickness, set in open marine pelagic sediment and containing greater than 2% organic carbon." Visually detected 'sapropels' do not always contain that amount of organic carbon. We have, therefore, adopted the definition of Van Santvoort et al. (1996), who define sapropels as distinct sediment layers with a organic carbon content that is significantly higher than that of the surrounding hemipelagic sediment and being deposited in an open marine environment. The youngest sapropel has been labelled S1 (Cita et al., 1977) and has been deposited between 5000 and 9000 years ago (Troelstra et al., 1991; Thomson et al., 1995; Van Santvoort et al., 1996). This sapropel is being subjected to diagenesis because of the diffusion of oxygen into its uppermost reaches, thus oxidising organic matter and giving rise to extensive remobilisation of redox-sensitive metals (De Lange et al., 1989; Pruysers et al., 1993; Higgs et al., 1994; Thomson et al., 1995; Van Santvoort et al., 1996). Burn-down of the sapropel occurs when the oxygen flux into the sediment is larger than the upward flux of reduced species that can be oxidised (Van Santvoort et al., 1996). As a consequence, this excess oxygen is used in the oxidation of the previously anoxic sapropelic sediments. Oxidation of the youngest sapropel develops distinct metal profiles, not only above, but also within the sapropel (see e.g. Fig. 1.2 in Chapter 1). This results in a change of the total composition of the initial, now oxidised, sapropel sediment as well as of the remaining, unoxidised, sapropel (Higgs et al., 1994; Thomson et al., 1995; Van Santvoort et al., 1996).

In recent years, some brine-filled basins with persisting anoxic conditions, e.g. Tyro, Bannock, Urania, Atalante and Discovery (Jongsma et al., 1983; De Lange and Ten Haven, 1983; Scientific Staff of Cruise Bannock 1984-12, 1985; MEDRIFF Consortium, 1995) have been discovered in the eastern Mediterranean. Two previously brine-filled basins, Kretheus and Poseidon, have been found in the Tyro Basin area (Fig. 4.1). Completely anoxic sediments have been reported for Tyro Basin (e.g. Troelstra, 1987), whereas a small oxic layer has been found lying on top of an anoxic sequence in Kretheus Basin (Troelstra, 1987) and Poseidon Basin. Organic matter is thought to be preserved better in anoxic brine basins, containing 2 mM H_2S (Luther et al., 1990), than it is in oxic, pelagic sediments, although Calvert and Pedersen (1992) have argued that organic carbon preservation in anoxic environments is not significantly different from that in oxic sediments. The occurrence of perfectly preserved radiolarians and of sulphate reduction in anoxic brine sediments but not in contemporaneous normal pelagic sediments in the eastern Mediterranean suggests that biogenic silica and reactive organic matter are preferentially preserved in these brine sediments, assuming similar inputs to these two basin types (Björklund and De Ruiter, 1987; Troelstra, 1987; Aghib, 1996; Henneke et al., 1997).

In this study, we compare new data on brine sediments with those on normal hemipelagic sediments from the same region and time interval, namely Holocene eastern Mediterranean sediments which include the S1 sapropel. We thereby use a multi-disciplinary approach, i.e. geochemical, micropalaeontological and radiometric methods. This will permit

us to establish potential changes from initial deposition to present-day recovery, hence preservation *vs.* removal mechanisms. Our new data indicate no alteration of the initial composition of S1-aged (former) brine sediments, whereas normal sapropel S1 sediments have undergone severe changes in composition due to burn-down.

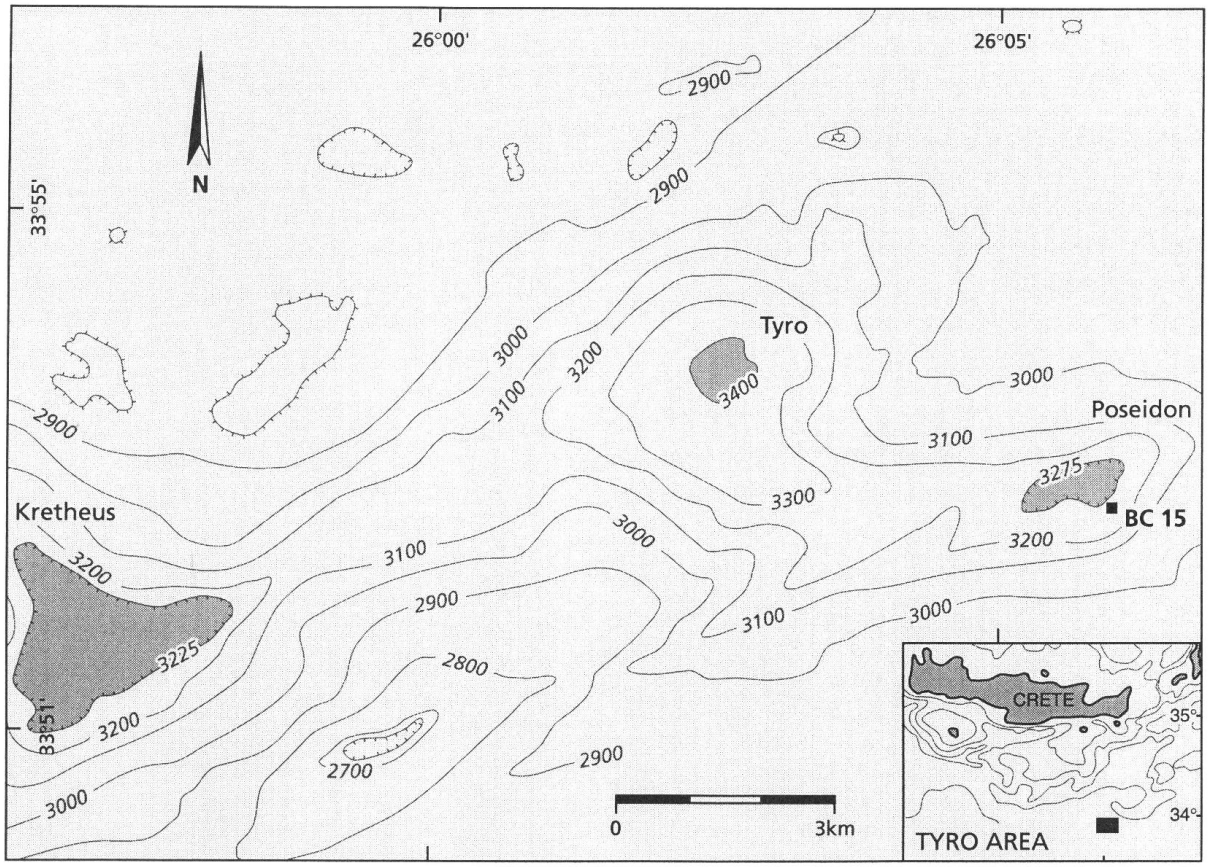

Figure 4.1 *The Tyro Basin area and its location with respect to Crete. The location of BC15 is marked.*

4.2 Material and methods

4.2.1 Sediment

During the 1991 MD69-Marflux cruise with R.V. *Marion Dufresne* boxcore BC15 (33˚51.4'N, 26˚05.5'E) was collected in Poseidon Basin at 3232 m water depth (Fig. 4.1). The recovered sediment column of 31.2 cm consists of hemipelagic, pteropod-rich mud (unit 1, 0 – 5.4 cm) overlying a dark-brown zone (unit 2, 5.4 – 6.6 cm), a cream-brownish layer (unit 3, 6.6 – 8.7 cm) and a coarse foraminifera ooze (unit 4, 8.7 – 12.3 cm). The sediment below 12.3 cm (unit 5) is heterogeneous in colour (dark grey / black-green / brown; Fig. 4.2A).

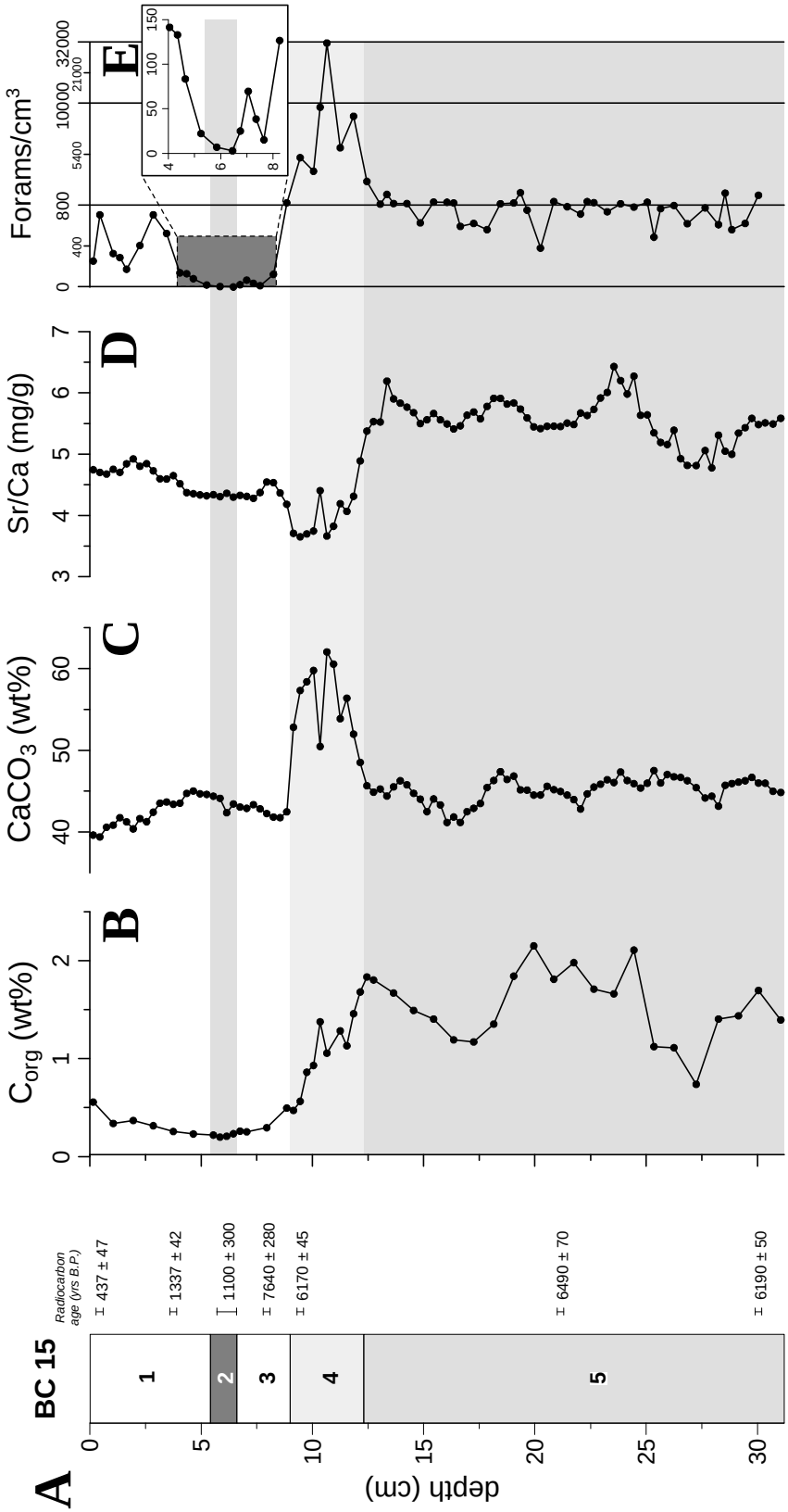
A
BC 15
Radiocarbon age (yrs B.P.)
437 ± 47
1337 ± 42
1100 ± 300
7640 ± 280
6170 ± 45
6490 ± 70
6190 ± 50
1
2
3
4
5
depth (cm)
B
Corg (wt%)
C
CaCO3 (wt%)
D
Sr/Ca (mg/g)
E
Foams/cm3

4.2.2 Sampling and chemical analysis

Pore water was extracted from one of the BC15 subcores following a shipboard routine (De Lange, 1992a). After two years of cold storage at 4˚C another subcore was divided into 3 mm thick slices. One half of each slice was dried at 50˚C and finely ground in an agate mortar, whereas the second half was kept for micropalaeontological studies (see below). Of each dried sample, 250 mg were digested in a mixture of hydrofluoric, nitric, and perchloric acids, and the digest was subsequently vaporised to dryness in Teflon® bombs. Final solutions were made in 1 M HCl and were analysed with an inductively coupled plasma atomic emission spectrometer (ICP-AES; ARL 34000) for Al, Ba, Ca, Fe, Mn, Sr, Ti and Zr. The quality of the analyses was monitored by the inclusion of in-house and international standards and precisions were always better than 2%. In addition, remeasurement (ICP-AES; Perkin Elmer Optima 3000) of some samples of this study and of Van Santvoort et al. (1996) in the same batch gave the same numbers for Ba. Consequently, observed differences (Fig. 4.8A) cannot be related to possible instrumental or measurement artifacts between the two series. In the same digest Se was measured by hydride generation AAS using a Perkin Elmer 3100 AAS in combination with a Perkin Elmer FIAS mercury/hydride chemifold and an XYZ autosampler.

The organic carbon content of dried samples was determined by first decalcifying the samples with 1 M HCl, then by oxidising the sample at 900˚C in a CuO oven and separating the evolved CO_2 cryogenically in a closed system. The pressure of the CO_2-gas in a fixed volume at room temperature is a measure for the organic carbon content of the sample. Included standards give a reproducibility better than 6%.

Total opal contents were measured using the automated leaching method described by Müller and Schneider (1993), and its reproducibity is better than 10%.

After appropriate dilution, the squeezed pore waters were analysed in Utrecht for Mn^{2+} and Fe^{2+} using a Perkin Elmer 4100 ZL Zeeman AAS. All samples were measured in triplicate. Reproducibility was better than 4% for Mn and better than 8% for Fe.

A sequential extraction was performed to determine the speciation of manganese and iron phases. This procedure consisted of eight steps: 250 mg of dried and ground sediment were subsequently extracted with: (1) 25 ml of a 1 M $MgCl_2$ solution (pH 8; absorbed ions; Ruttenberg, 1992); (2) 25 ml 2 M NH_4Cl (2× pH 9, 2× pH 8, 2× pH 7.5, 3× pH 7 respectively; carbonates; De Lange, 1992b; De Lange et al., 1994); (3) 25 ml of an ascorbic acid/sodium bicarbonate/sodium citrate solution (pH ~ 8; amorphous oxides; Kostka and Luther, 1994); (4) 25 ml 1 M NaAc pH 6 followed by 25 ml of 1 M NaAc pH 5 (remaining carbonates); (5) 25 ml of dithionite solution (pH 4.8; crystalline oxides; Kostka and Luther, 1994); (6) 20 ml of 20% HF (silicates; Lord, 1982; Pruysers et al., 1993); (7) 25 ml of concentrated

Left page: **Figure 4.2** *A) Core description and radiocarbon ages of BC15. Numbers indicate the zones as described in the text (core description). 1 = top; 2 = Mn-rich layer (dark-brown); 3 = cream-brownish layer; 4 = foraminifera ooze; 5 = heterogeneous organic-rich layer; B) Organic carbon vs. depth profile in BC15; C) $CaCO_3$ vs. depth profile in BC15; D) Sr/Ca ratio vs. depth profile in BC15; E) Amount of foraminifera per cm^3 vs. depth in BC15. Note the three different linear scales.*

HNO_3 (pyrite and other reduced phases; Lord, 1982; Pruysers et al., 1993); (8) 20 ml of a $HF/HNO_3/HClO_4$ mixture (residual phases; Lord, 1982; Pruysers et al., 1993). After each extraction the sediment was rinsed with distilled water. The extractants from steps 6 to 8 were each vaporised to dryness and the residue was subsequently dissolved in 1 M HCl. All solutions were analysed with ICP-AES (Perkin Elmer Optima 3000). The quality of the measurements was monitored by blanks and in-house standards. Reproducibility for Ca, Fe and Mn was better than 2%.

After drying at 50˚C, the samples for micropalaeontological analysis were weighed, then washed and sieved over mesh widths of 63, 150 and 595 μm. Sieve residues were weighed and the 150 – 595 μm size fraction for each sample was split into suitable aliquots containing about 200 planktonic foraminiferal specimens. These were identified and counted, and we here present results in relative abundances (%) with respect to total planktonic foraminifera.

^{14}C Accelerator Mass Spectrometry (AMS) dating was performed on handpicked foraminifera at the AMS-facility in Utrecht (the Netherlands). Experimental procedures follow Van der Borg et al. (1997).

4.3 Results

4.3.1 Radiocarbon dating

Seven samples have been dated using AMS-radiocarbon (Fig. 4.2A; Table 4.1). The samples at 0.45 and 3.75 cm give ages of 437 and 1337 $^{14}C_{nc}$-yrs ('nc' means uncorrected for the reservoir age) respectively, implying an average sedimentation rate of 3.67 cm/kyr for the top of the core. The sapropelic sediments and the foraminifera ooze have a rather uniform $^{14}C_{nc}$ age of 6170 to 6490 years. These ages fall in the range of 5000 to 9000 years reported for the most recent sapropel (S1) (Troelstra et al., 1991; Thomson et al., 1995; Van Santvoort et al., 1996). The ages in the Mn peak (1100 $^{14}C_{nc}$-yrs) and the interval between the foraminifera ooze and the Mn peak (7640 $^{14}C_{nc}$-yrs) deviate from the other ages in that the first appears too young and the latter too old. Due to the low amount of foraminifera (see below), only a few could be picked for the age determination in these samples (Table 4.1). Consequently, the extremely low sample sizes for these samples have resulted in a relatively large standard deviation, and in an extreme sensitivity to sampling artifacts. This will be discussed later.

4.3.2 Biogenic components

Benthic foraminifera are absent in BC15. The planktonic foraminiferal fauna of BC15 is rather homogeneous when compared to results from similar high-resolution investigations (Fig. 4.3; Rasmussen, 1991; Jorissen et al., 1993; Rohling et al., 1997; De Rijk et al., 1999; Hayes et al., 1999). Only in the upper 12.3 cm can some variability be observed in the planktonic fauna. The fauna between 12.3 cm and the beginning of the Mn-enriched layer (6.6 cm) shows increased abundances of colder water species such as *T. quinqueloba*, *G. scitula*, and right-coiled *N. pachyderma*, while the warm subtropical SPRUDTS-group is

at a low and a sharp drop occurs in *G. ruber* (Fig. 4.3). The upper part of this interval is characterised by extremely low abundances of foraminifera compared to the rest of the boxcore (Fig. 4.2E).

Elevated organic carbon contents are found below 12.3 cm, whereas the organic carbon values increase with depth within the foraminifera ooze (Fig. 4.2B). Following the definition of Van Santvoort et al. (1996), the sediment below 12.3 cm is considered to be sapropelic. Barium and selenium (Fig. 4.4) are elevated in this part compared to the upper 12.3 cm and closely follow the organic carbon content (cf. Fig. 4.2).

The $CaCO_3$ content (Fig. 4.2C) was calculated from the total Ca concentration. This is valid because 99% of total Ca is extracted in the carbonate steps of the sequential extraction (Chapter 7). A sediment trap study in the eastern Mediterranean has shown that most carbonate is biogenic (Chapters 2 and 3). The calculated $CaCO_3$ content, therefore, is a representation of biogenic carbonate. The carbonate content in the top 8.7 cm varies between 40 and 45 wt%, which is comparable to that found in sediments of the same age and similar depth of a nearby oxic core (T 83-48; Ten Haven et al., 1987). The foraminiferal ooze contains an enhanced amount of carbonates, namely up to about 60%. The sapropelic sediment has a slightly varying carbonate content of about 45%. When comparing Figs. 4.2C and 4.2E, it is obvious that the $CaCO_3$ content does not correlate with the amount of foraminifera. A recent sediment trap study in the eastern Mediterranean has shown that coccolithophores, and not foraminifera, are the major contributors to the present-day carbonate flux (Chapter 3).

Abundant radiolarians and other biogenic siliceous remains are observed in the sapropelic sediments below 12.3 cm in BC15, but are absent in the sediment above it. The opal content was also chemically determined for some samples (after Müller and Schneider, 1993; results in Table 4.2).

Table 4.1 *AMS-^{14}C ages (uncorrected years) on handpicked foraminifera and associated information, of some samples from BC15.*

Sample code	Depth (cm)	Notes	UtC-Nr.[1]	Weight (mg C)	^{14}C age (yrs BP ± 1σ)	δ^{13}C (‰)[2]
AA09129	0.3 – 0.6	oxic sed.	4557	0.95	437 ± 47	1
AA09140	3.6 – 3.9	oxic sed.	5676	0.8	1337 ± 42	0.3
AA09147 – AA 09149	5.7 – 6.6	Mn peak	4558	0.02	1100 ± 300	n.a.
AA09154	7.8 – 8.1		5677	0.03	7640 ± 280	n.a.
AA09159	9.3 – 9.6	foram ooze	4559	0.88	6170 ± 45	0.9
AA09198	21.0 – 21.3	sapropel	4560	0.73	6490 ± 70	0.7
AA09227	29.9 – 30.2	sapropel	4561	0.34	6190 ± 50	0.3

[1] *Laboratory number (UtC-xxxx) reference Utrecht AMS-facility*

[2] *Relative to PDB; n.a. = not available due to extremely small sample size*

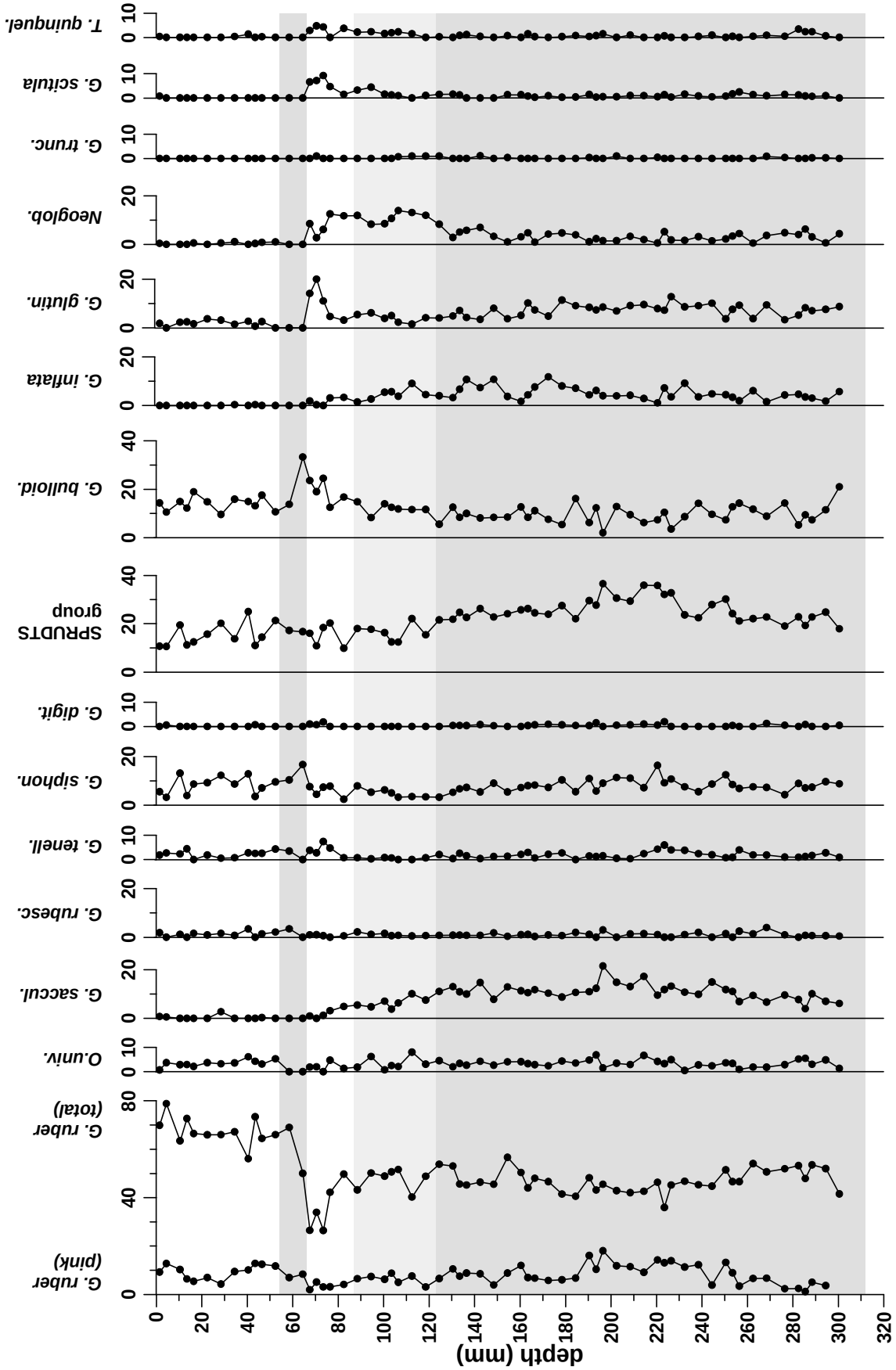
depth (mm)
0 20 40 60 80 100 120 140 160 180 200 220 240 260 280 300 320
G. ruber (pink)
G. ruber (total)
O.univ.
G. saccul.
G. rubesc.
G. tenell.
G. siphon.
G. digit.
SPRUDTS group
G. bulloid.
G. inflata
G. glutin.
Neoglob.
G. trunc.
G. scitula
T. quinquel.

4.3.3 Titanium and zirconium

Variation in the terrigenous composition is recorded by Ti/Al and Zr/Al ratios (Fig. 4.4C). In the sapropel (unit 5) these ratios are constant, whereas a strong variation occurs in units 3 and 4.

4.3.4 Manganese and iron

A sharp Mn peak is found between 5.4 and 6.6 cm with values up to 2 wt% (Fig. 4.5). The Mn speciation was determined using a sequential extraction (Table 4.3). Manganese (oxyhydr)oxides (from hereon referred to as Mn oxides) are mainly present in and above the Mn-enriched band, whereas some pyrite-bound Mn is found in the organic-rich part of the sediment below this band. Manganese incorporated into carbonates is found throughout the sediment, but concentrations are conspicuously higher below the Mn band (Table 4.3). Dissolved Mn^{2+} is absent in and above the Mn peak, whereas concentrations rapidly increase below the Mn peak (Fig. 4.5).

Results from the sequential extractions show that Fe oxides are mainly present in the top 8.7 cm, whereas pyrite (FeS_2) is present below this depth (Fig. 4.6). A small Fe oxide enrichment is recorded on top of the foraminifera ooze. Porewater Fe^{2+} remains below 1 μM, which is in contrast to the concentration usually found in and below the normal eastern Mediterranean sapropel S1 (concentrations up to 15 μM, Van Santvoort et al., 1996).

Table 4.2 *Opal content of some samples from BC15. 'Visible' indicates whether biogenic silica was observed, or not, during the micropalaeontological studies. 'Measured opal' indicates the chemically determined total opal content (after Müller and Schneider, 1993).*

Sample code	Depth (cm)	Visible	Measured opal (wt%)
AA09137	2.7 – 3.0	no	0.5
AA09165	11.1 – 11.4	no	2.4
AA09179	15.3 – 15.6	yes	2.2
AA09191	18.9 – 19.2	yes	3.4
AA09197	20.7 – 21.0	yes	6.3
AA09221	28.1 – 28.4	yes	2.6

Left page: **Figure 4.3** *Relative percentages of foraminifera vs. depth in BC15. Indicated zonations are identical to those in Fig. 4.2.*

4.4 Discussion

Biogenic silica is usually absent in eastern Mediterranean sediments. However, it can be found in high concentrations in brine sediments (Björklund and De Ruiter, 1987; Troelstra, 1987; Aghib, 1996). Opal only occurs below the foraminifera ooze in BC15, implying the initial deposition of this organic-rich sediment in a brine environment. The measured opal content of 2.2 to 6.3 wt% for the sapropelic sediments falls in the same range as that for sediments of the anoxic brine-filled Bannock Basin (Aghib, 1996). In contrast, the upper 12.3 cm appear to have been deposited initially in normal oxygenated bottom water conditions. Furthermore, faunal assemblages of the sediment from the Mn peak (5.4 – 6.6 cm) up to the top of BC15 indicate normal pelagic sedimentation.

4.5 Sequence and time of deposition of sediment intervals

4.5.1 Reservoir age correction

Extrapolation of the two ^{14}C ages in unit 1 to the sediment-water interface using a constant sedimentation rate of 3.67 cm kyr^{-1} results in a reservoir age of 314 yrs. This calculation is valid because of the complete recovery of the top sediment and the absence of benthic foraminifera and bioturbation marks. This calculated reservoir age for the eastern Mediterranean is 86 yrs younger than the open ocean average of 400 yrs measured by Stuiver et al. (1986) and Bard (1988). Stuiver et al. (1986) also report differences in the reservoir age for different regions, including the western Mediterranean, for which they found a deviation from the open ocean average of –135 ± 85 yrs. Our value for the eastern Mediterranean

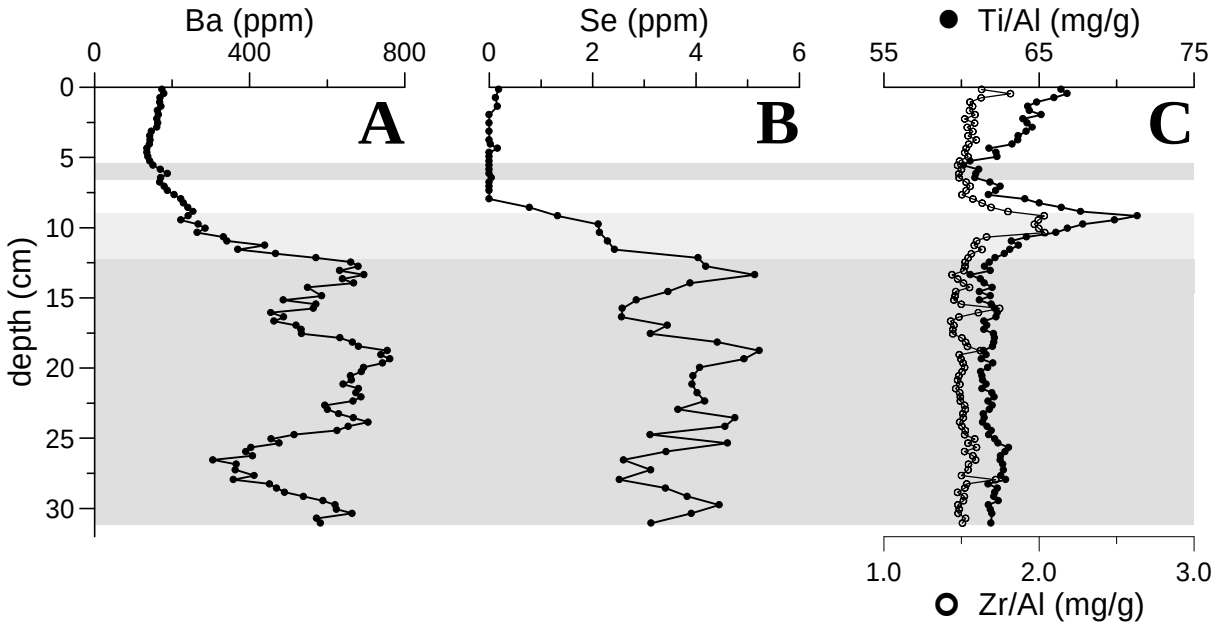

Figure 4.4 *A) Ba vs. depth in BC15; B) Se vs. depth in BC15; C) Ti/Al and Zr/Al vs. depth in BC15.*

(–86 yrs) falls in the same range as the one reported for the western Mediterranean basin. The lower reservoir age for the Mediterranean might be explained by a shorter turn-over time for the present-day Mediterranean compared to the major ocean basins (Kremling and Petersen, 1988). Therefore, we use the age of 314 yrs to correct the $^{14}C_{nc}$ ages for the reservoir effect, giving $^{14}C_c$ ages.

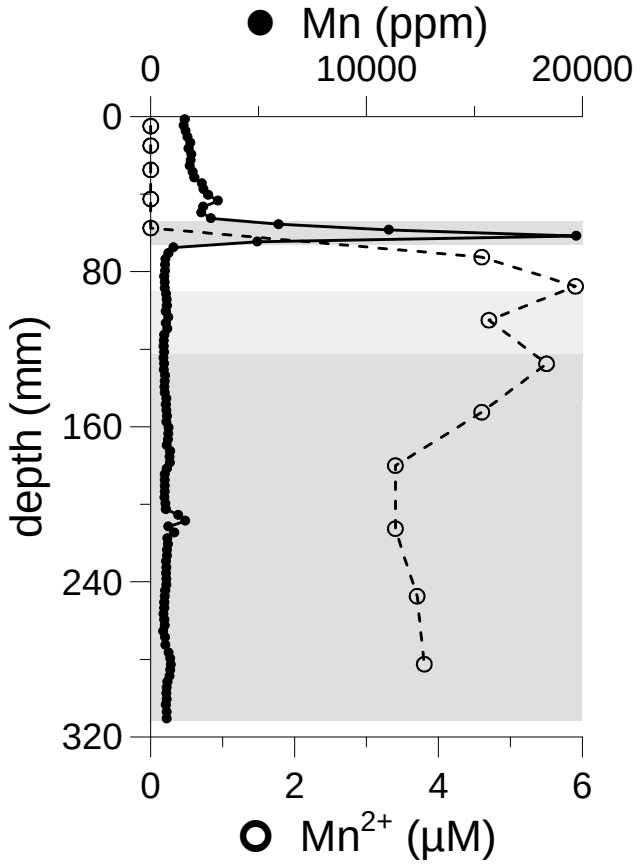

Figure 4.5 *Solid phase Mn (solid circles) and pore water Mn^{2+} (open circles) vs. depth in BC15.*

4.5.2 Redox boundaries

The redox conditions in the boxcore can be inferred from the pore-water-Mn^{2+} profile. The boundary between oxic and suboxic sediments is defined as the depth where dissolved Mn^{2+} increases rapidly (e.g. Froelich et al., 1979; Van Santvoort et al., 1996). Mn^{2+} is highly immobile in oxic environments, because it is oxidised and subsequently trapped into insoluble oxides, whereas concentrations rapidly increase in suboxic and anoxic sediments due to the instability of Mn oxides and the higher solubility product of Mn carbonates compared to Mn oxides (Middelburg et al., 1987). The present position of the oxic/suboxic boundary is, therefore, located at the depth of the Mn peak (Fig. 4.5). This is further substantiated by the Mn speciation in the boxcore. Manganese oxides are mainly present in and above the Mn peak, whereas Mn incorporated into carbonates is evidently higher in the sediment below the

Mn peak (Table 4.3). The pore-water-Mn^{2+} profile confirms such upward diffusion, oxidation and precipitation at the level of the Mn peak.

4.5.3 Timing of the Mn oxide peak

The time that would be needed to accumulate the Mn peak by upward diffusion of Mn^{2+} can be calculated by using the solid phase and pore water Mn concentrations according to the same procedure and parameters as Pruysers et al. (1993). The calculated time of 1600 years is only 200 years less than the ending of anoxic conditions in Poseidon Basin, based on the Cl-diffusion profile (1,800 years, Van Santvoort and De Lange, 1996). When extrapolating the inferred sedimentation rate of 3.67 cm kyr^{-1} from the top down to the Mn peak, the age of the peak lies between 1471 (top of Mn peak) and 1798 $^{14}C_c$-yrs (bottom). These ages are in conflict with the ^{14}C date recorded in the Mn peak (~ 800 $^{14}C_c$-yrs, corrected

Table 4.3 *Speciation of Mn in BC15 as determined by the sequential extraction. Manganese in carbonates was calculated from the sum of steps 1, 2 and 4; Mn in oxides from the sum of steps 3 and 5; Mn in pyrite by taking Mn recovered in step 7 (see section 4.2.2). Only the fractions relevant to the discussion in this paper have been included. Furthermore, the Mn-tot column only gives the values for the 18 extracted samples; all values are included in Fig. 4.5. It should be noted that the speciation of sample AA09146 is indicative of the Mn peak.*

Sample code	Depth (cm)	Mn-carb (ppm)	Mn-ox (ppm)	Mn-pyr (ppm)	Mn-tot[1] (ppm)	Recovery[2] (%)
AA09132	1.2 – 1.5	180	1382	1	1847	93
AA09137	2.7 – 3.0	139	1985	1	1949	116
AA09146	5.4 – 5.7	78	5346	1	5927	94
AA09152	7.2 – 7.5	338	111	1	690	86
AA09156	8.4 – 8.7	392	61	2	654	92
AA09160	9.6 – 9.9	507	101	25	754	100
AA09164	10.8 – 11.1	481	100	36	773	91
AA09172	13.2 – 13.5	370	94	79	674	101
AA09178	15.0 – 15.3	396	87	68	733	100
AA09183	16.5 – 16.8	439	101	73	809	98
AA09190	18.6 – 18.9	333	70	94	649	98
AA09198	21.0 – 21.3	481	85	76	821	97
AA09204	22.8 – 23.1	402	81	70	719	98
AA09207	23.7 – 24.0	398	90	88	740	97
AA09212	25.2 – 25.5	334	73	50	634	94
AA09221	28.1 – 28.4	538	93	80	941	95
AA09226	29.6 – 29.9	404	78	94	729	99
AA09230	30.9 – 31.2	406	91	66	746	96

[1] *Total-Mn as measured in the total digestion*

[2] *Sum of all sequential extraction steps divided by total-Mn × 100%*

for reservoir age). This age is, however, based on a very small amount of foraminifera (Fig. 4.2E, Table 1), thereby sensitive to contamination during sampling of the boxcore and considered not reliable; due to the upward extrusion of the boxcore and the incomplete removal of the outer rims of each slice, some contamination might have occurred by the inclusion of younger foraminifera in older slices. This hardly influences ^{14}C dating when having large amounts of foraminifera, but might be important when foraminifera numbers are low, such as in the Mn layer (Fig. 4.2E). The amount of Mn in the Mn peak can therefore be explained by the oxidation of upward diffusing Mn^{2+} and the subsequent precipitation of Mn oxides alone. In addition, results seem to agree that the border between units 2 (Mn peak) and 3 marks the end of sediment deposition within the anoxic brine around 1800 yrs BP. Consequently, the sediment from the Mn peak up to the sediment-water interface indicate normal pelagic deposition.

4.5.4 Timing of the sediment below the Mn oxide peak

The uniform faunal assemblage, the fairly constant ages and the occurrence of opal indicate that the sapropelic sediments (unit 5) consist of a slump generated and deposited within the brine. This is further substantiated by constant Ti/Al and Zr/Al profiles (Fig. 4.4C). These ratios are considered to be an indicator for the relative presence of heavy minerals in comparison to clay minerals. The heavy mineral fraction mainly resides in the coarser fraction (Schmitz, 1987; Shimmield, 1992). Uniform Ti/Al and Zr/Al ratios, as in the sapropelic unit, therefore indicate a uniform grain size distribution, thereby also pointing to redeposited sediment. These ratios fall in the same range as those recorded in the S1 sapropel in normal sediments (unpublished results). Because no grain size fractionation has occurred and the ratios are of the same magnitude, it is valid to compare this unit with sapropels in normal eastern Mediterranean sediments.

The explanation of the origin of the sediments from 6.6 – 12.3 cm in BC15 is not straightforward. Biostratigraphy may hold some clues, as a cool planktonic foraminiferal fauna occurs in this interval. Three intervals of several centuries duration have been reported with similar cool faunas in Holocene sequences in the Adriatic and Aegean Seas; one around 7000 yrs BP, one around 6300 yrs BP, and one following the Santorini eruption/explosion (Rohling et al., 1997; Hayes et al., 1999; De Rijk et al., 1999). The latter has recently been dated at 3356 years BP (Bruins and Van der Plicht, 1996). The oldest of these three periods is faunistically different from units 3 and 4 in BC15, in that it commonly contains high abundances of pink coloured morphotypes of *G. ruber*, which, in contrast, are scarce in the 6.6 – 12.3 cm interval in BC15. The faunal compositions of the middle (around 6300 yrs BP) and youngest periods with cool faunas are more similar to that in units 3 and 4 of BC15. Because of the occurrence of normal pelagic sediment with an age up to 1800 $^{14}C_c$-yrs overlying these units in BC15, it is more likely that the original sediment was deposited during the latest cooling event, i.e. the one following the Santorini explosion. The visible absence of opal and a relatively low organic carbon content suggest a source outside the brine basin. The slump might, therefore, have been separated at the seawater/brine interface (Rimoldi et al., 1996), resulting in a foraminifera-rich lower interval (unit 4) and a

foraminifera-poor upper interval (unit 3). The measured opal content in the lower foraminifera ooze together with an upward decreasing organic carbon content indicates some mixing with the upper part of the sapropel in the brine during redeposition. The ^{14}C dating, however, suggests a much older time of deposition. This might be explained by the commonly reported resedimentation/reworking processes which occur in brine basins, giving rise to the finding of old nannofossil species, even of Pliocene and Miocene age (Erba et al., 1987; Parisi et al., 1987), and thereby increasing the apparent age of the sediment.

4.5.5 Deposition summary

The sapropelic interval (unit 5) consists of a slump of organic-rich sediments generated and redeposited within the brine. This was followed by redeposition of sediments from outside the brine basin (units 3 and 4), whereby the brine structure caused a density-induced separation of the sediment. The base of unit 4 seems to have mixed with the upper part of unit 5. Both slumps (units 3 – 4 and unit 5) might have been caused by tectonic activity ultimately leading to the oxygenation of Poseidon Basin, 1800 yrs BP. After this oxygenation, normal pelagic sedimentation started. Near the base of these normal pelagic sediments, a Mn oxide peak was formed.

4.6 Diagenesis in Poseidon Basin sediment versus normal pelagic eastern Mediterranean sediment

4.6.1 Mn and Fe in normal pelagic eastern Mediterranean sediments

In normal eastern Mediterranean sediments, a downward-moving oxidation front exists on top of sapropel S1 (De Lange et al., 1989; Higgs et al., 1994; Thomson et al., 1995; Van Santvoort et al., 1996). Oxygen is not completely utilised at the sediment-water interface, diffusing into the sediment thereby oxidising previously anoxic, sapropelic, sediments. This type of diagenesis is non-steady-state, resulting in the so-called ‘double-manganese-peak’ feature. The upper peak is thought to be deposited either hydrogenically or by a fixation mechanism upon reoxygenation of the eastern Mediterranean deep water (Higgs et al., 1994; Van Santvoort et al., 1996). This peak has been broadened by bioturbation, and is typically 2 to 4 cm thick (e.g. Thomson et al., 1995). The lower peak results from the oxidation of upward diffusing Mn^{2+} and the subsequent precipitation of Mn oxides. It is accompanied by a large Fe oxide peak, which results from the oxidation of upward-diffusing Fe^{2+} and the subsequent precipitation of Fe oxides. With time and depth the progress of the oxidation front will slow down, thereby precipitating increasing amounts of Mn and Fe oxides at each subsequent level. Other redox-sensitive elements, such as I, Se and V, are also mobilised in a predictable sequence with regard to the oxidation front, forming distinct peaks near the redox front, above as well as within the remaining sapropel sediment (Thomson et al., 1995).

4.6.2 Mn and Fe in Poseidon Basin sediments

In Poseidon Basin sediments, a single, sharp, 1.2 cm thick Mn oxide peak exists, well above the organic-rich sediment (Fig. 4.5). The pore-water-Mn^{2+} profile indicates this peak to be the active boundary between oxic and suboxic sediments at present. The area around the Mn peak does not contain enhanced Fe oxide levels. Only a small Fe oxide peak is found 2.1 cm below the Mn peak (Fig. 4.6A), whereas in normal eastern Mediterranean sediments the lower Mn peak and the Fe oxide peak do not show a separation of more than 1 cm (Thomson et al., 1995; Van Santvoort et al., 1996; unpublished results). This separation is thought to be due to a preferential mobilisation of Mn relative to Fe due to thermodynamics and kinetics (Lynn and Bonatti, 1965; Froelich et al, 1979; Burdige and Gieskes, 1983; De Lange, 1986; Thomson et al., 1989; Pruysers et al., 1993; Stumm and Morgan, 1996). The absence of a clear link between the solid Mn and Fe oxide profiles in BC15 confirms, therefore, our earlier statement that no downward oxidation is taking place in this boxcore. This is further substantiated by pyrite, which shows, like organic carbon, no sharp boundary between the organic-rich and organic-poor sediments (Fig. 4.6B), in contrast with normal eastern Mediterranean sediments, where pyrite sharply increases just below the oxidation front. Moreover, a good correlation exists between pyrite and organic carbon in BC15 (compare Figs. 4.2B and 4.6B). The Mn/Fe ratio of the pyrite found in Poseidon Basin is

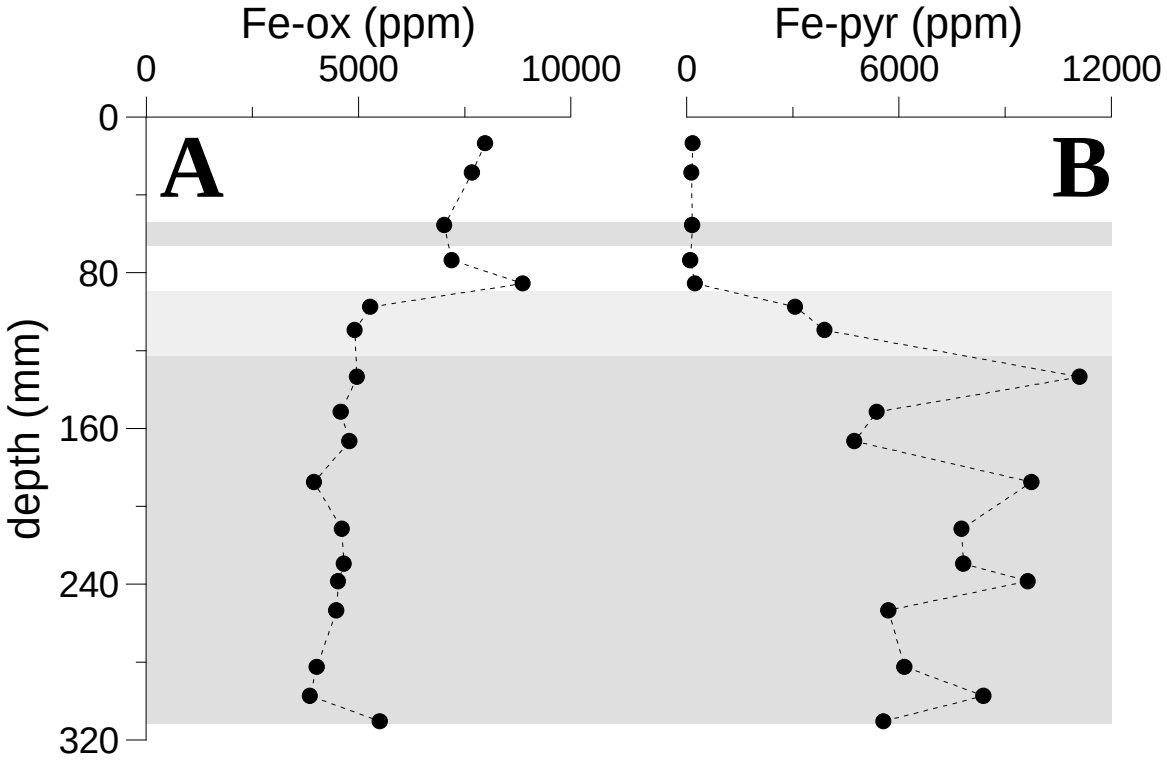

Figure 4.6 *Fe speciation as determined by the sequential extraction. A) Fe oxides vs. depth in BC15. Fe in oxides was determined by summation of steps 3 and 5; B) Fe-pyrite vs. depth in BC15. Fe in pyrite are the values measured in step 7. See section 4.2.2 for the description of the sequential extraction steps.*

about twice as high as that in the normal sapropel S1 pyrite (Fig. 4.7). The Mn^{2+} concentration is also twice as high in the pore water of the brine sediment of BC15 than it is in the pore water of normal sapropel S1 sediment (5 – 6 μM versus 2 – 3 μM; e.g. Van Santvoort et al., 1996). The Mn^{2+} concentration in BC15 is comparable to that found in the Tyro Basin brine (De Lange et al., 1990). The correspondence between the Mn/Fe ratio in pyrite and the Mn^{2+} in pore water indicates that formation of pyrite in BC15 took place in a brine environment. The Mn^{2+} concentration in the brine might have originally been controlled by either the input of Mn oxides, which are subsequently reduced, or by a combined equilibrium of Mn with sulphide and carbonate phases. The good relationship between pyrite and organic carbon suggests that pyrite formation in the brine environment of BC15 has been organic carbon limited (Berner, 1984). However, Henneke et al. (1997) found no good correlation of pyrite with the organic carbon content in the brine-filled Tyro and Bannock Basins. They proposed a mainly syngenetic and Fe-limited formation of pyrite. At this moment, we cannot give a satisfactory explanation for this difference.

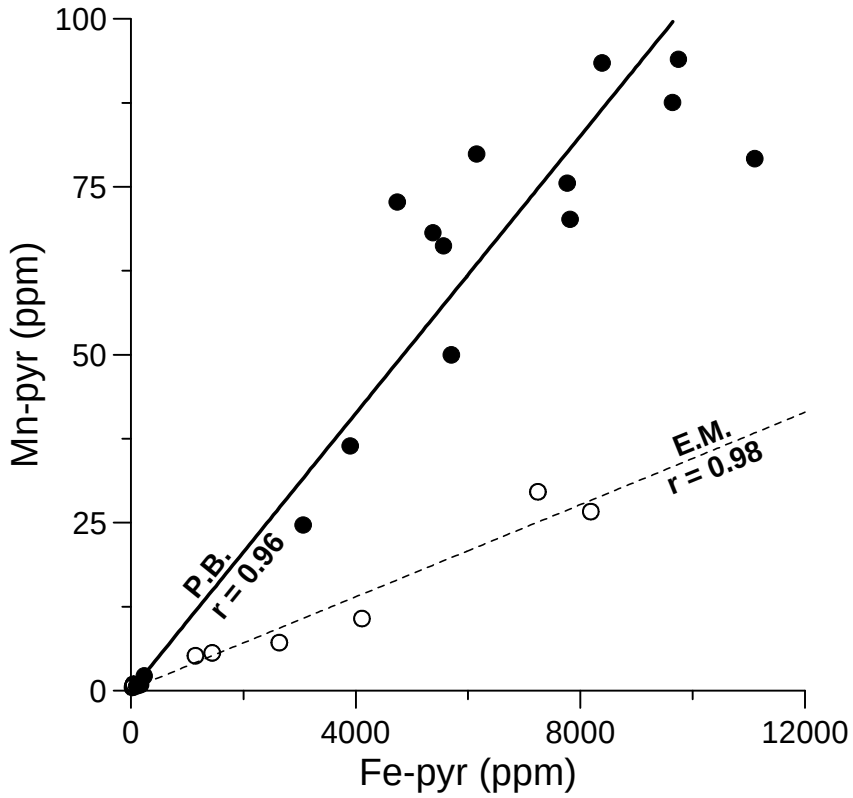

Figure 4.7 *Fe-pyrite vs. Mn-pyrite in BC15 (solid circles) and normal eastern Mediterranean sediments containing sapropel S1 (open circles). The solid line indicates a linear best fit forced through zero for BC15 (Mn_{pyr} (ppm) = 10.3×10^{-3} × Fe_{pyr} (ppm)), the hatched line a linear best fit for the normal sapropel S1 (Mn_{pyr} (ppm) = 3.4×10^{-3} × Fe_{pyr} (ppm) + 0.23). The results for the normal eastern Mediterranean sediments were obtained applying the sequential extraction to sediments from boxcore ABC26 (site BC12/UM26 of Van Santvoort et al., 1996)).*

4.6.3 Se in normal pelagic sediments and Poseidon Basin sediments

The absence of a downward-moving oxidation front is clearly indicated by the Se profile (Fig. 4.4). In oxidised sediments Se will be in the form of selenate (SeO_4^{2-}), which is a soluble species. Reduction of this species forms elemental Se and further reduction may even result in the formation of the selenide anion (Se^{2-}) (Howard, 1977; Brookins, 1988; Masscheleyn et al., 1990). The latter species are highly insoluble, giving rise to the preferential accumulation of Se in organic-rich sediments. In normal eastern Mediterranean sapropels, a large Se enrichment is encountered just below the redox front (Thomson et al., 1995; Van Santvoort et al., 1996). It forms upon the downward oxidation of the sapropel, where Se is mobilised when encountering oxygen. Subsequently, selenate continuously diffuses downwards, is reduced and concentrated just below the redox front. The Se profile resulting from such downward oxidation does not correlate with the organic carbon content (Fig. 4.8B). In sediments of Poseidon Basin, however, Se correlates well with the organic carbon content (Fig. 4.8B), and no enrichments are found near the oxic/suboxic boundary (Fig. 4.4B). Another redox-sensitive element, vanadium, is also enriched in the sapropel, correlating with the organic carbon content (see also Chapter 5; $V_{non-clay}$ (ppm) / C_{org} (wt%) = 29.3 with $R^2 = 0.94$). Like for Se, no diagenetic peak is found for V. Consequently, the sapropel sediments in BC15 have not been diagenetically altered by oxygen penetration. In addition, it appears that the distribution of Se, V and probably other trace elements still reflect their initial correlation with the organic carbon flux to sapropel S1 sediments in the eastern Mediterranean.

4.7 Preservation of organic-rich S1 sediments in the anoxic Poseidon brine compared to that in oxic pelagic sediments

4.7.1 Opal

High opal contents have been found in the organic-rich sediment of Poseidon Basin (Table 4.2), whereas in normal eastern Mediterranean sediments, including sapropels, insignificant amounts, if any, occur. The preservation of biogenic silica is thought to occur due to the high dissolved silica concentration in the brine (Björklund and De Ruiter, 1987). De Lange et al. (1990) measured a dissolved silica concentration of 266 μM in the Tyro brine, as opposed to concentrations of about 10 μM in eastern Mediterranean bottom water (Kremling and Petersen, 1981; Hydes et al., 1988). The high silica concentrations in the brine will result in a much lower opal dissolution rate, as this concentration lies much more near the saturation concentration of opal than that of normal eastern Mediterranean sediments. Consequently, opal is much better preserved in anoxic brine sediments than in oxic normal eastern Mediterranean sediments.

4.7.2 Carbonate

The average carbonate content is slightly higher in the sapropelic sediments (12.3 – 31.2 cm) than it is in the top sediments (0 – 6.6 cm) of BC15 (Fig. 4.2C). Nearby core T 83–48 (Ten Haven et al., 1987) shows no changes in the carbonate sedimentation in the

Holocene. The change of the average carbonate content in BC15, therefore, indicates that carbonates are preserved better in brine sediments. This agrees with the chemical reactions taking place in oxic compared to anoxic conditions. Namely, oxic breakdown of organic material produces acid, which dissolves some carbonates, whereas anoxic conditions produces bicarbonate, resulting in enhanced preservation of carbonates (De Lange et al., 1989). Sr/Ca ratios may give further information about the preservation of carbonates in marine sediments. The Sr/Ca ratio is thought to be indicative of the aragonite content in eastern Mediterranean sediments (Pruysers et al., 1991; Thomson et al., 1995), because aragonite contains more Sr than calcite due to the relative ease with which Sr can substitute Ca in the aragonite structure (e.g. Winland, 1969). Sr/Ca ratios of eastern Mediterranean sapropels are clearly higher than those found in recent oxic top sediments (Thomson et al., 1995), suggesting enhanced preservation of aragonite during periods of sapropel deposition. The average Sr/Ca ratio in the sapropel of BC15 is higher than that found in normal eastern Mediterranean sapropels of similar depths, 5.56 mg/g (Fig. 4.2D) versus 4.99 mg/g at about 3300 m water depth (unpublished results UM15, Van Santvoort et al., 1996). Brine conditions, therefore, seem to enhance aragonite preservation relative to normal sapropels*. The Sr/Ca ratio of the foraminifera ooze has the lowest value recorded in BC15, confirming that this ooze originates from outside the brine basin**.

4.7.3 Organic matter

Van Santvoort et al. (1996) have shown that Ba is a reliable indicator of organic carbon accumulation for unoxidised S1 sediments. In addition, Dymond et al. (1992) showed a clear relationship between organic carbon and barite fluxes in sediment traps. Therefore, Ba can be considered as a palaeoproxy for past organic carbon fluxes, even when diagenesis has removed most of the organic carbon signal. Indeed, Ba shows a good correlation with organic carbon in Poseidon Basin sediments (Fig. 4.4A). However, when Ba is plotted versus the organic carbon content (Fig. 4.8A), the resulting slope, i.e. the C_{org}/Ba ratio, is lower than for average eastern Mediterranean sapropels (Van Santvoort et al., 1996). At first glance this suggests lower preservation of organic matter in the brine, in contrast with other biogenic components (opal, carbonates). However, the lower C_{org}/Ba ratio in BC15 is thought partly to be due to the greater depth of BC15 compared to other cores, and the commonly recorded decrease of C_{org}/Ba ratios with depth in the water column (Von Breymann et al., 1990; Dymond et al., 1992; Van Santvoort et al., 1996). It may also in part be related to the unknown preserved Ba fraction in brine sediments compared to the normal average 30% preservation of Ba (Dymond et al., 1992). In view of the sulphate concentration of the Tyro brine being twice as high as that of normal sea water (De Lange et al., 1990), a better preservation of barite in brine compared to normal sediments is thought to result. This is likely to be the case, at least in the top 50 cm of brine sediment, where sulphate reduction

* Continuing research (Chapter 7) shows that the aragonite content measured by XRD is lower in the former brine sapropel than in the normal sapropel S1. See also footnote on page 65.

** The lower Sr/Ca in the foraminifera ooze is probably caused by the relatively low Sr/Ca ratio of foraminiferal calcite compared to e.g. coccolith calcite.

does not appear to take place at a significant rate (Henneke et al., 1997). Consequently, the lower C_{org}/Ba ratio in BC15 implies a better preservation of barite relative to organic carbon in brine sediments*, but is as yet inconclusive for the organic carbon preservation potential of brine relative to normal sediments.

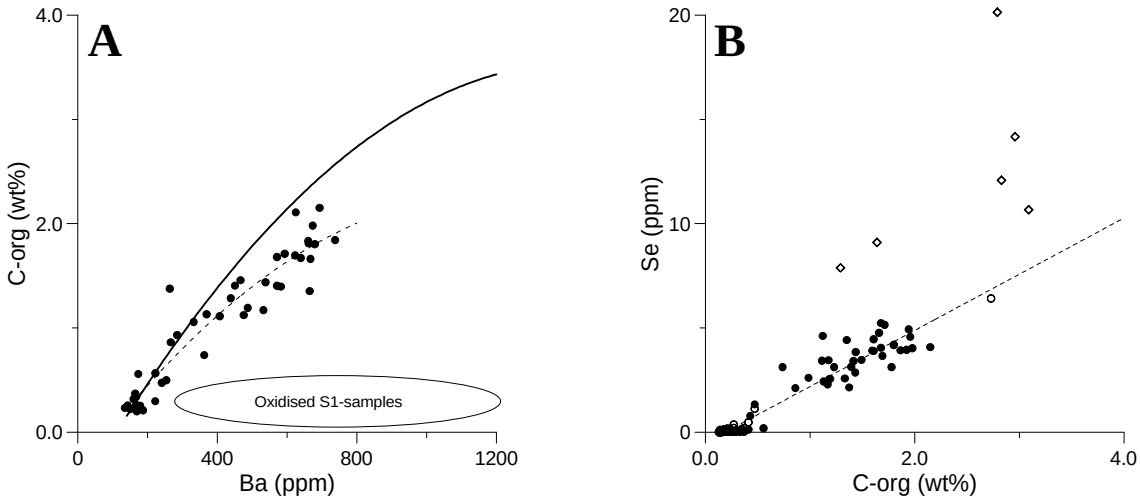

Figure 4.8 *A) Organic carbon vs. Ba in BC15 (dots) and its best polynomial fit (hatched line; C_{org} (wt%) = $-1.88\times10^{-6} \times (Ba)^2 + 4.48\times10^{-3} \times Ba - 0.373$; Ba in ppm) have been indicated. In addition, the best polynomial fit in normal eastern Mediterranean S1-sapropels (thick solid line) and the position of oxidised S1-samples have been given (Van Santvoort et al., 1996). B) Organic carbon vs. Se in BC15 (solid circles) and normal eastern Mediterranean top sediments (open symbols; unpublished results from boxcore UM 35). Open dymonds indicate values from diagenetic Se peaks in normal sediments. The hatched line indicates the best linear fit for BC15 samples (Se (ppm) = 2.7 × C_{org} (wt%) – 0.5).*

* Continuing research (Chapter 6) shows that there is no difference in the relationship between biogenic Ba (barite) and organic carbon between former brine and normal sapropel sediments, suggesting that preservation of barite compared to organic carbon is similar in these two types of sediment. See also footnote on page 65.

4.8 Conclusions

Several differences could be established in diagenesis and preservation of biogenic components, between anoxic brine sediments and oxic normal eastern Mediterranean sediments:

1) There has been no burn-down front in sapropel sediments deposited in Poseidon brine, whereas there is one in those deposited in the normal eastern Mediterranean basin.

2) Consequently, there has been no mobilisation of Se (and other trace elements) and the trace element / C_{org} ratio has been preserved in the brine but not in the normal sapropel sediments.

3) Biogenic opal, aragonite* and calcite have been better preserved in the brine than in the normal sapropel sediments.

4) The preservation of barite relative to that of organic carbon seems to be higher in shallow brine sediments than it is in unoxidised normal Mediterranean sediments**. However, our data are inconclusive for the preservation potential of organic carbon in brine relative to normal sediments, hence the difference of organic carbon preservation of brine compared to normal sediments.

Acknowledgements – This research was supported by MAST-1-MARFLUX (900022C), MAST-2-PALAEOFLUX (MAS2-CT93-0051), MAST-3-CLIVAMP (MAS3-CT95-0043) and MAST-3-SAP programmes. G. Nobbe, H. de Waard and P. Anten are acknowledged for their technical assistence. This chapter greatly benefited from the suggestions of three anonymous reviewers.

This is NSG (Netherlands Research School of Sedimentary Geology) paper nr. 98002.

* See footnotes on pages 65 and 82.

** See footnotes on pages 65 and 83.

Chapter 5

Sequential extraction of iron, manganese and related elements, tested on natural minerals and applied to eastern Mediterranean sediments

Abstract – A detailed sequential extraction scheme (MESEX) was developed to distinguish Fe and Mn phases in eastern Mediterranean sediments. First, the MESEX method was calibrated using a number of Fe and Mn containing natural minerals to obtain operationally defined carrier phases such as carbonate, amorphous oxides, crystalline oxides, aluminosilicates and pyrite. During further calibration, using MESEX on a mixed mineral standard of known composition, the various minerals were fairly well separated. Subsequently, MESEX was applied to two different types of Holocene eastern Mediterranean sediments from boxcores taken in (1) a former brine basin, and (2) a normal setting, including the organic-rich sapropel S1. The following are results obtained by the application of MESEX on these sediments.

The Mn(II)/Mn(III,IV) redox boundary in both boxcores is clearly distinguished. Carbonate-related Mn is enriched below this boundary, whereas Mn oxides only occur above the same boundary. A clear Fe(II)/Fe(III) redox boundary is present in the normal eastern Mediterranean sediments and is located just below the Mn(II)/Mn(III,IV) redox boundary. The Fe(II)/Fe(III) boundary closely coincides with the visible boundary between the lower unoxidised and the upper oxidised (burned-down) part of the original sapropel S1 interval. Pyrite is only present within the unoxidised interval, whereas Fe oxides are abundant above it. The Fe(II)/Fe(III) redox boundary in the former brine sediments resides on top of the organic-enriched sediments, as deduced from the distribution of Fe oxides and pyrite. As a result of burn-down of the sapropel S1 unit in the normal sediments, a vanadium peak has been formed below the oxidation front, whereas no such V peak was observed in the former brine sediments. This, together with the location of the Mn(II)/Mn(III,IV) redox boundary well above the organic-enriched sediments, suggests that no burn-down has taken place into the sapropelic sediments of the former brine basin, resulting in the preservation of the relationships of trace metal to organic carbon or pyrite. Concercing the trace metal fraction associated with reduced phases such as organic carbon and pyrite, MESEX suggests that Mn and Co are more associated with pyrite, wheras Ni, Cu and Zn, as well as V, are more related to organic matter.

On the basis of MESEX, variations have also been detected in the terrigenous component, i.e. aluminosilicates. $(Fe/Al)_{clay}$ and $(Mg/Al)_{clay}$ ratios are somewhat higher in sapropelic than in non-sapropelic sediments, suggesting a slightly higher chlorite content in the former. Several trace metal to Al ratios behave similarly. These results indicate that sources of terrestrial material have been different during sapropel times compared to the period immediately after it. On the other hand, the K/Al_{clay} ratio remains fairly constant with depth in the sediment, suggesting that no major changes may have occurred in the relative contribution of illite to the terrigenous fraction.

5.1 Introduction

The distribution of elements over different mineral phases may be used for the palaeo-environmental interpretation of the sedimentary record. This distribution can be measured by means of sequential extraction, in which sediment samples are suspended in solutions of successively increasing leaching strength. After each extraction step, the solutions are individually analysed. The results represent dissolution of different mineral phases as defined by the extraction procedure. Calibration of this method can be done by the extraction of pure minerals. The focus of this chapter is on the determination of the speciation of iron, manganese and related trace metals in eastern Mediterranean sediments, and on how this can be used for palaeo-environmental reconstructions of the sedimentary regime in the eastern Mediterranean during the Holocene.

Much sequential extraction work has been done on the speciation of iron (e.g. Lord, 1982; Canfield, 1989; Huerta-Diaz and Morse, 1990; Pruysers et al., 1991, 1993; Kostka and Luther, 1994), because of its specific redox chemistry. The variations of Fe (hydr)oxide and pyrite content in sediments have been used to define parameters such as degree of pyritisation (DOP; Berner, 1970). The speciation of other elements, like Mn and other trace metals, has been determined mainly in combination with Fe mineral extractions. This is specifically the case for the trace metal content of pyrite (Huerta-Diaz and Morse, 1990, 1992). Such extractions are mainly limited to the determination of (palaeo)redox chemistry of the sediments. However, other palaeo-environmental information can have been locked into minerals other than oxides and sulphides. The two most important ones are carbonates and clay minerals, both consisting of various minerals with each having a different chemical composition. Determination of their content and if possible their composition may yield insight in variations in palaeo-environmental conditions such as changes in terrestrial input sources. This will provide a broader picture than can be gained from the extraction of only Fe oxides and pyrite. Thus, results of broad sequential extractions will not only improve the insight in sediment composition, but also in initial and ongoing processes.

The eastern Mediterranean is a semi-enclosed basin very sensitive to global climatic changes, and its sediments record important global environmental variations. This is expressed by the occurrence of distinct organic-rich intervals (sapropels; Kidd et al., 1978) within otherwise organic-poor units. These sapropels have been attributed to intervals of enhanced palaeoproductivity and decreased oxygen content of the bottom water (see review by Rohling, 1994). Due to increased precipitation, river input is thought to have increased significantly during sapropel times (Kallel et al., 1997). This would then have resulted in an increase of nutrients in the photic zone, leading to higher productivity and possibly anoxic bottom waters. Because of the distinct compositional differences between the sedimentary units, sequential extractions are an appropriate tool to unravel environmental changes recorded in eastern Mediterranean sediments.

In this study, we developed a detailed sequential extraction scheme (MESEX) to differentiate carbonate-, clay-, oxide- and sulphide-bound Fe and Mn contents in sediments. We have used natural minerals and a mixed mineral standard (MMIN) to evaluate MESEX, and have applied it to eastern Mediterranean Holocene sediments which include the youngest

sapropel (S1). This enabled us to review variations in (palaeo)redox conditions and in the terrigenous component of the sediment, and in the relationship between trace metals and reduced fractions such as organic carbon and pyrite.

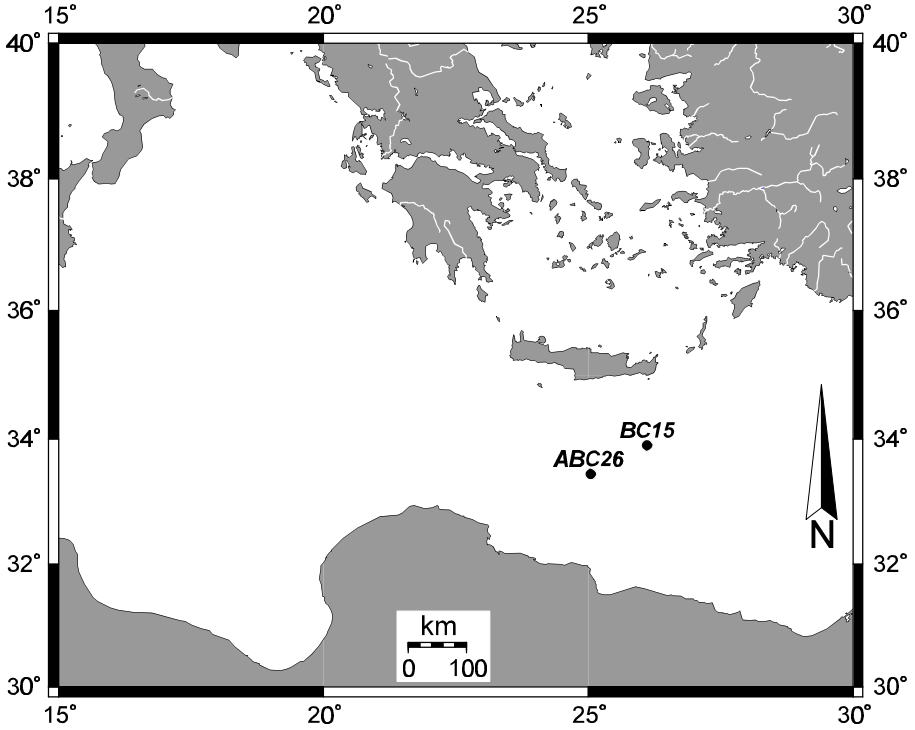

Figure 5.1 *Location of boxcores ABC26 (33°21.3'N, 24°55.4'E; water depth 2150 m) and BC15 (33°51.4'N, 26°05.5'E; water depth 3232 m) in the eastern Mediterranean.*

5.2 Materials and methods

5.2.1 Materials

A large number of natural minerals were used to evaluate the MESEX scheme. These were (with the appropriate element):

Fe: Fe-Mn nodules (from the Madeira Abyssal Plain), siderite ($FeCO_3$), haematite (Fe_2O_3), goethite (FeOOH), pyrite (FeS_2), ilmenite ($FeTiO_3$) and magnetite (Fe_3O_4)

Mn: Fe-Mn nodules (from the Madeira Abyssal Plain) and rhodochrosite ($MnCO_3$)

A standard with mixed natural minerals was prepared (MMIN; Table 5.1), containing a number of the minerals listed above, complemented by illite (which contributes a.o. Fe). In addition, samples were extracted from two eastern Mediterranean boxcores (BC15 and ABC26; Fig. 5.1).

The Fe-Mn nodules were obtained during the 1986 Madeira Abyssal Plain expedition of *R.V. Tyro* (De Lange et al., 1992), goethite and haematite from the in-house mineral collection at Utrecht University, and all other minerals from Wards.

Table 5.1 *The composition of MMIN, the mixed mineral standard prepared for this study.*

Mineral	Content (wt%)
illite	46.2
calcite	40.1
dolomite	10.0
pyrite	1.5
gypsum	0.7
goethite	0.6
haematite	0.5
manganite	0.3
barite	0.1

Table 5.2 *Overview of the MESEX sequential extraction scheme and its three variants (SE 1, SE2 and SE3).*

MESEX sequential extraction scheme				
Step	Variant SE1	Variant SE2	Variant SE3	Ref.
1	25 ml 1M $MgCl_2$ pH 5.3	25 ml 1M $MgCl_2$ pH 8	25 ml 2M NH_4Cl pH 9	1 2, 3
2	25 ml 2M NH_4Cl pH 9	2×25 ml 2M NH_4Cl pH 9	25 ml 2M NH_4Cl pH 9	2, 3
3	25 ml 2M NH_4Cl pH 9	2×25 ml 2M NH_4Cl pH 8		2, 3
4	25 ml 2M NH_4Cl pH 9	2×25 ml 2M NH_4Cl pH 7.5		2, 3
5	25 ml 2M NH_4Cl pH 9	3×25 ml 2M NH_4Cl pH 7		2, 3
6	25 ml ascorbic acid/sodium bicarbonate/sodium citrate solution (pH ~ 8)			4
7	25 ml 1 M NaAc pH 6			5
8	25 ml of 1 M NaAc pH 5			5
9	25 ml sodium dithionite / sodium citrate / sodium acetate solution (pH 4.8)			4
10	20 ml 20% HF [a]			6, 7
11	25 ml concentrated HNO_3 [a]			6, 7
12	10 ml 40% HF + 10 ml $HNO_3/HClO_4$ [a]			6, 7

[a] *Solutions have been decanted into Teflon vessels, vaporised to dryness and redissolved in 1 M HCl.*

References: (1) Ruttenberg (1992); (2) De Lange (1992b); (3) De Lange et al. (1994); (4) Kostka and Luther (1994); (5) Chapter 4; (6) Lord (1982); (7) Pruysers et al. (1993)

5.2.2 Methods

The MESEX scheme (Table 5.2) was designed in such a way that the different solvents would subsequently extract the following phases: absorbed ions ($MgCl_2$), carbonates (NH_4Cl), amorphous oxides (ascorbate), remaining carbonates (NaAc), crystalline oxides (dithionite), clay minerals (HF), pyrite and organic-bound metals (HNO_3) and residual minerals ($HF/HNO_3/HClO_4$).

In general, the method consisted of the following steps. Approximately 250 mg of sediment was accurately weighed. Samples from BC15 were extracted using the SE2 variant of MESEX, whereas those from ABC26 and MMIN were extracted using the slightly different SE3 variant. Lower weights were used for the natural minerals (see for the variant applied on each mineral Fig. 5.2). The samples were added to Teflon tubes. After shaking with the appropriate solvent (mostly ~ 16 hours), these tubes were centrifuged at 4000 rpm, after which the solution was decanted. Between all steps, the samples were washed with distilled water. In SE1 and SE2, these washes were disregarded, whereas in SE3, they were included in the total extract per step. All solutions were measured using an Inductively Coupled Plasma Atomic Emission Spectrometer (ICP-AES; Perkin Elmer Optima 3000) for Fe, Mn, V, Al, Ti, S, Ni, Co, Zn and Cu. The quality of the measurements was monitored by the inclusion of blanks and in-house standards. Reproducibility was generally within 2% for all elements.

All samples, including the pure minerals, were subjected to total destruction by digestion in a mixture of hydrofluoric, nitric, and perchloric acids, which was subsequently vaporised to dryness in Teflon vessels on a sand bath. Final solutions were made in 1 M HCl and were analysed with ICP-AES (BC15 and ABC26-B on an ARL 34000; all other samples, including ABC26-C, on a Perkin Elmer Optima 3000). Repeated analysis of in-house and international standards gave a reproducibility of < 2% for all elements, except for Co and Ni in BC15 (4% and 5%), and Co in ABC26-B (5%).

5.3 Results and discussion

First, the results of MESEX on pure Fe and Mn minerals will be discussed. This will allow us to evaluate how the sequentially applied extractants will distinguish the various minerals. Then, the interaction of a combination of pure minerals will be examined using the results on the mixed mineral standard MMIN. Finally, the results on the extraction of two eastern Mediterranean boxcores will be used to gain a better understanding of the environmental and diagenetic history of Holocene eastern Mediterranean sediments.

5.3.1 Natural minerals

The Fe and Mn minerals used in this study can be divided into three groups: carbonates, oxides and sulphides. The two carbonates used here are siderite and rhodochrosite. The suite of Fe and Mn oxides include Fe-Mn nodules, goethite, haematite, magnetite, and ilmenite. Pyrite was the only sulphide mineral subjected to sequential extraction.

5.3.1.1 Carbonates

Siderite and rhodochrosite are not extracted in considerable amounts during the first six steps of MESEX (Fig. 5.2), as opposed to other carbonate minerals (see Chapter 7). Dissolution of rhodochrosite appears to be pH dependent: the amount dissolved is highest in the HF step (pH 4.2), and decreasingly lower amounts are extracted in respectively NaAc (pH 5), $MgCl_2$ (pH 5.2) and NaAC (pH 6). An exception in this series is the dithionite (pH 4.8) step, which does not fit in this trend. Siderite is mainly dissolved in the dithionite and HF steps, i.e. similar to most Fe oxides (see section 5.3.1.2). Siderite, however, is not a common mineral in sub-recent to recent marine sediments (Haese, 1997, 2000) and will not be considered from hereon.

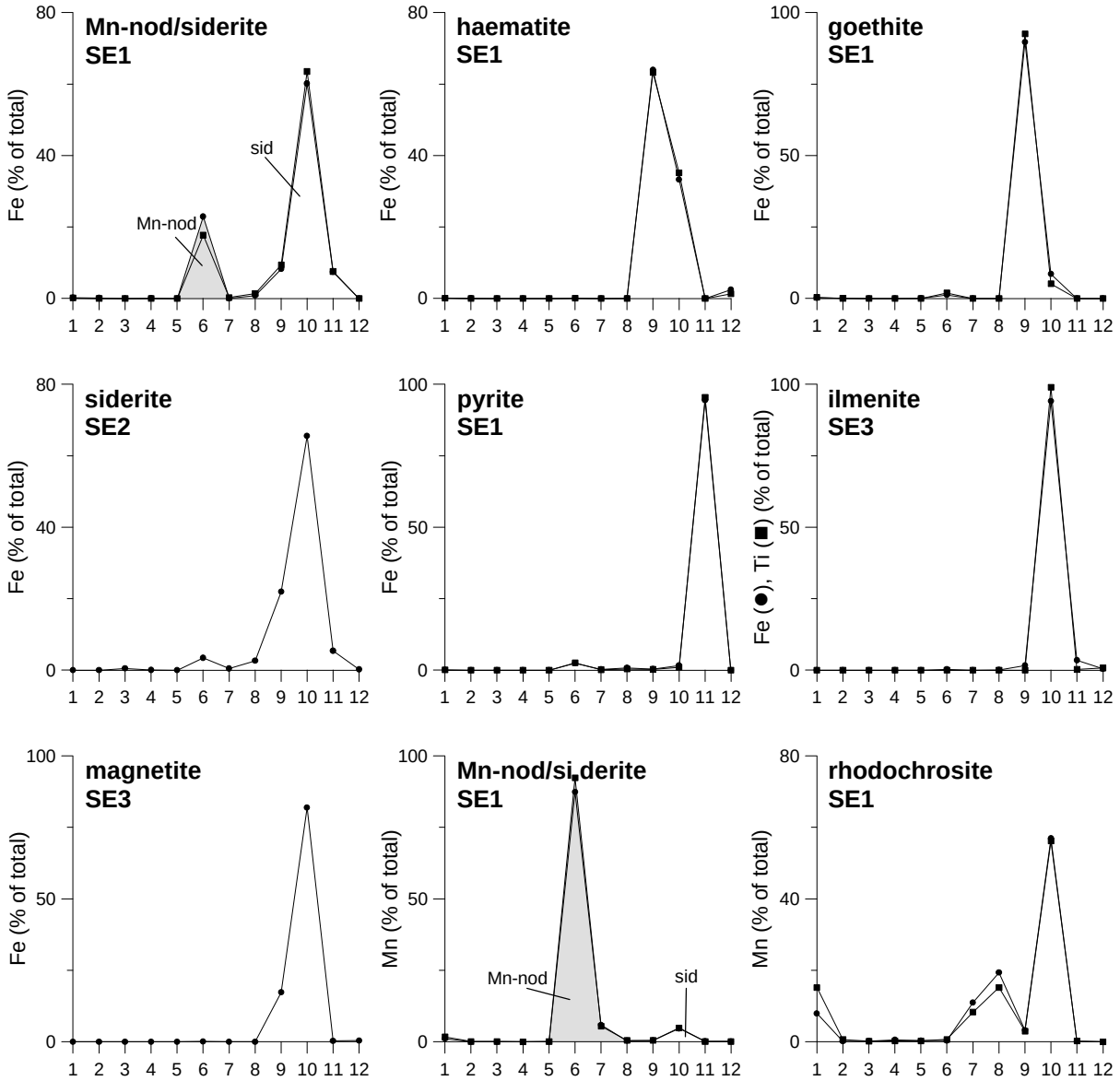

Figure 5.2 *The sequential extraction results for the pure minerals. Information on recovery and used scheme are included. The values for the Fe and Mn standards are reported in wt%.*

5.3.1.2. Oxides

Five different oxides were subjected to MESEX. The oxides of the Fe-Mn nodule are relatively easily extracted compared to the other four, and are completely dissolved using the ascorbate solution (step 6; Fig. 5.2; Table 5.3). Nodules contain easily dissolvable amorphous Mn and Fe oxides (Bernat et al., 1989) and are thus expected to dissolve in the ascorbate step. Goethite is also dissolved in small amounts in the ascorbate step (Table 5.3). Like haematite, goethite is mainly but not completely extracted in the dithionite step (Fig. 5.2; Table 5.3). The percentage of haematite and goethite which dissolves in the dithionite step appears to be rather constant, regardless of the total amount of mineral present. This might have two causes. Firstly, both minerals being natural, some Fe may be present in other phases that are not dissolved in dithionite but only in HF. This would result in similar percentages of Fe extracted in the dithionite step regardless of the total amount. Secondly, the reaction time in combination with reactive surface area might influence the amount of mineral dissolved. All mineral samples (except pyrite) were finely powdered, giving them similar grain sizes. If dissolution of haematite and goethite were slow and not instantaneous when applying the dithionite solution, the shaking time (i.e. the time in which the dithionite solution was in contact with the mineral sample) would have a profound effect on the possible amount of mineral dissolved. Having a similar grain size would result in similar percentages of the mineral dissolved, regardless of the total amount of mineral present. As goethite and haematite have been reported to completely dissolve in dithionite within an hour (Canfield, 1988), it is rather the first option, i.e. Fe mineral phases other than (hydr)oxides, that correspond to our findings.

The Fe dissolution potential, defined as the amount of Fe dissolved (in μg) divided by the weight used for sediment samples (in g; on average 0.25 g) and multiplied by 10^4 wt%/ppm, for goethite and haematite can be calculated for each sequential step. This is done to evaluate if, when applying a certain solvent to sediment samples, all goethite or haematite will be dissolved. For goethite, this potential is between 640 and 840 ppm for the ascorbate step, whereas it is at least 4 wt% for dithionite.

Table 5.3 *The extracted amounts of Fe for different Fe oxides in the ascorbate, dithionite and HF steps.*

Mineral	Fe-tot (mg)	Fe_{asc} (% of Fe-tot)	Fe_{dith} (% of Fe-tot)	Fe_{HF} (% of Fe-tot)
Mn-nod. 1	8.00	98.0%	–	–
Mn-nod. 2	4.42	99.1%	–	–
haematite 1	25.18	0.04%	64.0%	33.3%
haematite 2	33.17	0.10%	63.3%	35.2%
goethite 1	12.96	1.3%	89.7%	8.6%
goethite 2	10.98	1.9%	92.5%	5.1%
ilmenite	8.64	0.3%	1.6%	94.1%
magnetite	17.45	0.1%	17.2%	81.9%

The Fe dissolution potential for haematite in the dithionite step is 6.4 wt% at a minimum. Such high amounts are usually not found in sediments. Consequently, if present in samples, all goethite or haematite is expected to dissolve in the dithionite step, although goethite will already dissolve to some extent in the preceeding ascorbate step.

Ilmenite and magnetite are mainly extracted using HF, and only a relatively small amount dissolves in the dithionite step (Fig. 5.2; Table 5.3). However, the Fe dissolution potential of magnetite in the dithionite step is still 1.2 wt%, whereas that of ilmenite equals 560 ppm. In view of the quantities of these minerals normally found in marine sediments, most if not all crystalline Fe oxides will have been extracted after application of the dithionite solvent.

5.3.1.3 Pyrite

Dissolution of pyrite occurs predominantly in the HNO_3 step, although a small amount appears to be extracted in the ascorbate solution. The ratio between the amount of pyrite found in the ascorbate step to that in the HNO_3 step is 0.026 and 0.027 g/g respectively for the duplicate extractions, which had differing amounts of initial pyrite (61.9 and 101.4 mg pyrite respectively). Because the pyrite crystals had a similar grain size, this may point to the presence of some amorphous Fe oxides on the surface of the pyrite crystals. These Fe oxides may have formed by the slow oxidation of pyrite prior to, during or after the (gentle) grinding process. These (amorphous) Fe oxides will dissolve in the ascorbate solution.

5.3.2 MMIN

The extraction of single pure minerals has two major drawbacks. Firstly, the amount used in the sequential extraction schemes is usually much higher than the concentration found in normal sediments. This may result in saturation of the solvent when using the pure mineral, whereas in general sediment samples would not be saturated. Secondly, sediments are composed of a multitude of minerals. Because of matrix effects, a single mineral suspended in a solvent may show a dissolution behaviour different from when that mineral is a constituent of a mixture of several minerals. To overcome these problems, a homogenised standard of nine pure minerals was prepared (MMIN; Table 5.1). The proportion between these minerals resembles the composition of average Mediterranean sediments. This will allow us to assess the applicability of the sequential extraction scheme for this sediment. In the following sections, the efficiency of the sequential extraction of MMIN will be reviewed. Subsequently, we will discuss the behaviour of the Fe and Mn minerals present in MMIN.

5.3.2.1 The efficiency of the sequential extractions

The efficiency of the sequential extraction of MMIN can be evaluated by using the recovery for each element. The recovery for a specific element is defined as the sum of the concentrations of each step, divided by the concentration measured by using total digestion. For MMIN, the total recoveries are good for all elements except Al, K and Fe. These are much lower than 100% (Al and K: ~ 80%; Fe: 91%), which can be attributed to the loss of about 20% illite in the sample during the steps prior to the last four (in which it is extracted;

see section 5.3.2.4). This is likely to be caused by the small grain size of clay minerals, which are easily decanted resulting in a loss of sample. However, it will not affect data on e.g. element to aluminium (El/Al) ratios (see section 5.3.2.4). The sequential extraction data, therefore, still give a satisfactory picture of the mineral distribution in the sediment despite the sometimes lower recoveries for certain elements.

5.3.2.2 Manganite

Manganese in MMIN is mainly extracted in the ascorbate step (Fig. 5.3). The only major Mn containing mineral in MMIN is manganite (γ-MnOOH; measured Mn content 16.4 wt%), which contributes 521 ppm Mn. Quantification of Mn in this step (506 ppm) results in a recovery of 97.2%. This result, together with that of the extraction of ferromanganese nodules (see section 5.3.1.2), suggests that all Mn (oxy)hydroxides will be extracted in the ascorbate step.

5.3.2.3 Goethite, haematite and pyrite

Iron in MMIN (3.56 wt% Fe in total) is contributed by goethite, haematite, pyrite and illite. The sequential extraction results for Fe give a seemingly complicated picture (Fig. 5.3).

Pyrite is the most easily separable Fe mineral. It dissolves in the HNO_3 step (Fig. 5.2), and gives a recovery of 97.6%. This is based on the extracted sulphur in the HNO_3 step (0.49 wt% S; MMIN contains 0.50 wt% S in pyrite). When calculating pyrite-Fe from pyrite-S using the S/Fe molar ratio of 2, it is found that Fe in this step is slightly in excess over pyrite-S.

The amount of Fe extracted from MMIN in the ascorbate and dithionite steps is, respectively, 0.36 and 1.08 wt%. The contribution of Fe from amorphous oxides originating from the oxidation of some pyrite, to the ascorbate step can only be ~ 0.01 wt% Fe, based on the ratio between the amounts of Fe extracted in the ascorbate and HNO_3 steps in the single mineral extraction of pyrite (see section 5.3.1.3). Goethite and haematite contribute, respectively, 0.37 and 0.38 wt% Fe to MMIN. According to the natural mineral extraction, haematite is almost insoluble in the ascorbate step (Table 5.3). Therefore, nearly all of the Fe recovered during the ascorbate step can be attributed to goethite. This also means that all haematite must have dissolved in the dithionite step. However, the dithionite solution dissolves more Fe than can be explained by haematite alone. Most of this Fe is thought to come from illite (see next section).

In summary, during the sequential extraction of MMIN, goethite is extracted in the ascorbate step, whereas haematite is dissolved with dithionite. However, part of Fe extracted in the dithionite (pH 4.8) step is likely to originate from incongruous dissolution of illite (see next section). Pyrite is exclusively extracted in the HNO_3 step.

5.3.2.4 Illite

The illite used in this study contributes Al, K, Fe and Mg to MMIN. Aluminium and K, in MMIN almost solely from illite, are mainly extracted in the HF-step. However, Mg_{illite} is extracted in the HF as well as HNO_3 steps, whereas Fe_{illite} is dissolved in the dithionite and

HF steps.

Recovery of Mg, as well as some Na, Ca and Al, in the HNO_3 step is likely to be an extraction artifact due to the formation of a ralstonite-like mineral ($NaMgAlF_6.H_2O$) during the HF-step, as observed by Ingall et al. (1993). This is confirmed by the Mg/Al ratio of the HNO_3 solvent, which is 1.1 mol/mol. In our case, this mineral would have the formula $Na_{0.49}Ca_{0.33}Mg_{1.03}Al_{0.93}F_6.H_2O$. Therefore, prudence is called for when using HF, because some elements can reprecipitate and will only be redissolved in subsequent steps.

A large fraction of Fe_{illite} is dissolved in the dithionite step. When the total amount of $Fe_{haematite}$ is substracted from $Fe_{dithionite}$, this illite-attributed excess Fe corresponds to 0.70 wt% Fe in MMIN. Together with Fe_{illite} from the HF and $HF/HNO_3/HClO_4$ steps and excess Fe

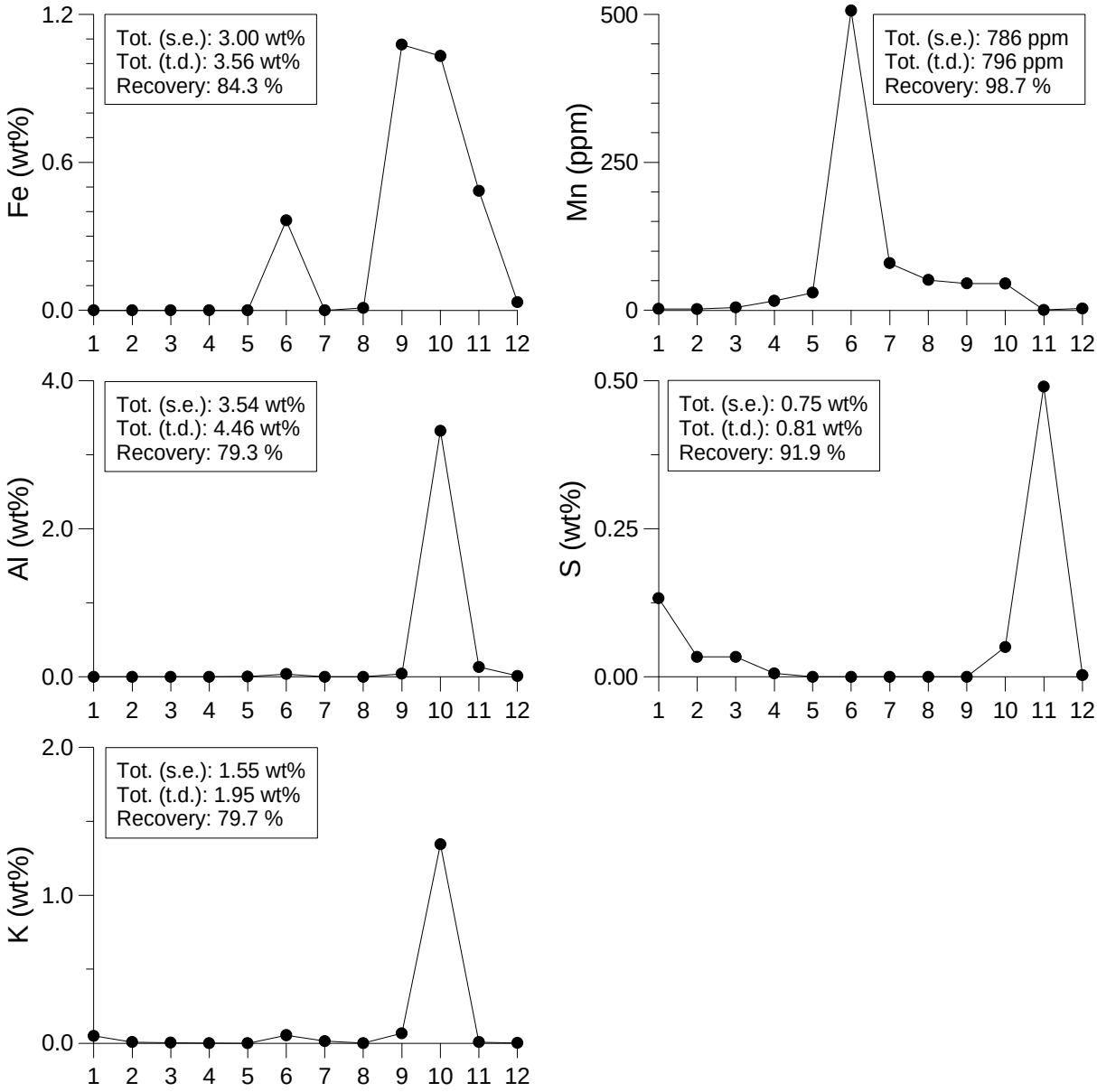

Figure 5.3 *The sequential extraction results using MESEX variant SE3 for MMIN (see Table 5.1), reported for Fe, Mn, Al, K and S. Information on the recovery is included.*

from the HNO_3 step (i.e. Fe_{HNO3} that is in excess over Fe_{pyrite} calculated from S_{pyrite}; see section 5.3.2.3), an Fe_{illite} recovery of 77.0% is calculated. This is close to recoveries of about 80% found for Al and K (see section 5.3.2.1). Therefore, it appears that there is incongruent dissolution of Fe_{illite} in the dithionite solution. X-Ray Diffraction analysis of the natural illite used in this study shows that the illite is not contaminated with Fe oxides. It has been observed that clay-Fe, e.g. in illite, chlorite and nontronite, is partially dissolved in acidic dithionite solutions (Slomp et al., 1996; Haese, 2000). Further evidence for the incongruent dissolution in dithionite of a part of the Fe contained in illite comes from sequential extractions of MMIN using slightly different schemes applied by S.J. Schenau (Utrecht University). A scheme similar to MESEX gives almost identical results for Fe dissolution in the ascorbate, dithionite and HF steps (Table 5.4, Schenau (1) scheme). However, application of a solution of dithionite at pH 7.6 (Ruttenberg, 1992), followed by extraction with 1 M HCl and then HF gives very different results, especially for the HF step (Table 5.4, Schenau (2) scheme). Quantification of the Fe dissolved in the ascorbate, dithionite (pH 7.6) and 1 M HCl steps equals the total amount of goethite and haematite in MMIN, whereas the amount of Fe contained in illite — now mainly in the HF step — is about equal to that calculated for MMIN from the MESEX result. This also indicates that the excess Fe extracted in (acidic) dithionite is likely to be present in illite. Therefore, using a low pH during the dithionite step may dissolve part of the Fe contained in illite and other clay minerals. However, the mechanism responsible for this is as yet unclear, because Al and Si are not extracted in significant amounts compared to Fe (compare Fe: 0.70 wt%; Al: 0.04 wt%; Si 0.09 wt%).

The 'clay fraction' of Al, K and Mg in MMIN consists of the amounts dissolved in steps 9 to 12, whereas that of Fe contains those of steps 10 and 12 plus the excess amounts of steps 9 and 11. Element to Al ratios of the clay fraction in MMIN confirm their relation to pure illite ($K/Al_{pure\ illite}$ = 0.42 g/g, $K/Al_{clay\ fraction}$ = 0.43 g/g; $Mg/Al_{pure\ illite}$ = 0.10 g/g, $Mg/Al_{clay\ fraction}$ = 0.11 g/g; $Fe/Al_{pure\ illite}$ = 0.53 g/g, $Fe/Al_{clay\ fraction}$ = 0.52 g/g). Consequently, the lower recoveries of K, Fe and Al (see section 5.3.2.1) do not influence the El/Al ratios of the clay mineral fraction.

Table 5.4 *The extracted Fe (wt%) in MMIN measured during the application of three slightly different sequential extraction schemes. (1) and (2): unpublished data S.J. Schenau; n.d. = not done.*

Fe (wt%) MMIN	**asc. acid**	**dithionite**		**1 M HCl**	**HF**	**HNO_3**	**$HF/HClO_4$/ HNO_3**	**Recovery (%)**
		pH 4.8	**pH 7.6**					
this study	0.364	1.077	x	n.d.	1.031	0.484	0.032	84.3
Schenau (1)[a]	0.413	1.097	x	n.d.	1.027	n.d.	0.521	87
Schenau (2)[b]	0.389	x	0.096	0.408	1.883	0.554	n.d.	94.3

[a] *This scheme is reported in Schenau (1999)*

[b] *S.J. Schenau, personal communication*

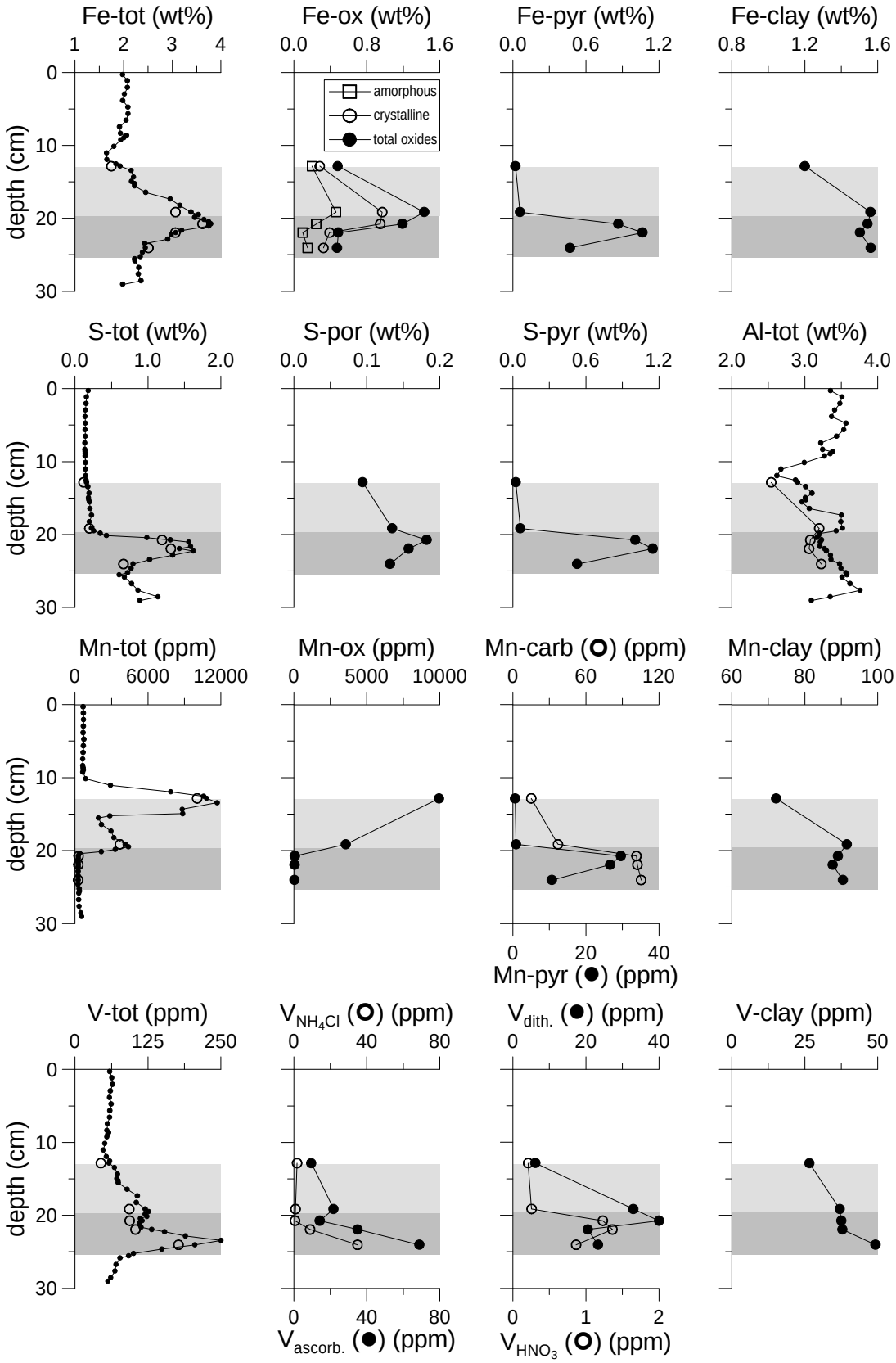
Fe-tot (wt%)
Fe-ox (wt%)
Fe-pyr (wt%)
Fe-clay (wt%)
amorphous
crystalline
total oxides
depth (cm)
S-tot (wt%)
S-por (wt%)
S-pyr (wt%)
Al-tot (wt%)
Mn-tot (ppm)
Mn-ox (ppm)
Mn-carb (O) (ppm)
Mn-clay (ppm)
Mn-pyr (●) (ppm)
V-tot (ppm)
V-clay (ppm)
V_NH4Cl (O) (ppm)
V_dith. (●) (ppm)
V_ascorb. (●) (ppm)
V_HNO3 (O) (ppm)

5.4 Sediments

Boxcore ABC26 contains a sediment sequence typical for the pelagic eastern Mediterranean (see also Chapter 1). It consists of oxic fine-grained sediments, which overlay organic-rich sapropel S1. Between these two sediment intervals, a red-brown oxidised sapropel zone can be distinguished, the top part of which is indicated by the upper Mn peak. Under the sapropel, hemipelagic gray clayey sediment is found. For the sequential extraction (MESEX variant SE3) we have selected five samples at the same depths in two subcores of ABC26; one is located at the top of the oxidised sapropel zone, one immediately above the visible, remaining sapropel, and three in the sapropel proper.

The sediment sequence of BC15, a boxcore recovered from a former brine basin, is described in detail in Chapter 4. Briefly, it contains a unit of organic-rich sediments, with an age comparable to sapropel S1, redeposited from within a brine environment. It is overlain by a unit consisting of an organic-enriched foraminifera ooze at its base and organic-poor oxic sediments almost devoid of foraminifers. This unit appears to be redeposited from outside the brine. On top lies a normal, oxic, sediment sequence accumulated after reoxygenation of the brine basin with a distinct Mn peak at its base. Eighteen samples throughout the boxcore were selected for sequential extraction (MESEX variant SE2).

In the following sections we will first briefly discuss the results of the extraction, then we will move on to discuss the results for the redox-sensitive elements Mn, Fe and V, and regard the differences in the palaeoredox history of the normal and of the former brine sediments. Then, the difference between the extraction results for the two ABC26 subcores will be used to draw conclusions about the affinity of the trace metal fraction associated with reduced mineral phases for organic matter or pyrite. Finally, metal to Al ratios of the clay mineral fraction will be compared between the different sedimentary units to establish the palaeo-environmental implications of these ratios.

5.4.1 Element speciation in ABC26 and BC15

For the samples of boxcore of ABC26-B, average recoveries for all elements except Al and V are close to 100% (compare the graphs containing the data on total digestion and the sum of all MESEX steps in Fig. 5.4). The slightly lower recovery of Al can be explained by the loss of some very fine-grained clay minerals during decanting of the extractants. The relatively low recovery of V (~ 80%) might be due to the incomplete dissolution of one or more V-containing refractory phases and/or to decanting of V-containing clay minerals and

Left page: **Figure 5.4** *The sequential extraction results for Fe, S, Al, Mn and V using MESEX variant SE3 for ABC26-B. The line/dot plots in the total element (El-tot) graphs are the concentrations found when applying total digestion, whereas the open circles report the total calculated by summing all steps of the sequential extraction. The explanation of the abbreviations is as follows: ox = oxides; pyr = pyrite; clay = clay minerals (aluminosilicates); por = pore water; carb = carbonates; NH_4Cl = sum of NH_4Cl steps; ascorb = ascorbate step; dith = dithionite step; HNO_3 = HNO_3 step.The dark-grey area indicates the unoxidised sapropel S1, whereas the light-grey area represents the oxidised sapropel zone. The values for amorphous and crystalline oxides were calculated according to Appendices 5-A and 5-B.*

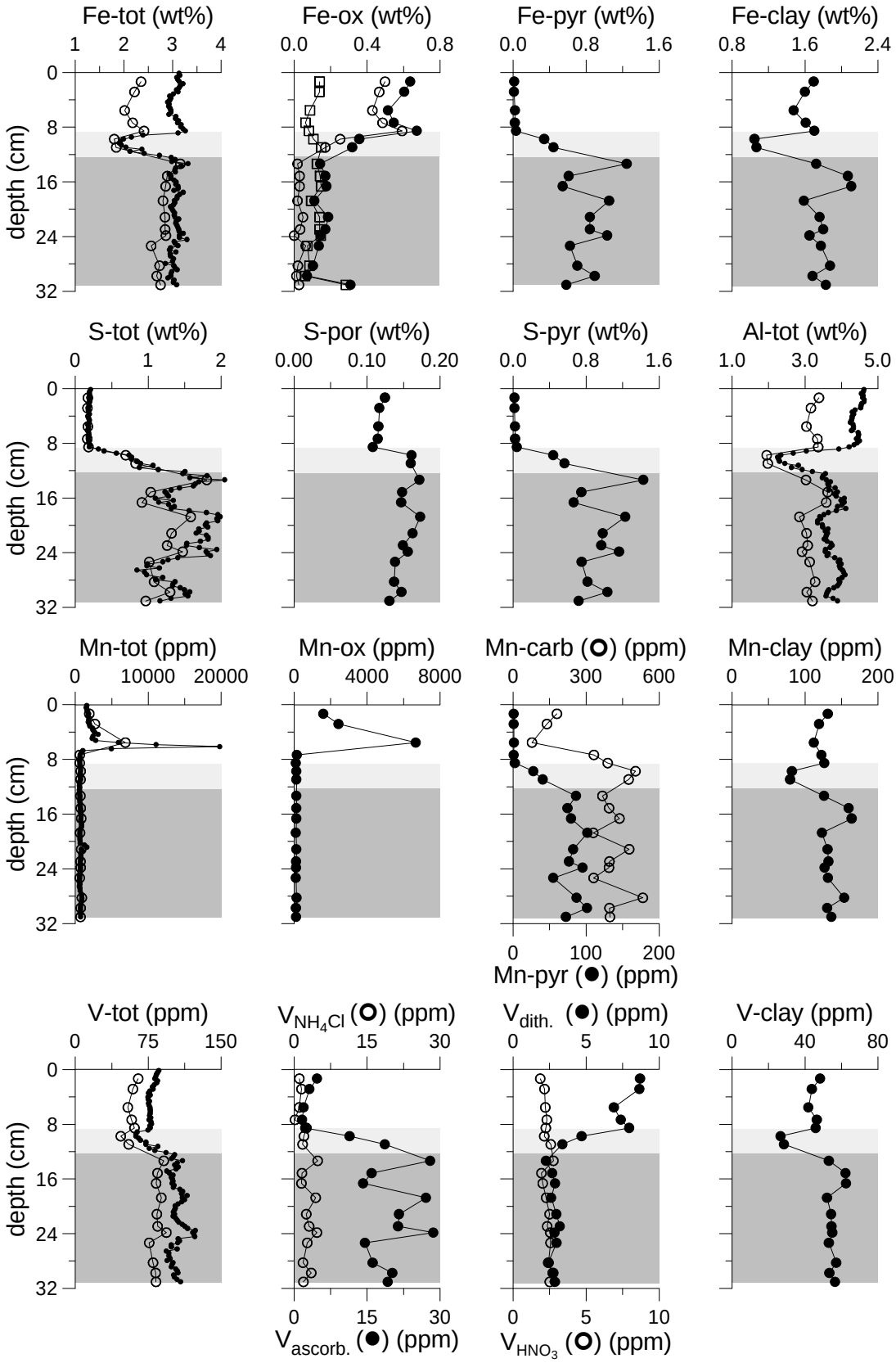
Fe-tot (wt%)
Fe-ox (wt%)
Fe-pyr (wt%)
Fe-clay (wt%)
S-tot (wt%)
S-por (wt%)
S-pyr (wt%)
Al-tot (wt%)
Mn-tot (ppm)
Mn-ox (ppm)
Mn-carb (O) (ppm)
Mn-clay (ppm)
Mn-pyr (●) (ppm)
V-tot (ppm)
V$_{NH_4Cl}$ (O) (ppm)
V$_{dith.}$ (●) (ppm)
V-clay (ppm)
V$_{ascorb.}$ (●) (ppm)
V$_{HNO_3}$ (O) (ppm)
depth (cm)

organic matter. Subcore ABC26-C (not shown) gives almost identical results. The recoveries of boxcore BC15 samples are relatively low for all elements except Mn (see the "total" graphs in Fig. 5.5). Decanting of fine-grained clay minerals, as indicated by Al might explain the low recovery of Fe and Al. Vanadium, again, has a relatively low recovery (~ 78%). Despite the relatively low recoveries for certain elements, the sequential extraction data give a representative picture of the mineral distribution in the sediment, similar recoveries were found for all samples.

Iron is mainly dissolved in five steps: ascorbate (step 6), dithionite (step 9), HNO_3 (step 11) and HF and HF/$HClO_4$/HNO_3 (steps 10 and 12, respectively). Results for the ascorbate and dithionite steps show abnormally high Fe concentrations in the organic-rich sediments of both ABC26 and BC15 (Appendices 5-A, 5-B). Because these sediment layers are reduced, Fe_{oxide} concentrations are expected to be low. In ABC26, Fe concentrations (~ 0.6 wt%) of the lowest two samples are comparable with the one for the uppermost, oxic sample. In BC15, the organic-rich samples have lower Fe concentrations than those from the oxic sediment, but are still rather high (Fe_{oxide} ~ 0.5 wt%). Passier and De Lange (1998) found low Fe_{oxide} contents in the remaining sapropel when applying dithionite to sapropel S1 in a boxcore (UM26), located close to the ABC26 site (no ascorbate extraction was performed). Sample handling and extraction of UM26 was done in an inert atmosphere, in contrast to our extraction. We think that the relatively high Fe content of the organic-rich samples in the ascorbate step is related to the oxidation of some pyrite, probably during oven-drying of the sediment. This is corroborated by the S/Na ratio of the first step, which is much higher than the pore water S/Na ratio in these samples. On the basis of this, we have applied a correction for $Fe_{ascorbate}$ so as to obtain the $Fe_{ascorbate}$ content which reflects its in-situ content (see Appendix 5-A). In Figures 5.4 and 5.5, the corrected $Fe_{ascorbate}$ contents are reported as $Fe_{amorphous\ oxides}$. The relatively high $Fe_{dithionite}$ concentration in the organic-rich samples is most probably related to the extraction of some clay minerals, as was demonstrated to have occurred for illite in the sequential extraction of MMIN. The extracted Mg content is also relatively high in this step and closely follows the total-Al profile, although Al concentrations are low in this step. In eastern Mediterranean sediments, illite and chlorite are abundant (Chamley, 1989). Especially chlorite has Fe and Mg as major elements. The ratio between Fe and Mg from clay minerals in the last three steps can then be used to distinguish between Fe_{oxide} and Fe_{clay} (see Appendix 5-B). In Figures 5.4 and 5.5 the corrected $Fe_{dithionite}$ contents are reported as $Fe_{crystalline\ oxides}$. Iron released in the HNO_3 step (step 11) can be attributed to pyrite, whereas Fe dissolved in steps 10 and 12 comes from clay minerals.

Left page: **Figure 5.5** *The sequential extraction results for Fe, S, Al, Mn and V using MESEX variant SE2 for BC15. The line/dot plots in the El-tot graphs are the concentrations found when applying total digestion, whereas the open circles report the total calculated by summing all steps of the sequential extraction. The legend for Fe-ox is the same as in Fig. 5.4. The explanation of the abbrevations can be found in the caption of Fig. 5.4. The dark-grey area denotes sapropelic sediments, the light-grey area the organic-enriched and foraminifera-rich zone. The values for amorphous and crystalline oxides were calculated according to Appendices 5-A and 5-B.*

Like Fe, Mn is found in oxides and clay minerals, but also as a trace element in carbonates and pyrite. The Mn oxides are mainly amorphous. Sulphur is mostly found in the first step (from precipitated pore water salts) and in pyrite (step 11). Aluminium is mostly extracted in the last three steps, indicating its relation to clay minerals.

Vanadium gives interesting extraction results. Part of the diagenetic peak in the lower half of the sapropel in ABC26 is dissolved in the NH_4Cl steps and, more importantly, in the ascorbate step. In BC15, relatively much V in the organic-rich sediment is dissolved in the NH_4Cl and ascorbate steps. In the dithionite step (V-dith), V follows more or less the Fe oxide profile in both boxcores.

5.4.2 Mn(II)/Mn(III,IV) redox boundary and diagenesis: Mn oxides and Mn carbonates

The location of the Mn(II)/Mn(III,IV) redox boundary is a measure for the depth down to which the pore water contains oxygen. Manganese will precipitate as $MnO_{1.5–2}$ in oxygen-containing sediments, whereas Mn containing carbonates are in equilibrium with Mn^{2+} (Middelburg et al., 1987). Therefore, comparison between the oxide and carbonate profiles of Mn will reveal the location of the redox boundary. The upper two samples of ABC26 (taken at the upper and lower Mn peak; Fig. 5.4) clearly contain high concentrations of Mn oxides, whereas all samples in the sapropel are almost devoid of these minerals. In the latter samples, however, Mn is present in carbonates (Fig. 5.4). This shows that the Mn(II)/Mn(III,IV) redox boundary is located exactly at the top of the present sapropel, and that oxygen has penetrated this sediment down to this depth. Although we have no porewater data for this core, porewater Mn^{2+} and oxygen data from nearby boxcore UM26 confirm the location of this boundary and the absence of oxygen below it. In BC15, the Mn(II)/Mn(III,IV) redox boundary is located at the large Mn_{total} peak. Manganese in the sediment from the top down to the Mn peak is mainly present as amorphous Mn oxides. $Mn_{carbonate}$, however, is relatively enriched below the peak, indicating equilibrium between Mn^{2+} and Mn containing carbonates (Fig. 5.5). This is confirmed by the pore water Mn^{2+} concentration, which also increases drastically below this Mn oxide peak (see also Chapter 4). This means that the sediment below the Mn peak is currently oxygen-depleted.

The results for the sequential extraction of ABC26 indicate that both Mn_{total} peaks consist of Mn oxides. The upper peak has been identified throughout the deep eastern Mediterranean and has a nearly uniform age (~ 5 kyr; Thomson et al., 1995). It is thought to be deposited either hydrogenically or by a fixation mechanism upon reoxygenation of the eastern Mediterranean deep water (Higgs et al., 1994; Van Santvoort et al., 1996). Commonly, the upper Mn peak is now taken as an indicator for the upper boundary of the original sapropel deposition. The lower Mn oxide peak has been formed by the oxidation of upward diffusing Mn^{2+}. This lower peak shows a gradual increase with depth with an abrupt ending at the present Mn(II)/Mn(III,IV) redox boundary. With time and depth, the progress of the oxidation front slows down, due to continuing (oxic) sedimentation which increases the distance between front and sediment-water interface. This causes precipitation of increasing amounts of Mn oxides at each subsequent level (e.g. Higgs et al., 1994; Thomson et al.,

1995). A minor Mn source for these oxides is Mn in pyrite, which is now only present in the visible unoxidised sapropel (Fig. 5.4), but which is oxidised by a downward moving oxidation front. However, most of the Mn that formed the lower Mn peak originates from reductive dissolution and subsequent diffusive transport of Mn^{2+} from sediment intervals well below sapropel S1, as demonstrated by the characteristic form of pore water Mn^{2+} profiles in sapropel S1 (Van Santvoort et al., 1996; Chapter 4).

The single large Mn_{total} peak in BC15 also consists of Mn oxides (compare Mn_{oxide} and Mn_{total} in Fig. 5.5). The sharpness of the peak indicates that bioturbation and a downward prograding oxidation front have not been active in the top of this boxcore. In Chapter 4 it is inferred that this peak has probably been deposited upon reoxygenation of the previously anoxic Poseidon Basin.

5.4.3 Fe(II)/Fe(III) redox boundary and diagenesis: Fe oxides and pyrite

Iron is the most abundant redox-sensitive metal. Oxygen-enriched sediments are characterised by a diversity of Fe oxides, such as goethite and haematite. Oxygen-depleted marine sediment, however, mostly contains an abundance of Fe sulphides, of which pyrite is dominant (e.g. Passier et al., 1996, 1997). In eastern Mediterranean sediments, the Fe(II)/Fe(III) redox boundary is situated close to the downward moving oxidation front (e.g. Van Santvoort et al., 1996).

In ABC26, the Fe(II)/Fe(III) redox boundary is located slightly below the Mn(II)/Mn(III,IV) redox boundary. This is indicated by the highly enriched concentration of Fe oxides just above and below the top of the present sapropel. The lower one of these two samples also contains a high amount of pyrite, still present in the remaining sapropel (Fig. 5.4). The Fe(II)/Fe(III) redox boundary is, therefore, located close to this sample. This means that there is a separation between the Fe and Mn redox boundaries, a phenomenon often seen in sediments and thought to be the result of thermodynamics and kinetics (Lynn and Bonatti, 1965; Froelich et al., 1979; Burdige and Gieskes, 1983; De Lange, 1986; Pruysers et al., 1993; Thomson et al., 1995; Stumm and Morgan, 1996). The Fe oxide content gradually increases with depth until immediately above the visible sapropel. These oxides have been precipitated as the result of oxidation of upward diffusing Fe^{2+}. One of the major Fe sources for these oxides is pyrite, which is completely removed as the downward moving oxidation front progresses.

In BC15, the absence of a downward moving oxidation front is not only indicated by the Mn versus depth profile (Fig. 5.5), but also by the fairly constant Fe oxide content in the uppermost part of the core. A faint Fe oxide peak at 9 cm likely indicates the present Fe(II)/Fe(III) redox boundary. This is confirmed by the presence of pyrite below this depth only (Fig. 5.5). Consequently, in this core the Mn and Fe redox boundaries are more widely separated than in ABC26. This is probably due to the organic matter contents, changing more gradually versus depth and being slightly lower than in ABC26.

The shifts in total Al, Fe-clay, and Mn-clay in ABC26 and BC15 correspond nicely with the respective carbonate contents of these samples (Chapters 4, 7), the upper sample in ABC26 containing 60 wt%, the other samples 50 wt%, i.e. a non-carbonate content of 40 and

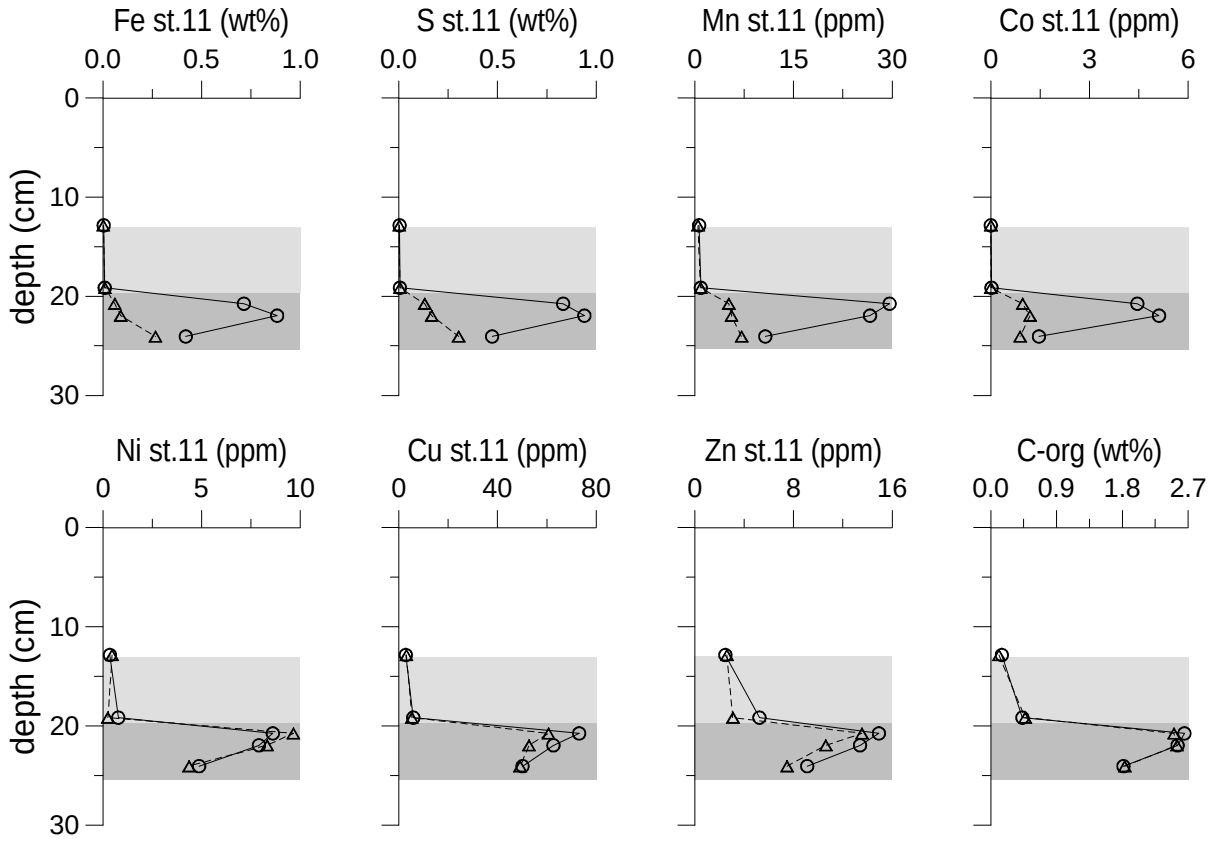

Figure 5.6 *Concentrations of Fe, S, Mn, Co, Ni, Cu and Zn in the HNO_3 step (= step 11) vs. depth in boxcore ABC26 samples. Also plotted is the organic carbon content vs. depth. Circles indicate samples from ABC26 subcore B, triangles samples from ABC26 subcore C.*

50 wt% respectively. This 25% relative increase is exactly reflected in all these parameters. A similar correspondence exists for these parameters and V-clay in BC15, but not for V-clay in ABC26 (see below).

5.4.4 Other redox-sensitive elements: Vanadium

Vanadium is also an element sensitive to changes in redox conditions. It has two prominent redox species, namely vanadate (V(V)), which prevails under oxic conditions, and V(IV), which is common as vanadyl (VO^{2+}) in reduced environments (Breit and Wantly, 1991). Both species are surface reactive, but vanadyl will be adsorbed far more strongly in natural waters (Wehrli and Stumm, 1989). Consequently, vanadium is thought to be removed from solution under reducing conditions (Emerson and Huested, 1991). In addition, vanadyl is often associated with organic ligands, humic and fulvic acids, and porphyrins (Cheshire et al., 1977; Wehrli and Stumm, 1989; Emerson and Huested, 1991; Antipenko et al., 1996). In the case of the oxidation of the previously reduced sapropel, vanadyl is oxidised to V(V) and diffuses downwards until it is again reduced and removed from solution. This occurs a few centimetres below the oxidation front, as can clearly be seen in the total-V profile of ABC26,

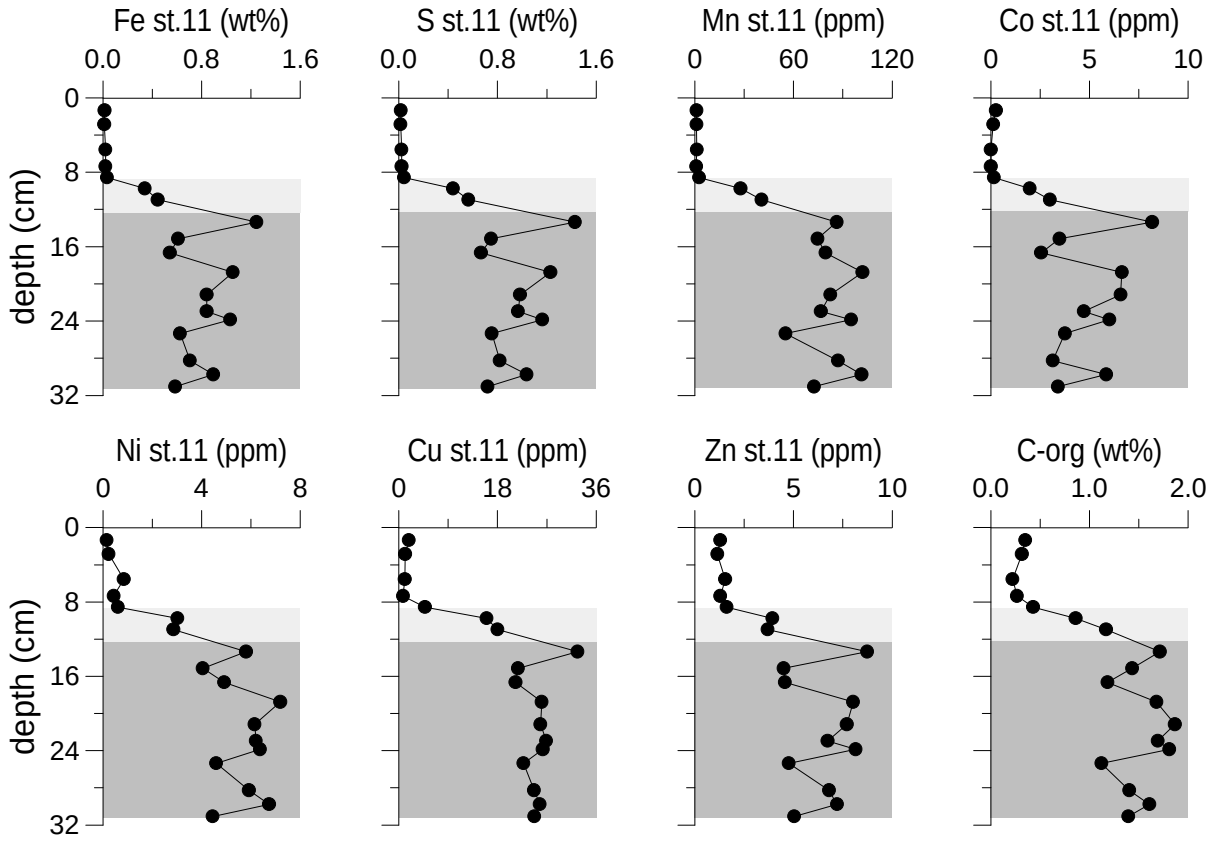

Figure 5.7 *Concentrations of Fe, S, Mn, Co, Ni, Cu and Zn in the HNO_3 step (= step 11) vs. depth in boxcore BC15. The organic carbon content vs. depth is also given.*

where a strong V peak exists near the bottom of the sapropel (Fig. 5.4). It is, however, unknown to which phase(s) this vanadium is attached. In the sequential extraction, most of this reduced excess V is released during the NH_4Cl steps and especially in the ascorbate step (Fig. 5.4). A separate 0.5 M NaOH extraction of the same samples also dissolved most of the V peak (unpublished results). The latter extraction is thought to release humic components, but also some oxides. Since there is no correlation between V recovered in the NH_4Cl and ascorbate steps and V present in Fe and Mn oxides, most of the excess vanadium is thought to be present as vanadyl absorbed to organic ligands matter. This is confirmed by the results found in BC15, where the concentration of reduced vanadium species, extracted in the NH_4Cl and ascorbate steps, is much higher in the organic-rich sediments, closely following the organic carbon profile (Fig. 5.5). The absence of a vanadium peak is, again, evidence for the absence of redox diagenesis in BC15 and allows for the determination of initial V/C_{org} ratios (see Chapter 4).

5.4.5 Trace element distribution in the HNO_3 step

The two subcores of ABC26 give almost identical results for all elements in all steps with the exception of the HNO_3 step, which extracts pyrite and organic-bound elements. The

profiles of Fe and S, indicative of pyrite, differ considerably between these cores, whereas the organic carbon content does not (Fig. 5.6). It appears that the state of diagenesis differs between these two closely spaced subcores, a phenomenon also encountered by Thomson et al. (1995) in two eastern Mediterranean subcores from the same multicorer. This strong difference allows us to determine whether some trace elements are related more to pyrite or more to organic carbon. It appears that Mn and Co have profiles comparable to pyrite, whereas Ni, Cu and Zn follow the pattern of organic carbon (Fig. 5.6). In BC15,organic carbon and pyrite give comparable profiles, hence the trace element distributions of Mn, Co, Ni, Cu and Zn do not differ significantly (Fig. 5.7). However, there are small but distinctly detectable differences. In the upper, oxic part of the boxcore, Zn, Ni and Cu that were dissolved in the HNO_3 step, concord with the presence of organic matter, whereas Fe, S, Mn and Co have concentrations close to zero. Therefore, we conclude that Mn and Co extracted with HNO_3 are mainly associated with pyrite, whereas Ni, Cu and Zn appear to be associated with organic matter.

In boxcore ABC26, ongoing redox diagenesis has resulted in the lowering of the upper boundary of the original sapropelic, organic-rich sediment. A penetrating oxygen front will

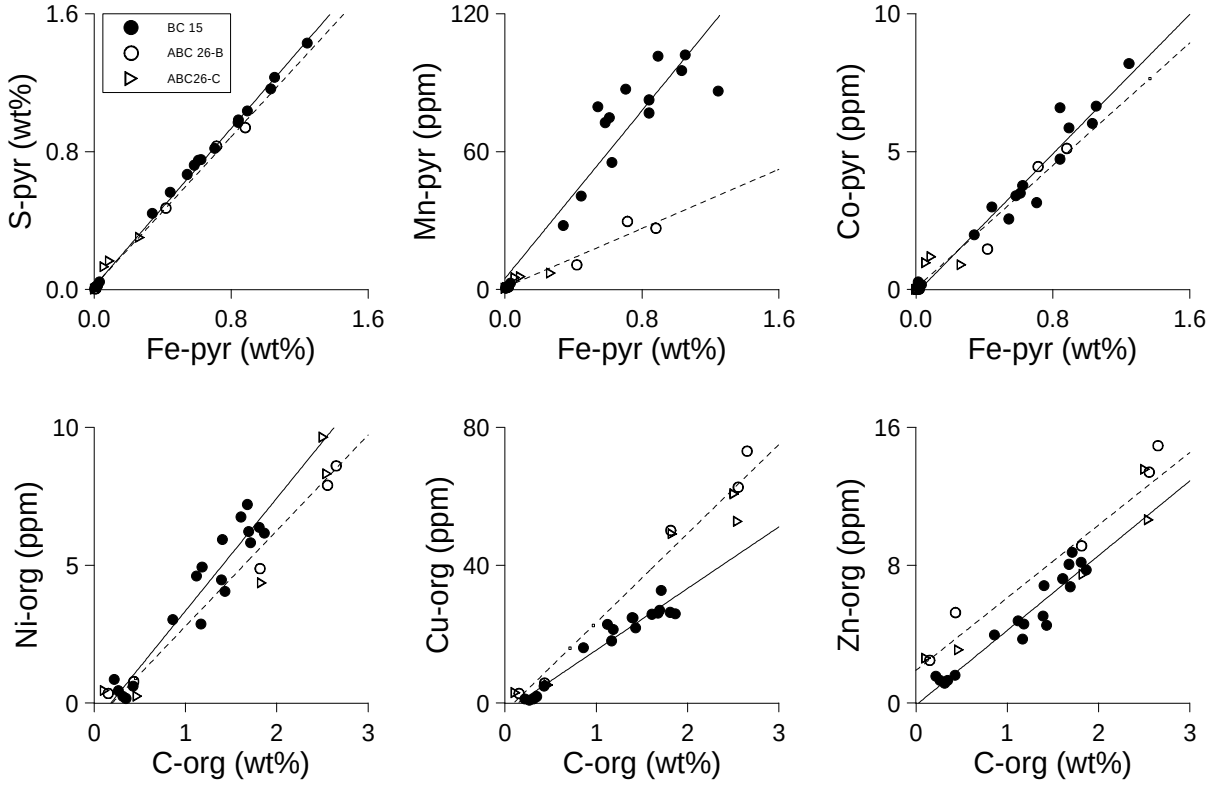

Figure 5.8 *Pyritic Fe vs. S_{pyr}, Mn_{pyr} and Co_{pyr}, and organic carbon vs. Ni_{org}, Cu_{org} and Zn_{org}. The differentiation between pyrite and organic matter is based on the findings plotted in Fig. 5.6. Solid circles indicate BC15 samples, open circles ABC26-B, and open triangles ABC26-C. The solid line is the best linear fit in BC15, the dotted line the best linear fit in ABC26 (based on all ten samples).*

affect not only the oxidised sediment, but also the deeper, visibly unaltered sapropel. This is for example seen in the profile of V (Fig. 5.4), in which a strong V spike is present within the still-present unoxidised part of the last sapropel. Whether the downward moving oxidation front has caused changes in the element distribution of the original sapropel might be inferred from the comparison between ABC26, containing possibly affected sapropelic sediments, and BC15, in which no redox diagenesis has taken place (Fig. 5.8). The S/Fe ratio of BC15 and ABC26 is almost identical, indicating that pyrite present in the original sapropel is not changed diagenetically and may also have retained its initial trace element content. This is corroborated by the relationship between Co and pyrite, which shows no difference between the two boxcores. However, manganese in pyrite is about twice as low in ABC26 relative to BC15. In Chapter 4 this is attributed to a different original Mn porewater content during formation of the pyrite. The original trace metal content in pyrite appears to be preserved if the sediment remains under oxygen-free conditions. Nearly the same appears to apply for organic matter and associated Ni, Cu and Zn for ABC26 and BC15 (Fig. 5.8). Similar relationships occur within each core, whereas only minor variations are present between the two cores. A downward moving oxidation front apparently affects neither pyrite nor the organic material that is present below such a front.

5.4.6 Terrigenous components

At present, input from Saharan dust is the major terrestrial source in most of the central eastern Mediterranean (Krom et al., 1999; Chapter 2). During periods of sapropel formation, river input drastically increased in the eastern Mediterranean, changing the character of the terrigenous component in sediments due to mineralogical differences of the source areas (Dominik and Stoffers, 1979; Krom et al., 1999). Clay minerals are the major component of the terrigenous fraction in pelagic sediments. There are a number of different clay minerals, each having characteristic compositions, expressed in differences in major element concentrations. Illite, e.g., contains primarily K, chlorite Fe and Mg, whereas kaolinite only contributes Al.

By using the MESEX scheme, differences in the terrigenous fraction can be measured, because clay minerals and heavy minerals are relatively insoluble and are only extracted using HF and $HF/HClO_4/HNO_3$ (steps 10 and 12, respectively). Because Al is a distinctive terrigenous component, element to Al ratios of the clay fraction of MESEX give information about changes in the terrigenous raction. These ratios were calculated for both boxcores (Table 5.5). For ABC26, there is no significant change in the K/Al ratio, suggesting that no relative changes in the relative illite content of the terrigenous fraction has occurred at this site. The Fe/Al and Mg/Al ratios, though fairly constant, are somewhat higher in the middle of the original sapropel, with values gradually decreasing towards the top and the bottom of the sapropel. In BC15, ratios are relatively constant within each of the distinguished zones, as seen from the 1σ standard deviation, but vary signifantly between these zones. The K/Al ratio is similar in the upper, oxic zone and the sapropel. Fe/Al and Mg/Al ratios are clearly enhanced in the sapropel. The higher Fe/Al and Mg/Al ratios in the sapropelic sediments of both boxcores indicate a relatively higher input of chlorite compared to other clay minerals,

Table 5.5 *Element/Al ratios found for the clay mineral fraction of the sequential extraction (see for calculation section 5.3.2.4) in samples from ABC26-B and BC15. Also shown are literature data on average shales and average marine clays.*

Boxcore and sample description		Fe/Al_{cl} (g/g)	Mg/Al_{cl} (g/g)	K/Al_{cl} (g/g)	Mn/Al_{cl} (mg/g)	V/Al_{cl} (mg/g)	Ni/Al_{cl} (mg/g)	Co/Al_{cl} (mg/g)	Zn/Al_{cl} (mg/g)	Cu/Al_{cl} (mg/g)
ABC26	**description**									
12.8 cm	upper Mn peak	0.483	0.251	0.248	2.49	1.10	1.56	0.157	1.04	0.269
19.1 cm	lower part of oxidised zone	0.494	0.262	0.244	2.60	1.20	1.68	0.195	1.08	0.310
20.7 cm	upper part of visible sapropel	0.506	0.273	0.244	2.76	1.26	1.65	0.189	1.24	0.698
21.9 cm	sapropel	0.493	0.261	0.244	2.68	1.27	1.69	0.200	1.28	0.657
24.0 cm	sapropel	0.487	0.245	0.249	2.60	1.58	1.44	0.197	1.14	0.473
BC15	**description**									
0.0-8.7 cm	oxic zone (n=5)	0.499 ± 0.011	0.307 ± 0.004	0.274 ± 0.007	2.77 ± 0.15	1.43 ± 0.03	2.12 ± 0.10	0.227 ± 0.009	0.69 ± 0.03	0.576 ± 0.062
8.7-12.3 cm	foraminifer- and organic-enriched zone (n=2)	0.540 ± 0.001	0.303 ± 0.013	0.286 ± 0.014	3.38 ± 0.13	1.42 ± 0.04	2.23 ± 0.09	0.246 ± 0.004	0.89 ± 0.02	0.716 ± 0.012
12.3-31.2 cm	sapropel (n=11)	0.573 ± 0.010	0.348 ± 0.010	0.265 ± 0.002	3.67 ± 0.22	1.79 ± 0.05	2.60 ± 0.07	0.256 ± 0.008	0.75 ± 0.05	0.754 ± 0.088
Literature values for shales*										
Shale (1)		0.590	0.188	0.333	10.63	1.63	0.85	0.238	1.19	0.563
Shale (2)		0.511	0.152	0.272	9.24	1.41	0.87	0.217	0.98	0.543
Mean shale (3)		0.545	0.182	0.278	9.66	1.48	0.77	0.216	1.36	0.443
Average post-Archean shale (4)		0.505	0.133	0.307	8.52	1.50	0.55	0.230	0.85	0.500

* *References: (1) Turekian and Wedepohl (1961); (2) Krauskopf (1967); (3) Bowen (1979); (4) Taylor and McLennan (1985)*

a fact which is commonly observed in eastern Mediterranean sapropels (Chamley, 1989). This points to more humid climatic conditions on land, and to changes in terrestrial input in concert with the deposition of sapropels. These changes may have been induced by enhanced rainfall in sapropel times, which would have resulted in an increase of the input of riverine material. Also, the source(s) for atmospheric dust may have shifted. Both could result in a change of the clay mineral composition (see also Krom et al., 1999).

Trace element (El) to aluminium ratios of the clay fraction show a trend similar to that of the Fe/Al and Mg/Al ratios (Table 5.5). They appear to be enriched in the sapropelic samples. The variations in the absolute value of the El/Al ratios between the two boxcores may relate to the different locations of the boxcores. Although they are in the same general

area, currents may distribute clay minerals differently in different regions. However, this does not change the actual trend.

Comparison between the MESEX measured El/Al ratios of the terrigenous fraction of eastern Mediterranean sediments and reported values for average shales (Table 5.5) shows that, although most of our El/Al ratios are in the same range as these average values, sequential extraction is necessary to establish the correct El/Al ratios of the terrigenous fraction in each sediment sample. This is important when, for example, the non-clay mineral fraction of a certain metal is calculated by making use of the total El and total Al contents, to avoid significant errors in these calculations (see also Chapter 6).

5.5 Conclusions

Calibration of the MESEX sequential extraction scheme for single natural Fe and Mn minerals indicates that ascorbate (step 6) dissolves amorphous Fe and Mn oxides and, in part, goethite. Dithionite (step 9) extracts the main part of goethite and haematite, and some magnetite and ilmenite. Remaining oxides dissolve completely in the HF-step (step 10). However, in view of the amount of Fe extracted, most if not all Fe oxides will have been dissolved after the application of the dithionite step. Concentrated HNO_3 (step 11) extracts pyrite completely. Rhodochrosite dissolution occurs in many steps, but more is dissolved with decreasing pH.

The MESEX results of a mixed mineral standard indicate that haematite, pyrite, illite (except for Fe) and manganite are dissolved in the expected step(s). However, goethite is completely, rather than partly, extracted in the ascorbate step. Another exception is the apparently incongruent dissolution of Fe associated with illite in the dithionite (pH 4.8) step.

Application of the MESEX scheme to sediments of two eastern Mediterranean boxcores gives a good indication of the distribution of Fe, Mn, S, Al and V over different minerals. In normal eastern Mediterranean sediments (boxcore ABC26), the Mn(II)/Mn(III,IV) redox boundary is located on top of the remaining sapropel. Below this depth, the sediment is oxygen-depleted. The Fe(II)/Fe(III) redox boundary is located just below the Mn(II)/Mn(III,IV) redox boundary. Iron and Mn have a progressively larger oxide peak from the top of the original sapropel, at the depth of the upper Mn oxide peak, to the top of the presently visible sapropel, at the base of the lower Mn peak, caused by the increasingly slower downward-moving oxidation front. In the former brine sediments (boxcore BC15), a large sharply defined Mn oxide peak constitutes the active Mn(II)/Mn(III,IV) redox boundary. In contrast to normal eastern Mediterranean sediment, the Fe(II)/Fe(III) redox boundary occurs well below the Mn(II)/Mn(III,IV) redox boundary and a clear Fe oxide enrichment is absent. Vanadium extracted in the NH_4Cl and ascorbate steps appears to be derived from the large diagenetic V peak in ABC26, whereas in BC15, NH_4Cl- and ascorbate-extracted V is only found in the organic-rich sediments and occurs in close association with organic carbon. Therefore, NH_4Cl- and ascorbate-extractable V is thought to be absorbed as vanadyl to organic ligands (such as humic acids). The results for the redox-sensitive elements Mn, Fe and V suggest that a downward moving oxidation front has had a major impact on metal

speciation in normal eastern Mediterranean sediments, whereas this front is absent in the former brine sediment. This observation makes the latter sediment suitable for palaeoclimatic analysis, especially with regard to the initial trace metal relationships with reduced phases such as organic matter and pyrite.

A similar organic carbon profile combined with a vastly different pyrite profile for otherwise identical samples in the two subcores of ABC26, have allowed us to determine the speciation of Mn, Co, Ni, Zn and Cu released in the HNO_3 step. Manganese and Co appear to be associated with pyrite, whereas Ni, Zn and Cu are more closely related to organic matter. Comparison with the former brine sediments of BC15 indicates that the relationships of Mn and Co to pyrite and Ni, Zn and Cu to organic carbon have not changed in the still remaining, visible sapropel of normal eastern Mediterranean sediments (ABC26).

The sequential extraction results also indicate that the relative illite content of the terrigenous fraction is rather constant with time, as is indicated by the similar K/Al ratios in most sediment samples. The slightly higher Fe/Al and Mg/Al ratios of the clay mineral fraction in sapropel S1 in normal eastern Mediterranean sediments suggest a somewhat higher abundance of chlorite in that period. The trace element to aluminium ratios of clay minerals behave mostly similar to the terrigenous Fe/Al and Mg/Al ratios. In the former brine sediments, these differences between present-day terrigenous El/Al ratios and ratios in the organic-enriched sediments are more pronounced. All of these results indicate that a change in the source of the terrigenous input has occurred between the deposition of sapropel and non-sapropel sediments.

Acknowledgements – P. Anten, A. van Leeuwen, G. Nobbe and H. de Waard are thanked for their analytical assistence. This chapter was significantly improved through thorough reading by C.H. van der Weijden and S.J. Schenau. The latter is also thanked for making sequential extraction results on MMIN available.

This study was supported by MARFLUX (MAST1-90022C), PALAEOFLUX (MAS2-CT93-0051) and SAP (MAS3-CT97-0137) European programmes.

Appendix 5-A

In the organic-rich samples of BC15 as well as ABC26, Fe released in the ascorbate step is much higher than expected. Also, the S/Na ratio in the first step (Table 5-A.1) is higher than measured pore water values (unpublished results). This suggests that, during sample handling, some pyrite has been oxidised. To correct for this effect, the following procedure has been used:

1. First, excess S in step 1 is calculated: $S_{excess,\ step\ 1} = Na_{step\ 1} \times (S/Na)_{pore\ water}$.
2. Then, it is assumed that all S_{excess} has been released from pyrite, and the oxidised Fe_{pyrte} is calculated: $Fe_{oxidised\ pyrite} = S_{excess,\ step\ 1} \times 55.85/64.12$. This assumption is feasible because in sapropel S1 from a nearby boxcore Passier and De Lange (1998) found no AVS but all reduced S to be pyrite-S.
3. Finally, it is assumed that the iron from the oxidised pyrite has been extracted in the ascorbate step, and both $Fe_{amorphous\ oxides}$ and Fe_{pyrite} are calculated:
    a) $Fe_{amorphous\ oxides} = Fe_{step\ 6} - Fe_{oxidised\ pyrite}$
    b) $Fe_{pyrite} = Fe_{step\ 11} + Fe_{oxidised\ pyrite}$

Table 5-A.1 summarizes the calculated values for all samples from boxcores BC15 and ABC26.

Table 5-A.1 *Calculation of the correction of Fe-pyr using S/Na from step 1 and Fe from the ascorbate step. Boxcore ABC26-B has sample numbers beginning with 77, boxcore ABC26-C sample numbers beginning with 78.*

BC15

Sample	depth	S st1	S/Na st.1	Fe st.6	Fe st.11	S xs st.1	Fe-pyr oxid.	Fe6-Fepyroxid	S por	Fe pyr	S pyr
	cm	wt%	g/g	wt%	wt%	wt%	wt%	wt%	wt%	wt%	wt%
AA09132	1.35	0.125	0.117	0.139	0.014	0.000	0.000	0.139	0.125	0.014	0.016
AA09137	2.85	0.116	0.117	0.138	0.011	0.000	0.000	0.139	0.117	0.011	0.014
AA09146	5.55	0.125	0.127	0.094	0.013	0.009	0.008	0.086	0.116	0.021	0.022
AA09152	7.35	0.129	0.132	0.074	0.008	0.014	0.012	0.062	0.115	0.020	0.023
AA09156	8.55	0.123	0.133	0.094	0.019	0.015	0.013	0.081	0.108	0.032	0.042
AA09160	9.75	0.238	0.174	0.173	0.273	0.077	0.067	0.106	0.161	0.341	0.440
AA09164	10.95	0.267	0.196	0.242	0.351	0.108	0.094	0.149	0.160	0.445	0.564
AA09172	13.35	0.414	0.283	0.336	1.035	0.242	0.211	0.125	0.172	1.246	1.428
AA09178	15.15	0.288	0.228	0.264	0.488	0.140	0.122	0.142	0.148	0.610	0.749
AA09183	16.65	0.278	0.222	0.263	0.429	0.132	0.115	0.148	0.147	0.544	0.666
AA09190	18.75	0.345	0.234	0.243	0.903	0.172	0.150	0.093	0.173	1.053	1.230
AA09198	21.15	0.309	0.223	0.266	0.715	0.146	0.127	0.139	0.163	0.842	0.983
AA09204	22.95	0.289	0.228	0.262	0.72	0.140	0.122	0.140	0.149	0.842	0.967
AA09207	23.85	0.315	0.237	0.284	0.894	0.159	0.139	0.146	0.156	1.032	1.163
AA09212	25.35	0.258	0.219	0.177	0.520	0.120	0.104	0.072	0.138	0.625	0.752
AA09221	28.25	0.302	0.258	0.227	0.562	0.165	0.144	0.084	0.137	0.706	0.817
AA09226	29.75	0.286	0.228	0.181	0.774	0.139	0.121	0.060	0.147	0.895	1.035
AA09230	31.05	0.221	0.198	0.362	0.506	0.090	0.079	0.284	0.131	0.585	0.720

ABC26

Sample	depth	S st1	S/Na st.1	Fe st.6	Fe st.11	S xs st.1	Fe-pyr oxid.	Fe6–Fepyroxid	S por	Fe pyr	S pyr
	cm	wt%	g/g	wt%	wt%	wt%	wt%	wt%	wt%	wt%	wt%
77912	12.85	0.108	0.104	0.216	0.004	0.021	0.018	0.198	0.088	0.022	0.024
77933	19.15	0.179	0.123	0.512	0.009	0.057	0.050	0.462	0.122	0.059	0.062
77938	20.75	0.322	0.184	0.398	0.714	0.175	0.152	0.246	0.147	0.867	1.007
77942	21.95	0.344	0.217	0.279	0.882	0.211	0.184	0.096	0.133	1.066	1.150
77949	24.05	0.178	0.124	0.201	0.419	0.058	0.050	0.150	0.120	0.469	0.530
78010	12.85	0.078	0.089	0.191	0.002	0.005	0.004	0.187	0.074	0.006	0.007
78035	19.15	0.141	0.093	0.524	0.010	0.013	0.011	0.513	0.128	0.021	0.018
78040	20.75	0.614	0.343	0.609	0.059	0.464	0.404	0.205	0.150	0.463	0.595
78044	21.95	0.927	0.554	0.697	0.090	0.786	0.685	0.012	0.141	0.775	0.952
78049	24.05	0.382	0.295	0.303	0.266	0.273	0.238	0.065	0.109	0.504	0.576

Appendix 5-B

The dithionite step (step 9) released more Fe than expected in the organic-rich samples of BC15 and of ABC26 (see for the original Fe_{dith} profile of BC15 Fig. 4.6A in Chapter 4). We have seen earlier (see section 5.3.2.4) that dithionite may dissolve some Fe from clay minerals. Although Al and K are low in this step, Mg is rather high and follows the total Al profile. This suggests that Mg from clay minerals is also released to some extent in the dithionite step. Because Fe and Mg are closely related in clay minerals, especially in chlorite, we have used the following procedure to distinguish between Fe_{clay} and $Fe_{crystalline\ oxides}$ in the dithionite step:

1. First, the Fe/Mg ratio of the clay minerals in the last three steps (steps 10 to 12) is calculated. For Mg, all three steps are used, whereas for Fe, only steps 10 and 12 are used (step 11 releases only Fe_{pyrite}, as suggested by the neglible $Fe_{step\ 11}$ content in the oxic samples). Also, the Fe/Mg ratio of the dithionite step is calculated to compare it with the ratio for the last three steps. In all but one sample, the former ratio is higher than than the latter, suggesting that the following correction procedure is feasible.
2. Then, $Fe_{clay,\ step\ 9}$ is calculated: $Fe_{clay,\ step\ 9} = Mg_{step\ 9} \times (Fe/Mg)_{steps\ 10–12}$
3. Finally, $Fe_{crystalline\ oxides}$ is calculated: $Fe_{crystalline\ oxides} = Fe_{step\ 9} – Fe_{clay,\ step\ 9}$.

Table 5-B.1 summarizes the calculated values for all samples from boxcores BC15 and ABC26.

Table 5-B.1 *Calculation of the separation of Fe in the dithionite step between Fe-oxide and Fe-clay using Mg in this step. Boxcore ABC26-B has sample numbers beginning with 77, boxcore ABC26-C sample numbers beginning with 78.*

BC15

Sample	depth	Mg st.9	Fe st.9	Mg 10–12	Fe 10,12	Fe/Mg 10–12	Fe/Mg 9	Fe cl 9	Fe ox 9
	cm	wt%	wt%	wt%	wt%	g/g	g/g	wt%	wt%
AA09132	1.35	0.161	0.765	0.858	1.428	1.66	4.76	0.268	0.497
AA09137	2.85	0.172	0.750	0.797	1.315	1.65	4.36	0.284	0.466
AA09146	5.55	0.169	0.694	0.769	1.209	1.57	4.11	0.265	0.428
AA09152	7.35	0.173	0.753	0.865	1.339	1.55	4.34	0.269	0.484
AA09156	8.55	0.198	0.926	0.809	1.367	1.69	4.67	0.335	0.591
AA09160	9.75	0.106	0.450	0.457	0.849	1.86	4.23	0.198	0.252
AA09164	10.95	0.102	0.345	0.521	0.893	1.71	3.38	0.175	0.170
AA09172	13.35	0.153	0.270	0.892	1.471	1.65	1.77	0.252	0.018
AA09178	15.15	0.168	0.300	1.121	1.801	1.61	1.78	0.270	0.030
AA09183	16.65	0.169	0.299	1.148	1.837	1.60	1.77	0.270	0.029
AA09190	18.75	0.135	0.232	0.867	1.375	1.59	1.72	0.214	0.018
AA09198	21.15	0.143	0.286	0.912	1.523	1.67	2.00	0.238	0.048
AA09204	22.95	0.148	0.287	0.898	1.546	1.72	1.94	0.254	0.032
AA09207	23.85	0.165	0.251	0.864	1.399	1.62	1.52	0.251	0.000
AA09212	25.35	0.158	0.334	0.874	1.503	1.72	2.12	0.271	0.063
AA09221	28.25	0.136	0.252	0.963	1.644	1.71	1.85	0.232	0.020
AA09226	29.75	0.159	0.262	0.909	1.434	1.58	1.65	0.250	0.012
AA09230	31.05	0.162	0.298	0.926	1.557	1.68	1.84	0.272	0.026

ABC26

Sample	depth	Mg 9	Fe 9	Mg 10–12	Fe 10,12	Fe/Mg 10–12	Fe/Mg 9	Fe 9 cl	Fe 9 ox
	cm	wt%	wt%	wt%	wt%	g/g	g/g	wt%	wt%
77912	12.85	0.091	0.432	0.637	1.051	1.65	4.76	0.150	0.282
77933	19.15	0.103	1.143	0.820	1.386	1.69	11.05	0.175	0.968
77938	20.75	0.101	1.123	0.780	1.367	1.75	11.12	0.177	0.946
77942	21.95	0.093	0.555	0.762	1.339	1.76	5.95	0.164	0.391
77949	24.05	0.102	0.510	0.750	1.376	1.83	5.01	0.187	0.323
78010	12.85	0.096	0.454	0.608	1.005	1.65	4.73	0.159	0.296
78035	19.15	0.104	1.217	0.836	1.402	1.68	11.65	0.175	1.042
78040	20.75	0.106	1.502	0.807	1.395	1.73	14.16	0.184	1.319
78044	21.95	0.092	0.773	0.785	1.378	1.75	8.42	0.161	0.612
78049	24.05	0.106	0.449	0.751	1.342	1.79	4.25	0.189	0.26

Chapter 6

A novel selective extraction for barite from marine sediments

Abstract – A sequential extraction method (BASEX) was developed to determine the different Ba fractions in sediments. Calibration of BASEX with pure barite and a home-made mixed mineral standard showed that barite is separated from all other major Ba containing mineral phases, such as clay minerals and Fe and Mn oxides.

Application of BASEX to eastern Mediterranean sediments, including sapropel S1, revealed that the enrichment in Ba concentrations observed in this sapropel consists mainly of barite. The relationship of barite-Ba with organic carbon in sapropel S1 sediments appears to be independent of water depth, of organic matter fluxes and of the sedimentation rate for cores ranging from 2150 to 3300 m water depth. This indicates that organic carbon remineralisation has been virtually absent in the water column deeper than 2150 m. This might have been caused by suboxic to anoxic conditions present in the deep eastern Mediterranean basin during the formation of sapropel S1.

Because of the constant relationship between barite and organic carbon in sapropelic sediments, we suggest that the barite content can be used to quantify the initial organic carbon content of the sediment in the oxidised sapropel interval.

6.1 Introduction

Changes in primary productivity record the climatic variability through time. The most important products of primary productivity are carbonates, opal, and organic carbon. These products are, however, recycled in varying amounts while settling through the water column and during early diagenesis in the sediment, which decreases their usability as a proxy for primary productivity in the past. Therefore, several researchers have looked for other, more robust proxies for palaeoproductivity, of which barite is one of the most promising. In sediment traps, a correlation was found between the vertical fluxes of organic carbon and particulate barite (Dymond et al., 1992; Francois et al., 1995; Dehairs et al., 2000). Although seawater is usually undersaturated with respect to barite (Church and Wolgemuth, 1972; Monnin et al., 1999), this mineral is thought to precipitate within sulphate-rich micro-environments associated with decaying organic matter or as the result of the dissolution of barium-rich celestite tests of acantharia, both causing localised supersaturation with respect to barite (Dehairs et al., 1980, 1990; Bishop, 1988; Bernstein et al., 1992; Dymond et al., 1992; Francois et al., 1995; Dymond and Collier, 1996). Accordingly, the sedimentary Ba concentration is considered to be an important tracer for palaeoproductivity (Bishop, 1988; Dymond et al., 1992; Francois et al., 1995). There are, however, two potential problems associated with the application of this proxy. Firstly, only part of the bulk-Ba consists of barite-Ba, and only the latter is related to palaeoproductivity (e.g. Gingele and Dahmke, 1994). Secondly, during sulphate reduction, barite may be mobilised and reprecipitated

elsewhere (Van Os et al., 1991; Von Breymann et al., 1992; McManus et al., 1994, 1998).

The most widely applied method in which Ba is used as a proxy for palaeoproductivity is to determine bulk concentrations of sedimentary Ba, or normative Ba/Al ratios to correct for carbonate dilution. Using this approach, it is assumed that barite is the major Ba contributor in the sediment. In many marine environments, however, silicate-bound Ba (detrital Ba) constitutes a significant fraction of the bulk Ba concentration. In addition, some Ba may be present in Fe-Mn oxides, or associated with organic matter, opal or carbonates (e.g. Gingele and Dahmke, 1994). To correct for the contribution of detrital Ba, the biogenic barite content (Ba_{bio}) is usually estimated with the equation (e.g. Dymond et al., 1992):

$$Ba_{bio} = Ba_{total} - Al_{total} \times (Ba/Al)_{aluminosilicates} \quad (1)$$

The $Ba/Al_{aluminosilicate}$ ratio for detrital material may vary between 2.5 and 10 mg/g, depending

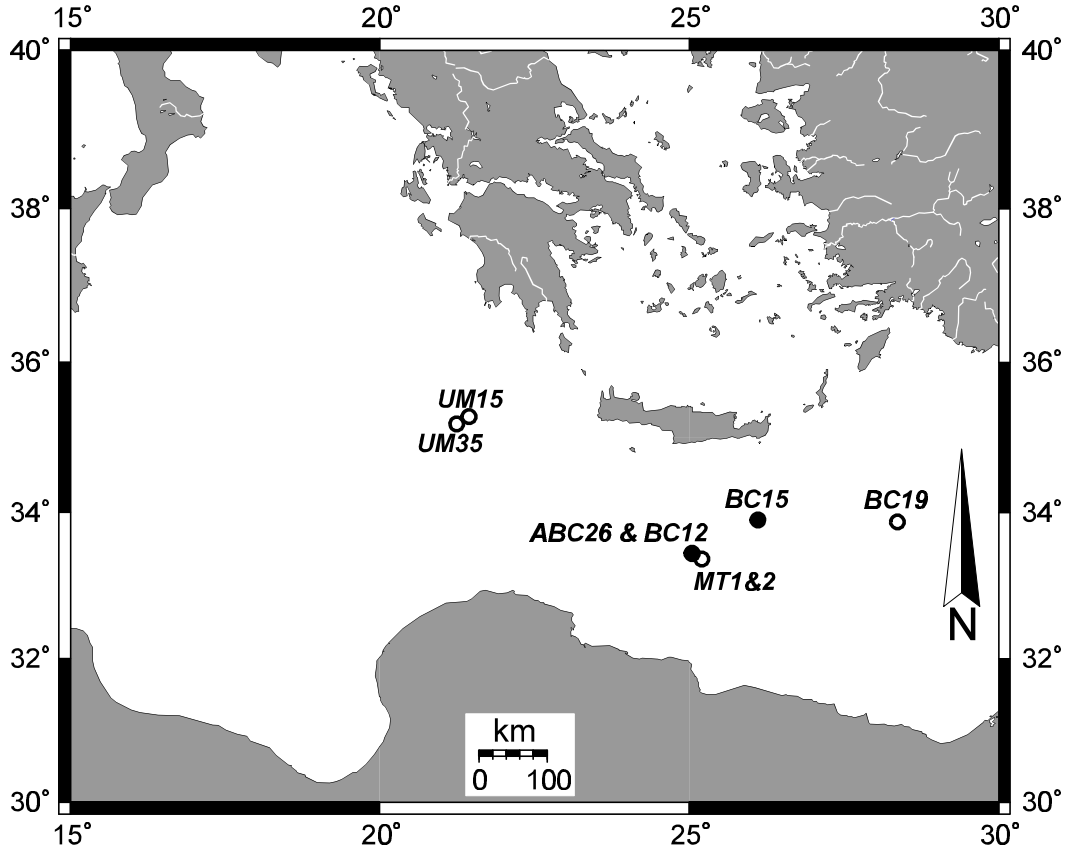

Figure 6.1 *Location of boxcores ABC26 (33°21.3'N, 24°55.4'E; water depth 2150 m) and BC15 (33°51.4'N, 26°05.5'E; water depth 3232 m) in the eastern Mediterranean. Also shown are the locations of the other boxcores of which organic carbon and Ba data are used in Fig. 6.7B: BC12 (located at 33˚23.56'N, 25˚01.03'E; 2211 m water depth); MT1 (33˚18.38'N, 25˚10.93'E; 2217 m); MT2 (33˚18.18'N, 25˚11.88'E; 2275 m); UM15 (35˚17.39'N, 21˚24.82'E; 3308 m); UM35 (35˚11.04'N, 21˚12.54'E; 2672 m); BC19 (33°47.65'N, 28°36.20'E; 2750 m).*

on the composition of the aluminosilicate source (Dymond et al., 1992; Gingele and Dahmke, 1994; Gingele et al., 1999). For sedimentary environments such as continental margin sediments, receiving a high contribution of detrital Ba (> 50%), it has been shown that Ba_{bio} cannot be adequately estimated due to large uncertainties in the detrital Ba/Al ratio (Dymond et al., 1992; Gingele and Dahmke, 1994; Gingele et al., 1999).

Several attempts have been made to directly determine the barite content in marine sediments, such as by X-ray diffraction (Gingele and Dahmke, 1994). At present, the only available methods to obtain quantitative information on the Ba speciation in sediments are sequential extraction techniques. They involve the application of a sequence of solvents to determine the operationally defined solid speciation of an element. Tribovillard et al. (1996) presented a four-step extraction scheme (after Lyle (1984)) to determine Ba speciation and distinguished: 1) carbonate and exchangeable cations (NaAc (1 M) + HAc, pH 5); 2) organically bound cations (Na dodecylsulphate (1%) + $Na_2B_4O_7$ (0.1 M), pH 9) ; 3) cations bound to the oxyhydroxide fraction (NH_2OH-HCl, pH 5); and 4) a residual fraction (HF). The barite content was then determined from the difference between bulk-Ba and the sum of these four steps. These authors and Des Combes et al. (1999) applied this scheme to Indian Ocean sediments to obtain estimates of palaeoproductivity. Similar extraction techniques have also been used to obtain $\delta^{34}S$, $^{87}Sr/^{86}Sr$ and ^{226}Ra contents in barite in order to determine palaeovariations of these isotopes in seawater (Paytan et al., 1993, 1996, 1998; Martin et al., 1995).

The present study examines the barite dissolution potential in a number of solvents. A chemical extraction method (BASEX) is presented for an easy determination of the barite contents in marine sediments. Eastern Mediterranean sediments are used to demonstrate the applicability of this method. These sediments are very suitable for the determination of environmental changes, because the area is highly sensitive to global climatic variations, as is expressed in the cyclic occurrence of organic-rich intervals (sapropels; Kidd et al., 1978) in otherwise organic-poor sediments (see review by Rohling, 1994). Variations between wet and dry periods in this region have caused changes in palaeoproductivity and in the composition of terrigenous material (Dominik and Stoffers, 1979; Kallel et al., 1997; Krom et al., 1999). This cyclicity allowed us to link chemical extraction data with these environmental parameters.

6.2 Materials and methods

6.2.1 Materials

Natural barite (Ba: 53 wt%; S: 13 wt%; Sr: 2.5 wt%) obtained from Wards was finely powdered before being subjected to sequential extraction. Also, a standard made up by mixing natural minerals with known compositions was prepared (MMIN; Table 6.1) and sequentially extracted. The composition was chosen so as to resemble average eastern Mediterranean sediment. The MMIN-minerals important for this study are barite ($BaSO_4$) and illite, which contains some Ba.

In addition, selected sediment samples were extracted from two eastern Mediterranean

Table 6.1 *The composition of MMIN, the mixed mineral standard prepared for this study.*

Mineral	Content (wt%)
illite	46.2
calcite	40.1
dolomite	10.0
pyrite	1.5
gypsum	0.7
goethite	0.6
haematite	0.5
manganite	0.3
barite	0.1

boxcores (BC15 and ABC26; Fig. 6.1). Boxcore ABC26, recovered during the 1987 Anoxic Basin Cruise with R.V. *Tyro*, contains a sediment sequence typical for the pelagic eastern Mediterranean (De Lange et al., 1989; Higgs et al., 1994; Thomson et al., 1995, 1999; Van Santvoort et al., 1996). We have analysed samples from two subcores of boxcore ABC26 (ABC26-B and ABC26-C). In each of the subcores five samples were selected for sequential extraction; one is located at the top of the oxidised zone, one from just above the remaining sapropel, and three from the sapropel proper. The sediment sequence of BC15, a boxcore recovered from a former brine basin during the 1991 MD69-Marflux cruise with R.V. *Marion Dufresne*, is described in detail in Chapter 4. Eighteen samples from this boxcore, covering all units, were selected for sequential extraction. Barium and Al data from six other boxcores (see Fig. 6.1 for locations) available at Utrecht University were used for comparison with the two cores subjected to BASEX.

6.2.2 Methods

The extraction scheme used in this study (BASEX; Table 6.2) was originally developed to extract successively the following phases (see also Chapter 4): absorbed ions ($MgCl_2$; only BC15), carbonates (NH_4Cl), amorphous oxides (ascorbate), remaining carbonates (NaAc), crystalline oxides (dithionite), clay minerals (HF), pyrite and organic-bound metals (HNO_3), and residual minerals ($HF/HNO_3/HClO_4$). In general, the method consisted of the following steps. Approximately 250 mg of sediment (less for pure barite) was accurately weighed. The samples were added to Teflon tubes. After shaking with 25 ml of the appropriate solvent (~ 16 hours), these tubes were centrifuged at 4000 rpm, after which the solution was decanted. Between all steps, the samples were washed with distilled water and then subjected to the following step.

A separate extraction was performed on BC15 samples in demineralised water. Fifteen ml water was added to 250 mg sediment. After shaking for 1 day, the tubes were centrifuged at 4000 rpm and, subsequently, the solutions decanted.

The bulk composition of all samples, including pure barite, were determined by total digestion in a mixture of hydrofluoric, nitric, and perchloric acids, which was subsequently vaporised to dryness in Teflon vessels on a sand bath. The residue was dissolved in HCl, with a final concentration of 1 M.

All of the above solutions were analysed for Ba and Al using Inductively Coupled Plasma Atomic Emission Spectrometry (ICP/AES; solutions of BC15 and ABC26-B samples on an ARL34000; all other solutions on a Perkin Elmer Optima 3000). The quality of the

Table 6.2 *Overview of the BASEX scheme used for the eastern Mediterranean sediments.*

BASEX scheme				
Step	***BC15, barite***	**Ref.**	***ABC26, MMIN***	**Ref.**
1	25 ml 1 M $MgCl_2$ pH 8	1	25 ml 2 M NH_4Cl pH 9	2, 3
2	2×25 ml 2 M NH_4Cl pH 9	2, 3	25 ml 2 M NH_4Cl pH 9	2, 3
3	2×25 ml 2 M NH_4Cl pH 8			2, 3
4	2×25 ml 2 M NH_4Cl pH 7.5			2, 3
5	3×25 ml 2 M NH_4Cl pH 7			2, 3
6	25 ml ascorbic acid/sodium bicarbonate/sodium citrate solution (pH ~ 8)			4
7	25 ml 1 M NaAc pH 6			5
8	25 ml of 1 M NaAc pH 5			5
9	25 ml sodium dithionite / sodium citrate / sodium acetate solution (pH 4.8)			4
10	20 ml 20% HF [a]			6, 7
11	25 ml concentrated HNO_3 [a]			6, 7
12	10 ml 40% HF + 10 ml $HNO_3/HClO_4$ [a]			6, 7

[a] *Solutions have been decanted into Teflon vessels, vaporised to dryness and redissolved in 1 M HCl.*
References: (1) Ruttenberg (1992); (2) De Lange (1992b); (3) De Lange et al. (1994); (4) Kostka and Luther (1994); (5) Chapter 4; (6) Lord (1982); (7) Pruysers et al. (1993)

measurements was monitored by the inclusion of blanks, in-house and international standards. Reproducibility of these standards was better than 2% for both elements.

The organic carbon content of dried samples from boxcores BC15 and ABC26 was determined by decalcification of the samples with 1 M HCl prior to oxidation at 900°C in a CuO oven and subsequent cryogenical separation of the evolved CO_2 in a closed system. The pressure of the CO_2 gas in a fixed volume at room temperature is a measure for the organic carbon content of the sample. Included standards give a reproducibility better than 6%. Organic carbon data on BC15 samples are taken from Chapter 4.

Barium and organic carbon fluxes were calculated using the following equation:

$$\left.\begin{matrix} Ba-AR \\ C_{org}-AR \end{matrix}\right\} = 0.1 \times LSR \times DBD \times C \qquad (2)$$

where Ba-AR and C_{org}-AR are the accumulation rates of respectively Ba and organic carbon (g m^{-2} yr^{-1}), LSR the linear sedimentation rate (cm kyr^{-1}), DBD the dry bulk density (g cm^{-3}) and C the concentration of Ba or organic carbon in the sediment (in wt%).

6.3 Results and discussion

First, we will evaluate the dissolution potential of pure barite in each of a number of sequentially applied solvents. Subsequently, the BASEX scheme will be evaluated using the extraction results of the mixed mineral standard MMIN. Finally, these findings will be used to interpret and discuss results from extractions applied to eastern Mediterranean sediment samples.

6.3.1 Pure barite

The total Ba recovery in the BASEX scheme (51.2 mg of pure barite) is only 30% (sum of all steps is 8.0 mg Ba, whereas 27.0 mg Ba was expected). This indicates that all extractants were saturated with respect to barite. The mineral dissolves best in HF and $HF/HClO_4/HNO_3$, but significant amounts are extracted in all other steps, with the exception of the dithionite step (Fig. 6.2A). The Ba concentration in the solvents is much higher than would be expected on the basis of the solubility product of barite (Fig. 6.2B). Dissolution of barite is influenced by a number of factors. Dove and Czank (1995) showed that the dissolution rate of barite decreases with increasing pH in the range of pH 2 to 5, but was almost independent of pH in neutral to basic solutions. This is consistent with the relatively constant Ba concentrations in the four NH_4Cl solutions with pH values ranging from 9 to 7 (Fig. 6.2B, steps 2 to 5 in Table 6.2). Furthermore, barite solubility has a positive relationship with the ionic strength of the solution. Blount (1977) calculated the barite solubility as a function of the molality of the solution using an extended Debye-Hückel equation. For 1 and 2 molal NaCl solutions (25°C, 1 bar), barite solubility is 0.077 and 0.106 mmol/kg, respectively. Most of our results are between 0.07 and 0.11 mM (Fig. 6.2B). The first step (1 M $MgCl_2$) has a similar Ba concentration of 0.108 mM, similar to that for 2 molal NaCl, although the ionic strength of 1 M $MgCl_2$ is 1.5× higher. The 2 M NH_4Cl steps (steps 2 to 5)

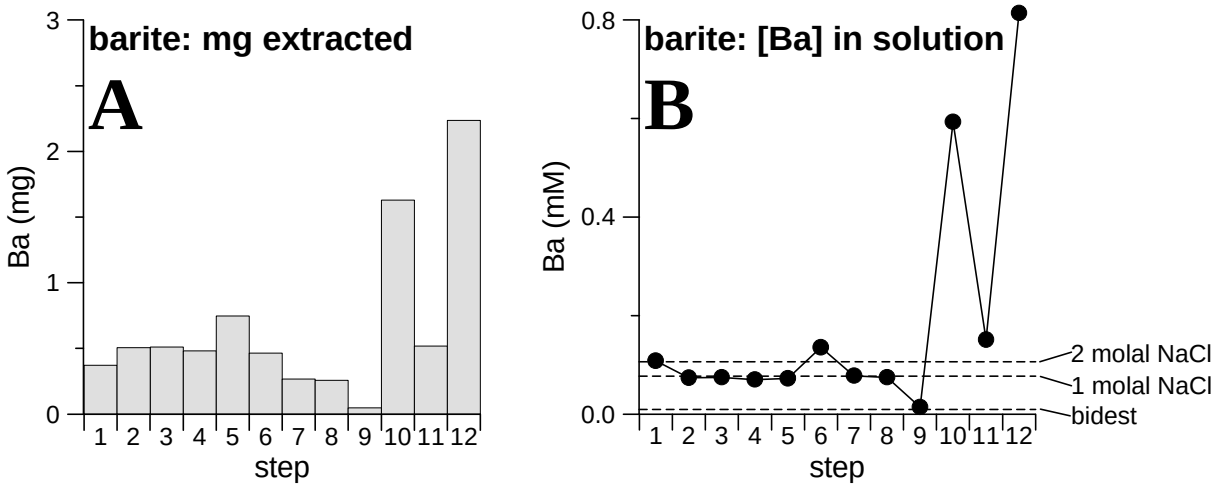

Figure 6.2 *BASEX results for pure barite per step. A) The total amount of Ba extracted per step (in mg); B) The concentration of Ba in each solvent (mmol/l). The horizontal dotted lines indicate the expected Ba concentration in demineralised water (bidest), 1 m NaCl, and 2 m NaCl (Blount, 1977).*

give Ba concentrations which correspond to the calculated values for barite dissolution in 1 molal NaCl. The ascorbate step (step 6) gives a higher than expected barite solubility, possibly due to the formation of a Ba complex with citrate. The two 1 M NaAc extractions (steps 7 and 8), with a ionic strength comparable to 1 molal NaCl, have Ba concentrations of 0.078 and 0.075 mM respectively. The dithionite extraction (step 9), however, has — despite the presence of citrate — a Ba concentration close to that of the demineralised water extraction; this may be related to sulphate produced by the oxidation of dithionite, causing reduction of the Ba concentration. In conclusion, it appears that a higher ionic strength of the solvent has, in general, a positive effect on barite solubility.

On the basis of these results, we have calculated the apparent barite dissolution potential for each step, which we define as the amount of Ba (μg) dissolved in that step, divided by 0.25 g (the amount of sediment sample used in the sequential extraction). The $MgCl_2$ (pH 8) step has a barite dissolution potential of ~ 1500 ppm Ba, whereas for each 25 ml NH_4Cl step this is ~ 1000 ppm Ba. In total, this amounts to about 1 wt% Ba in the first five steps. This is much higher than the Ba concentrations usually found in (organic-rich) sediments (Dymond et al., 1992; Gingele and Dahmke, 1994; Van Santvoort et al., 1996; Nijenhuis and De Lange, 2000). Consequently, most if not all barite in natural samples would be extracted in the first five steps. However, some prudence is called for. These values are maximum estimates of the barite dissolution potential in our sequential extraction for pure barite alone. Barite solubility in natural samples may be affected by matrix effects due to the presence of other minerals.

Barite is relatively soluble in the last three steps (steps 10 to 12; Fig. 6.2). Because of the low pH of these solutions, SO_4^{2-} associates with H^+ and forms HSO_4^-, which reduces the overall SO_4^{2-} concentrations, thus enhancing barite solubility. However, we cannot explain why barite extracted in the concentrated HNO_3 step (step 11) is much lower than it is in HF (step 10) or $HF/HNO_3/HClO_4$ (step 12).

6.3.2 MMIN: Barite and illite (Ba)

The standard MMIN (Table 6.1) contains two significant Ba contributors, namely barite (518 ppm Ba) and illite (208 ppm Ba). Two distinct fractions are extracted, one in the first five sequential steps, the other in the last three (Fig. 6.3). Quantification of the Ba extracted in these two fractions results in 515 ppm in the first fraction and 212 ppm in the second one. This indicates that there is a good separation between the barite and illite-Ba fractions, with Ba_{barite} constituting the first one (recovery: 99.4%) and Ba_{illite} the second one (recovery: 101.5%). The high solubility of barite in the NH_4Cl extraction has already been discussed above for the pure mineral. The measured value of about 145 ppm Ba found for MMIN in the NH_4Cl pH 9 steps (steps 1 and 2) is much lower than the barite dissolution potential of about 1000 ppm in a 250 mg sample determined for pure minerals. However, all barite is still dissolved within the first five steps of the sequential extraction scheme.

Illite dissolution is expected mainly in HF and $HF/HClO_4/HNO_3$ (steps 10 and 12). However, most Ba_{illite} appears to be extracted in the HNO_3 step (step 11). This is very likely a matrix artifact due to the formation of a ralstonite-like mineral ($NaMgAlF_6.H_2O$), as found

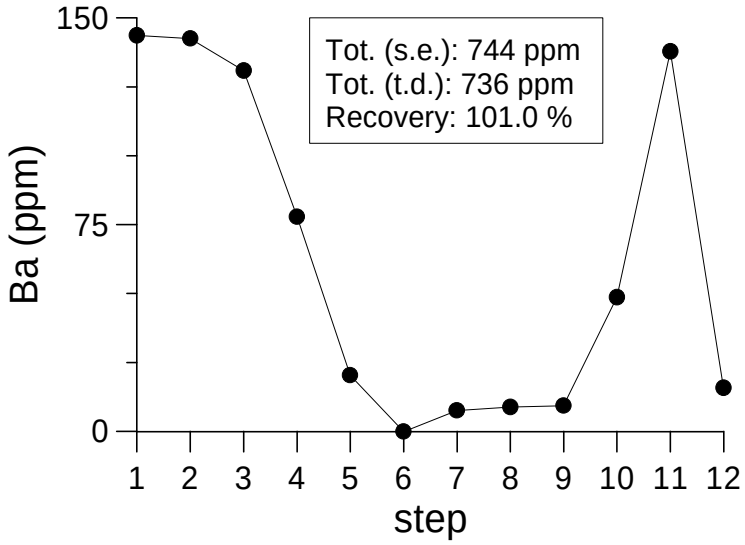

Figure 6.3 *The results on Ba from the sequential extraction of MMIN using the BASEX scheme.*

by Ingall et al. (1993). This mineral is formed during the HF step, and is easily dissolved in the subsequent HNO_3 step. The Mg/Al ratio in the HNO_3 step of MMIN suggests that a ralstonite-like mineral is indeed formed in the previous HF step (see Chapter 5). On the basis of its concentration in the HNO_3 step, Ba also appears to be incorporated in this mineral. Therefore, taking the sum of the Ba concentrations of the last three sequential steps only will result in an accurate assessment of clay-bound Ba.

6.3.3. Eastern Mediterranean sediments

Pelagic sediments in the eastern Mediterranean are mainly a mixture of biogenic carbonate and terrigenous material (e.g. Chapters 2, 3, 5, 7). Clay-bound Ba may, therefore, be an important component of the bulk-Ba flux. The BASEX scheme permits the separation between Ba_{clay} and Ba_{barite}, thus enabling a direct assessment of the relationship between Ba_{barite} (= Ba_{bio}) and organic carbon.

Total Ba contents in BC15 and ABC26 show the same downcore distribution as the organic carbon concentration (Figs. 6.5A,E). In BC15, total Ba is closely correlated to the organic carbon content throughout the core, whereas in ABC26 this is true except for the interval from 20 to 13 cm. This interval represents the part of the sapropel that was reoxidised during diagenesis (the oxidised sapropel interval; De Lange et al., 1989; Higgs et al., 1994; Thomson et al., 1995, 1999; Van Santvoort et al., 1996).

Barium extraction results show distinct differences between the sedimentological units in both boxcores (Fig. 6.4). For the units enriched in organic carbon in ABC26 and BC15, including the oxidised sapropel interval in ABC26, the profile of the sequentially extracted Ba per sample resembles the one for MMIN (Fig. 6.3). Clearly, in these samples, the amount of Ba_{barite} is much larger than that of Ba_{clay}. The oxic sediment of both boxcores has a distinctly

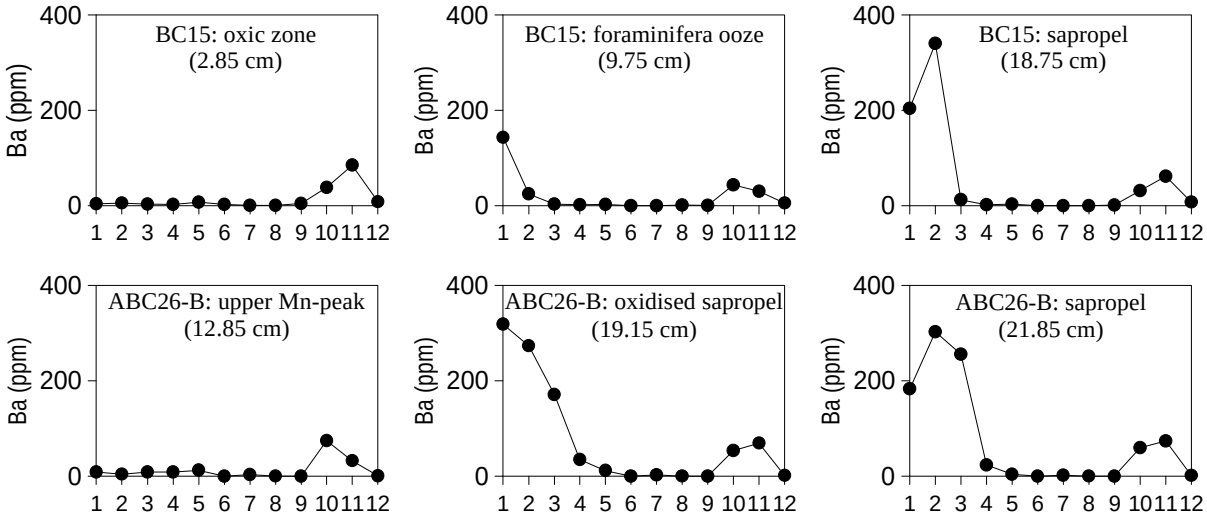

Figure 6.4 *Results on Ba in different lithological units from the sequential extraction of eastern Mediterranean sediments using the BASEX scheme. The upper three graphs depict, from left to right, typical BC15-profiles found in the oxic samples, the organic-enriched/foraminifera-rich zone, and the sapropel. The lower three show, from left to right, typical ABC26-profiles from the upper Mn peak, the oxidised sapropel interval, and the remaining sapropel.*

lower Ba_{barite} content, whereas Ba bound to clay minerals is in the same order of magnitude as in the organic-enriched sediments. The high amount of Ba extracted in the early BASEX steps (i.e. steps 1 to 5) of sapropelic sediment samples is, therefore, indicative for a significant barite content. However, these sediment samples do not have a composition known in advance, as was the case for MMIN, so other Ba minerals have to be excluded, such as witherite ($BaCO_3$), which is about 25 times more soluble than barite and dissolves easily in NH_4Cl (unpublished data). To investigate this, a demineralised water extraction was applied to a number of BC15 samples to determine the amount of Ba that dissolves in pure water. The calculated solubility product for barite would then indicate whether barite or witherite is present. The log $K'_{sp,\ barite}$ ($= -9.71 \pm 0.06$ mol^2 l^{-2}) in the organic-rich samples, calculated from the Ba^{2+} and SO_4^{2-} concentrations determined in the demi-water extraction (n=23), is close to the expected log $K'_{sp,\ barite}$ of –9.98 (Blount, 1977), whereas the samples in the oxic part had undetectable Ba concentrations. This is further evidence for the dissolution of barite rather than another Ba mineral in the first five BASEX steps. Other fractions, including Ba bound to Mn and Fe oxides, contribute only little to total Ba (Figs. 6.5D,H). In conclusion, the organic-rich sediments of both cores contain a large fraction of Ba in barite (Figs. 6.5B,F). Most if not all excess Ba — i.e. the Ba fraction not associated with aluminosilicates — can thus be attributed to barite. Barium incorporated in aluminosilicates is a significant portion of total Ba (Figs. 6.5C,G). These results confirm those of Thomson et al. (1995), who showed that almost all Ba in the interval with enhanced total Ba concentrations is present in the form of small barite crystals (typically 1–3 μm) and only a trivial amount of Ba is sorbed by oxyhydroxides.

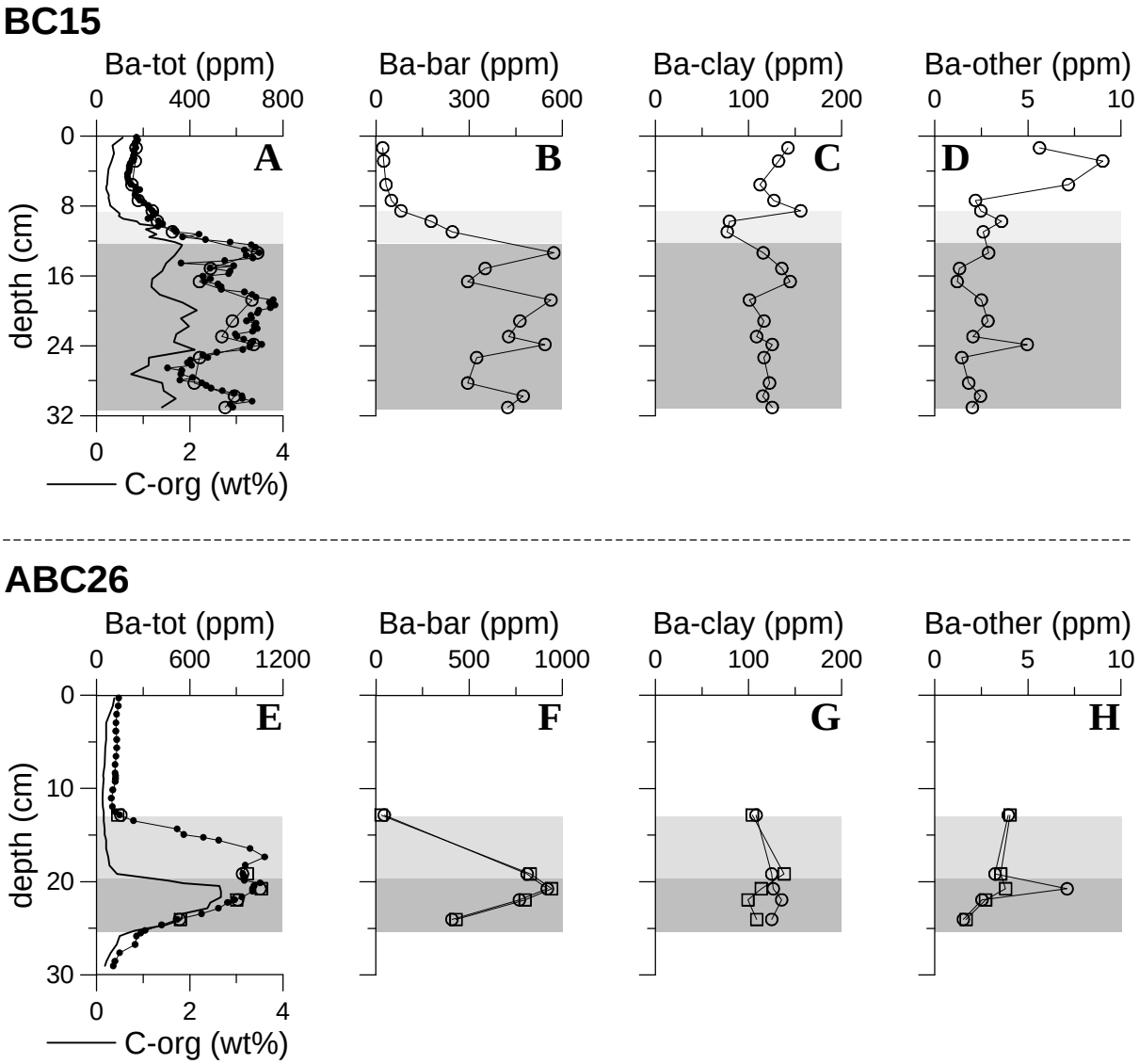

Figure 6.5 *Depth profiles of total digestion (filled circles) and BASEX (open symbols) results in the eastern Mediterranean boxcores. The BASEX results of the two subcores of ABC26 were differentiated (circles and squares). A, E) Total Ba and organic carbon of BC15 (A) and ABC26 (E). Filled dots indicate total digestion, open symbols the sum of all BASEX steps, whereas the thick solid line indicates the organic carbon content; B, F) Ba_{barite} (sum of steps 1 to 5) in BC15 (B) and ABC26 (F); C, G) Ba_{clay} (sum of steps 10 to 12) in BC15 (C) and ABC26 (G); D, H) Ba_{other} (sum of steps 6–9, thus including Ba in oxides) in BC15 (D) and ABC26 (H). The dark-grey area indicates organic-rich sediments. The light-grey area in A–D represents organic-enriched foraminifera ooze; in E–H, it indicates the oxidised sapropel zone.*

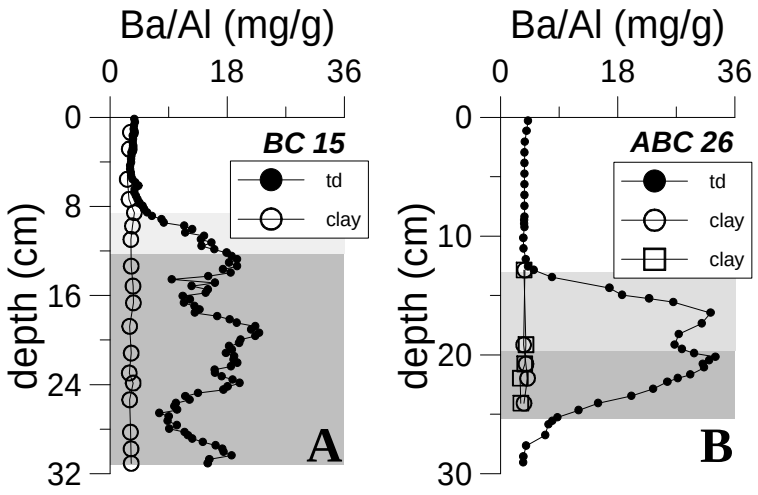

Figure 6.6 *Depth profiles of Ba/Al in BC15 (A) and ABC26 (B). Filled circles indicate total digestion results, open symbols* Ba_{clay} *divided by total Al. The two ABC26 subcores have been plotted individually (circles and squares).*

The BASEX method allows the determination of the Ba/Al ratio of the clay mineral fraction (Fig. 6.6). For BC15, an average $(Ba/Al)_{clay}$ ratio of 3.04 ± 0.37 mg/g is found for the oxic samples, whereas the organic-rich ones have a ratio of 3.23 ± 0.21 mg/g. The $(Ba/Al)_{clay}$ of all ABC26 samples is 3.63 ± 0.33 mg/g. This is slightly higher than the ratios in BC15, and might reflect small differences in the source material due to its different location, mainly with respect to the proximity of the Saharan desert, which is thought to be the major source of dust deposition in the eastern Mediterranean (e.g. Guerzoni, 1997, and references therein). The values and variability observed for the $(Ba/Al)_{clay}$ ratios have implications for the calculation of Ba_{excess} using Eq. (1). The $(Ba/Al)_{clay}$ ratios found here are much lower than those reported for continental crust or shales (Table 6.3). The latter values are often used in other studies for the determination of the Ba_{bio} content of sediments (e.g. Dymond et al., 1992; Gingele and Dahmke, 1994; Gingele et al., 1999; Dehairs et al., 2000). Our results indicate that it is important to know the exact ratio in each sample, because detrital Ba/Al ratios differ (1) per area, e.g. in relation to the proximity of the detrital source(s), and (2) within one core, e.g. due to changes in environmental conditions that can cause a shift in detrital source(s). Otherwise, when using a constant, estimated Ba/Al ratio for the detrital fraction, the calculated Ba_{bio} content may deviate considerably from the actual value.

In normal oceanic settings, a decrease of the C_{org}/Ba_{bio} ratio with water depth is observed, in sediment traps as well as in surface sediments (Dymond et al., 1992; Von Breymann et al., 1992; Francois et al., 1995; Dymond and Collier, 1996; Dehairs et al., 2000). This has been explained by continued organic matter degradation and barite formation while particles are settling through the water column (e.g. Bishop, 1988; Dymond and Collier, 1996). Accordingly, the C_{org}/Ba_{bio} ratio of suspended matter and sediment decreases with water depth. However, the relationship between barite-Ba and C_{org} ($C_{org} = 0.0162 \times (Ba_{bio})^{0.755}$,

Table 6.3 *A number of Ba/Al ratios cited in the literature. These values are often used for the correction of bulk-Ba to calculate Ba_{bio}. The measured Ba/Al_{clay} ratio of eastern Mediterranean sediments is also given.*

Type of material	Ba/Al (mg/g)	Reference
Shale	7.25	Turekian and Wedepohl (1961)
Crust	5.16	Taylor (1964)
Shale	5.99	Krauskopf (1967)
Mean shale	6.25	Bowen (1979)
Upper continental crust	6.84	Taylor and McLennan (1985)
Average post-Archean shale	6.50	Taylor and McLennan (1985)
Upper continental crust	8.63	Wedepohl (1995)
Continental crust	7.34	Wedepohl (1995)
BC15, oxic samples (n=5)	3.04 ± 0.37	this study
BC15, org.-rich samples (n=13)	3.23 ± 0.21	this study
ABC26, all samples (n=10)	3.63 ± 0.33	this study

R^2 = 0.96, n = 21) appears to be the same for the organic-rich sediments of both eastern Mediterranean boxcores, although they were collected at water depths differing more than 1000 m (Fig. 6.7A). To substantiate this, Ba_{bio} was calculated for a number of other eastern Mediterranean boxcores using Eq. (1). The detrital Ba/Al ratios used for the boxcores, which were all retrieved from areas in close proximity to ABC26 (BC12, MT1, MT2), or from the eastern Mediterranean (UM15, UM35, BC19), were based on the values determined above for BC15 and ABC26. This assumption may introduce a maximum estimated error of ~ 10% for these cores. The relationship between C_{org} and Ba_{bio} appears to be similar to that found for ABC26 and BC15 (Fig. 6.7B), again regardless of the water depth of the core. Taking all data together, this relationship is $C_{org} = 0.0247 \times (Ba_{bio})^{0.706}$ (R^2 = 0.83, n = 71). When the organic carbon and Ba_{bio} fluxes are calculated for each boxcore using Eq. 2, their relationship gives a straight line with a positive intercept on the C_{org} axis (Fig. 6.8). This positive intercept can be explained by a relatively constant input of refractory organic carbon, which will not induce barite formation in the water column. These cores represent samples with a range of water depths (2150 – 3300 m), sedimentation rates (2.8 – 5.3 cm kyr^{-1}), and organic carbon fluxes (0.27 – 1.05 g m^{-2} yr^{-1}). Consequently, the linearity of the C_{org} *vs.* Ba_{bio} relationship suggests that the ratio between marine organic matter — i.e. C_{org} minus refractory organic carbon — and biogenic Ba in sapropel S1 is rather constant, regardless of water depth, sedimentation rate, organic matter fluxes or concentrations (Figs. 6.8, 6.9). Therefore, it appears that a decrease of the ratio between marine organic carbon and biogenic Ba with water depth between 2150 and 3300 m is not observed in the eastern Mediterranean during deposition of sapropel S1.

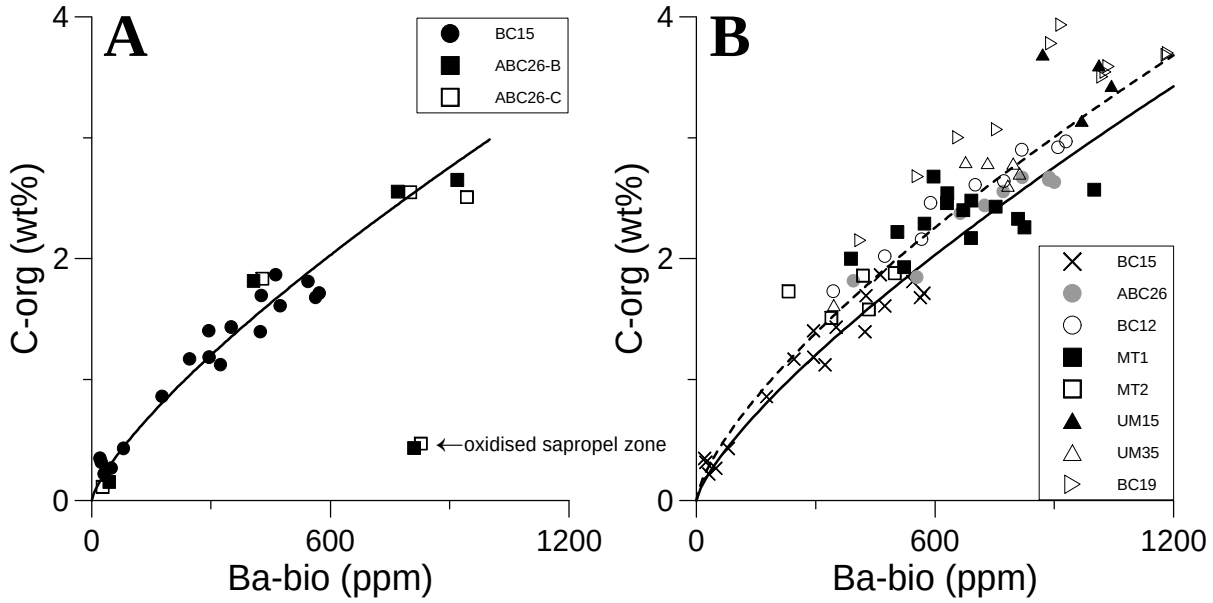

Figure 6.7 *A) Ba_{bio} vs. organic carbon in BC15 (circles) and ABC26 (squares). Ba_{bio} values are the results found in the sequential extraction for barite-Ba. The solid line is the best fit, represented by ($C_{org} = 0.0162 \times (Ba_{bio})^{0.755}$. The upper three samples of BC15 and the upper two of both ABC26 subcores were excluded when calculating the fit; B) Ba_{bio} vs. organic carbon for a number of eastern Mediterranean boxcores. Ba_{bio} was calculated using Eq. (1), using an estimated, constant, $Ba/Al_{aluminosilicates}$ for each boxcore, except for the samples of BC15, which show the sequential extraction results. The solid line is the same as the fit projected in Fig. 6.7A. The dashed line is a best fit for all data, represented by $C_{org} = 0.0247 \times Ba_{bio}^{0.706}$.*

It is believed that during deposition of sapropels in the eastern Mediterranean, part of the water column was suboxic to anoxic due to stagnation of the circulation by the formation of a low density surface water layer caused by highly increased precipitation (e.g. Rohling, 1994; Kallel et al., 1997). In basins with present-day suboxic to anoxic deep waters, such as the Black Sea and the Cariaco Basin, it has been observed that most organic matter degradation takes place at the oxic-anoxic interface (Karl and Knauer, 1991; Thunell et al., 2000). Organic matter fluxes only decrease very slowly if at all within deeper parts of an anoxic water column (Karl and Knauer, 1991). This suggests a relatively slow decay of organic matter in the suboxic water column, and would result in a C_{org}/Ba_{bio} ratio that would not significantly change with depth. If organic matter remineralisation would continue during settling in the water column, then the C_{org}/Ba_{bio} ratio would have decreased with water depth because of increased barite formation with continuing organic matter breakdown. This can also be seen in the sapropel S1 interval of eastern Mediterranean boxcores, where the C_{org}/Ba_{bio} relationships shows no trend with water depth, despite the range of depth between 2150 and 3300 m. In reported C_{org}/Ba_{bio} depth profiles for oxic water columns such as in the Pacific and the Atlantic Oceans, this ratio decreases in the order of 25% between 2150 and 3300 m (Dymond et al., 1992; Francois et al., 1995; Gingele et al., 1999). Although the

eastern Mediterranean C_{org}/Ba_{bio} ratios fall in the same range as these other published values, the eastern Mediterranean data set is more consistent because biogenic Ba was directly measured. Therefore, the recorded absence of a decrease of the C_{org}/Ba_{bio} ratios in eastern Mediterranean sapropel S1 sediments is believed to suggest that remineralisation was practically absent in the part of the water column between 2150 and 3300 m, indicating that this part of the water column might have been suboxic to anoxic. Hence, the export flux of organic carbon and Ba_{bio} at a certain depth is higher during the deposition of sapropel S1 sediments than otherwise. This concords with the observation that if sedimentation rates are low such as in the eastern Mediterranean, the preservation of organic matter is enhanced when the water column is oxygen-deficient (Canfield, 1994; Van der Weijden et al., 1999; Nijenhuis and De Lange, 2000). For the oxidised sapropel interval, this means that, although C_{org} has been removed due to oxygen burn-down, the enhanced barite content still records the initial higher C_{org} levels (cf. Van Santvoort et al., 1996).

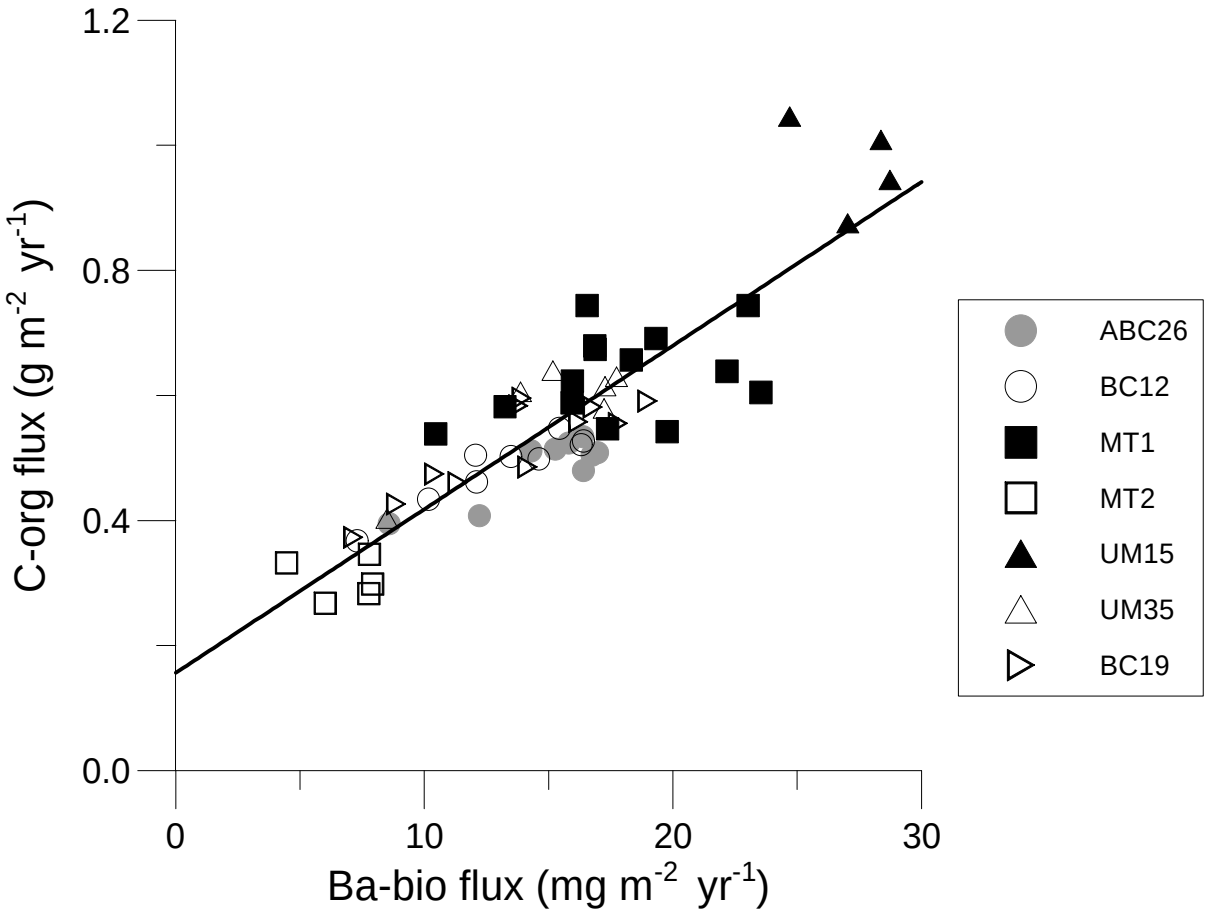

Figure 6.8 *The Ba_{bio} flux vs. organic carbon flux of sapropel S1 samples with an organic carbon content > 1.5 wt%. Fluxes were calculated by taking into account sedimentation rate and dry bulk density. The thick line represents the best linear fit: C_{org}-flux = 0.0262 × Ba_{bio}-flux + 0.156 (n=58; R^2 = 0.79).*

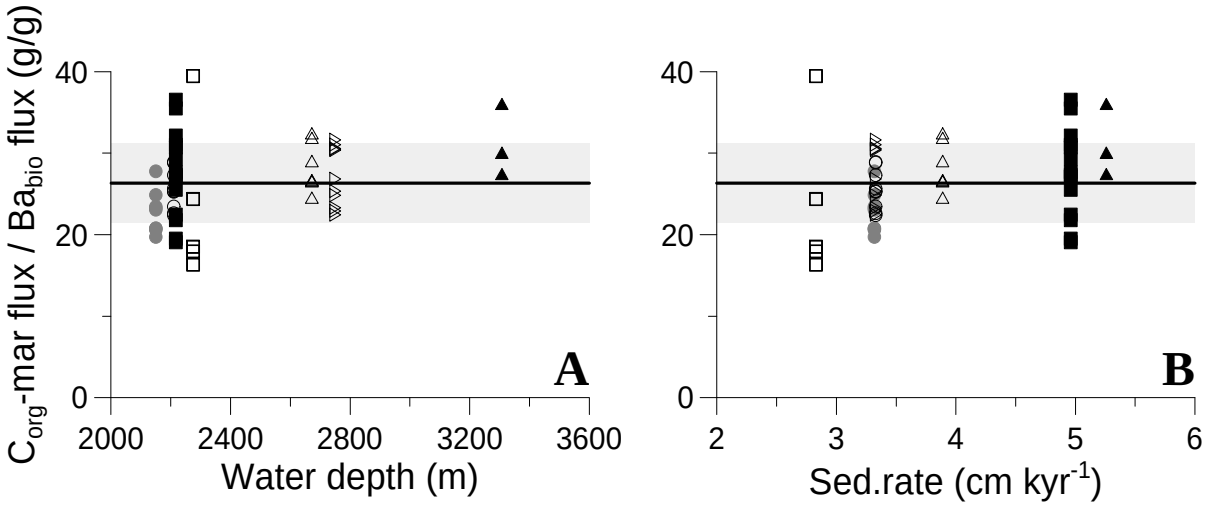

Figure 6.9 *The ratio between the fluxes of marine organic matter flux and biogenic Ba versus A) water depth, and B) sedimentation rate. The solid line indicates the average ratio, the grey area the 1σ standard deviation (n = 58). The different symbols represent different boxcores (for the legend, see Fig. 6.8).*

6.3.4. Implications for future research

As shown by the results on pure barite, a mixed mineral standard and eastern Mediterranean sediments, Ba speciation can be assessed in a relatively simple way. The sequential extraction scheme presented in this study (Table 6.2) was originally developed to determine the elemental speciation in the carbonate, oxide, reduced and terrigenous fractions of marine sediments. If only Ba speciation is needed, the extraction can be simplified. We suggest the following BASEX scheme for the easy determination of Ba speciation in sediments (use shaking times, sample volumes and related procedures as mentioned in section 6.2.2 and Table 6.2):

Step 1: 25 ml demineralised water (to dissolve precipitated porewater salts)
Step 2: 6 × 25 ml 2M NH_4Cl pH 7 (barite; the number of times to apply 25 ml NH_4Cl depends on the approximate amount of barite present in the sample)
Step 3: 2 × 25 ml 1M NaAc (to remove excess carbonate; only necessary for samples which have a high carbonate content)
Step 4: 25 ml Na-dithionite (Ba in oxides)
Step 5: 25 ml HF/HNO_3HClO_4 (clay-bound Ba)

Our results in combination with data from Blount (1977) and Dove and Czank (1995) indicate that barite can be determined by sequential extraction. Previously, e.g. for the analysis of $\delta^{34}S$, $^{87}Sr/^{86}Sr$ and ^{226}Ra activity in barite, strong extractants, like HF, have been used to remove other minerals so that only barite remains for isotope analysis (Paytan et al., 1993, 1996, 1998; Martin, 1995). Our results indicate that this might result in the premature

dissolution of some barite crystals, in particular the smaller ones. An entirely different approach is, therefore, sometimes more adequate. However, as carbonate dissolves along with barite during this extraction, this method is not suitable for the analysis of $^{87}Sr/^{86}Sr$ in barite. One of the major advantages of the extraction approach is, that even microscopically unrecognisable barite can still be isolated from the sediment matrix using a relatively simple extraction procedure, which would permit the accurate quantification of the total barite contents and the determination of e.g. $\delta^{34}S$ of barite.

6.4 Conclusions

A sequential extraction scheme was developed that distinctly separates Ba in barite, oxides and clay minerals. The method proved very effective on an artificial mixed mineral standard and was subsequently applied to eastern Mediterranean sediments. In this way, not only barite and clay-bound Ba contents, but also the aluminosilicate Ba/Al ratio, were accurately determined in these sediments. This ratio is much lower than literature values for marine shales and continental crust that are normally used in Ba_{bio} calculations.

Eastern Mediterranean sapropel S1 sediments exhibit the same relationship between organic carbon and biogenic Ba, regardless of water depth, location or sedimentation rate. This is likely to be due to the cessation of organic matter breakdown in the possibly suboxic to anoxic part of the water column, tentatively set to be from no more than 2150 m to at least 3300 m.

The results of this study support the use of barite for the quantification of the initial organic carbon content in the sediments of the oxidised sapropel interval.

Acknowledgements – P. Anten, G. Nobbe and H. de Waard are thanked for their analytical assistence. Thorough reading by C.H. van der Weijden and S.J. Schenau has significantly improved this chapter.

This study was supported by MARFLUX (MAST1-90022C), PALAEOFLUX (MAS2-CT93-0051) and SAP (MAS3-CT97-0137) European programmes.

Chapter 7

Sequential extraction of aragonite, calcite and dolomite from eastern Mediterranean sediments

Abstract – A novel sequential extraction method for carbonates (CASEX) has been developed to differentiate between aragonite/calcite and dolomite. Dolomite can be reliably quantified as shown by the extraction of a prepared standard of known mineral contents. In addition, Mg/Ca and Sr/Ca ratios for bulk $CaCO_3$ can be determined without the influence of dolomite. The Sr/Ca ratio of the first CASEX step is a good indicator for the relative aragonite content in sediment cores.

Application of the CASEX method to eastern Mediterranean sediments has yielded the following results. The dolomite content and the Mg/Ca ratio of carbonate (i.e. aragonite and calcite) are lower in the most recent sapropel S1 than they are in younger sediments. These observations correspond to the sapropel being formed during a relatively humid period with relatively low dust deposition rates and a relatively high river run-off. Accordingly, the dolomite content is indicative for the relative contribution of dust to the terrigenous fraction, whereas the carbonate (i.e. aragonite and calcite) Mg/Ca ratio is dependent on surface water salinity. The major part of the decrease in the carbonate Mg/Ca ratio can be attributed to such a change in salinity, whereas differences in the species composition of flora and fauna may contribute additionally. In contrast, most of the change in the carbonate Sr/Ca ratio observed in eastern Mediterranean sediments must have been caused by a change in ecology rather than salinity.

7.1 Introduction

Carbonate composition has become a major topic of interest in sedimentary and palaeo-environmental analysis. This study will introduce a novel approach to determine the relative contributions of different carbonate minerals. It is done by the gradual leaching of carbonates, meanwhile monitoring the leached Ca, Mg and Sr concentrations. Our novel extraction — hereafter referred to as the CASEX method — allows for the correct assessment of the dolomite content in sediments as well as Mg/Ca and Sr/Ca ratios of $CaCO_3$.

The analysis of the relative contributions of different major carbonate minerals, i.e. calcite, aragonite and dolomite, can up till now only be done on a semi-quantitative basis by X-Ray Diffraction (XRD). Relatively little attention has been paid to variations in bulk carbonate Mg/Ca and Sr/Ca ratios as a result of environmental change. Magnesium and Sr are known to be incorporated relatively easily into carbonate. This incorporation appears to be mainly related to temperature, although salinity and pH play a role as well (Delaney et al., 1985; Nürnberg, 1995; Nürnberg et al., 1996; Lea et al., 1999). This has been confirmed by palaeo-environmental studies on recent and subrecent sediments, where foraminiferal Mg/Ca and Sr/Ca ratios correlate well with the $\delta^{18}O$ record (Savin and Douglas, 1973; Bender et al., 1975; Rosenthal and Boyle, 1993; Puechmaille, 1994; Rosenthal et al., 1997), although prudence is in order, because these ratios may be affected by selective dissolution (Brown and

Elderfield, 1996).

The extraction method was applied to eastern Mediterranean sediments to determine the response of the carbonate minerals and their composition to changes in the sedimentary regime. The eastern Mediterranean has undergone significant repetitive environmental changes, making its sediments excellent material for studying changes in sediment composition related to different environmental conditions. Distinct organic-rich intervals (sapropels; Kidd et al., 1978) occur within otherwise organic-poor units. The occurrence of these intervals has been attributed to enhanced palaeoproductivity and decreased oxygen content of the bottom water (see review by Rohling, 1994). Due to increased precipitation, river input must have increased significantly during sapropel times (Rossignol-Strick et al., 1982; Kallel et al., 1997; Rossignol-Strick et al., 1998). This resulted not only in a decrease in salinity but also in an increase of nutrients in the photic zone, leading to higher productivity and possibly anoxic bottom waters. Eastern Mediterranean top sediment contains the most recent sapropel (S1), deposited in the Holocene, between 5 and 9 kyrs BP (e.g. Cita et al., 1977; Thomson et al., 1995). Geochemical profiles across the Holocene sediment display the same features throughout the deep eastern Mediterranean (see also Chapter 1). Usually, unoxidised sapropel sediment is overlain by a reddish-brown layer which has an increased amount of Fe and Mn oxides due to the action of a downward-moving oxidation front (e.g. Higgs et al., 1994; Thomson et al., 1995; Van Santvoort et al., 1996). On top of this oxidised sapropel zone, a strong Mn oxide enrichment is always present, denoting the end of

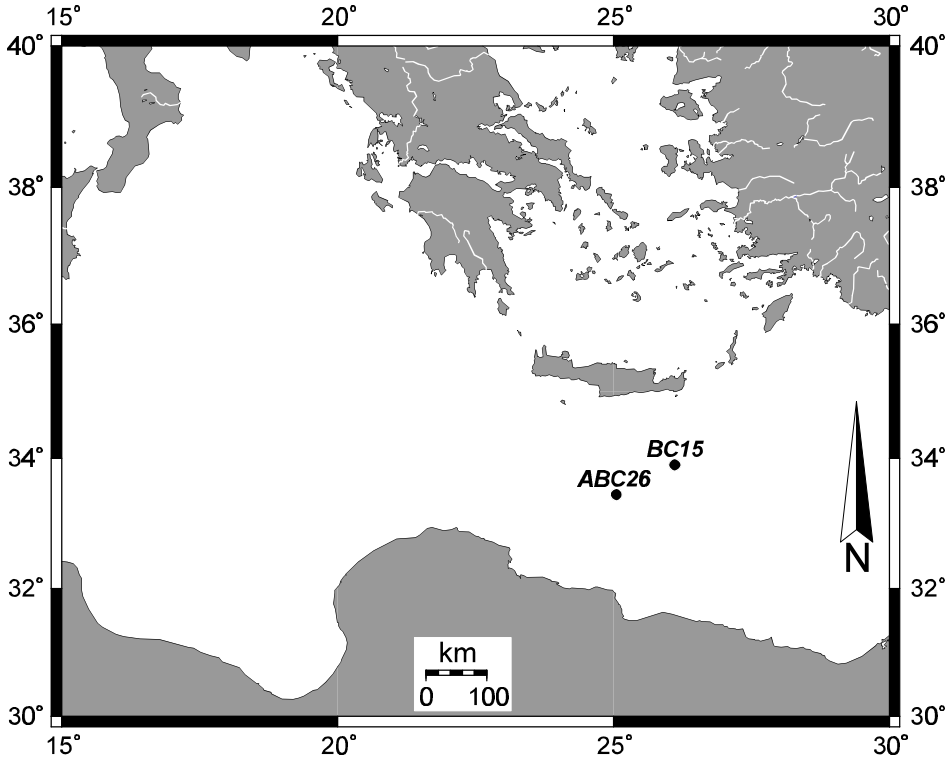

Figure 7.1 *Location of boxcores ABC26 (33°21.3'N, 24°55.4'E; water depth 2150 m) and BC15 (33°51.4'N, 26°05.5'E; water depth 3232 m) in the eastern Mediterranean.*

sapropel sedimentation.

In this chapter, first the CASEX method and its results on a known mixed mineral standard will be introduced. Subsequently, the results of the application of CASEX to eastern Mediterranean sediments will be discussed and interpreted.

7.2 Materials and methods

7.2.1 Materials

A mixture of minerals with a known composition was prepared and used as a standard (MMIN; Table 7.1) for the sequential extraction. The contribution of each mineral was chosen in such a way to be representative for eastern Mediterranean sediment. The MMIN minerals important for this paper are calcite ($CaCO_3$), dolomite ($CaMg(CO_3)_2$) and gypsum ($CaSO_4.2H_2O$).

In addition, samples of two eastern Mediterranean boxcores (BC15 and ABC26; Fig. 7.1) were extracted. Boxcore ABC26 was recovered from a water depth of 2150 m and contains a sediment sequence typical for the pelagic eastern Mediterranean. We have analysed samples from two subcores of ABC26 (ABC26-B and ABC26-C). In both subcores five samples were selected for sequential extraction: one from the upper Mn peak, another one in the oxidised sapropel zone close above the visible sapropel, and three from the sapropel proper.

Table 7.1 *The composition of MMIN, the mixed mineral standard prepared for this study.*

Mineral	Content (wt%)
illite	46.2
calcite	40.1
dolomite	10.0
pyrite	1.5
gypsum	0.7
goethite	0.6
haematite	0.5
manganite	0.3
barite	0.1

The sediment sequence of BC15, a boxcore recovered from a former brine basin at 3232 m water depth, is described in detail in Chapter 4. Briefly, it contains a unit of organic-rich sediments contemporary to sapropel S1, but redeposited from within a brine environment. It is overlain by a unit consisting of a foraminifer- and organic-enriched ooze at its base and organic-poor sediments almost devoid of foraminifers; this unit has been redeposited from outside the brine. On top lies a normal sediment sequence accumulated after reoxygenation of the brine basin with a distinct Mn peak at its base. Eighteen samples from this boxcore were selected for sequential extraction.

7.2.2 Methods

The CASEX method (Table 7.2), was composed in such a way that the different solvents would subsequently extract the following phases: absorbed ions ($MgCl_2$; only BC15), carbonates (NH_4Cl), amorphous oxides (ascorbate), and remaining carbonates (NaAc). The pH of the NH_4Cl and NaAc solutions was adjusted by adding NH_3 and HAc respectively.

In general, the CASEX method consisted of the following procedure. Approximately

250 mg of sediment was accurately weighed. The samples were put in Teflon tubes. After shaking with the appropriate solvent (~ 16 hours), these tubes were centrifuged at 4000 rpm, after which the solution was decanted. Between all steps, the samples were washed with distilled water. All solutions, including the washes (except for BC15), were measured using an Inductively Coupled Plasma Atomic Emission Spectrometer (ICP/AES; Perkin Elmer Optima 3000) for Ca, Mg, Sr, Al and S. The quality of the measurements was monitored by the inclusion of blanks and in-house standards. Reproducibility of these standards was better than 2% for Ca, Mg, Sr and Al, and better than 4% for S. Because wash solutions following individual extraction steps from the BC15 extraction series were not analysed, concentrations were corrected using known solubility products and volumes, and using the results from an in-house standard (MM91; mixed eastern Mediterranean sediment) employed in all series. This was necessary due to some carbonate dissolution during these washes.

Table 7.2 *Overview of the CASEX method used in this study.*

CASEX scheme				
Step	***BC15***	**Ref.**	***ABC26, MMIN***	**Ref.**
1	25 ml 1 M $MgCl_2$ pH 8	1	25 ml 2 M NH_4Cl pH 9	2, 3
2	2×25 ml 2 M NH_4Cl pH 9	2, 3	25 ml 2 M NH_4Cl pH 9	2, 3
3	2×25 ml 2 M NH_4Cl pH 8			2, 3
4	2×25 ml 2 M NH_4Cl pH 7.5			2, 3
5	3×25 ml 2 M NH_4Cl pH 7			2, 3
6	25 ml ascorbic acid/sodium bicarbonate/sodium citrate solution (pH ~ 8)			4
7	25 ml 1 M NaAc pH 6			5
8	25 ml of 1 M NaAc pH 5			5

References: (1) Ruttenberg (1992); (2) De Lange (1992b); (3) De Lange et al. (1994); (4) Kostka and Luther (1994); (5) Chapter 4.

All samples, including calcite, dolomite and gypsum, were subjected to total digestion by oven heating them at 95°C in a mixture of hydrofluoric, nitric, and perchloric acids. The solutions, which were kept in Teflon vessels, were subsequently vaporised to dryness on a sand bath. Final solutions were made in 1 M HCl and were analysed with ICP/AES (BC15 and ABC26-B on an ARL 34000; all other samples on a Perkin Elmer Optima 3000). International and in-house standards were always included, giving reproducibilities better than 2% for Ca, Mg, Sr, Al and S.

X-Ray Diffraction (Philips PW1730/10; Kα radiation, Cu target) analysis of powdered sediment samples (two from BC15, five from ABC26-C) was used for the semi-quantitative determination of calcite, dolomite and aragonite. The ratios of the maximum intensities of the

(104) peak of calcite, the (104) peak of dolomite and the (111) peak of aragonite were individually calibrated according to Milliman (1974) for semi-quantitative calibrations. To convert peak ratios to actual concentrations of calcite, dolomite and aragonite, the following procedure was used. First, it is assumed that total Ca is equal to all carbonate-Ca. This assumption will not introduce a large error, because Ca in eastern Mediterranean sediments is almost exclusively related to carbonates (see section 7.3). The following equation is then true:

$$Ca_{total} = Ca_{cc} + Ca_{dol} + Ca_{arag} = \frac{40.08}{100.08} \times cc + \frac{40.08}{184.41} \times dol + \frac{40.08}{100.09} \times arag \qquad (1)$$

where Ca_{total} is total Ca measured by total digestion (wt%), Ca_{cc}, Ca_{dol} and Ca_{arag} the amount of Ca contributed by calcite, dolomite and aragonite respectively (wt%), and cc, dol and arag are the contents of calcite, dolomite and aragonite respectively (wt%). Eq. 1 is then rewritten as:

$$cc = \frac{Ca_{total}}{\frac{40.08}{100.09} + \frac{40.08}{184.41} \times \frac{dol}{cc} + \frac{40.08}{100.09} \times \frac{arag}{cc}} \qquad (2)$$

Total Ca, and the dol/cc and arag/cc ratios (from the calibrated XRD peak intensity ratios) are known, so the calcite, and subsequently the dolomite and aragonite contents can be calculated.

7.3 Results and discussion

The results of the sequential extraction on the mixed mineral standard MMIN will be shown first, and related to the different mineral phases present in MMIN. These findings will then be used for the interpretation of the CASEX results of eastern Mediterranean sediment samples. Finally, the environmental implications will be discussed.

7.3.1 MMIN

The sequential extraction of single minerals has two major drawbacks. Firstly, the amount used in the sequential extractions is usually much higher than the amount found during the extraction of normal sediments. This may result in saturation of the solvent when using a single mineral, whereas sediment samples would generally not be saturated. Secondly, sediments are composed of a multitude of minerals. A mixture of different minerals will react differently towards a certain solvent compared to a single mineral because of the interaction between minerals with different solubilities, hence creating a variable matrix. To avoid these problems, a homogenised standard of nine minerals with known compositions was prepared (MMIN; Table 7.1). The proportion between these minerals resembles their content in average Mediterranean sediments. This will allow us to assess the applicability of the CASEX scheme to our sediment samples.

Table 7.3 *The amount of Ca, Mg and Sr found per mineral and for the total standard, including the recoveries per element. Total (s.e.) designates the total amount found in the sequential extraction, total (t.d.) the total amount expected based on the total digestion results for the individual minerals.*

MMIN		calcite	dolomite	gypsum	total
Ca	total (s.e.)	161580	23648[a]	1616[b]	186844
(ppm)	total (t.d.)	160407	24039	1588	186034
	recovery%	*100.7%*	*98.4%*	*101.8%*	*100.4%*
Mg	total (s.e.)	2176	14883	14.4[b]	17073
(ppm)	total (t.d.)	1815	15129	14.2	16958
	recovery%	*119.9%*	*98.4%*	*101.8%*	*100.7%*
Sr	total (s.e.)	66.2	47.3[a]	23.4[b]	137
(ppm)	total (t.d.)	64.3	48.0	23.0	135
	recovery%	*103.0%*	*98.4%*	*101.8%*	*101.1%*

[a] *calculated using El/Mg ratio found for pure dolomite*

[b] *calculated using El/S ratio found for pure gypsum*

The efficiency of the sequential extraction of MMIN is good, with total recoveries for Ca, Mg and Sr of respectively 100.4, 101.7 and 101.0 % (Table 7.3). Calcium is a major component of calcite, dolomite and gypsum. Gypsum was included in MMIN to represent Ca present in salts which precipitate due to the evaporation of pore water during drying of sediments. Although Ca in gypsum has only a minor contribution to bulk Ca, it is important to know when it will be extracted to avoid errors in the calculation of carbonate-Ca, because gypsum-Ca might be an important contributor in a single step. Calcium is mainly extracted in the NH_4Cl and NaAc steps (Fig. 7.2). A slightly higher amount of Ca is extracted in the first than in the second step, although both steps consist of NH_4Cl (pH 9). The concentration of S extracted in the first step (0.13 wt%) equals the total amount of S_{gypsum} present in MMIN. Using the known composition of gypsum, the contribution of Ca, Mg and Sr derived from gypsum can be calculated* (Table 7.3).

Calcite and dolomite can also be distinguished. Calcite is more soluble than dolomite, which is reflected in the Mg/Ca ratio of the carbonates in the successive CASEX steps (Fig. 7.3A). At first, this ratio is low and decreases until step 4. Subsequently, it increases from step 5 onwards. The amount of Mg extracted in steps 5 to 8 (1.51 wt%) equals the total amount of Mg contributed by dolomite. The Ca content from steps 1 to 8 remaining after substraction of Ca contributed by gypsum and dolomite, is 16.2 wt%, which is exactly the contribution of calcite to MMIN. Therefore, distinction between calcite and dolomite is possible by summation of the released Mg, beginning with the step in which the Mg/Ca ratio starts to increase, and ending with the NaAc (pH 5) step.

* Note: For sediment samples, the Ca/S ratio of (average) seawater (or, when available, of the porewater) should be used for the determination of Ca originally from porewater.

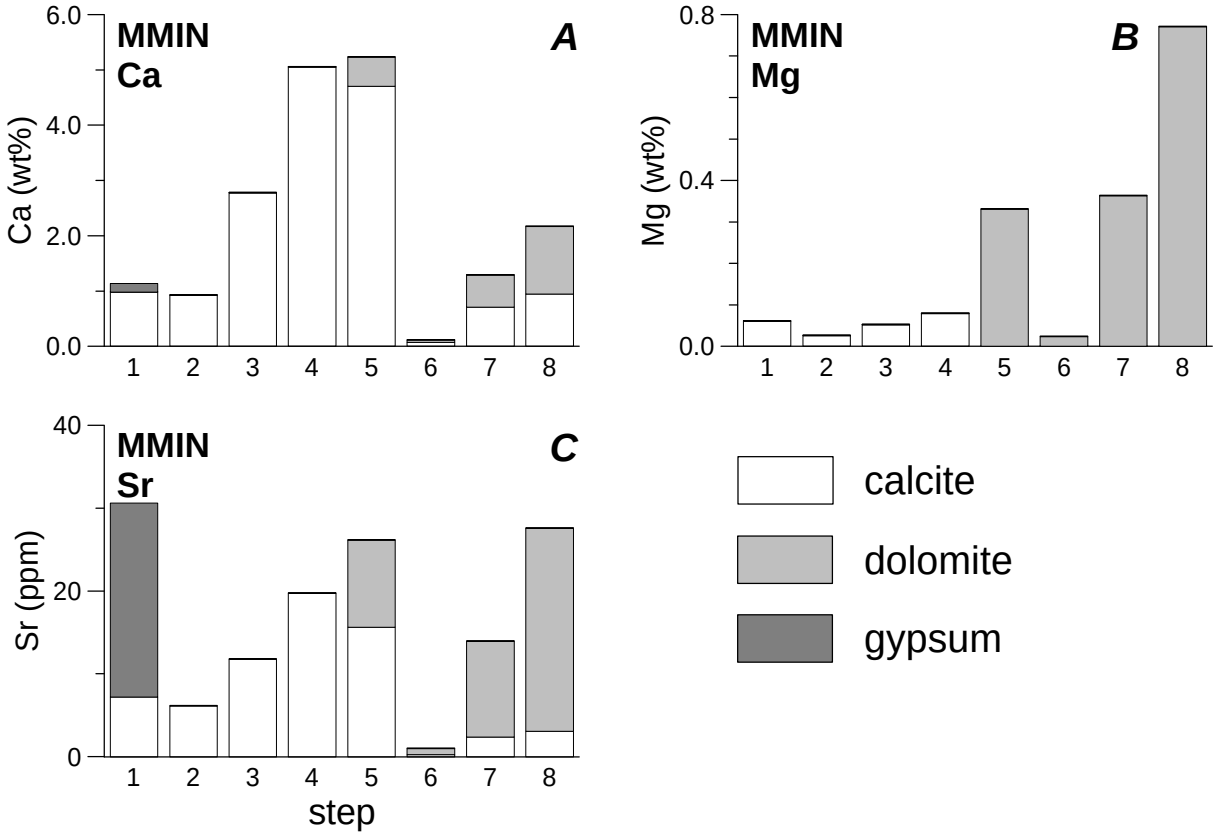

Figure 7.2 *The sequential extraction results of MMIN (see Table 7.1), for A) Ca, B) Mg, and C) Sr. Relative contributions by calcite, dolomite and gypsum have been indicated (see text).*

Magnesium is mainly present in dolomite and calcite. Quantification of $Mg_{calcite}$ gives a recovery of 120%, possibly due to some dissolution of dolomite in step 4 (Table 7.3). This will hardly affect the quantification of dolomite in sediments, but may introduce a small error in the calculation of the Mg/Ca ratio of calcite. For successive sediment samples, this relative overestimation will not have a significant effect on the trend of the Mg/Ca ratio of $CaCO_3$.

Strontium is present in calcite, dolomite and gypsum. Quantification of Sr_{gypsum} and $Sr_{dolomite}$ on the basis of S_{gypsum} and $Mg_{dolomite}$ respectively, allows for the determination of $Sr_{calcite}$ and gives a Sr recovery of ~ 100% for all minerals. The decrease of the Sr/Ca ratio of calcite (as for the Mg/Ca ratio in steps 1–4) indicates that some recrystallisation of carbonates may take place during the extraction (Fig. 7.3B).

7.3.2 Sediments

7.3.2.1 Efficiency of the sequential extraction of sediment samples

To assess the efficiency of the CASEX method for the sediment samples, we need to include the non-carbonate fraction together with the carbonate fraction. Therefore, recovery is defined as:

$$Recovery = \frac{sum\ of\ all\ concentrations\ of\ a\ certain\ element}{concentration\ of\ that\ element\ measured\ by\ total\ digestion} \times 100\% \quad (3)$$

In all sediment samples, the carbonate fraction of Ca and Sr is very high compared to the non-carbonate fraction, indicating that Ca and Sr are mainly present in carbonates (Table 7.4). Magnesium, however, is also present in high concentrations in the non-carbonate fraction, that is in clay minerals. The recoveries of Mg from the ABC26 samples are all close to 100%. In BC15, the recovery of Mg is somewhat lower, which may be caused by some loss of very fine-grained clay minerals decanted during the extraction procedure (see also Chapter 5).

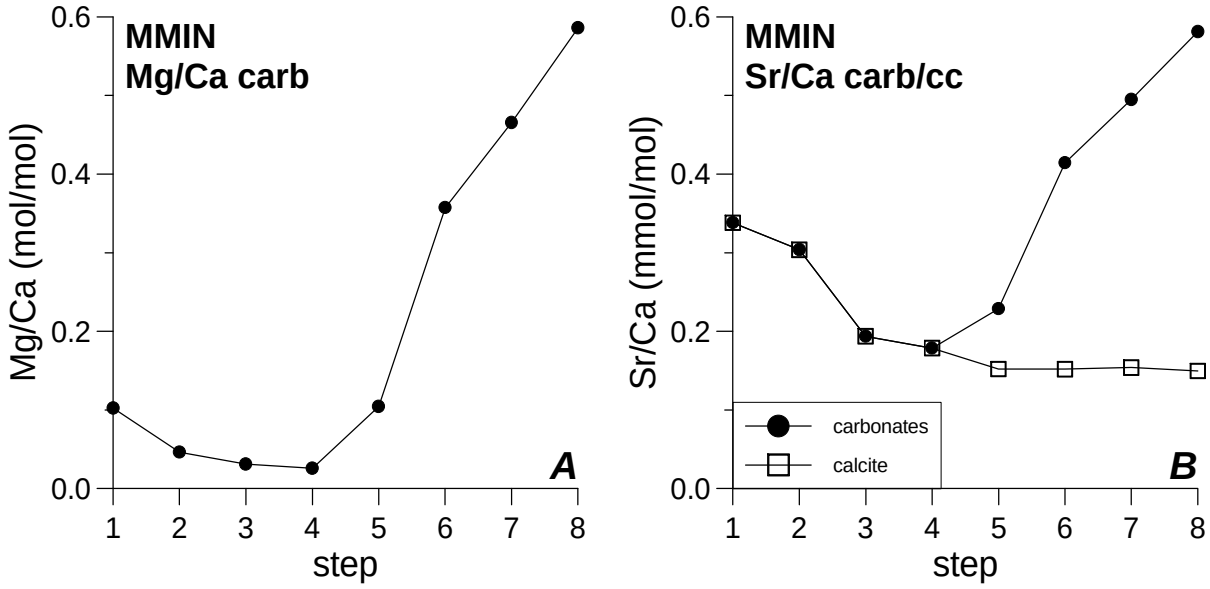

Figure 7.3 *A) Mg/Ca ratio (mol/mol) in each of the sequential extraction steps of the carbonate fraction of MMIN; B) Sr/Ca ratio (mmol/mol) of the carbonate and calcite fractions of MMIN.*

7.3.2.2 Calcite and aragonite ($CaCO_3$) versus dolomite ($CaMg(CO_3)_2$)

As inferred from the sequential extraction of MMIN, calcite and dolomite can be distinguished by using the Mg/Ca ratio of each step. This holds true for the eastern Mediterranean sediment samples subjected to CASEX. Despite the higher $CaCO_3$ content of ABC26 (50%) relative to MMIN (40%) and the concordantly higher number of steps (5 *vs.* 4 steps; cf. Figs. 7.3A, 7.4B) needed to dissolve most $CaCO_3$, similar results are found for the development of the Mg/Ca ratio in consecutive steps. Analogous results are found when comparing samples of BC15 (42% $CaCO_3$) and ABC26 (Figs. 7.4A,B). Consequently, the amount of dolomite present in each eastern Mediterranean sediment sample can be quantified.

Results from BC15 indicate that the dolomite content of the oxic intervals is clearly higher than that of the sapropel (Fig. 7.5E). In ABC26, dolomite is lowest in the upper part of the visible sapropel, with a trend to higher values towards the top and bottom of the original sapropel (Fig. 7.5K). Calcium carbonate, which includes calcite as well as aragonite, correlates well with the total Ca content of both boxcores (compare Figs. 7.5A and 7.5D (BC15) and Figs. 7.5G and 7.5J (ABC26)).

Although XRD analysis only gives semi-quantitive results for calcite, dolomite and

Table 7.4 *Recovery results of Ca, Mg and Sr for all boxcore samples. "El st.1–8" (El = element) designates the total for steps 1 to 8 (the 'carbonate steps'), "El-rest" the total for the rest of the steps, "El td" the total as found in the total digestion, and "Rec%" the recovery for that element.*

Sample code	Depth (cm)	Ca st.1–8 (wt%)	Ca-rest (wt%)	Ca td (wt%)	Rec%	Mg st.1–8 (wt%)	Mg-rest (wt%)	Mg td (wt%)	Rec%	Sr st.1–8 (ppm)	Sr-rest (ppm)	Sr td (ppm)	Rec%
BC15													
AA09132	1.35	15.8	0.2	17.1	93.8%	0.87	1.18	2.42	84.9%	731	47	801	97.1%
AA09137	2.85	16.8	0.2	17.4	97.9%	0.88	1.12	2.41	82.8%	772	46	818	100.0%
AA09146	5.55	17.1	0.1	18.2	94.7%	0.96	1.09	2.44	83.9%	729	39	785	97.8%
AA09152	7.35	16.8	0.1	17.7	95.6%	0.90	1.20	2.43	86.3%	702	41	757	98.2%
AA09156	8.55	16.4	0.2	17.1	97.2%	1.04	1.16	2.45	90.0%	692	47	744	99.3%
AA09160	9.75	23.2	0.1	23.9	97.4%	0.71	0.66	1.48	92.9%	849	23	882	99.0%
AA09164	10.95	23.2	0.1	24.8	93.8%	0.63	0.73	1.51	90.4%	897	21	946	97.0%
AA09172	13.35	17.5	0.1	18.2	97.0%	0.68	1.21	2.09	90.9%	1076	33	1125	98.6%
AA09178	15.15	16.8	0.1	17.4	97.1%	0.69	1.48	2.25	95.9%	917	33	966	98.4%
AA09183	16.65	15.7	0.1	16.8	94.0%	0.68	1.51	2.37	92.3%	853	34	919	96.5%
AA09190	18.75	16.9	0.1	19.0	89.7%	0.70	1.16	2.06	90.5%	1005	28	1105	93.4%
AA09198	21.15	16.6	0.1	18.4	90.7%	0.72	1.22	2.14	90.8%	915	30	1002	94.3%
AA09204	22.95	16.9	0.1	18.8	90.8%	0.75	1.21	2.19	89.6%	1018	31	1110	94.5%
AA09207	23.85	17.4	0.1	19.4	90.4%	0.73	1.19	2.15	89.7%	1105	30	1202	94.4%
AA09212	25.35	16.9	0.1	19.5	87.4%	0.83	1.20	2.28	88.7%	932	35	1039	93.0%
AA09221	28.25	16.6	0.1	17.7	94.7%	0.77	1.27	2.27	89.8%	875	35	936	97.2%
AA09226	29.75	17.6	0.1	19.1	92.5%	0.72	1.24	2.16	91.0%	987	31	1066	95.5%
AA09230	31.05	17.1	0.1	18.4	93.8%	0.77	1.25	2.26	89.7%	956	34	1024	96.7%
ABC26-B													
77912	12.85	23.8	0.1	24.0	99.5%	1.15	0.73	1.85	101.5%	1031	28	1067	99.2%
77933	19.15	20.6	0.2	21.3	97.5%	0.84	0.92	1.75	100.9%	1202	33	1250	98.8%
77938	20.75	19.8	0.2	20.4	98.3%	0.84	0.88	1.66	104.0%	1295	33	1313	101.2%
77942	21.95	20.2	0.2	20.6	98.7%	0.87	0.85	1.66	104.1%	1325	35	1423	95.6%
77949	24.05	20.5	0.1	21.0	98.4%	0.99	0.85	1.80	102.5%	1511	36	1584	97.7%
ABC26-C													
78010	12.25	24.1	0.1	24.8	97.8%	1.22	0.70	1.90	101.5%	1014	27	1030	101.0%
78035	19.75	20.6	0.2	21.4	97.0%	0.81	0.94	1.74	100.6%	1216	33	1222	102.2%
78040	21.25	19.7	0.2	20.3	97.7%	0.83	0.91	1.59	109.6%	1305	32	1252	106.8%
78044	22.45	19.9	0.2	21.1	95.1%	0.87	0.88	1.65	105.5%	1388	33	1399	101.6%
78049	23.95	20.0	0.2	20.9	96.8%	0.97	0.86	1.77	103.3%	1456	38	1470	101.7%

aragonite because of the dependence of measured peak intensities on e.g. grain size and grinding time (Milliman, 1974), it can be used to show trends between different samples. The dolomite content determined by XRD is in fair agreement with the content derived from the sequential extractions (Table 7.5). Therefore, we are confident that the sequential extraction results give a correct representation of the dolomite content in these sediments.

The Mg/Ca ratio of sequential steps prior to the dolomite extraction decreases from the first step up to step 4 or 5 (Figs. 7.4A,B). Sediments may include Mg-containing calcites

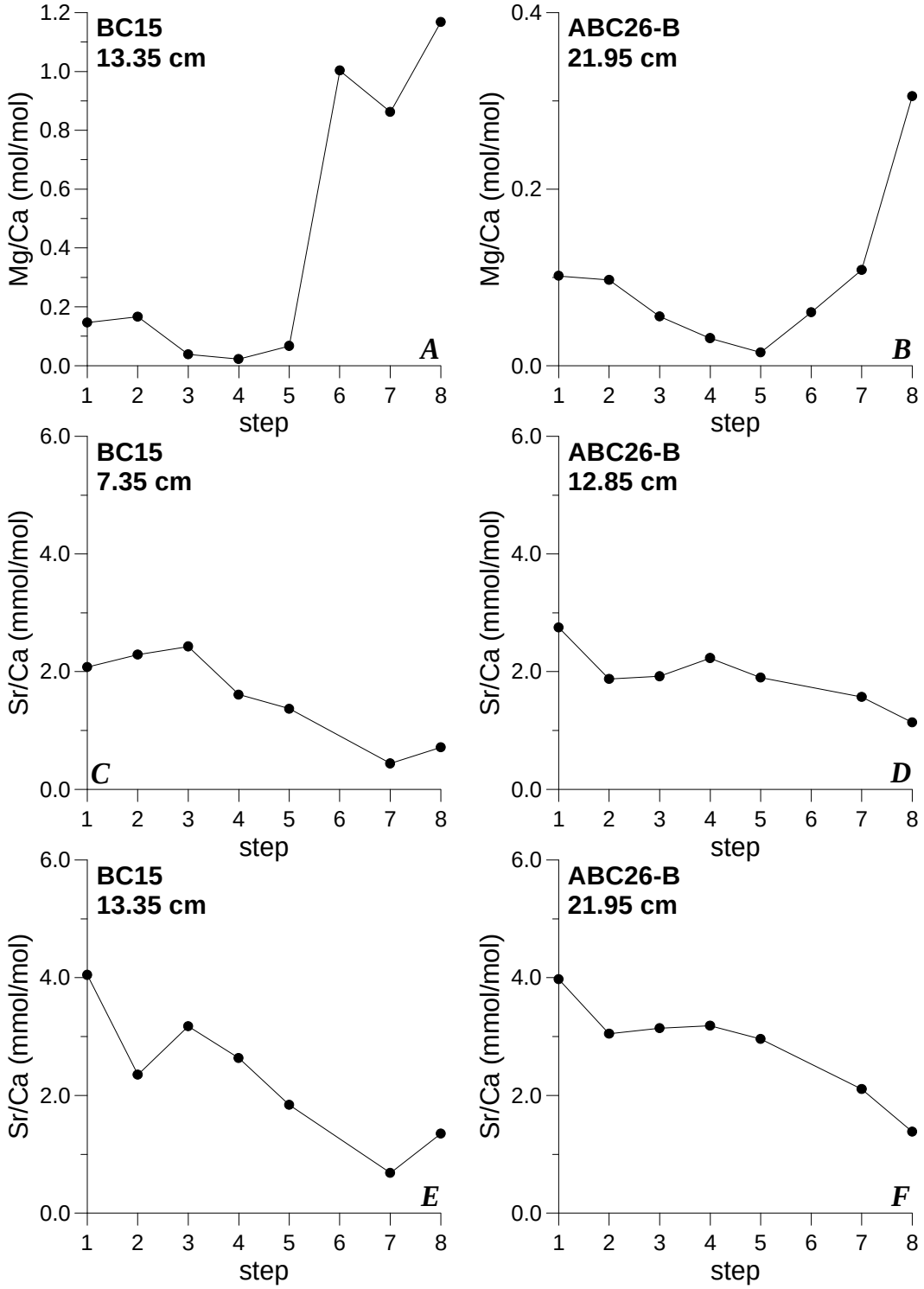

Figure 7.4 *A–B) Typical development of the Mg/Ca ratio (mol/mol) in BC15 (A) and ABC26-B (B); C–D) Typical development of the Sr/Ca ratio (mmol/mol) in oxic sediment samples from BC15 (C) and ABC26-B (D); E–F) Typical development of the Sr/Ca ratio (mmol/mol) in sapropel samples from BC15 (E) and ABC26-B (F). The depth of all shown samples is designated in the graphs.*

with a range of different Mg contents (e.g. Milliman, 1974), hence with slightly different solubilities. A higher Mg content would correspond to a slightly higher solubility. The decrease of the Mg/Ca ratio in consecutive extraction steps can, therefore, be explained by the selective dissolution of a range of Mg-containing calcites. Because of the decrease of the Mg/Ca ratio in these succerssive steps, dissolution of dolomite can be excluded.

7.3.2.3 Aragonite

Precipitation experiments and theoretical calculations have shown that Sr is enriched in aragonite compared to calcite (e.g. Winland, 1969). In subsequent extraction steps, the Sr/Ca ratio is initially high and decreases slowly (Figs. 7.4C,D). Aragonite is slightly more soluble than calcite and is, therefore, likely to dissolve predominantly in the first extraction step. The Sr/Ca ratio of the first step, therefore, may represent the relative content of aragonite compared to calcite. In general, aragonite appears to be higher in the sapropel than in the overlying oxic sediments and to follow the trend of the bulk sediment Sr/Ca ratio (Fig. 7.6). This is further substantiated by the XRD-derived aragonite content of a few selected samples (Table 7.5; Figs. 7.6A,C), which agree nicely with the relative Sr/Ca ratio in step 1.

7.3.3 Environmental history of eastern Mediterranean sediments

To the best of our knowledge, no data are available on the Calcite Compensation Depth (CCD) in the eastern Mediterranean, but the Aragonite Compensation Depth (ACD) is reported to be at about 3000 m water depth (Berger, 1978). However, in boxcore UM4 from 3309 m water depth, pteropods are still found in abundance (Chapter 2), which suggests that the ACD is even deeper than 3300 m. Consequently, the CCD must also be deeper than 3300 m. Furthermore, even fragile coccolithophores, such as *Oolithothus fragilis*, *Discosphaera tubifera* and *Umbilicosphaera* spp., are present in the surface sediment of boxcore UM15 (3308 m water depth; Chapter 3) and in sediment trap samples at 3000 m water depth (Chapter 3). This means that the carbonate contents in both boxcores of this study have not been subject to dissolution.

At present, input from Saharan dust is the major terrestrial source in most of the central eastern Mediterranean (Dulac et al., 1996; Guerzoni et al., 1997; Krom et al., 1999; Chapter 2). During periods of sapropel formation, river input drastically increased (Rossignol-Strick et al., 1982; Kallel et al., 1997; Rossignol-Strick et al., 1998), changing the character of the terrigenous component in sediments due to mineralogical differences of the source areas (Dominik and Stoffers, 1979; Krom et al., 1999). Also, the relative humidity during sapropel times was higher (Kallel et al., 1997), which would have a negative effect on the amount of dust formation in Northern Africa, the major source area for Saharan dust (Dominik and Stoffers, 1979). Dolomite is a component of wind-blown dust (Chester et al., 1977) and could be an indicator for the relative importance of dust deposition with regard to the total terrigenous component. The results presented here (Figs. 7.5E and 7.5K) show that the dolomite content is much lower in sapropelic than in non-sapropelic sediments. However, the variation in dolomite content and bulk sediment Mg/Al ratio do not correspond (compare Figs. 7.5E and 7.5F, and 7.5K and 7.5L). Bulk sediment Al and Mg/Ca profiles

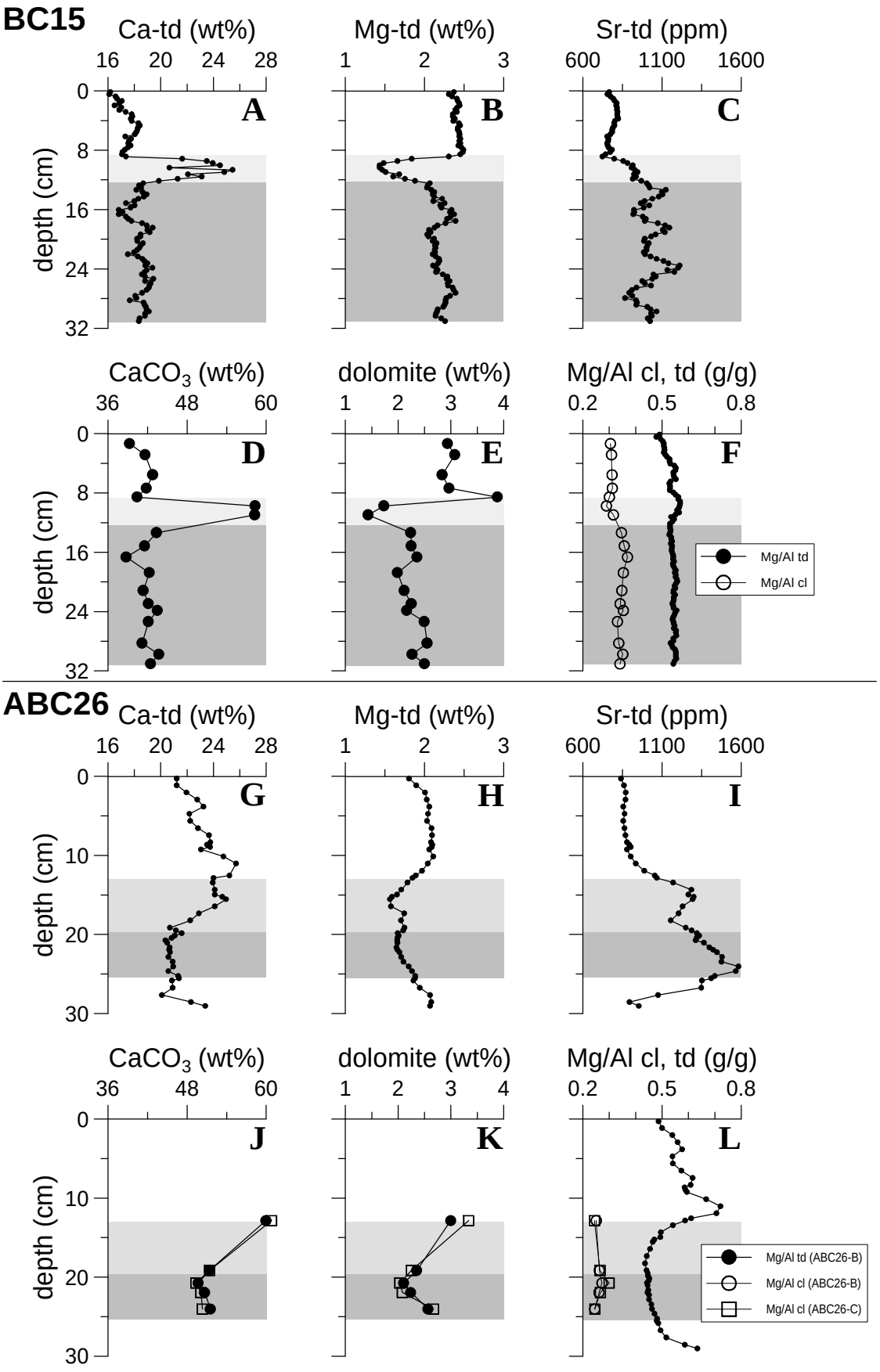
BC15
Ca-td (wt%)
16 20 24 28
Mg-td (wt%)
1 2 3
Sr-td (ppm)
600 1100 1600
A
B
C
depth (cm)
0 8 16 24 32
CaCO3 (wt%)
36 48 60
dolomite (wt%)
1 2 3 4
Mg/Al cl, td (g/g)
0.2 0.5 0.8
D
E
F
Mg/Al td
Mg/Al cl
ABC26
Ca-td (wt%)
16 20 24 28
Mg-td (wt%)
1 2 3
Sr-td (ppm)
600 1100 1600
G
H
I
depth (cm)
0 10 20 30
CaCO3 (wt%)
36 48 60
dolomite (wt%)
1 2 3 4
Mg/Al cl, td (g/g)
0.2 0.5 0.8
J
K
L
Mg/Al td (ABC26-B)
Mg/Al cl (ABC26-B)
Mg/Al cl (ABC26-C)

Table 7.5 *Results on calcite, dolomite and aragonite contents for the samples subjected to XRD-analysis, and calculated from the total Ca content and relative XRD peak intensities (see methods). For comparison, CASEX results for the same samples have been included.*

Sample	Depth (cm)	$Calcite_{XRD}$ (wt%)	$Aragonite_{XRD}$ (wt%)	$Dolomite_{XRD}$ (wt%)	$Dolomite_{seq.extr.}$ (wt%)
BC15					
AA09156	8.55	37.3	2.3	4.7	4.2
AA09190	18.75	41.0	5.3	1.9	2.3
ABC26-C					
78010	12.25	57.1	2.9	3.4	3.3
78035	19.75	43.6	8.8	1.8	2.3
78040	21.25	41.8	7.9	1.8	2.0
78044	22.45	43.6	7.6	2.4	2.1
78049	23.95	40.4	9.9	2.7	2.7

(Figs. 7.7B–C,E–F) are very similar, in contrast to bulk sediment Ca and Mg/Al profiles (Figs. 7.5A,F,G,L). This indicates that most of the variations in the Mg/Al ratio are related to differences in the Mg content of clay minerals. This illustrates that in general the Mg/Al ratio cannot be used as a proxy for the relative variations of dolomite in a sediment column, unless dolomite is a major constituent, e.g. in the Indian Ocean, in areas close to sabkhas (Reichart et al., 1997). However, by using the CASEX method it is possible to correctly assess not only the sedimentary dolomite content and variations therein, but also the variations in the Mg/Al ratio of clay minerals (see also Chapter 5; Figs. 7.5F,L).

Aragonite is a $CaCO_3$ polymorph slightly more soluble than calcite. A number of faunal and floral species, such as green algae, aragonitic bryozoans and pteropods, have an aragonite instead of a calcite test (e.g. Milliman, 1974). Aragonite is richer in Sr than calcite (Winland, 1969; Sutherland et al., 1984). However, eastern Mediterranean pteropods appear to be relatively poor in Sr (Sr/Ca = 1.65 mmol/mol; Chapter 2). Increases in the bulk sediment Sr/Ca ratio and aragonite content, such as found in eastern Mediterranean sapropels (Figs. 7.6B and 7.6D; Table 7.5), are, therefore, not related to an increased number of

Left page: **Figure 7.5** *A–C) Total digestion (td) results of BC15 for Ca (A), Mg (B) and Sr (C); D–E) CASEX results of BC15 for calcite plus aragonite (D) and dolomite (E); F)The bulk sediment (td) Mg/Al ratio (g/g) and the Mg/Al ratio of the clay mineral fraction (cl) in BC15; G–I) Total digestion results of ABC26 for Ca (G), Mg (H) and Sr (I); J–K) CASEX results of ABC26 (filled circles and open squares designate ABC26-B and ABC26-C respectively) for calcite plus aragonite (J) and dolomite (K); L) The bulk sediment (td) Mg/Al ratio (g/g) and the Mg/Al ratio (g/g) of the clay mineral fraction (cl) in ABC26. The dark-grey zones in the graphs of BC15 and ABC26 line out the (visible) sapropel. The light-grey zone in the figures of BC15 delineates the foraminifera ooze, whereas the light-grey interval in ABC26 is the oxidised sapropel zone.*

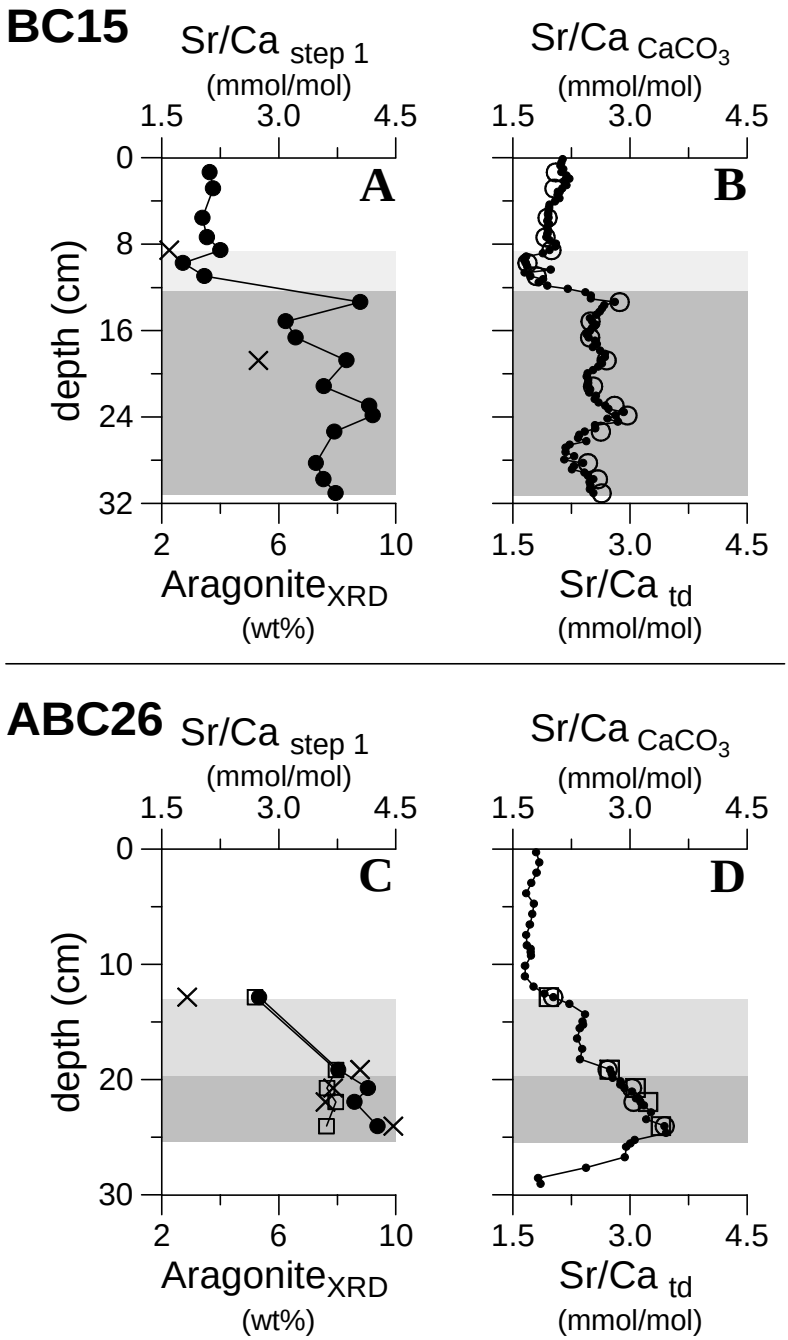

Figure 7.6 *A) Sr/Ca ratio (mmol/mol) of the first CASEX step (filled circles) and the XRD-determined aragonite content (crosses) in wt% of BC15; B) The Sr/Ca ratio of calcite plus aragonite ($CaCO_3$) in mmol/mol (open circles) and the bulk sediment Sr/Ca ratio (mmol/mol) (filled circles) in BC15; C) Sr/Ca ratio (mmol/mol) of the first CASEX step and the XRD-determined aragonite content in wt% of ABC26. Filled circles and open squares designate the Sr/Ca ratio of the first CASEX step in ABC26-B and ABC26-C respectively, whereas crosses indicate the aragonite content; D) The Sr/Ca ratio of calcite plus aragonite ($CaCO_3$) in mmol/mol (open symbols) and the bulk sediment Sr/Ca ratio (mmol/mol) (filled circles) in ABC26. Circles designate ABC26-B, squares ABC26-C.*

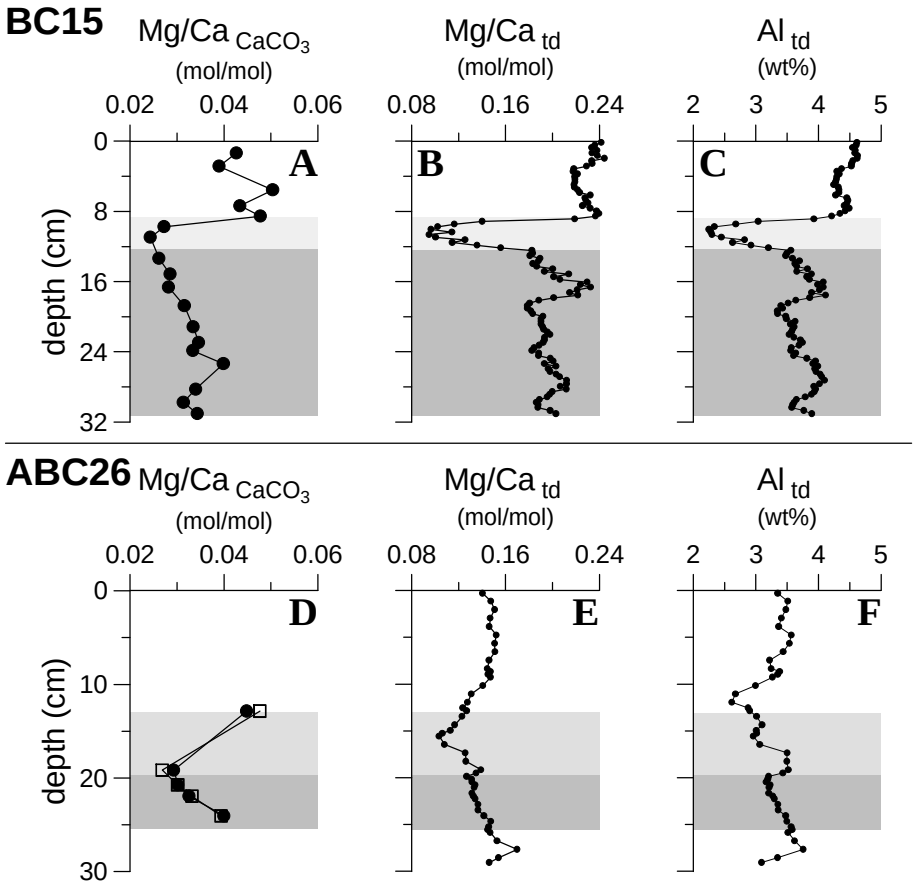

Figure 7.7 *A) The Mg/Ca ratio of calcite plus aragonite ($CaCO_3$) (mol/mol) in BC15; B) The bulk sediment Mg/Ca ratio (mol/mol) in BC15; C) The bulk sediment Al content of BC15 (see also Chapter 5); D) The Mg/Ca ratio of $CaCO_3$ (mol/mol) in ABC26. Filled circles and open squares designate ABC26-B and ABC26-C respectively; E) The bulk sediment Mg/Ca ratio (mol/mol) in ABC26-B; F) The bulk sediment Al content of ABC26 (see also Chapter 5).*

pteropods, as implied by Sutherland et al. (1984), but are most likely related to an increase in some other as yet undetermined fine-grained aragonite phase. This is in line with Milliman and Müller (1973), who concluded on the basis of XRD-analyses of eastern Mediterranean sediments that the aragonite was not associated with pteropods, but rather with the fine-grained lutite fraction (see also Chapter 2). Similar results were found for Pacific and Atlantic sediments (Hampt Andreasen and Delaney, 2000).

The CASEX method has allowed the determination of the Mg/Ca and Sr/Ca ratios of $CaCO_3$(including calcite as well as aragonite). The Mg/Ca ratios of samples from ABC26 are at a minimum in the original sapropel, and those in BC15 are lowest in the organic-rich sapropel sediments (Figs. 7.7A,C). This might be caused by a lower temperature, a decreased salinity, enhanced postdepositional dissolution, or variations in the relative amount of biogenic carbonate species (foraminifers, coccolithopores, pteropods, calcareous dinoflagellates), each having different Mg/Ca and Sr/Ca in their tests (Milliman, 1974).

Another possibility is the decreased occurrence of inorganically precipitated magnesian calcitic cement (Milliman and Müller, 1973). Holocene sea surface temperatures were relatively stable during the last 8000 years (Kallel et al., 1997), excluding lower temperatures as a possible cause for the lower Mg/Ca values. Enhanced postdepositional carbonate dissolution (Brown and Elderfield, 1996) can be discounted for the eastern Mediterranean S1 sapropel because carbonate preservation is higher, not lower, during its deposition due to the euxinic environment (see e.g. Chapter 4). However, the three other mechanisms that may lead to a lower Mg/Ca value are possible; these are: 1) decreased surface water salinity, 2) variations in flora and fauna, and 3) decreased inorganic precipitation of magnesian calcite.

1) Decreased surface water salinity

Surface water salinity was indeed lower, because rainfall was significantly enhanced during sapropel times (e.g. Kallel et al., 1997). Estimates for the decrease in surface water salinity near the two boxcore sites is in the order of 4‰ (Kallel et al., 1997). Investigations on the behaviour of the Mg/Ca ratio in relation to salinity in laboratory cultures show that a 4‰ salinity decrease results in the percentual lowering of the Mg/Ca ratio in foraminifers of ~ 16% (Lea et al., 1999) to ~ 25% (Nürnberg et al., 1996). In comparison, the results on our boxcores give a decrease of the bulk calcite Mg/Ca ratio of about 35% during sapropel deposition (Figs. 7.7A,D), suggesting that a decrease in surface water salinity might indeed have had a major impact on the Mg/Ca ratio of bulk $CaCO_3$.

2) Variations in flora and fauna

Fauna and flora in sapropels is different compared to that in other sedimentary units (e.g. Cita et al., 1977; Rasmussen, 1991; Vismara-Schilling and Coulbourn, 1991; Castradori, 1993; Rohling et al., 1993; Schmiedl et al., 1998; Negri et al., 1999). There exist not only varations in the Mg/Ca ratio within different groups of species, but also within one group (e.g. Milliman, 1974; Lea et al., 1999; Elderfield and Ganssen, 2000). Consequently, fauna and flora with different species and groups of species may be partly responsible for the observed profiles.

3) Decreased inorganic precipitation of magnesian calcite

The content of magnesian calcite cement is reported to decrease during sapropel times (Milliman and Müller, 1973), which means that such a decrease can also be partly responsible for the lower carbonate Mg/Ca ratios in sapropel S1. Such a decrease is likely to be related to generally lower salinities during that period.

In summary, the decreased surface water salinity appears to be mainly responsible for the decreased Mg/Ca ratio of bulk $CaCO_3$ in sapropel S1 sediments, either directly by adapted uptake by organisms or by reduced precipitation of high-Mg calcite. A different flora and fauna may have had an additional influence.

The Sr/Ca ratios of $CaCO_3$ are almost identical to bulk sediment Sr/Ca ratios (Figs. 7.6B and 7.6D). They are relatively high in the organic-rich sediments of BC15 and ABC26 compared to the upper, oxic sediments. As seen earlier (section 7.3.2.3), this is likely to reflect the relative abundance of aragonite in the sapropelic sediments (Figs. 7.6A,C; Table 7.5). In contrast to carbonate Mg/Ca, temperature and salinity do not have such a large effect on carbonate Sr/Ca in single species (Lea at al., 1999). Variations in the Sr/Ca ratio must, therefore, for the greater part be due to changes in fauna and flora.

7.4 Conclusions

The results of the extraction of a mixed mineral standard show that the novel CASEX method can differentiate between calcite and dolomite and give an indication of the aragonite content. The dolomite content of sapropelic sediments is lower than that of overlying oxic sediment, which suggests that dust deposition decreased during sapropel times. This corresponds with the enhanced humidity for that period. The dolomite content determined by CASEX corresponds nicely with that determined by XRD, but deviates considerably from bulk Mg/Al ratios. As a consequence, total sediment Mg/Al and Mg/Ca ratios cannot 'a priori' be considered representative for either the dolomite content or for the Mg/Ca ratio of carbonate. In this study, most of the Mg/Al variations appear to be related to differences in the Mg content of clay minerals. Thus, bulk sediment Mg/Al ratios cannot be used for the indication of dolomite, whereas the CASEX method, better than XRD, can correctly assess the dolomite content in sediments. In contrast, the Sr/Ca ratio of the total sediment is almost entirely determined by the carbonate fraction.

The CASEX method also allows for the determination of Mg/Ca and Sr/Ca ratios of bulk $CaCO_3$ (including calcite as well as aragonite). The Mg/Ca ratio is significantly lower, whereas the Sr/Ca ratio is higher in the organic-rich sapropelic sediment. Quantification of the possible effect of a decrease in salinity strongly suggests that decreased surface water salinity may be the main cause for the observed Mg/Ca profile, in line with the enhanced humidity of that period. Faunal and floral changes may also have a possible (minor) contribution to the observed decrease in Mg/Ca. However, the Sr/Ca profile mainly reflects changes in the faunal and floral composition. The increased Sr/Ca suggests relatively higher amounts of aragonite in the sapropel, corroborated by the semi-quantitive XRD-analysis of aragonite.

Acknowledgements – P. Anten, A. van Leeuwen, G. Nobbe and H. de Waard are thanked for their analytical assistence. Thorough reading by C.H. van der Weijden and S.J. Schenau has greatly improved this manuscript.

This study was supported by MARFLUX (MAST1-90022C), PALAEOFLUX (MAS2-CT93-0051) and SAP (MAS3-CT97-0137) European programmes.

References

Aghib F.S. (1996) Anoxic versus oxic sedimentation in the Bannock Basin area, 35,000 yrs B.P. to present. *Riv. It. Paleontol. Stratigr.* 102, 293-302.

Anderson R.F., Bacon M.P. and Brewer P.G. (1983a) Removal of ^{230}Th and ^{231}Pa from the open ocean. *Earth Planet. Sci. Lett.* 62, 7-23.

Anderson R.F., Bacon M.P. and Brewer P.G. (1983b) Removal of ^{230}Th and ^{231}Pa at ocean margins. *Earth Planet. Sci. Lett.* 66, 73-90.

Andreae M.O. (1986) The ocean as a source of atmospheric sulfur compounds. *In:* Buat-Ménard P. (ed.) The role of air-sea exchange in geochemical cycling, *Reidel, Dordrecht,* 331-362.

Antipenko V.R., Zemtseva L.I. and Pevneva G.S. (1996) Methods of quantitative analysis for metal porphyrins in oils and related natural materials. *Geochem. Int.* 33, 96-104.

Antoine D., Morel A. and André J.-M. (1995) Algal pigment distribution and primary production in the eastern Mediterranean as derived from coastal zone color scanner observations. *J. Geophys. Res.* 100, 16193-16209.

Bacon M.P. (1984) Glacial to interglacial changes in carbonate and clay sedimentation in the Atlantic Ocean estimated from ^{230}Th measurements. *Isotope Geoscience* 2, 97-111.

Bacon M.P., Huh C.-A., Fleer A.P. and Deuser W.G. (1985) Seasonality in the flux of natural radionuclides and plutonium in the deep Sargasso Sea. *Deep-Sea Res.* 32, 273-286.

Baker E.T., Milburn H.B. and Tennant D.A. (1988) Field assessment of sediment trap efficiency under varying flow conditions. *J. Mar. Res.* 46, 573-592.

Balch W.M., Kilpatrick K.A. and Tres C.C. (1997) The 1991 coccolithophore bloom in the central North Atlantic. 1. Optical properties and factors affecting their distribution. *Limnol. Oceanogr. 41*, 1669-1683.

Balopoulos E., Theocharis A., Price B., Heussner S., Souvermezoglou A., Kontoyiannis H., Nakopoululou C., Varnavas S., Collins M.B., Apostolopoulou M., Ignatiades L., Gotsi O. and Theodoru A. (1996) A synthesis of preliminary results from multidisciplinary oceanographic studies in the South Aegean Sea and the straits of Cretan Arc. *Second workshop of the Mediterranean Target Project, Crete 1996, Extended abstract*, 224-232.

Bard E. (1988) Correction of accelator mass spectrometry ^{14}C ages measured in planktonic foraminifera: Paleoceanographic implications. *Paleoceanography.* 3, 635-645.

Behrenfeld M.J., Bale A.J., Kolber Z.S., Aiken J. and Falkowski A. (1996) Confirmation of iron limitation of phytoplankton photosynthesis in the equatorial Pacific Ocean. *Nature* 383, 508-511.

Bender M.L., Lorens R.B. and Williams D.F. (1975) Sodium, magnesium and strontium in the tests of planktonic foraminifera. *Micropaleontology* 21, 448-459.

Bergametti G., Gomes L., Remoudaki E., Desbois M., Martin D. and Buat-Ménard M.P. (1989) Present transport and deposition patterns of African dusts to the north-western Mediterranean. *In:* Leinen M. and Sarnthein M. (eds) Paleoclimatology and paleometeorology; modern and past patterns of global atmospheric transport. *NATO ASI Series C* 282, 227-252.

Bergametti G., Remoudaki E., Losno R., Steiner E., Chatenet B. and Buat-Menard P. (1992) Source, transport and deposition of atmospheric phosphorus over the northwestern

Mediterranean. *J. Atm. Chem.* 14, 501-513.

Berger W.H. (1978) Deep-sea carbonate: pteropod distribution and the aragonite compensation depth. *Deep-Sea Res.* 25, 447-452.

Berland B.R., Benzhitski A.G., Zensira P., Burlakova Z.P., Georgieva L.V., Izmestieva M.A., Kholodov V.I. and Maestrini S.Y. (1988) Conditions hydrologiques estivales en Méditerranée, répartition du phytoplancton et de la matière organique. *Oceanol. Acta* 9, 163-177.

Bernard F. and Lecal J. (1953) Role des flagellés calcaires dans la sédimentation actuelle en Méditerranée. *Publ. 19th geol. Congres, Algiers 1952* (4), 11-23.

Bernat M., Causse C., Perseil E.A. and Féraud G. (1989) Variations of element distribution in ferromanganese nodules and its bearing on growth rates. *Mineral. Deposita* 24, 258-269.

Berner R.A. (1970) Sedimentary pyrite formation. *Amer. J. Sci.* 270, 1-23.

Berner R.A. (1984) Sedimentary pyrite formation: An update. *Geochim. Cosmochim. Acta* 48, 605-615.

Bernstein R.E., Byrne R.H., Betzer P.R. and Greco A.M. (1992) Morphologies and transformations of celestite in seawater: The role of acantharians in strontium and barium geochemistry. *Geochim. Cosmochim. Acta* 56, 3273-3279.

Bishop J.K.B. (1988) The barite-opal-organic carbon association in ocean particulate matter. *Nature* 332, 341-343.

Björklund K.R. and De Ruiter R. (1987) Radiolarian preservation in eastern Mediterranean anoxic sediments. *Mar. Geol.* 75, 271-281.

Blount C.W. (1977) Barite solubilities and thermodynamic quantities up to 300°C and 1400 bars. *Amer. Mineral.* 62, 942-957.

Bonelli P., Braga Marcazzan G.M. and Cereda E. (1996) Elemental composition and air trajectories of African dust transported in northern Italy. *In:* Guerzoni S. and Chester R. (eds.) The impact of desert dust across the Mediterranean. *Environm. Sci. Technol. Libr.* 11, 275-283. *Kluwer Academic Publishers, Dordrecht.*

Bowen H.J.M. (1979) Environmental chemistry of the elements. *Academic Press, London,* 333 pp.

Breit G.N. and Wanty R.B. (1991) Vanadium accumulation in carbonaceous rocks: A review of geochemical controls during deposition and diagenesis. *Chem. Geol.* 91, 83-97.

Broerse A.C., Ziveri P., Van Hinte J.E. and Honjo S. (2000) Coccolithophore export production, seasonal species composition, and coccolith-$CaCO_3$ fluxes in the NE Atlantic (34˚N 21˚W and 48˚N 21˚W). *Deep-Sea Res. II* 47, 1877-1905.

Brookins D.G. (1988) Eh-pH diagrams for geochemistry. *Springer-Verlag, Berlin,* 176 pp.

Brown C.W. and Yoder J.A. (1994) Distribution pattern of coccolithophorid blooms in the Western North Atlantic Ocean. *Continent. Shelf Res.* 14, 175-197.

Brown S.J. and Elderfield H. (1996) Variations in Mg/Ca and Sr/Ca ratios of planktonic foraminifera caused by postdepositional dissolution: Evidence of shallow Mg-dependent dissolution. *Paleoceanography* 11, 543-551.

Bruins H.J. and Van der Plicht J. (1996) The exodus enigma. *Nature* 382, 213-214.

Buat-Ménard P., Davies J., Remoudaki E., Miquel J.C., Bergametti G., Lambert C.E., Ezat U., Quétel C., La Rosa J. and Fowler S.W. (1989) Non-steady-state biological removal of atmospheric particles from Mediterranean surface waters. *Nature* 340, 131-134.

Burdige D.J. and Gieskes J.M. (1983) A pore water/solid phase diagenetic model for manganese in marine sediments. *Amer. J. Sci.* 283, 29-47.

Calvert S.E. (1983) Geochemistry of Pleistocene sapropels and associated sediments from the Eastern Mediterranean. *Oceanol. Acta* 6, 255-267.

Calvert S.E. and Pedersen T.F. (1992) Organic carbon accumulation and preservation in marine sediments: How important is anoxia? *In:* Whelan J. and Farrington J.W. (eds.) Organic matter: Productivity, accumulation, and preservation in recent and ancient sediments. *Columbia University Press, New York,* 231-263.

Calvert S.E., Nielsen B. and Fontugne M.R. (1992) Evidence from nitrogen isotope ratios for enhanced productivity during formation of eastern Mediterranean sapropels. *Nature* 359, 223-225.

Canfield D.E. (1988) Sulfate reduction and the diagenesis of iron in anoxic marine sediments. *PhD thesis, Yale University,* 248 pp.

Canfield D.E. (1989) Reactive iron in marine sediments. *Geochim. Cosmochim. Acta* 53, 619-632.

Canfield D.E. (1994) Factors influencing organic carbon preservation in marine sediments. *Chem. Geol.* 114, 315-329.

Castradori D. (1993) Calcareous nannofossils and the origin of eastern Mediterranean sapropels. *Paleoceanography* 8, 459-471.

Chamley H. (1989) Clay sedimentology. *Springer-Verlag*, 623 pp.

Charlson R. J., Lovelock J.E., Andrea M.O. and Warren S.G. (1987). Oceanic phytoplankton, atmospheric sulfur, cloud albedo and climate. *Nature* 326, 655-661.

Chen J.H., Edwards P.L. and Wasserburg G.J. (1986) ^{238}U, ^{234}U and ^{232}Th in seawater. *Earth Planet. Sci. Lett.* 80, 241-251.

Cheshire M.V., Berrow M.L., Goodman B.A. and Mundie C.M. (1977) Metal distributions and nature of some Cu, Mn and V complexes in humic and fulvic acid fractions of soil organic matter. *Geochim. Cosmochim. Acta* 41, 1131-1138.

Chester R.. Baxter G.G., Behairy A.K.A., Connor K., Cross D., Eldersfield H. and Padgham R.C. (1977) Soil-sized eolian dusts from the lower troposphere of the eastern Mediterranean Sea. *Mar. Geol.* 24, 201-217.

Church T.M. and Wolgemuth K. (1972) Marine barite saturation. *Earth Planet. Sci. Lett.* 15, 35-44.

Cita M.B., Vergnaud-Grazzini C., Robert C., Chamley H., Ciaranfi N. and d'Onofrio S. (1977) Paleoclimatic record of a long deep sea core from the eastern Mediterranean. *Quatern. Res.* 8, 205-235.

Colley S., Thomson J., Wilson T.R.S. and Higgs N.C. (1984) Post-depositional migration of elements during diagenesis in brown clay and turbidite sequences in the North East Atlantic. *Geochim. Cosmochim. Acta* 48, 1223-1235.

Colley S., Thomson J. and Newton P.P. (1995) Detailed ^{230}Th, ^{232}Th and ^{210}Pb fluxes recorded by the 1989/90 BOFS sediment trap time-series at 48˚N, 20˚W. *Deep-Sea Res. I* 42, 833-848.

Conte M.H., Weber J.C. and Ralph N. (1998) Episodic particle flux in the deep Sargasso Sea: an organic geochemical assessment. *Deep-Sea Res. I* 45, 1819-1841.

Correggiari A., Guerzoni S., Lenaz R., Quarantotto G. and Rampazzo G. (1989) Dust deposition in the central Mediterranean (Tyrrhenian and Adriatic Seas): Relationships with marine

sediments and riverine input. *Terra Nova* 1, 549-558.

Dachs J., Bayona J.M., Fowler S.W., Miquel J.C. and Albaigés J. (1986) Vertical fluxes of polycyclic aromatic hydrocarbons and organochlorine compounds in the western Alboran Sea (southwestern Mediterranean). *Mar. Chem.* 52, 75-86.

Dehairs F., Chesselet R. and Jedwab J. (1980) Discrete suspended particles of barite and the barium cycle in the open ocean. *Earth Planet. Sci. Lett.* 49, 528-550.

Dehairs F., Goeyens L., Stroobants N., Bernard P., Goyet C., Poisson A. and Chesselet R. (1990) On suspended barite and the oxygen minimum in the southern ocean. *Global Biogeochem. Cycles* 4, 85-102.

Dehairs F., Fagel N., Antia A.N., Peinert R., Elskens M. and Goeyens L. (2000) Export production in the Bay of Biscay as estimated from barium - barite in settling material: a comparison with new production. *Deep-Sea Res. I* 47, 583-601.

De Lange G.J. and Ten Haven H.L. (1983) Recent sapropel formation in the eastern Mediterranean. *Nature* 305, 797-798.

De Lange G.J. (1986) Early diagenetic reactions in interbedded pelagic and turbiditic sediments in the Nares Abyssal Plain (western North Atlantic): Consequences for the composition of sediment and interstitial water. *Geochim. Cosmochim. Acta* 50, 2543-2561.

De Lange G.J., Middelburg J.J. and Pruysers P.A. (1989) Discussion: Middle and Late Quaternary depositional sequences and cycles in the eastern Mediterranean. *Sedimentology* 36, 151-158.

De Lange G.J., Middelburg J.J., Van der Weijden C.H., Catalano G., Luther G.W. III, Hydes D.J., Woittiez J.R.W. and Klinkhammer G.P. (1990) Composition of anoxic hypersaline brines in the Tyro and Bannock Basins, eastern Mediterranean. *Mar. Chem.* 31, 63-88.

De Lange G.J. (1992a) Shipboard routine and pressure-filtration system for pore-water extraction from suboxic sediments. *Mar. Geol.* 109, 77-81.

De Lange G.J. (1992b) Distribution of various extracted phosphorus compounds in the interbedded turbiditic/pelagic sediments of the Madeira Abyssal Plain, eastern North Atlantic. *Mar. Geol.* 109, 115-139.

De Lange G.J., Van Os B. and Poorter R. (1992) Geochemical composition and inferred accretion rates of sediments and manganese nodules from a submarine hill in the Madeira Abyssal Plain, eastern North Atlantic. *Mar. Geol.* 109, 171-194.

De Lange G.J., Van Os B., Pruysers P.A., Middelburg J.J., Castradori D., Van Santvoort P., Müller P.J., Eggenkamp H. and Prahl F.G. (1994) Possible early diagenetic alteration of palaeo proxies. *NATO ASI Series* I 17, 225-258.

Delaney M.L., Bé A.W.H. and Boyle E.A. (1985) Li, Sr, Mg, and Na in foraminiferal calcite shells from laboratory culture, sediment traps, and sediment cores. *Geochim. Cosmochim. Acta* 49, 1327-1341.

Des Combes H.J., Caulet J.-P. and Tribovillard N.P. (1999) Pelagic productivity changes in the equatorial area of the northwest Indian Ocean during the last 400,000 years. *Mar. Geol.* 158, 27-55.

De Rijk S., Hayes A. and Rohling E.J. (1999) Eastern Mediterranean sapropel S1 interruption: an expression of the onset of climatic deterioration around 7 ka BP. *Mar. Geol.* 153, 337-343.

De Visser J.P., Ebbing J.H.J., Gudjonsson L., Hilgen F.J., Jorissen F.J., Verhallen P.J.J.M. and

Zevenboom D. (1989) The origin of rhythmic bedding in the Pliocene Trubi Formation of Sicily, southern Italy. *Palaeogeogr. Palaeoclimatol. Palaeoecol.* 69, 45-66.

Dominik J. and Stoffers P. (1979) The influence of Late Quaternary stagnations on clay sedimentation in the eastern Mediterranean Sea. *Geol. Rundsch.* 68, 302-317.

Dove P.M. and Czank C.A. (1995) Crystal chemical controls on the dissolution kinetics of the isostructural sulfates: Celestite, anglesite, and barite. *Geochim. Cosmochim. Acta* 59, 1907-1915.

Dugdale R.C. and Wilkerson F.P. (1988) Nutrient sources and primary production in the Eastern Mediterranean. *Oceanol. Acta* 9, 179-184.

Dulac F., Moulin C., Lambert C.E., Guillard F., Poitou J., Guelle W., Quétel C.R., Schneider X. and Ezat U. (1996) Quantitative remote sensing of African dust transport to the Mediterranean. *In:* Guerzoni S. and Chester R. (eds.) The impact of desert dust across the Mediterranean. *Environm. Sci. Technol. Libr.* 11, 25-49. *Kluwer Academic Publishers, Dordrecht.*

Dymond J., Suess E. and Lyle M. (1992) Barium in deep-sea sediment: a geochemical proxy for paleoproductivity. *Paleoceanography* 7, 163-181.

Dymond J. and Collier R. (1996) Particulate barium fluxes and their relationships to biological productivity. *Geochim. Cosmochim. Acta* 43, 1283-1308.

Elderfield H. and Ganssen G. (2000) Past temperature and ^{18}O of surface ocean waters inferred from foraminiferal Mg/Ca ratios. *Nature* 405, 442-445.

Emerson S.R. and Huested S.S. (1991) Ocean anoxia and the concentrations of molybdenum and vanadium in seawater. *Mar. Chem.* 34, 177-196.

Erba E., Parisi E. and Cita M.B. (1987) Stratigraphy and sedimentation in the western Strabo Trench, Eastern Mediterranean. *Mar. Geol.* 75, 57-75.

Fisher N.S., Cochran J.K., Krishnaswami S. and Livingstone H.D. (1988) Predicting the oceanic flux of radionuclides on sinking biogenic debris. *Nature* 335, 622-625.

Francois R., Honjo S., Manganini S.J. and Ravizza G.E. (1995) Biogenic barium fluxes to the deep sea: Implications for paleoproductivity reconstruction. *Global Biogeochem. Cycles* 9, 289-303.

Froelich P.N., Klinkhammer G.P., Bender M.L., Luedtke N.A., Heath G.R., Cullen D., Dauphin P., Hammond D., Hartman B. and Maynard V. (1979) Early oxidation of organic matter in pelagic sediments of the eastern equatorial Atlantic: suboxic diagenesis. *Geochim. Cosmochim. Acta* 43, 1075-1090.

Gard G. (1989) Variation in coccolith assemblages during the last glacial cycle in the high and mid-latitude Atlantic and Indian Oceans. *In:* Nannofossils and their applications, proceedings of the International Nannofossil Association conference, London, 1987. Br. Micropaleontol. Soc. Ser. Ellis Horwood, pp. 108-121.

Gingele F. and Dahmke A. (1994) Discrete barite particles and barium as tracers of paleoproductivity in South Atlantic sediments. *Paleoceanography* 9, 151-168.

Gingele F.X., Zabel M., Kasten S., Bonn W.J. and Nürnberg C.C. (1999) Biogenic barium as a proxy for paleoproductivity: Methods and limitations of application. *In:* Fischer G. and Wefer G. (eds) Use of proxies in paleoceanography: Examples from the South Atlantic. *Springer-Verlag Berlin Heidelberg*, 345-364.

Gordeyev V.V. and Lisitsyn A.P. (1978) The average chemical composition of suspensions in the

world's rivers and the supply of sediments to the ocean by streams. *Doklady, Earth Sci. Section* 238, 150-153.

Graham D.W., Bender M.L., Williams D.F. and Keigwin L.D. (1982) Strontium-calcium ratios in Cenozoic planktonic foraminifera. *Geochim. Cosmochim. Acta* 46, 1281-1292.

Guerzoni S., Molinaroli E. and Chester R. (1997) Saharan dust inputs to the western Mediterranean Sea: depositional patterns, geochemistry and sedimentological implications. *Deep-Sea Res. II* 44, 631-654.

Güllü G.H., Ölmez I. and Tuncel G. (1996) Chemical concentrations and elements size distributions of aerosols in the eastern Mediterranean during strong dust storms. *In:* Guerzoni S. and Chester R. (eds.) The impact of desert dust across the Mediterranean. *Environm. Sci. Technol. Libr.* 11, 339-347. *Kluwer Academic Publishers, Dordrecht.*

Gust G., Byrne R.H., Bernstein R.E., Betzer P.R. and Bowles W. (1992) Particle fluxes and moving fluids: experience from synchronous trap collections in the Sargasso Sea. *Deep-Sea Res.* 39, 1071-1083.

Haese R.R. (1997) Beschreibung und Quantifizierung frühdiagenetischer Reaktionen des Eisens in Sedimenten des SüdAtlantiks. *Berichte Fachbereich Geowissenschaften Univ. Bremen* 99, 118 pp.

Haese R.R. (2000) The reactivity of iron. *In:* Schulz H.D. and Zabel M. (eds.) Marine geochemistry. *Springer-Verlag Berlin Heidelberg*, 233-261.

Haidar A.T., Thierstein H.R. and Deuser W.G. (2000) Calcareous phytoplankton standing stocks, fluxes and accumulation in Holocene sediments off Bermuda (N. Atlantic). *Deep-Sea Res. II* 47, 1902-1938.

Hampt Andreasen G. and Delaney M.L. (2000) Bulk calcite size fraction distribution and Sr/Ca composition for deep-sea sediments at selected age horizons. *Mar. Geol.* 169, 185-205.

Hayes A., Rohling E.J., De Rijk S., Kroon D. and Zachariasse W.J. (1999) Mediterranean planktonic foraminiferal faunas during the last glacial cycle. *Mar. Geol.* 153, 239-252.

Henneke E., Luther G.W. III, De Lange G.J. and Hoefs J. (1997) Sulphur speciation in anoxic hypersaline sediments from the eastern Mediterranean Sea. *Geochim. Cosmochim. Acta* 61, 307-321.

Heussner S. and Monaco A. (1996) The MTP sediment trap experiments: highlights on particle fluxes through the eutrophic and oligotrophic systems of the Mediterranean Sea. *Second workshop of the Mediterranean Target Project, Crete 1996, Extended abstract*, 233-239.

Higgs N.C., Thomson J., Wilson T.R.S. and Croudace I.W. (1994) Modification and complete removal of eastern Mediterranean sapropels by postdepositional oxidation. *Geology* 22, 423-426.

Hilgen F.J. (1991) Astronomical calibration of Gauss to Matuyama sapropels in the Mediterranean and implication for the geomagnetic polarity time scale. *Earth Planet. Sci. Lett.* 104, 226-244.

Hilgen F.J., Krijgsman W., Langereis C.G., Lourens L.J., Santarelli A. and Zachariasse W.J. (1995) Extending the astronomical (polarity) time scale into the Miocene. *Earth Planet. Sci. Lett.* 136, 495-510.

Höll C., Karwath B., Rühlemann C., Zonneveld K.A.F. and Willems H. (1999) Palaeoenvironmental information gained from calcareous dinoflagellates: the late Quaternary eastern and western tropical Atlantic Ocean in comparison. *Palaeogeogr.*

Palaeoclimatol. Palaeoecol. 146, 147-164.

Holligan P.M., Viollier M., Harbour D.S., Camus P. and Champagne-Philippe M. (1983) Satellite and ship studies of coccolithophore production along a continental shelf edge. *Nature* 304, 339-342.

Honjo S., Manganini S.J. and Cole J.J. (1982) Sedimentation of biogenic matter in the deep ocean. *Deep-Sea Res.* 29, 609-625.

Howard J.H. (1977) Geochemistry of selenium: formation of ferroselite and selenium behaviour in the vicinity of oxidising sulfide and uranium deposits. *Geochim. Cosmochim. Acta* 41, 1665-1678.

Huerta-Diaz M.A. and Morse J.W. (1990) A quantitative method for determination of trace metal concentrations in sedimentary pyrite. *Mar. Chem.* 29, 119-144.

Huerta-Diaz M.A. and Morse J.W. (1992) Pyritization of trace metals in anoxic marine sediments. *Geochim. Cosmochim. Acta* 56, 2681-2702.

Hydes D.J., De Lange G.J. and De Baar H.J.W. (1988) Dissolved aluminium in the Mediterranean. *Geochim. Cosmochim. Acta* 52, 2107-2114.

Ingall E.D., Bustin R.M. and Van Capellen P. (1993) Influence of water column anoxia on the burial and preservation of carbon and phosphorus in marine shales. *Geochim. Cosmochim. Acta* 57, 303-316.

Jarvis I. and Higgs N. (1987) Trace-element mobility during early diagenesis in distal turbidites: late Quaternary of the Madeira Abyssal Plain, N Atlantic. *In:* Weaver P.P.E. and Thomson J. (eds) Geology and geochemistry of abyssal plains. *Geol. Soc. Spec. Publ.* 31, 179-213.

Jongsma D., Fortuin A.R., Huson W., Troelstra S.R., Klaver G.T., Peters J.M., Van Harten D., De Lange G.J. and Ten Haven L. (1983) Discovery of an anoxic basin within the Strabo Trench, eastern Mediterranean. *Nature* 305, 795-797.

Jordan R., Meixhun Z., Eglinton G. and Weaver P.P.E. (1996) Coccolith and alkenone stratigraphy and paleoceanography at an upwelling site off NW Africa (ODP 658 C) during the last 130,000 years. *In:* A. Moguivelesky and R. Whatley (eds.) Microfossil and Oceanic Environments, *University of Wales, Aberystwyth Press*, pp. 111-130.

Jorissen F.J., Asioli A., Borsetti A.M., Capotondi L., De Visser J.P., Hilgen F.J., Rohling E.J., Van der Borg K., Vergnaud-Grazzini C. and Zachariasse W.J. (1993) Late Quaternary central Mediterranean biochronology. *Mar. Micropaleontol.* 21, 169-189.

Kadko D. (1980) ^{230}Th, ^{226}Ra and ^{222}Rn in abyssal sediments. *Earth Planet. Sci. Lett.* 49, 360-380.

Kalberer M., Fischer G., Pätzold J., Donner B., Segl M. and Wefer G. (1993) Seasonal sedimentation and stable isotope records of pteropods off Cap Blanc. *Mar. Geol.* 113, 305-320.

Kallel N., Paterne M., Duplessy J.-C., Vergnaud-Grazzini C., Pujol C., Labeyrie L., Arnold M., Fontugne M. and Pierre C. (1997) Enhanced rainfall in the Mediterranean region during the last sapropel event. *Oceanol. Acta* 20, 697-712.

Karl D.M. and Knauer G.A. (1991) Microbial production and particle flux in the upper 350 m of the Black Sea. *Deep-Sea Res.* 38, suppl. 2, 5921-5942.

Khripounoff A. and Crassous P. (1994) Particulate material degradation in sediment traps at 2000 m depth on the Meriadzeck Terrace (Bay of Biscay). *Deep-Sea Res. I* 41, 821-829.

Kidd R.B., Cita M.B. and Ryan W.B.F. (1978) Stratigraphy of Eastern Mediterranean sapropel sequences recovered during DSDP Leg 42A and their paleoenvironmental significance.

In: Hsü K.J., Montadert L. et al., Initial reports of the Deep-Sea Drilling Project 42, *U.S. Govt. Printing Office, Washington D.C.*, 421-443.

Kleijne A. (1993) Morphology, taxonomy and distribution of extant coccolithophorids (calcareous nannoplankton), *PhD dissertation, Vrije Universiteit Amsterdam,* 321 pp.

Knappertsbusch M. (1993) Geographic distribution of living and Holocene coccolithophores in the Mediterranean Sea. *Mar. Micropaleontol.* 21, 219-247.

Kostka J.E. and Luther G.W. III (1994) Partitioning and speciation of solid phase iron in saltmarsh sediments. *Geochim. Cosmochim. Acta* 58, 1701-1710.

Krauskopf, K.B. (1967) Introduction to geochemistry. *McGraw-Hill, Inc., New York,* 617 pp.

Kremling K. and Petersen H. (1981) The distribution of zinc, cadmium, copper, manganese and iron in waters of the open Mediterranean Sea. *"Meteor" Forsch. Ergebn. Reihe A/B* 23, 5-14.

Krinsley D. and Bieri R. (1959) Changes in the chemical composition of pteropod shells after deposition on the sea floor. *J. Paleontol.* 33, 682-684.

Krom M.D., Brenner S., Kress N., Neori A. and Gordon L.I. (1992) Nutrient dynamics and new production in a warm-core eddy from the Eastern Mediterranean Sea. *Deep-Sea Res.* 39, 467-480.

Krom M.D., Michard A., Cliff R.A. and Strohle K. (1999) Sources of sediment to the Ionian Sea and western Levantine basin of the Eastern Mediterranean during S-1 sapropel times. *Mar. Geol.* 160, 45-61.

Kullenberg B. (1952) On the salinity of water contained in marine sediments. *Medd. Oceanogr. Inst. Goteborg* 21, 1-38.

Lal D. (1977) The oceanic microcosm of particles. *Science* 198, 997-1009.

Lea D.W., Mashiotta T.A. and Spero H.J. (1999) Controls on magnesium and strontium uptake in planktonic foraminifera determined by live culturing. *Geochim. Cosmochim. Acta* 63, 2369-2379.

Li W.K.W., Yacobi Y.Z. and Wood A.M. (1993) Ultraphytoplankton in the eastern Mediterranean Sea: Towards deriving phytoplankton biomass from flow cytometric measurements of abundance, fluorescence and light scatter. *Mar. Ecol. Prog. Ser.* 102, 79-97.

Lord C.J. III (1982) A selective and precise method for pyrite determination in sedimentary materials. *J. Sed. Petr.* 52, 664-666.

Lototoskaya A., Ziveri P., Ganssen G.M., and Van Hinte J.E. (1998) Calcareous nannoflora response to Termination II at 45˚ N, 25˚ W (northeast Atlantic). *Mar. Micropaleontol.* 34, 47-70

Lourens L.J. (1994) Astronomical forcing of Mediterranean climate during the last 5.3 million years. *Ph.D. dissertation, Utrecht Univ.*, 247 pp.

Luther G.W. III, Catalano G., De Lange G.J. and Woittiez J.R.W. (1990) Reduced sulphur in the hypersaline anoxic basins of the Mediterranean Sea. *Mar. Chem.* 31, 137-152.

Lyle M., Heath G.R. and Robbins J.M. (1984) Transport and release of transition elements during early diagenesis: Sequential leaching of sediments from MANOP Sites M and H. Part I. pH 5 acetic acid leach. *Geochim. Cosmochim. Acta* 48, 1705-1715.

Lynn D.C. and Bonatti E. (1965) Mobility of manganese in diagenesis of deep-sea sediments. *Mar. Geol.* 3, 457-474.

Martin E.E., Macdougall J.D., Herbert T.D., Paytan A. and Kastner M. (1995) Strontium and neodymium isotopic analyses of marine barite separates. *Geochim. Cosmochim. Acta* 59, 1353-1361.

Martin J.H., Coale K.H., Johnson K.S., Fitzwater S.E., Gordon R.M., Tanner S.J., Hunter C.N., Elrod V.A., Nowicki J.L., Coley T.L., Barber R.T., Lindley S., Watson A.J., Van Scoy K., Law C.S., Liddicoat M.I., Ling R., Stanton T., Stockel J., Collins C., Anderson A., Bidigare R., Ondrusek M., Latasa M., Millero F.J., Lee K., Yao W., Zhang J.Z., Friederich G., SakamotoC., Chavez F., Buck K., Kolber Z., Greene R., Falkowski P., Chisholm S.W., Hoge F., Swift R., Yungel J., Turner S., Nightingale P., Hatton A., Liss P. and Tindale N.W. (1994) Testing the iron hypothesis in ecosystems of the equatorial Pacific Ocean. *Nature* 371, 123-129.

Martin J.-M. and Meybeck M. (1979) Elemental mass-balance of material carried by major world rivers. *Mar. Chem.* 7, 173-206.

Masscheleyn P.H., Delaune R.D. and Patrick W.H. (1990) Transformations of selenium as affected by sediment oxidation-reduction potential and pH. *Environ. Sci. Technol.* 24, 91-96.

Matrai P.A. and Keller M.D. (1993) Dimethylsulfide in a large-scale coccolithophore bloom in the Gulf of Maine. *Continent. Shelf Res.* 13, 831-843.

McCorkle D.C., Martin P.A., Lea D.W. and Klinkhammer G.P. (1995) Evidence of a dissolution effect on benthic foraminiferal shell chemistry: $\delta^{13}C$, Cd/Ca, and Sr/Ca results from the Ontong Java Plateau. *Paleoceanography* 10, 699-714.

McIntyre A., Bé A.W.H. and Roche M.B. (1970) Modern Pacific Coccolithophorida: A paleontological thermometer. *Trans. New York Acad. Sci.* 32, 720-731.

McManus J., Berelson W.M., Klinkhammer G.P., Kilgore T.E. and Hammond D.E. (1994) Remobilization of barium in continental margin sediments. *Geochim. Cosmochim. Acta* 58, 4899-4907.

McManus J., Berelson W.M., Klinkhammer G.P., Johnson K.S., Coale K.H., Anderson R.F., Kumar N., Burdige D.J., Hammond D.E., Brumsack H.J., McCorkle D.C. and Rushdi A. (1998) Geochemistry of barium in marine sediments: Implications for its use as a paleoproxy. *Geochim. Cosmochim. Acta* 62, 3453-3473.

MEDRIFF Consortium (1995) Three brine lakes discovered in the seafloor of the Eastern Mediterranean. *Eos Trans.* 76, 313+318.

Mercone D., Thomson J., Croudace I.W., Siani G., Paterne M. and Troelstra S. (2000) Duration of S1, the most recent sapropel in the eastern Mediterranean Sea, as indicated by accelerator mass spectrometry radiocarbon and geochemical evidence. *Paleoceanography* 15, 336-347.

Middelburg J.J., De Lange G.J. and Van der Weijden C.H. (1987) Manganese solubility control in marine pore waters. *Geochim. Cosmochim. Acta* 51, 759-763.

Milliman J.D. and Muller J. (1973) Precipitation and lithification of magnesian calcite in the deep-sea sediments of the eastern Mediterranean sea. *Sedimentology* 20, 29-45.

Milliman J.D. (1974) Marine carbonates. *Springer-Verlag, Berlin,* 375 pp.

Milliman J.D. (1993) Production and accumulation of calcium carbonate in the ocean: budget of a nonsteady state. *Global Biogeochem. Cycles* 7, 927-957.

Miquel J.C., Fowler S.W., La-Rosa J. and Buat-Ménard P. (1994) Dynamics of the downward

flux of particles and carbon in the open northwestern Mediterranean Sea. *Deep-Sea Res. I* 41, 243-261.

Molfino B. and McIntyre A. (1990) Precessional Forcing of Nutricline Dynamics in the Equatorial Atlantic. *Science* 249, 766-769.

Molinaroli E., Guerzoni S. and Rampazzo G. (1993) Contribution of Saharan dust to the Central Mediterranean Basin. Geol. *Soc. Amer. Spec. Pap.* 284, 303-312.

Monnin C., Jeandel C., Cattaldo T. and Dehairs F. (1999) The marine barite saturation state of the world's oceans. *Mar. Chem.* 65, 253-261.

Moore W.S. and Dymond J. (1988) Correlation of ^{210}Pb removal with organic carbon fluxes in the Pacific Ocean. *Nature* 331, 339-341.

Moulin C., Lambert C.E., Dulac F. and Dayan U. (1997) Control of atmospheric export of dust from North Africa by the North Atlantic Oscillation. *Nature* 387, 691-694.

Müller P.J. and Schneider R. (1993) An automated leaching method for the determination of opal in sediments and particulate matter. *Deep-Sea Res. I* 40, 425-444.

Murray R.W. and Leinen M. (1996) Scavenged excess aluminum and its relationship to bulk titanium in biogenic sediments from the central equatorial Pacific Ocean. *Geochim. Cosmochim. Acta* 60, 3869-3878

Negri A., Capotondi L. and Keller J. (1999) Calcareous nannofossils, planktonic foraminifera and oxygen isotopes in the late Quaternary sapropels of the Ionian Sea. *Mar. Geol.* 157, 89-103.

Neuer S., Ratmeyer V., Davenport R., Fischer G. and Wefer G. (1997) Deep water particle flux in the Canary Island region: seasonal trends in relation to long-term satellite derived pigment data and lateral sources. *Deep-Sea Res. I* 44, 1451-1466.

Nijenhuis I.A., Schenau S.J., Van der Weijden C.H., Hilgen F.J., Lourens L.J. and Zachariasse W.J. (1996) On the origin of upper Miocene sapropelites: A case study from the Faneromeni section, Crete (Greece). *Paleoceanography* 11, 633-645.

Nijenhuis I.A., Bosch H.-J., Sinnighe Damsté J.S., Brumsack H.-J. and De Lange G.J. (1999) Organic matter and trace element rich sapropels and black shales: a geochemical comparison. *Earth Planet. Sci. Lett.* 169, 277-290.

Nijenhuis I.A. and De Lange G.J. (2000) Geochemical constraints on Pliocene sapropel formation in the eastern Mediterranean. *Mar. Geol.* 163, 41-63.

Nolet G.J. and Corliss B.H. (1990) Benthic foraminiferal evidence for reduced deep-water circulation during sapropel deposition in the eastern Mediterranean. *Mar. Geol.* 94, 109-130.

Nürnberg D. (1995) Magnesium in tests of *Neogloboquadrina pachyderma* sinistral from high northern and southern latitudes. *J. Foraminif. Res.* 25, 350-368.

Nürnberg D., Bijma J. and Hemleben C. (1996) Assessing the reliability of magnesium in foraminiferal calcite as a proxy for water mass temperatures. *Geochim. Cosmochim. Acta* 60, 803-814.

Okada H. and Honjo S. (1973) The distribution of oceanic coccolithophorids in the Pacific. *Deep-Sea Res.* 20, 355-374.

Okada H. and McIntyre A. (1979) Seasonal distribution of modern coccolithophores in the Western North Atlantic Ocean. *Mar. Biol.* 54, 319-328.

Olausson E. (1961) Studies of deep-sea cores. *Rep. Swed. Deep-Sea Exped. 1947-1948* 8 (6),

336-391.

Parisi E., Erba E. and Cita M.B. (1987) Stratigraphy and sedimentation in the anoxic Bannock Basin (Eastern Mediterranean). *Mar. Geol.* 75, 93-117.

Passier H.F., Middelburg J.J., Van Os B.J.H. and De Lange G.J. (1996) Diagenetic pyritisation under eastern Mediterranean sapropels caused by downward sulphide diffusion. *Geochim. Cosmochim. Acta* 60, 751-763.

Passier H.F., Middelburg J.J., De Lange G.J. and Böttcher M.E. (1997) Pyrite contents, microtextures, and sulfur isotopes in relation to formation of the youngest eastern Mediterranean sapropel. *Geology* 25, 519-522.

Passier H.F. and De Lange G.J. (1998) Sedimentary sulfur and iron chemistry in relation to the formation of eastern Mediterranean sapropels. *In:* Robertson A.H.F, Emeis K.-C., Richter C. and Camerlenghi A. (Eds.) *Proc. ODP, Sci. Results*, 160: College Station, TX (Ocean Drilling Program), 249-259.

Paytan A., Kastner M., Martin E.E., Macdougall J.D. and Herbert T. (1993) Marine barite as a monitor of seawater strontium isotope composition. *Nature* 366, 445-449.

Paytan A., Moore W.S. and Kastner M. (1996) Sedimentation rate as determined by ^{226}Ra activity in marine barite. *Geochim. Cosmochim. Acta* 60, 4313-4319.

Paytan A., Kastner M., Campbell D. and Thiemens M.H. (1998) Sulfur isotopic composition of Cenozoic seawater sulfate. *Science* 282, 1459-1462.

Peterson M.L., Hernes P.J., Thoreson D.S., Hedges J.I., Lee C. and Wakeham S.G. (1993) Field evaluation of a valved sediment trap. *Limnol. Oceanogr.* 38, 1741-1761.

Pruysers P.A., De Lange G.J. and Middelburg J.J. (1991) Geochemistry of eastern Mediterranean sediments: Primary sediment composition and diagenetic alteration. *Mar. Geol.* 100, 137-154.

Pruysers P.A., De Lange G.J., Middelburg J.J. and Hydes D.J. (1993) The diagenetic formation of metal-rich layers in sapropel-containing sediments in the eastern Mediterranean. *Geochim. Cosmochim. Acta* 57, 527-536.

Puechmaille C. (1994) Mg, Sr and Na fluctuations in the test of modern and recent *Globigerina bulloides*. *Chem. Geol.* 116, 147-152.

Quétel C.R., Remoudaki E., Davies J.E., Miquel J.-C., Fowler S.W., Lambert C.E., Bergametti G. and Buat-Ménard P. (1993) Impact of atmospheric deposition on particulate iron flux and distribution in northwestern Mediterranean waters. *Deep-Sea Res. I* 40, 989-1002.

Ramaswamy V., Nair R.R., Manganini S., Haake B. and Ittekkot V. (1991) Lithogenic fluxes to the deep Arabian Sea measured by sediment traps. *Deep-Sea Res.* 38, 169-184.

Rasmussen T.L. (1991) Benthonic and planktonic foraminifera in relation to the Early Holocene stagnation in the Ionian Basin, Central Mediterranean. *Boreas* 20, 357-376.

Reichart G.J., Den Dulk M., Visser H.J., Van der Weijden C.H. and Zachariasse W.J. (1997) A 225 kyr record of dust supply, paleoproductivity and the oxygen minimum zone from the Murray Ridge (northern Arabian Sea). *Palaeogeogr., Palaeoclimat., Palaeoecol.* 134, 149-169.

Riegman R., Stolte W. and Noordeloos A.A.M. (1998) A model system approach to biological forcing: the example of *Emiliania huxleyi*. Final Report Subproject (b): Physiology. NIOZ-Rapport 1998-8, Netherlands Institute for Sea Research, 32 pp.

Rimoldi B., Alexander J. and Morris S. (1996) Experimental turbidity currents entering

density-stratified water: analogues for turbidites in Mediterranean hypersaline basins. *Sedimentology* 43, 527-540.

Robarts R.D., Waiser M.J. and Yacobi Y.Z. (1996) Bacterial abundance, biomass, and production in relation to phytoplankton biomass in the Levantine Basin of the Southeastern Mediterranean Sea. *Mar. Ecol. Prog. Ser.* 137, 273-281.

Rohling E.J. and Gieskes W.W.C. (1989) Late Quaternary changes in Mediterranean Intermediate Water density and formation rate. *Paleoceanography* 4, 531-545.

Rohling E.J., Jorissen F.J., Vergnaud Grazzini C. and Zachariasse W.J. (1993) Northern Levantine and Adriatic Quaternary planktic foraminifera; Reconstruction of paleoenvironmental gradients. *Mar. Micropaleontol.* 21, 191-218.

Rohling E.J. (1994) Review and new aspects concerning the formation of eastern Mediterranean sapropels. *Mar. Geol.* 122, 1-28.

Rohling E.J., Jorissen F.J. and De Stigter H.C. (1997) 200 years interruption of Holocene sapropel formation in the Adriatic Sea. *J. Micropaleontol.*, 16, 97-108.

Rosenthal Y. and Boyle E.A. (1993) Factors controlling the fluoride content of planktonic foraminifera: An evaluation of its paleoceanographic applicability. *Geochim. Cosmochim. Acta* 57, 335-346.

Rosenthal Y., Boyle E.A. and Slowey N. (1997) Temperature control on the incorporation of magnesium, strontium, fluorine, and cadmium into benthic foraminiferal shells from Little Bahama Bank: Prospects for thermocline paleoceanography. *Geochim. Cosmochim. Acta* 61, 3633-3643.

Rossignol-Strick M., Nesteroff W., Olive P. and Vergnaud-Grazzini C. (1982) After the deluge: Mediterranean stagnation and sapropel formation. *Nature* 295, 105-110.

Rossignol-Strick M. (1983) African monsoons, an immediate climate response to orbital forcing. *Nature* 304, 46-49.

Rossignol-Strick M. (1985) Mediterranean Quaternary sapropels, an immediate response of the African monsoon to variation of insolation. *Palaeogeogr. Palaeoclimatol. Palaeoecol.* 49, 237-263.

Rossignol-Strick M., Paterne M., Bassinot F.C., Emeis K.-C. and De Lange G.J. (1998) An unusual mid-Pleistocene monsoon period over Africa and Asia. *Nature* 392, 269-272.

Roth P.H. and Berger W.H. (1975) Distribution and dissolution of coccoliths in the South and central Pacific. Cushman Found. *Foraminif. Res.* 13, 87-113.

Ruttenberg K.C. (1992) Development of a sequential extraction method for different forms of phosphorus in marine sediments. *Limnol. Oceanogr.* 37, 1460-1482.

Savin S.M. and Douglas R.G. (1973) Stable isotope and magnesium geochemistry of recent planktonic foraminifera from the South Pacific. *Geol. Soc. Amer. Bull.* 84, 2327-2342.

Schenau S.J. (1999) Cycling of phosphorus and manganese in the Arabian Sea during the Late Quaternary. *Geol. Ultraiect.* 182, 183 pp.

Schenau S.J., Antonarakou A., Hilgen F.J., Lourens L.J., Nijenhuis I.A., Van der Weijden C.H. and Zachariasse W.J. (1999) Organic-rich layers in the Metochia section (Gavdos, Greece): evidence for a single mechanism of sapropel formation during the past 10 My. *Mar. Geol.* 153, 117-135.

Schmiedl G., Hemleben C., Keller J. and Segl M. (1998) Impact of climatic changes on the benthic foraminiferal fauna in the Ionian Sea during the last 330,000 years.

Paleoceanography 13, 447-458.

Schmitz B. (1987) The TiO_2/Al_2O_3 ratio in the Cenozoic Bengal abyssal fan sediments and its use as a paleostream energy indicator. *Mar. Geol.* 76, 195-206.

Schneidermann N. (1977) Selective dissolution of recent coccoliths in the Atlantic Ocean. *In:* Ramsay A.T.S. (ed.) *Oceanic micropaleontology, v.2,* Acad. Press, London, 1009-1053.

Scientific Staff of Cruise *Bannock* 1984-12 (1985) Gypsum precipitation from cold brines in an anoxic basin in the eastern Mediterranean. *Nature* 314, 152-154.

Shimmield G.B. (1992) Can sediment geochemistry record changes in coastal upwelling palaeoproductivity? Evidence from northwest Africa and the Arabian Sea. *In:* Prell C.P. and Emeis K.C. (eds) Upwelling systems: Evolution since the early Miocene. *Geol. Soc. Spec. Publ.* 64, 29-46.

Sigl W., Chamley H., Fabricius F., Giroud d'Argoud G. and Müller J. (1978) Sedimentology and environmental conditions of sapropels. *In:* Hsü K.J., Montadert L. et al., Initial reports of the Deep-Sea Drilling Project 42, *U.S. Govt. Printing Office, Washington D.C.*, 445-465.

Slomp C.P., Van der Gaast S.J. and Van Raaphorst W. (1996) Phosphorus binding by poorly crystalline iron oxides in North Sea sediments. *Mar. Geol.* 52, 55-73.

Sprengel C., Baumann K.-H. and Neuer S. (2000) Seasonal and interannual variations of coccolithophore fluxes and species composition in sediment traps north of Gran Canaria (29°N 15°W). *Mar. Micropaleontol.* 39, 157-178.

Sprovieri R., Thunell R. and Howell M. (1986) Paleontological and geochemical analyses of three laminated sedimentary units of late Pliocene-Early Pleistocene age from the Monte San Nicola section in Sicily. *Riv. Ital. Paleontol. Stratigr.* 102, 77-104.

Steinmetz J.C. (1991) Calcareous nannoplankton biocoenosis: Sediment trap studies in the Equatorial Atlantic, Central Pacific, and Panama Basin. *Ocean Biocoenosis Series No. 1,* Woods Hole Oceanographic Institution, 85 pp.

Stuiver M., Pearson G.W. and Braziunas T. (1986) Radiocarbon age calibration of marine samples back to 9000 cal yr BP. *Radiocarbon* 28, 980-1021.

Stumm W. and Morgan J.J. (1996) Aquatic chemistry. *John Wiley and Sons Inc., New York,* 1022 pp.

Sutherland H.E., Calvert S.E. and Morris R.J. (1984) Geochemical studies of the recent sapropel and associated sediment from the Hellenic Outer Ridge, eastern Mediterranean Sea. I: Mineralogy and chemical composition. *Mar. Geol.* 56, 79-92.

Taylor S.R. (1964) Abundance of chemical elements in the continental crust: a new table. *Geochim. Cosmochim. Acta* 28, 1273-1285.

Taylor S.R. and McLennan S.M. (1985) The continental crust: its composition and evolution. *Blackwell Scientific Publications, Oxford,* 312 pp.

Ten Haven H.L., De Lange G.J. and McDuff R.E. (1987) Interstitial water studies of Late Quaternary Eastern Mediterranean sediments with emphasis on early diagenetic reactions and evaporitic salt influences. *Mar. Geol.* 75, 119-136.

Tennant D.A. and Baker E.T. (1992) A fast, high-precision splitter for particle suspensions. *Mar. Geol.* 108, 247-252.

Thomson J., Wilson T.R.S., Culkin F. and Hydes D.J. (1984) Non-steady state diagenetic record in eastern equatorial Atlantic sediments. *Earth Planet. Sci. Lett.* 71, 23-30.

Thomson J., Colley S., Higgs N.C., Hydes D.J., Wilson T.R.S. and Sørensen J. (1987)

Geochemical oxidation fronts in NE Atlantic distal turbidites and their effects in the sedimentary record. *In:* Weaver P.P.E. and Thomson J. (eds) Geology and geochemistry of abyssal plains. *Geol. Soc. Spec. Publ.* 31, 167-177.

Thomson J., Higgs N.C., Wilson T.R.S., Croudace I.W., De Lange G.J. and Van Santvoort P.J.M. (1995) Redistribution and geochemical behaviour of redox-sensitive elements around S1, the most recent eastern Mediterranean sapropel. *Geochim. Cosmochim. Acta* 59, 3487-3501.

Thomson J., Mercone D., De Lange G.J. and Van Santvoort P.J.M. (1999) Review of recent advances in the interpretation of eastern Mediterranean sapropel S1 from geochemical evidence. *Mar. Geol.* 153, 77-89.

Thunell R.C., Williams D.F. and Kennett J.P. (1977) Late Quaternary paleoclimatology, stratigraphy and sapropel history in Eastern Mediterranean deep-sea sediments. *Mar. Micropaleontol.* 2, 371-388.

Thunell R.C., Varela R., Llano M., Collister J., Muller-Karger F. and Bohrer R. (2000) Organic carbon fluxes, degradation, and accumulation in an anoxic basin: Sediment trap results from the Cariaco Basin. *Limnol. Oceanogr.* 45, 300-308.

Tribovillard N.-P., Caulet J.-P., Vergnaud-Grazzini C., Moureau N. and Tremblay P. (1996) Lack of organic matter accumulation on the upwelling-induced Somalia margin in a glacial-interglacial transition. *Mar. Geol.* 133, 157-182.

Troelstra S.R. (1987) Late Quaternary sedimentation in Tyro and Kretheus Basins, southeast of Crete. *Mar. Geol.* 75, 77-91.

Troelstra S.R., Ganssen G.M., Van der Borg K. and De Jong A.F.M. (1991) A late quaternary stratigraphic framework for eastern Mediterranean sapropel S1 based on AMS ^{14}C dates and stable oxygen isotopes. *Radiocarbon* 33, 15-21.

Turekian K.K. and Wedepohl K.H. (1961) Distribution of the elements in some major units of the earth's crust. *Geol. Soc. Amer. Bull.* 72, 175-192.

Turley C.M. (1997) The changing Mediterranean Sea - A sensitive ecosystem? *Abstr. Vol., Int. Conference "Progress in oceanography of the Mediterranean Sea", Rome, Nov. 17-19, 1997.* pp. 65-66.

Van der Weijden C.H. (1993) Geochemical signatures preserved in sediments of Semaforo and Vrica sections (Calabria, Italy) and their relations with variations of the sedimentary regime. *Palaeogeogr., Palaeoclimat., Palaeoecol.* 103, 203-221.

Van der Weijden C.H., Middelburg J.J., De Lange G.J., Van der Sloot H.A., Hoede D. and Woittiez J.R.W. (1990) Profiles of the redox-sensitive trace elements As, Sb, V, Mo and U in the Tyro and Bannock Basins (eastern Mediterranean). *Mar. Chem.* 31, 171-186.

Van der Weijden C.H., Reichart G.J. and Visser H.J. (1999) Enhanced preservation of organic matter in sediments deposited within the oxygen minimum zone in the northeastern Arabian Sea. *Deep-Sea Res. I* 46, 807-830.

Van Os B.J.H., Middelburg J.J. and De Lange G.J. (1991) Possible diagenetic mobilization of barium in sapropelic sediment from the eastern Mediterranean. *Mar. Geol.* 100, 125-136.

Van Os B.J.H., Lourens L.J., Hilgen F.J., De Lange G.J. and Beaufort L. (1994) The formation of Pliocene sapropels and carbonate cycles in the Mediterranean: Diagenesis, dilution, and productivity. *Paleoceanography* 9, 601-617.

Van Santvoort P.J.M. and De Lange G.J. (1996) Messinian salt fluxes into the present-day

Eastern Mediterranean: implications for budget calculations and stagnations. *Mar. Geol.* 132, 241-251.

Van Santvoort P.J.M., De Lange G.J., Thomson J., Cussen H., Wilson T.R.S., Krom M.D. and Ströhle K. (1996) Active post-depositional oxidation of the most recent sapropel (S1) in sediments of the eastern Mediterranean Sea. *Geochim. Cosmochim. Acta* 60, 4007-4024.

Van Santvoort P.J.M., De Lange G.J., Langereis C.G., Dekkers M.J. and Paterne M. (1997) Geochemical and paleomagnetic evidence for the occurrence of "missing" sapropels in eastern Mediterranean sediments. *Paleoceanography* 12, 773-786.

Van der Borg K., Alderliesten C., De Jong A.F.M., Van den Brink A., De Haas A.P., Kersemaekers H.J.H. and Raaymakers J.E.M.J. (1997) Precision and mass fractionation in ^{14}C analysis with AMS. *Nucl. Instr. Meth. Phys. Res. B* 123, 97-101.

Vismara-Schilling A. and Coulbourn W.T. (1991) Benthic foraminiferal thanatofacies associated with Late Pleistocene to Holocene anoxic events in the eastern Mediterranean Sea. *J. Foraminif. Res.* 21, 103-125.

Von Breymann M.T., Suess E. and Lyle M.W. (1990) Depth dependent enrichment of barium and copper in the Peru margin and Nazca Plate sediments; utility as productivity proxies. *Eos Transactions* 71, 116-117.

Von Breymann M.T., Emeis K.-C. and Suess E. (1992) Water depth and diagenetic constraints on the use of barium as a palaeoproductivity indicator. *In:* Summerhayes C.P., Prell W.L. and Emeis K.-C. (eds) Upwelling systems: Evolution since the early Miocene. *Geol. Soc. Spec. Publ.* 64, 273-284.

Wedepohl K.H. (1995) The composition of the continental crust. *Geochim. Cosmochim. Acta* 59, 1217-1232.

Wefer G. and Fischer G. (1993) Seasonal patterns of vertical particle flux in equatorial and coastal upwelling areas of the eastern Atlantic. *Deep-Sea Res. I* 40, 1613-1645.

Wehrli N. and Stumm W. (1989) Vanadyl in natural waters: Adsorption and hydrolysis promote oxygenation. *Geochim. Cosmochim. Acta* 53, 69-77.

Westbroek P., Brown C.W., Van Bleijswijk J., Brownlee C., Brummer G.J., Conte M., Egge J., Fernández E., Jordan R., Knappertsbusch M., Stefels J., Veldhuis M., Van der Wal P. and Young J. (1993) A model system approach to biological climate forcing: the example of *Emiliania huxleyi*. *Global Planet. Change* 8, 27-46.

Wilson T.R.S., Thomson J., Colley S., Hydes D.J. and Higgs N.C. (1985) Early organic diagenesis: The significance of progressive subsurface oxidation fronts in pelagic sediments. *Geochim. Cosmochim. Acta* 49, 811-822.

Wilson T.R.S., Thomson J., Hydes D.J., Colley S., Culkin F. and Sørensen J. (1986) Oxidation fronts in pelagic sediments: diagenetic formation of metal-rich layers. *Science* 232, 972-975.

Winland H.D. (1969) Stability of calcium carbonate polymorphs in warm, shallow seawater. *J. Sediment. Petrol.* 39, 1579-1587.

Yacobi Y. Z., Zohary T., Kress N., Hecht A., Robarts R.D., Waiser M., Wood A.M. and Li W.K.W. (1995) Chlorophyll distribution throughout the southeastern Mediterranean in relation to the physical structure of the water mass. *J. Mar. Syst.* 6, 179-189.

Ziveri P., Grandi C. and Stefanetti A. (1995) Biogenic fluxes in Bannock Basin: first results from a sediment trap study (November 1991 - May 1992). *Rend. Fis. Acc. Lincei* s. 9 v. 6,

131-145.

Ziveri P., De Lange G.J., Rossignol-Strick M., Schrader H. and Thomson J. (1996) Biogechemical Cycles in the eastern Mediterranean; Actuo (seasonal/annual) variations. 2nd Workshop of Mediterranean Target Project, 217-221.

Ziveri P. and Thunell R.C. (2000) Coccolithophore export production in Guaymas Basin, Gulf of California: response to climate forcing. *Deep-Sea Res. II* 47, 2073-2100.

Ziveri P., Erba. E. Grandi C. Stefanetti A. and Cita M. (in prep.) Biogenic fluxes in the central eastern Mediterranean Basin from a sediment trap investigation.

Zohary T. and Robarts R.D. (1998) Experimental study of microbial P limitation in the eastern Mediterranean. *Limnol. Oceanogr.* 43, 387-395.

Zonneveld K.A.F., Höll C., Janofske D., Karwath B., Kerntopf B., Rühlemann C. and Willems H. (1999) Calcareous dinoflagellate cysts as palaeo-environmental tools. *In:* Fischer G. and Wefer G. (eds.) Use of proxies in paleoceanography: Examples from the South Atlantic. *Springer-Verlag, Berlin Heidelberg*, pp. 145-164.

Inleiding en samenvatting

1.1 Het onderzoeksgebied

De Middellandse Zee is een groot bekken dat vrijwel geheel omgeven is door landmassa's. De Middellandse Zee ligt geklemd tussen het Afrikaanse continent, dat zich ten zuiden bevindt, en Eurazië in het noorden. De enige verbinding met de oceaan is via de ondiepe Straat van Gibraltar. De Middellandse Zee zelf wordt over het algemeen verdeeld in twee delen, een westelijk en een oostelijk (Figuur 1.1), die van elkaar gescheiden zijn door de drempel (verhoging van de zeebodem) in de Straat van Sicilië. Tegenwoordig is de hoeveelheid water dat verdampt groter dan dat via neerslag aangevuld wordt. Dit resulteert in een anti-estuariene circulatie; voedselarm oppervlaktewater van de Atlantische Oceaan stroomt de Middellandse Zee in, terwijl voedselrijk water van gemiddelde diepte (tussen oppervlaktewater en diepzeewater in) de Middellandse Zee uitstroomt. Door deze uitvoer van voedingsstoffen kan de huidige Middellandse Zee beschouwd worden als een voedselwoestijn. De totale productie van organisch materiaal is erg laag in vergelijking met de wereldoceaan, en 85% van de primaire productie in de oostelijke Middellandse Zee vloeit naar de microbiële voedselketen (Turley, 1997). De populaties van fytoplankton worden gedomineerd door picoplankton, en de bacteriële biomassa is ongeveer 50% van de totale biomassa (Robarts et al., 1996). Tegenwoordig bevatten sedimenten in de oostelijke Middellandse Zee vooral een terrigene fractie en een carbonaatfractie, terwijl de gehalten aan organisch materiaal en biogeen opaal erg laag zijn.

1.2 Vorming van sapropelen

De Zweedse Diepzee-expeditie in 1948 bracht de wereld het eerste bewijs voor het bestaan van intervallen met organisch-rijk sediment in de oostelijke Middellandse Zee (Kullenberg, 1952). In de daarop volgende jaren is vastgesteld dat deze organisch-rijke sedimenten op een zeer regelmatige manier voorkomen in grotendeels organisch-arme intervallen. De organisch-rijke sedimenten zijn zowel in sedimentkernen van de bodem van de oostelijke Middellandse Zee gevonden (b.v. Cita et al., 1977; Kidd et al., 1978; Calvert et al., 1983; Pruysers et al., 1991; Van Santvoort et al., 1997; Nijenhuis et al., 1999) als in ontsluitingen op land van zeer snel omhooggekomen zeebodem (b.v. Sprovieri et al., 1986; De Visser et al., 1989; Van der Weijden et al., 1993; Van Os et al., 1994; Nijenhuis et al., 1996; Schenau et al., 1999). Deze organisch-rijke sedimentlagen, die in ieder geval voorkomen sinds het Mioceen (de geologische periode van 23,7 tot 5,3 miljoen jaar geleden), worden sapropelen genoemd. Kidd et al. (1978) stelde de volgende definitie voor sapropelen voor: "duidelijk gescheiden lagen, meer dan 1 cm dik, die zich bevinden in open-marien sediment en meer dan 2% organisch koolstof bevatten". Deze definitie is echter nogal beperkend, hetgeen Van Santvoort et al. (1996) noopte tot de volgende verfijning: "duidelijk onderscheiden sedimentlagen met een gehalte aan organisch koolstof dat significant hoger is dan dat van het omliggende hemipelagische sediment, en die afgezet zijn in een open-mariene

omgeving". Het regelmatige voorkomen van sapropelen in de sedimenten van de oostelijke Middellandse Zee is in verband gebracht met variaties in de excentriciteit van de baan van de Aarde en met variaties in de helling (obliquiteit) en de precessie van de aardas (b.v. Rossignol-Strick, 1983, 1985; Hilgen, 1991; Lourens, 1994; Hilgen et al., 1995). De vorming van sapropelen wordt vooral bepaald door de precessie, welke een cyclus van ongeveer 23000 jaar heeft. Afzetting van sapropelen gebeurt wanneer de hoeveelheid zonnestraling op het noordelijk halfrond maximaal is doordat de precessie van de aardas het minimum heeft bereikt.

Er is steeds meer bewijs dat sapropelen worden gevormd gedurende perioden met een vochtig klimaat ten tijde van het precessieminimum (Rossignol-Strick et al., 1982; Rossignol-Strick, 1985; Kallel et al., 1997). Deze omstandigheden zorgden voor een verhoogde toevoer van rivierwater en voedingsstoffen naar het Middellandse-Zeebekken. Er wordt echter nog steeds gediscussieerd over de oorzaak van het hoge gehalte aan organisch materiaal in sapropelen. De verhoogde toevoer van zoet water kan hebben gezorgd voor de ontwikkeling van oppervlaktewater met een laag zoutgehalte (saliniteit), waardoor de circulatie van het diepe water werd verminderd. Zo'n stagnerende waterkolom zou hebben geleid tot zuurstofarm (suboxisch) of zuurstofloos (anoxisch) bodemwater, waardoor een betere preservatie van organisch materiaal bevorderd werd (Olausson, 1961; Cita et al., 1977; Nolet en Corliss, 1990). Er is ook gesuggereerd dat een stijging van de mariene productiviteit de oorzaak was van sapropelvorming, in elk geval veel meer dan verhoogde preservatie van organisch materiaal (Calvert et al., 1983; Calvert et al., 1992). Rohling en Gieskes (1989) voegden beide scenario's samen en opperden dat zich een duidelijk "Diep Chlorofyl Maximum" kan hebben ontwikkeld in de eufotische zone (de zone van het oppervlaktewater waarin het zonlicht binnendringt), waardoor de primaire productiviteit gestimuleerd werd.

1.3 Pekelbekkens

In 1983 werd in de oostelijke Middellandse Zee, tijdens de expeditie van het onderzoeksschip *Tyro*, op een diepte van ~ 3400 meter een bekken ontdekt gevuld met pekel (zeewater verzadigd aan zout) (De Lange en Ten Haven, 1983; Jongsma et al., 1983). Iets later werd westelijker, op een diepte van ~ 3500 meter, een dergelijk bekken ontdekt door het onderzoeksschip *Bannock* (Wetenschappelijke Staf van Cruise Bannock 1984-2, 1985). Deze zogenaamde pekelbekkens, genoemd naar het schip dat ze ontdekte (respectievelijk Tyrobekken en Bannockbekken) zijn zuurstofloos doordat de hoge dichtheid van de pekel in deze bekkens vermenging met het zuurstofrijke gewone Middellands-Zeewater voorkómt. In de buurt van het Tyrobekken zijn ook nog twee sub-bekkens, het Kretheusbekken en het Poseidonbekken, ontdekt. Deze twee bekkens waren vroeger met pekel gevuld, maar nu niet meer. In het midden van de jaren negentig zijn in de nabijheid van het Bannockbekken nog drie pekelbekkens gevonden: het Urania-, het Atalante- en het Discoverybekken (MEDRIFF Consortium, 1995).

Deze pekelbekkens bieden een unieke mogelijkheid om sedimentatie te vergelijken die — in dezelfde tijdsperiode — onder zuurstofrijke en zuurstofarme omstandigheden

plaatsvond. Het voorkomen van perfect gepreserveerde radiolariën en van sulfaatreductie in de zuurstofloze sedimenten die werden afgezet in de pekel, en het ontbreken ervan in zuurstofrijk pelagisch sediment dat in de oostelijke Middellandse Zee in dezelfde tijdsperiode is afgezet, suggereert dat — onder aanname van gelijksoortige aanvoer van deze twee typen sediment — biogeen silica (opaal) en reactief organisch materiaal beter worden gepreserveerd in de pekelbekkens (Björklund en De Ruiter, 1987; Troelstra, 1987; Aghib, 1998; Henneke et al., 1997).

1.4 Diagenese van sapropel S1

Na afzetting ondergaan sapropelen significante chemische veranderingen (diagenese). Men heeft gevonden dat de profielen van organisch materiaal in Holocene sedimenten sterk variëren in de oostelijke Middellandse Zee, maar dat de distributie van verschillende metalen juist op elkaar lijkt (b.v. Pruysers et al., 1991, 1993; Higgs et al., 1994; Thomson et al., 1995, 1999; Van Santvoort et al., 1996; zie Figuur 1.2). Deze specifieke eigenschap kan ook worden teruggevonden in organisch-rijke turbidieten op de Abyssale Vlakte van Madeira (De Lange et al., 1989). Deze turbidieten hebben blootgestaan aan diagenese door een zich omlaag bewegend oxidatiefront (b.v. Colley et al., 1984; Thomson et al., 1984, 1987; Wilson et al., 1985, 1986; Jarvis en Higgs, 1987). Dit heeft geleid tot de hypothese dat sapropelen, die altijd ingeschakeld zitten tussen organisch-arm sediment, onderhevig zijn geweest aan een soortgelijk oxidatieproces. Hierdoor zijn significante hoeveelheden van organisch materiaal en andere gereduceerde fasen zoals pyriet verwijderd uit het bovenste gedeelte van de sapropel, en zijn diverse metalen geredistribueerd in het sediment.

De meeste onderzoeken hebben zich gespitst op de jongste sapropel (S1), die in het Holoceen (de geologische periode die de laatste 10000 jaar aangeeft) is afgezet. Deze sapropel bevat het meest verse geochemische bewijs voor de diagenese van sapropelen, terwijl ook de ouderdom ervan kan worden bepaald met behulp van radioactief koolstof (^{14}C) (b.v. Thomson et al., 1995, 1999). De “inbranding” van deze sapropel heeft gezorgd voor gedeeltelijke of zelfs complete verwijdering van het hoge gehalte aan organisch materiaal, waardoor er moeilijkheden ontstonden met de precieze datering van het einde van de afzetting van de sapropel. De periode waarbinnen sapropel S1 is afgezet, is nu vastgesteld op ~ 9000–5000 jaar geleden (Troelstra et al., 1992; Thomson et al., 1995, 1999; Mercone et al., 2000), waarbij het einde van de afzetting wordt gemarkeerd door het niveau van de bovenste verrijking van het sediment aan mangaan (Figuur 1.2).

1.5 Dit proefschrift

In dit proefschrift worden recente sedimentfluxen (d.w.z. de sedimentdeeltjes die vanuit het oppervlaktewater zinken richting de zeebodem) in de pelagische oostelijke Middellandse Zee bestudeerd. Ook wordt de geochemie onderzocht van Holocene sedimenten, inclusief sapropel S1, die zijn afgezet in zowel een normaal milieu als in een voormalig pekelbekken in de oostelijke Middellandse Zee. Figuur 1.1 toont de locaties van

de sedimentval (recente fluxen) en de bestudeerde sedimentkernen (Holocene sedimenten).

Hoofdstukken 2 en 3 gaan over recente sedimentfluxen in de oostelijke Middellandse Zee. Deze zijn gemeten met behulp van een sedimentval in de periode van november 1991 tot augustus 1994 op een waterdiepte van 3000 meter. In hoofdstuk 2 worden vooral de fluxen van de totale massa, van de belangrijkste terrigene en carbonaat-gerelateerde elementen (aluminium (Al), calcium (Ca), magnesium (Mg) en strontium (Sr)) en van ^{230}Th besproken. Hoofdstuk 3 behandelt de biogene fluxen, waarvan die van coccolithoferen (algen die een kalkskelet produceren) en kalkdinoflagellaten (thoracosphaeriden) de belangrijkste zijn. Vrijwel alle fluxen tonen een sterke seizoensinvloed, waarbij de hoogste fluxen tijdens de vroege lente van 1992 en 1993 en gedurende de late lente en vroege zomer van 1994 zijn gemeten. De enige uitzondering is de flux van complete coccosferen, waarvan de maximale flux in de winter plaatsvindt. Een vergelijking tussen historische jaarreeksen van door een satelliet ("Coastal Zone Colour Scanner") gemeten chlorofyl-gehalten (pigment) en de reeks van de fluxen gemeten in de sedimentval geeft aan dat er zich een periode van vier tot zes maanden bevindt tussen het maximum in de primaire productiviteit in het oppervlaktewater en de maximum flux gemeten in de sedimentval. Alleen de flux van coccosferen gemeten in de sedimentval is het hoogst ongeveer één maand nadat de pigmentconcentratie in het oppervlaktewater maximaal is. Deze laatste waarde wordt meestal ook in andere oceanen gevonden. De opvangefficiëntie van de sedimentval, berekend uit de gemeten ^{230}Th-flux in de val, bedraagt slechts 23%. Tevens is de flux van Al in de sedimentval ongeveer viermaal lager dan de Al-flux in nabijgelegen bovenste sediment. Carbonaatfluxen in de sedimentval, berekend uit de flux van Ca, zijn relatief zelfs nog lager vergeleken met de accumulatie van carbonaten in het bovenste sediment. De jaarlijkse flux van coccolithoforen is veel lager dan gepubliceerde fluxen die zijn waargenomen in de meeste andere oceanen, zelfs indien wordt gecorrigeerd voor de opvangefficiëntie. Dit bevestigt dan ook de lage primaire productiviteit in de oostelijke Middellandse Zee. Carbonaatoplossing is verwaarloosbaar op de diepte van de sedimentval en op de zeebodem, getuige het feit dat ook zeer fragiele coccolithofoorsoorten aanwezig zijn in beider sediment. De relatief lagere flux van totaal carbonaat in vergelijking met de terrigene flux — de laatste komt vooral tot uiting in de Al-flux — wordt deels veroorzaakt door het veel lagere gehalte aan grote (> 32 μm) foraminiferen (eencelligen met een kalkschaal) en pteropoden (planktonische gastropoden) in de monsters van de sedimentval dan in het bovenste sediment. Kwantificering van de terrigene flux in de sedimentval geeft aan dat woestijnstof uit de Sahara waarschijnlijk het grootste aandeel in deze flux heeft. Coccolithoforen zijn de belangrijkste bestanddelen van de biogene carbonaatflux in de oostelijke Middellandse Zee, gevolgd door thoracosphaeriden. *Emiliania huxleyi* en *Florisphaera profunda* zijn de meest voorkomende coccolithofoorsoorten in zowel de monsters van de sedimentval als het bovenste sediment.

In de hoofdstukken 4 tot en met 7 worden de metaalgehalten in de vaste fase en de verdeling van die metalen over verschillende mineraalfracties in normale sedimenten en in sedimenten uit een voormalig pekelbekken in de oostelijke Middellandse Zee besproken. De nadruk ligt op de diagenese van sapropel S1, dan wel het ontbreken daarvan, en op de daaruit voortvloeiende relaties tussen metalen en organisch materiaal.

In hoofdstuk 4 wordt de recente geschiedenis van sedimenten van het, vroeger met pekel gevulde en zuurstofloze, Poseidonbekken behandeld. De geochemie van deze sedimenten wordt vergeleken met sediment dat is afgezet in een voor de oostelijke Middellandse Zee normaal milieu. Op basis van ouderdommen bepaald via radioactief koolstof (AMS-^{14}C-methode) en op basis van geochemische en foraminiferenzones kunnen drie hoofdintervallen in de sedimentkern uit het Poseidonbekken worden onderscheiden. Van beneden naar boven in de kern zijn dat: (1) Organisch-rijk sediment dat geresedimenteerd is in het met pekel gevulde bekken zelf en dat dezelfde leeftijd heeft als sapropel S1 in normale sedimenten; (2) Sediment dat een typische koel-waterfauna van foraminiferen bevat en dat van de randen van het bekken de pekel is ingegleden toen die nog aanwezig was; (3) Oxisch (zuurstofrijk) pelagisch sediment dat is afgezet nadat, ongeveer 1800 jaar geleden, de zuurstofloze pekel vervangen was door zuurstofrijk bodemwater. Dicht bij de basis van deze laatste eenheid hebben zich mangaanoxiden opgehoopt. Deze verrijking aan mangaan markeert de huidige grens tussen zuurstofrijke en zuurstofarme milieus in het sediment. Een zich langzaam naar beneden bewegend oxidatiefront — iets wat meestal in normale sapropel-S1-sedimenten wordt gevonden — heeft zich nooit gevormd in de sedimenten van het Poseidonbekken. Dit heeft tot gevolg gehad dat de relatie die bestaat tussen organisch materiaal en aan organisch materiaal gerelateerde sporenelementen, b.v. seleen (Se), is behouden in de organisch-rijke sedimenten van het Poseidonbekken. Dit in tegenstelling tot normale sedimenten, waarin deze positieve relatie volledig verdwenen is. Het hoge gehalte aan opaal in de organisch-rijke sedimenten van het Poseidonbekken laat zien dat biogeen opaal beter gepreserveerd blijft ten opzichte van normale sapropel-S1-sedimenten. Het carbonaatgehalte van de sedimenten in het pekelbekken is tevens iets hoger dan in nabijgelegen normaal sediment van dezelfde leeftijd. Dit suggereert een ietwat betere preservatie van carbonaten in het pekelbekken.

In hoofdstuk 5 worden de bevindingen van hoofdstuk 4 in meer detail onderzocht met behulp van een gedetailleerd sequentieel-extractieschema (MESEX). Dit schema is toegepast op zowel normale Holocene sedimenten uit de oostelijke Middellandse Zee als op sedimenten van het Poseidonbekken (zie Figuur 1.2 voor typische profielen van metaalconcentraties in deze normale sedimenten). De grens tussen tweewaardig en drie- tot vierwaardig mangaan (Mn(II)/Mn(III,IV)) kan duidelijk worden onderscheiden in beide typen sediment. Aan carbonaat gerelateerde mangaan is namelijk verrijkt onder deze grens, terwijl mangaanoxiden alleen boven deze grens voorkomen. Er is een duidelijke grens tussen twee- en driewaardig ijzer (Fe(II)/Fe(III)) aanwezig in de normale sedimenten van de oostelijke Middellandse Zee. Deze bevindt zich net onder de Mn(II)/Mn(III,IV)-grens en valt ongeveer samen met het zichtbare grensvlak tussen het eronder liggende niet-geoxideerde en het bovenliggende geoxideerde deel van de oorspronkelijke sapropel S1. IJzersulfide, in de vorm van pyriet, is alleen aanwezig in het niet-geoxideerde interval, terwijl ijzeroxiden erboven veelvuldig voorkomen. De relatief grote afstand tussen de redoxgrenzen van Mn(II)/Mn(III,IV) en Fe(II)/Fe(III) in de sedimenten van het voormalige pekelbekken bevestigt dat er geen actieve oxidatie van de organisch-rijke eenheid in deze sedimenten heeft plaatsgevonden. Dit heeft geresulteerd in het behoud van de relatie tussen spoormetalen en organisch koolstof. Dit

wordt nog verder gestaafd door de profielen van vanadium (V), eveneens een metaal dat gevoelig is voor overgangen tussen reductie en oxidatie (redoxgevoelig). In normale sedimenten in de oostelijke Middellandse Zee heeft zich onder het oxidatiefront een grote diagenetische verrijking aan V gevormd. De MESEX-methode suggereert dat dit gemobiliseerde vanadium waarschijnlijk als vanadyl geadsorbeerd zit aan organisch materiaal. De correlatie van dit overschot aan V (dat wil dus zeggen het vanadium dat niet in kleimineralen zit) met organisch materiaal is echter volledig verdwenen. In de sedimenten uit het voormalige pekelbekken is V niet gemobiliseerd, wat blijkt uit de goede correlatie van het V-overschot met organisch materiaal. De MESEX-methode toont ook, door het vergelijken van de resultaten van twee sedimentkernen die zeer dicht bij elkaar liggen, dat de fractie van Mn en kobalt (Co) zich bevindend in gereduceerde mineraalfasen, voornamelijk geassocieerd is met pyriet, terwijl nikkel (Ni), koper (Cu) en zink (Zn) in deze fasen meer gerelateerd zijn aan organisch materiaal. In de overgebleven, zichtbare sapropel in de normale sedimenten van de oostelijke Middellandse Zee hebben deze laatstgenoemde elementen nog altijd hun oorspronkelijke relatie met organisch koolstof, zoals te zien is wanneer deze relatie vergeleken wordt met die in sedimenten van het voormalige pekelbekken. Op basis van de MESEX-methode konden kleine veranderingen in de samenstelling van de terrigene fractie (aluminosilicaten) worden vastgesteld. De Fe/Al_{klei}- en Mg/Al_{klei}-verhoudingen zijn iets hoger in sapropelen dan in normale pelagische sedimenten, hetgeen een verhoogd gehalte aan chloriet in eerstgenoemde sedimenten impliceert. Verhoudingen tussen verschillende sporenelementen en Al gedragen zich evenzo. Deze resultaten suggereren dat de bronnen van terrigeen materiaal ten tijde van sapropelafzetting verschilden van die in de direct erop volgende periode. Anderzijds blijft het profiel van de K/Al_{klei}-verhouding tamelijk constant, hetgeen betekent dat er zich geen grote veranderingen hebben voorgedaan in de relatieve bijdrage van illiet aan de kleimineraalfractie.

Hoofdstuk 6 presenteert een nieuw sequentieel-extractieschema (BASEX), dat bariet succesvol scheidt van andere mineraalfasen die barium (Ba) bevatten. Toepassing van de BASEX-methode op zowel sedimenten uit het Poseidonbekken als normale Holocene sedimenten uit de oostelijke Middellandse Zee toont aan dat het grootste deel van de hoge Ba-concentratie in sapropel S1 (Figuur 1.2) zich bevindt in bariet. De relatie van bariet-Ba (= biogeen Ba) met organisch koolstof in niet-geoxideerde sapropelsedimenten lijkt onafhankelijk van de waterdiepte, van de fluxen van organisch materiaal en van de sedimentatiesnelheid voor sedimentkernen afkomstig van diepten tussen 2150 en 3300 meter. Dit geeft aan dat remineralisatie van organisch materiaal vrijwel afwezig is geweest in de waterkolom dieper dan 2150 meter. Dit kan zijn veroorzaakt door de suboxische tot anoxische omstandigheden die heersten in het diepe gedeelte van het bekken van de oostelijke Middellandse Zee gedurende de vorming van sapropel S1. Hoewel de in dit proefschrift gemeten C_{org}/Ba-verhoudingen in hetzelfde bereik liggen als andere, gepubliceerde waarden, kan gesteld worden dat, omdat in dit proefschrift biogeen Ba rechtstreeks is gemeten, de hier getoonde waarden consistenter zijn dan andere die zijn gebaseerd op geschatte gehalten van biogeen Ba. Vanwege de vergelijkbare relatie tussen bariet en organisch koolstof over de hele oostelijke Middellandse Zee kan het hoge barietgehalte in het geoxideerde gedeelte van de

sapropel gebruikt worden om het oorspronkelijke gehalte van organisch koolstof in het sediment te kwantificeren.

In hoofdstuk 7 wordt een sequentiële-extractiemethode (CASEX) gepresenteerd waarmee verschillende carbonaatfasen, zoals aragoniet, calciet en vooral dolomiet, kunnen worden onderscheiden. Bovendien kunnen de verhoudingen van Mg/Ca en Sr/Ca in de totale carbonaatfractie bepaald worden zonder de invloed van dolomiet ($CaMg(CO_3)_2$). De CASEX-methode is toegepast op zowel sedimenten uit het Poseidonbekken als op normale Holocene sedimenten uit de oostelijke Middellandse Zee. Het dolomietgehalte en de verhoudingen van Mg/Ca en Sr/Ca in de totale carbonaatfractie (d.i. zonder dolomiet) zijn lager tijdens de afzetting van sapropel S1 dan in de periode erna. Deze waarnemingen komen overeen met het feit dat de vorming van de sapropel gebeurde in een relatief nat klimaat, waarin de aanvoer van woestijnstof relatief laag en de toevoer van rivieren relatief hoog waren. In dit opzicht geeft het dolomietgehalte de relatieve bijdrage van woestijnstof aan de terrigene fractie weer. De lagere Mg/Ca-verhoudingen in sapropelsedimenten worden vooral veroorzaakt door een lager zoutgehalte van het oppervlaktewater. Verschillen in de soorten die deel uitmaken van de flora en fauna zouden deels ook de oorzaak van een lagere verhouding kunnen zijn. In tegenstelling daarmee moet het grootste deel van de verandering in de Sr/Ca-verhouding toegeschreven worden aan veranderingen in de ecologie.

Acknowledgements

In the course of my years at Utrecht University, many people have, in some way, contributed to the road which ultimately led to this thesis. I thank them all for the help they have provided somewhere along the way.

First of all, I am indebted to Gert de Lange for providing me the opportunity to do this extremely fascinating research. Although the road was long and not always as smooth as it could have been, the final goal has been reached with this thesis. I am also very grateful to Kees van der Weijden, who helped me crossing the finishing line by doing numerous re-reads and by having fruitful discussions with me in the latter stages of my work on this dissertation.

For their valuable input in the writing process, I thank Patrizia Ziveri (Vrije Universiteit Amsterdam / University of Milan), Eelco Rohling and John Thomson (both Southampton Oceanographic Centre). Working with them has shown that multi-disciplinary research is indispensable in our field of research.

For their analytical assistance, I am grateful to Helen de Waard, Gijs Nobbe, Paul Anten, Anita van Leeuwen, Arnold van Dijk, Thea Broer, Geert Ittman, Gerrit van het Veld and Arie de Jong.

During my years in Utrecht, I have had numerous discussions with colleagues to tackle the problems of the eastern Mediterranean. Of them, I especially mention Patrick van Santvoort, Peter Pruysers, Hilde Passier, Ivar Nijenhuis and Gert-Jan Reichart. I also thank Gerard van den Berg and Christof Meile for being roommates at the institute. Furthermore, other colleagues I have had in the last six years — and they were many — have made my stay in Utrecht as pleasurable as can be. They include Pieter Kleingeld, Dineke van de Meent, Mark van Alphen, Hendrik-Jan Visser, Thomas Keijzer, Arthur Schmidt, Dick Schipper, Marcel Hoefs, Hans Hage, Ronald Jonckbloedt, Ding Mei, Berend Wilkens, Niels Hartog, Mariëtte Wolthers, Gernot Nehrke, Gerben Mol, Dorinda van der Linden, Sieger van der Laan, Ralf Haese and Caroline Slomp. A special thanks goes to Olaf Schuiling, who made such a big impression on me when I first began my study.

One colleague in particular has been a help throughout the years. I am indebted to Sjoerd Schenau for all the discussions we have had about each other's data and for the countless re-reads of earlier drafts of the manuscript, thereby greatly improving their quality.

Last but certainly not least, I am grateful to my parents and my brother, whose quiet support over the years has strengthened me. Also, I thank my colleagues at Centrale Financiën Instellingen (Team GGB), where I am currently employed via PinkRoccade TopTalenT (formerly TAS Top Talent), and Albert Goense of PinkRoccade TopTalenT for being so enthusiastic about my dissertation and giving me the time to finish it.

Curriculum Vitae

Arrian Rutten werd op 21 september 1972 in Dongen geboren. In 1984 begon hij zijn middelbare schoolopleiding VWO aan het Bisschoppelijk College Schöndeln te Roermond. In maart 1987 verhuisde hij naar Spijkenisse, alwaar hij zijn VWO-opleiding voortzette aan de Openbare Scholengemeenschap Ring van Putten. Deze opleiding werd in 1990 afgesloten met het Atheneum-B-diploma (met Latijn). In datzelfde jaar begon hij met zijn studie aan de Universiteit Utrecht, waar hij in 1991 het propedeutisch examen Geologie *cum laude* behaalde. In juni 1994 werd door hem het doctoraal examen Geochemie *cum laude* behaald. Aansluitend werd hij assistent-in-opleiding bij de vakgroep Geochemie te Utrecht. Het in deze hoedanigheid verrichte onderzoek aan sedimenten in de oostelijke Middellandse Zee heeft geresulteerd in dit proefschrift. Momenteel werkt hij als ICT-consultant bij PinkRoccade TopTalenT.

“Is a dream a lie if it don’t come true, or is it something worse?”

Bruce Springsteen – The river

"A sudden silence hit the Earth. If anything it was worse than the noise. For a while, nothing happened.

The great ships hung motionless in the sky, over every nation on Earth. Motionless they hung, huge, heavy, steady in the sky, a blasphemy against nature. Many people went straight into shock as their minds tried to encompass what they were looking at. The ships hung in the sky in much the same way that bricks don't.

And still nothing happened.

Then there was a slight whisper, a sudden spacious whisper of open ambient sound. Every hi fi set in the world, every radio, every television, every cassette recorder, every woofer, every tweeter, every mid-range driver in the world quietly turned itself on.

Every tin can, every dustbin, every window, every car, every wine glass, every sheet of rusty metal became activated as an acoustically perfect sounding board.

Before the Earth passed away it was going to be treated to the very ultimate in sound reproduction, the greatest public address system ever built. But there was no concert, no music, no fanfare, just a simple message.

'People of Earth, your attention please,' a voice said, and it was wonderful. Wonderful perfect quadrophonic sound with distortion levels so low as to make a brave man weep.

'This is Prostetnic Vogon Jeltz of the Galactic Hyperspace Planning Council,' the voice continued. *'As you will no doubt be aware, the plans for development of the outlying regions of the Galaxy require the building of a hyperspatial express route through your star system, and regrettably your planet is one of those scheduled for demolition. The process will take slightly less than two of your Earth minutes. Thank you.'*

The PA died away.

Uncomprehending terror settled on the watching people of Earth. The terror moved slowly through the gathered crowds as if they were iron filings on a sheet of board and a magnet was moving beneath them. Panic sprouted again, desperate fleeing panic, but there was nowhere to flee to.

Observing this, the Vogons turned on their PA again. It said:

'There's no point in acting all surprised about it. All the planning charts and demolition orders have been on display in your local planning department in Alpha Centauri for fifty of your Earth years, so you've had plenty of time to lodge any formal complaint and it's far too late to start making a fuss about it now.'

The PA fell silent again and its echo drifted off across the land. The huge ships turned slowly in the sky with easy power. On the underside of each a hatchway opened, an empty black square.

By this time somebody somewhere must have manned a radio transmitter, located a wavelength and broadcast a message back to the Vogon ships, to plead on behalf of the planet. Nobody ever heard what they said, they only heard the reply. The PA slammed back into life again. The voice was annoyed. It said:

'What do you mean you've never been to Alpha Centauri? For heaven's sake mankind, it's only four light years away you know. I'm sorry, but if you can't be bothered to take an interest in local affairs that's your own lookout.

'Energize the demolition beams.'

Light poured out of the hatchways.

'I don't know,' said the voice on the PA, *'apathetic bloody planet, I've no sympathy at all.'* It cut off.

There was a terrible ghastly silence.

There was a terrible ghastly noise.

There was a terrible ghastly silence.

The Vogon Constructor Fleet coasted away into the inky starry void."

Douglas Adams – The hitchhiker's guide to the galaxy (excerpt)